MIT LIBRARIES DUPL 1
3 9080 00576532 3

TECTONIC EVOLUTION OF THE MT. OLYMPOS REGION, GREECE

by

Elizabeth Renee Schermer

B.S. Geology, Stanford University
(1982)

B.A. English, Stanford University
(1982)

Submitted to the Department of
Earth, Atmospheric, and Planetary Sciences
In Partial Fulfillment of the Requirements for the Degree of

Doctor of Philosophy

at the

Massachusetts Institute of Technology

February, 1989

©Elizabeth R. Schermer 1989. All rights reserved
The author hereby grants to MIT permission to reproduce and to distribute copies of this thesis document in whole or in part.

Signature of Author: _____
Department of Earth, Atmospheric, & Planetary Sciences, MIT
September 6, 1988

Certified by: _____
B. Clark Burchfiel
Thesis Supervisor

Accepted by: _____
T. H. Jordan
Chairman, Department Committee

MASSACHUSETTS INSTITUTE OF TECHNOLOGY
APR 11 1989
LIBRARIES

TECTONIC EVOLUTION OF THE MT. OLYMPOS REGION, GREECE

by

Elizabeth Renee Schermer

Submitted to the Department of Earth, Atmospheric, and Planetary Sciences
on September 6, 1988 in partial fulfillment of the requirements for the degree of
Doctor of Philosophy

ABSTRACT

In the Mt. Olympos region, N. Greece, Paleozoic continental basement and cover sequences were subducted and later thrust over Mesozoic-Eocene carbonate platform strata during the Mesozoic to Tertiary collision of the Apulian and European plates. Five major structural units have been identified: The lowest unit (Olympos unit), is composed of parautochthonous, very low-grade Mesozoic platform carbonates and Lutetian (Eocene) flysch. Previous workers have correlated the Olympos unit with the margin of the Apulian plate. This is overlain in thrust contact by the Ambelakia unit, a tectonically complex sequence of blueschist-facies metabasalts and metasediments. Preliminary major and trace element and isotope geochemistry studies suggest that parts of the Ambelakia unit were derived from a volcanic arc. The third unit, the Pierien unit, consists of blueschist-facies Paleozoic granitic gneiss overlain by Mesozoic marble, internally imbricated and thrust over the Olympos and Ambelakia units. Blueschist-greenschist transition facies quartzofeldspathic and amphibolitic gneiss and schist of the fourth unit, the Pierien unit, are found in both thrust and normal fault contact over lower units. The highest unit, the ophiolite unit, includes late Jurassic ophiolitic rocks generally in normal fault contact over all lower units.

Based on a combination of field, geochronologic, and petrologic data, I recognize the following sequence of events related to the collision of Apulia and Europe during the Alpine orogeny: D0): Amphibolite facies metamorphism and deformation of the Pierien and Infrapierien units may include both early Alpine and Paleozoic events that can not be differentiated in the study area. D1) Thrust imbrication, mylonitization, NE-SW trending isoclinal folds, and blueschist-greenschist facies metamorphism of continental nappes (Pierien,Infrapierien) may have signaled the beginning of collision. D2) Blueschist-facies metamorphism of the Ambelakia unit and parts of the Pierien unit was accompanied by the formation of foliation, isoclinal folds, and NE-SW mineral lineation. Thrust faults that juxtaposed the Pierien, Infrapierien, and Ambelakia units were active during this event. D3) Thrusting of Ambelakia and Pierien units over the Olympos unit produced NE-SW trending isoclinal folds and stretching lineations and 50-300 m thick mylonite zones at thrust faults. Sense-of-shear indicators indicate the hanging wall moved towards SW over the footwall. Thrusting produced ductile fabrics but did not overprint the blueschist-facies mineral assemblages formed during D2 with higher temperature phases. D4) Thrust faults were folded by close to open NW-SE trending folds. These folds were previously interpreted (Barton, 1975) to represent NE-directed thrusting of basement rocks over parautochthon; however, this event overprints the older, thrust-related fabrics. F4 folds rotated thrust faults to produce apparent normal sense of shear on thrusts on the W margin of the Olympos window. D5) Low-angle normal faults locally cut out 3-6 km of structural section and displace ophiolitic rocks down to NNE and NE so they are in fault contact with all lower structural units. D6) Broad folding about NE-SW axes caused further steepening of thrust surfaces and preserved low-angle normal fault segments on the NW and SE flanks of Mt. Olympos. D7) High-angle normal faults juxtapose ophiolitic rocks against the lower parts of the Olympos unit on the eastern flank of Mt. Olympos and cut Neogene and Quaternary conglomerates. Brittle extensional structures in D7 affect both hanging wall and footwall, indicating extension occurred at a relatively shallow level.

The SW-vergence of the major thrusting events (D2, D3) indicates that the ocean from which the ophiolitic terranes were derived originally lay NE of the carbonate platform of Apulia (Olympos unit). This in turn suggests that only one ocean basin lay between Apulia and Europe in this region prior to Paleocene collision. The D2 and D3 events are interpreted to represent A-type subduction of the continental basement and cover of part of the Apulian plate.

Diffusive-loss profiles in 40Ar/39Ar spectra from hornblende, white mica, and biotite samples indicate that the upper two structural units preserve evidence of four distinct thermal events while the lower units were affected only by Eocene and younger events. Temperatures of the thermal events are

broadly constrained by the closure temperatures of the dated minerals; however Ar loss during the Eocene events may have been controlled by deformation and recrystallization rather than (temperature-controlled) volume diffusion from existing mineral grains: 1) 295-300 Ma crystallization of granitic intrusions, with cooling from >550°C to <325°C by 285 Ma; 2) ~100 Ma greenschist to blueschist-greenschist transition facies metamorphism (T~400-500°C) and imbrication of continental thrust sheets; 3) 53-61 Ma blueschist facies metamorphism and deformation of the basement and continental margin units (Ambelakia and Pierien units) at T<350-400°C; 4) 36-40 Ma thrusting of blueschists over the Olympos carbonate platform, and metamorphism at T<350°C. A fifth event is indicated by diffusive-loss profiles in microcline spectra from the basement units. These are interpreted to reflect the beginning of decompression and cooling to T<100-150°C at 16-23 Ma, associated with normal faulting which continued until Quaternary time. During early to middle Tertiary, an average cooling rate of >10°C/Ma below metamorphic temperatures of ~350-400°C allowed preservation of the blueschist facies mineral assemblages as they were uplifted from depths of >20 km.

Incomplete resetting of mica ages in all units constrains the temperature of metamorphism during continental (A-type) subduction to T≤350°C, the approximate closure temperature for Ar in muscovite. Ar release spectra from phengites grown during Eocene metamorphism and deformation record the ages of Ar loss events.

A-type subduction resulted in the superposition of high pressure-low temperature assemblages on earlier higher T, lower P assemblages. Four metamorphic events can be distinguished; an earlier greenschist facies (M1), two blueschist facies events (M2,M3) and a late- to post-kinematic prehnite-pumpellyite facies event (M4). Pressures and temperatures of M2 and M3 metamorphism have been estimated from phase assemblages and compositions of sodic amphiboles and pyroxenes and the phengite content of white mica. These constraints indicate P-T conditions of T<250°C, P≥4-6 kb in the Olympos unit; P ~6-8 kb; T ~250-350°C in the Ambelakia unit; and P ~6-8kb, T ~300-425°C in the Pierien unit. Blueschist-greenschist transition facies metamorphic conditions in the Infrapierien unit are estimated at P ~3-6kb and T ~350-500°C.

A speculative tectonic model for the pressure-temperature-time evolution of the Mt. Olympos region includes the following: A-type subduction may have begun prior to final collision of the Apulian and European plates, but blueschist facies metamorphism and further basement imbrication began at roughly the same time as the collision. Basement rocks followed a counter-clockwise P-T path, as pressures initially increased contemporaneously with decreasing temperatures. Subsequent events evolved from blueschist facies through prehnite-pumpellyite facies. Subduction of the continental crust proceeded by stripping off thin thrust sheets of the uppermost basement and cover and by continual underthrusting of cool surface material to depths ≥20km. Underthrusting maintained low temperatures at these depths for ~20 Ma until decompression and cooling occurred by erosion and normal faulting. The period of extension and decompression appears to have begun approximately at the same time as the opening of the Aegean back-arc basin and was superimposed on the previously-formed thrust belt.

Thesis supervisor: Dr. B. Clark Burchfiel

Title: Schlumberger Professor of Geology

ACKNOWLEDGEMENTS

This thesis was financially supported by a National Science Foundation Graduate Fellowship, a Grant-in-Aid of Research from Sigma Xi, a Geological Society of America Research Grant, and the departmental Student Research Fund . Field work was funded by support from the Schlumberger Corporation to Clark Burchfiel.

My greatest thanks go to Clark Burchfiel, who suggested Greece as a field area in the first place, and let me have the freedom and time to develop the ideas presented in this thesis. His help in the field, in figuring out the "big picture", and pointing out the significance of many things I might have overlooked has been invaluable. Kip Hodges also provided scientific, editorial, and emotional support at many crucial moments; without his help, Chapter 5 would probably not exist. Stan Hart kept me aware of all the problems inherent in geochronology, and generously allowed the use of his lab for the Rb/Sr and Sm/Nd work.

My other committee members Peter Crowley and Nafi Toksöz were very helpful in providing valuable comments and criticisms. Dan Lux at the University of Maine let me flounder in his argon lab and helped in the analysis of the data in chapter 4. Fred Frey and Pilalamarri Ila were extremely helpful with neutron activation analysis. Bruce Wardlaw of the U.S.G.S. examined many samples for conodonts, but to no avail. David Howell's unflagging enthusiasm and encouragement of my scientific career is also greatly appreciated. Dave Larue also provided much encouragement and the opportunity to visit the Caribbean under the guise of speaking at the University of Puerto Rico.

I also thank Dimitrios Papanikolaou for logistical support in Greece and helpful discussions on metamorphism in the Hellenides. His graduate assistants Themios Lekkas and Christos Sideris helped me get through the maze of bureaucracy needed to start field work in Greece. Professor Mariolakis also was very helpful in obtaining my field work permit.

The Papadimitriou family of Kastanea-Servia and the Tzikas family of Elassona were my home away from home during three long field seasons. Their warmth, generosity, and friendliness, and their patient listening to my bumbling of the Greek language will never be forgotten.

My field assistants Becky Cleaver, Barb Lycan, Mo Smith, and Sarah Kruse put up with the hardships of warm weather, beautiful beaches, fresh Greek salads and berries, and Bouzouki music and dancing without complaining. Fortunately,

the "wolves", the late-night visits from strangers and the hard work were also treated with much patience.

Ken Burrhus and Levent Gulen provided much help in the isotope lab, and many thanks go to Steve Recca and Tim Grove for help on the microprobe and much free time. Larry McKenna and Doug Walker were very generous to provide XRF analyses of many samples.

Many current and former graduate students have made my time at M.I.T. both interesting and enjoyable, and I have learned much from you all. The tectonics students, including Dave Klepacki, Doug Walker, Peter Crowley, Peter Tilke, Zhang Pei-Zhen, Jim Knapp, Larry McKenna, Laurence Page, David Silverberg, Allison McFarlane, David Dinter, Mary Hubard, Barb Sheffels, Cindy Ebinger, and Joann Stock are thanked for putting up with my questions and anxiety attacks. Mike Baker, Tanya Furman, Don Hickmott, Jane Selverstone, Tom Sisson and Tom Juster endured many ignorant petrologic questions. Vincent Salters not only helped me survive the clean lab and the world of isotope geochemistry, but spent many valuable late hours helping me get through the last-minute crunch. Tom Sisson made sure I learned that there are other challenges in life besides thesis-writing; thanks for the patience with my rock- and ice-climbing attempts and my aversion to bad weather and crummy skiing conditions!

Mary Hubbard and Barb Sheffels have been great friends and provided many excuses for Toscaninis and all manner of procrastination activities. Mary Reid and Brian Taras made the early years here much more enjoyable; I appreciate the many late-night conversations, Thai food and friendship. Mary Reid and Jim Sample are also especially thanked for help with drafting and for stabilizing the last-minute chaos.

The MIT women's ice hockey team helped me survive the long winters in Boston; without them I might have moved to a place where the skiing is good. Four years of teamwork and great coaching (thanks, Brian) was one of the most important contributions to my education. I also thank the women's rugby team for letting me extend my enthusiasm for contact sports through the fall and spring.

Last, but not least, I thank my parents and family for putting up with my boondoggling around the world, even if they're still not sure it's really in the pursuit of scientific knowledge. Scott Eilbers provided the lure of three weeks of rafting down the Colorado to finally get me finished and back out west.

TABLE OF CONTENTS

ABSTRACT ii
ACKNOWLEDGEMENTS iv
TABLE OF CONTENTS vi

Chapter 1: INTRODUCTION AND GEOLOGIC BACKGROUND 1
Introduction 2
Organization 5
Methods 5
Geological Framework of the Mt. Olympos Region 6
Geologic setting of the Internal Hellenides 6
Previous work 11

Chapter Two: TECTONOSTRATIGRAPHY 13
INTRODUCTION 14
OLYMPOS UNIT 14
Introduction 14
Carbonate rocks 18
Flysch 19
Metamorphism and Deformation 20
Introduction 22
"Type section" description 23
Metapelites and metapsammites 26
Marbles and calc-schists 26
Pink dolomitic breccia 26
Mica schists 27
Metavolcanic rocks 27
Ambelakia rocks in other parts of Olympos-Ossa region 28
FLAMBOURON CONTINENTAL BASEMENT UNITS 29
Introduction and previous work 29
Pierien unit 29
Introduction 29
Pre?Carboniferous gneisses, granites and granodiorites 29
Mica schists, augen schists, amphibolites 32
Marbles 33
Geochronology 33
Infrapierien unit 33
Introduction 33
Livadi granite-gneiss 34
Interbedded quartzofeldspathic and amphibolite gneisses 34
Overlying metasedimentary rocks 35
Blueschists and Mn-rich schists 36
Marbles 36
OPHIOLITE 37
Introduction 37
Regional relations 37
Livadi ophiolite complex 37
Other ophiolitic rocks in the Olympos region 39
Ultramafic rocks 39
Mafic rocks 40
Carbonate and clastic rocks overlying(?) the ophiolite 40
NEOGENE AND QUATERNARY 41
GEOCHEMISTRY OF META-IGNEOUS ROCKS 42
Ambelakia unit 42
Trace Elements 42

Rb/Sr and Sm/Nd isotopes 43
Pierien and Infrapierien units 43
Ophiolite unit 43
Discussion: Paleogeography of the Olympos region 44
Olympos unit 44
Ambelakia unit 45
Pierien and Infrapierien units 45
Ophiolite unit 46
CONCLUSIONS 46
Appendix A2: Geochemical data 47

Chapter Three: STRUCTURAL EVOLUTION OF SUBDUCTED CONTINENTAL CRUST, MT. OLYMPOS REGION, GREECE 52
INTRODUCTION 53
Geologic setting 54
Previous work 57
Purpose of this study 58
Summary of events 59
GEOMETRIC, CHRONOLOGIC, AND KINEMATIC CHARACTERISTICS OF THE DEFORMATION IN THE OLYMPOS REGION 59
D0: Pre-Alpine deformation and medium-grade metamorphism 61
D1: Early to middle Cretaceous folding and basement imbrication 61
Ophiolite unit 62
Pierien and Infrapierien units 62
Ambelakia unit 68
D1 relative timing 68
Absolute timing constraints 72
D1 kinematics 72
D2: latest Cretaceous to early Eocene blueschist-facies metamorphism and deformation 73
Ophiolite unit 76
Infrapierien unit 76
Pierien unit 79
Ambelakia unit 82
The Sparmou thrust 82
D2 relative timing 83
Ophiolite unit 83
Infrapierien unit 83
Pierien and Ambelakia units 89
D2 kinematics 89
D3: Late Eocene SW-directed emplacement of metamorphic nappes over the Olympos carbonate platform 90
Pierien and Infrapierien units 90
Ambelakia unit 91
Olympos unit 91
The Olympos Thrust 97
D3 relative timing 98
D3 kinematics 98
D4: NW-SE folding 99
D4 relative timing 100
D4 kinematics 100
D5: Low-angle normal faults 103
D5 relative timing 107
D5 kinematics 108
D6: NE-SW open folds 109
D6 relative timing 111
D6 kinematics 111

D7: High-angle normal faults 111
D7 relative timing 112
D7 kinematics 112
DISCUSSION 117
Summary of deformational events in the Mt. Olympos region 117
Regional implications of deformational events 117
Intracontinental subduction 119
Significance of D5 and D7 normal faulting 121
CONCLUSIONS 123
APPENDIX A3 Stereographic projections of structural data 124

Chapter Four: TEMPERATURE-TIME HISTORY OF SUBDUCTED CONTINENTAL CRUST, MT. OLYMPOS REGION, GREECE 128
INTRODUCTION 129
Geologic setting of the Internal Hellenides 130
Previous geochronological studies 135
Sample selection and analytical methods 136
RESULTS 138
Ambelakia Unit 138
Pierien Unit 140
Infrapierien Unit. 150
DISCUSSION 153
Closure temperatures and the discrepancy between Rb/Sr and Ar/Ar ages 154
Age gradients in white mica and microcline spectra 156
Excess Argon 163
Temperature-time history of the Pelagonian zone during Alpine orogenesis 163
Paleozoic 164
Mesozoic 165
Tertiary 167
CONCLUSIONS 172
Acknowledgements 173
Table 4.1 174
Table 4.2 181

Chapter 5: METAMORPHIC PETROLOGY AND P-T HISTORY 182
INTRODUCTION 183
PETROGRAPHIC CHARACTERISTICS OF METAMORPHIC ASSEMBLAGES 183
M1: Greenschist-Amphibolite facies metamorphism 184
Granitic rocks 184
Pelites 188
Metabasites 189
Carbonate rocks 197
M2 and M3: High P-Low T metamorphism 197
Granitic rocks 198
Pelites 198
Metabasites 199
Carbonate rocks 202
Metagraywacke and meta-arkosic sandstone 203
M4: Prehnite-pumpellyite facies metamorphism 207
METAMORPHIC MINERAL COMPOSITIONS 207
Analytical Methods 207
Amphiboles 208
Sodic pyroxenes 209
Epidote 216
White mica 217
Chlorite 218

Pumpellyite 221
Feldspars 221
Garnet 221
Biotite 222
Chloritoid and paragonite 222
RELATIVE AND ABSOLUTE AGES OF METAMORPHISM AND DEFORMATION 222
M1: Mid-Cretaceous greenschist-amphibolite facies metamorphism in the Ophiolite, Pierien, and Infrapierien units 223
M2: Early Eocene blueschist facies metamorphism, Pierien and Ambelakia units 224
M3: late Eocene blueschist-facies metamorphism in the Pierien, Ambelakia, and Olympos units 225
M4: cooling and decompression under prehnite-pumpellyite facies conditions 225
DISCUSSION: CONSTRAINTS ON CONDITIONS OF METAMORPHISM 226
Constraints from mineral equilibria and the stability of index minerals 229
Mineral stability fields 229
Lawsonite 229
Pumpellyite and Prehnite 229
Sodic amphibole 230
Epidote and actinolite 230
Phase equilibria constraints on P,T conditions 231
M1: Greenschist-amphibolite facies metamorphism 231
M2, M3, and M4: Blueschist and Prehnite-Pumpellyite facies metamorphism 231
Thermobarometric constraints 232
Garnet-biotite geothermometry 233
Garnet-chlorite geothermometry 233
Phengite geobarometry 238
Constraints from sodic and calcic amphibole compositions 241
Constraints from sodic pyroxene compositions 244
PRESSURE-TEMPERATURE-TIME EVOLUTION OF THE MT. OLYMPOS REGION: A SPECULATIVE TECTONIC MODEL 246
CONCLUSIONS 250

Chapter 6: CONCLUSIONS: TECTONIC HISTORY OF THE MT. OLYMPOS REGION 251
Introduction 252
Summary of constraints on the tectonic history 252
Structural and Metamorphic Evolution 254
Characteristics of continental collision and subduction 255
Significance of normal faulting and the preservation of blueschists 257
A-type subduction: problems and possible solutions 258
CONCLUSIONS 260

REFERENCES 261

Chapter 1: INTRODUCTION AND GEOLOGIC BACKGROUND

Introduction

Continent-continent collision is one of the most important mountain-building processes. The mountain ranges of the Alpine-Tethyan orogen are the result of the convergence between and collision of the African and European plates that accompanied the closure of the Tethys ocean. Although the Alps are one of the most intensely-studied orogens, there is still much that we do not understand about collisional orogeny. For example, it has been recognized for many years that the large amounts of shortening recorded in the cover rocks cannot be accounted for by restoration onto the presently exposed basement. This implies that some of the basement has disappeared, or been subducted. The concept of disappearance of the basement rocks, called "verschlucking" by Ampferer (1906), or A-type subduction by Bally (1975), was originally proposed for the Eastern Alps, and has been more recently applied to other collisional orogens (e.g. Trumpy, 1963; Milnes, 1978; Burchfiel, 1980; Hodges et al, 1982). Inasmuch as it is well-known that subduction of significant amounts of continental crust is required throughout the Alpine orogen, the processes by which the subduction occurs remain poorly understood even after many years of study.

During the Alpine orogeny in Greece, the African plate collided with the European plate to form the Hellenic Alps. Deformation began in the internal (eastern) Hellenides with intrusion of middle Jurassic granites and obduction of middle Jurassic ophiolites in latest Jurassic time, and continued episodically through Cretaceous and Tertiary time as deformation progressed from east to west into the external Hellenides. The collision resulted in A-type subduction of the leading edge of the Apulian plate (African promontory). Fragments of partially subducted crust are exposed in the Mt. Olympos region, the subject of this thesis. The continental lithologies were metamorphosed under high pressure - low temperature conditions and thrust over carbonate platform strata. Although the metamorphism and its relation to deformation have been the subject of study for many years, considerable controversy still exists as to the number, age, and regional significance of various deformation phases, and there is little agreement on the paleogeographic reconstruction of the region (see Robertson and Dixon, 1984 for a useful introduction to the many problems).

The peaks of Mt. Olympos (Figure 1.1) are formed by carbonate rocks that are thought to correlate with the external Hellenides (Godfriaux, 1968; Fleury and Godfriaux, 1974) The carbonate rocks are exposed in a tectonic window through

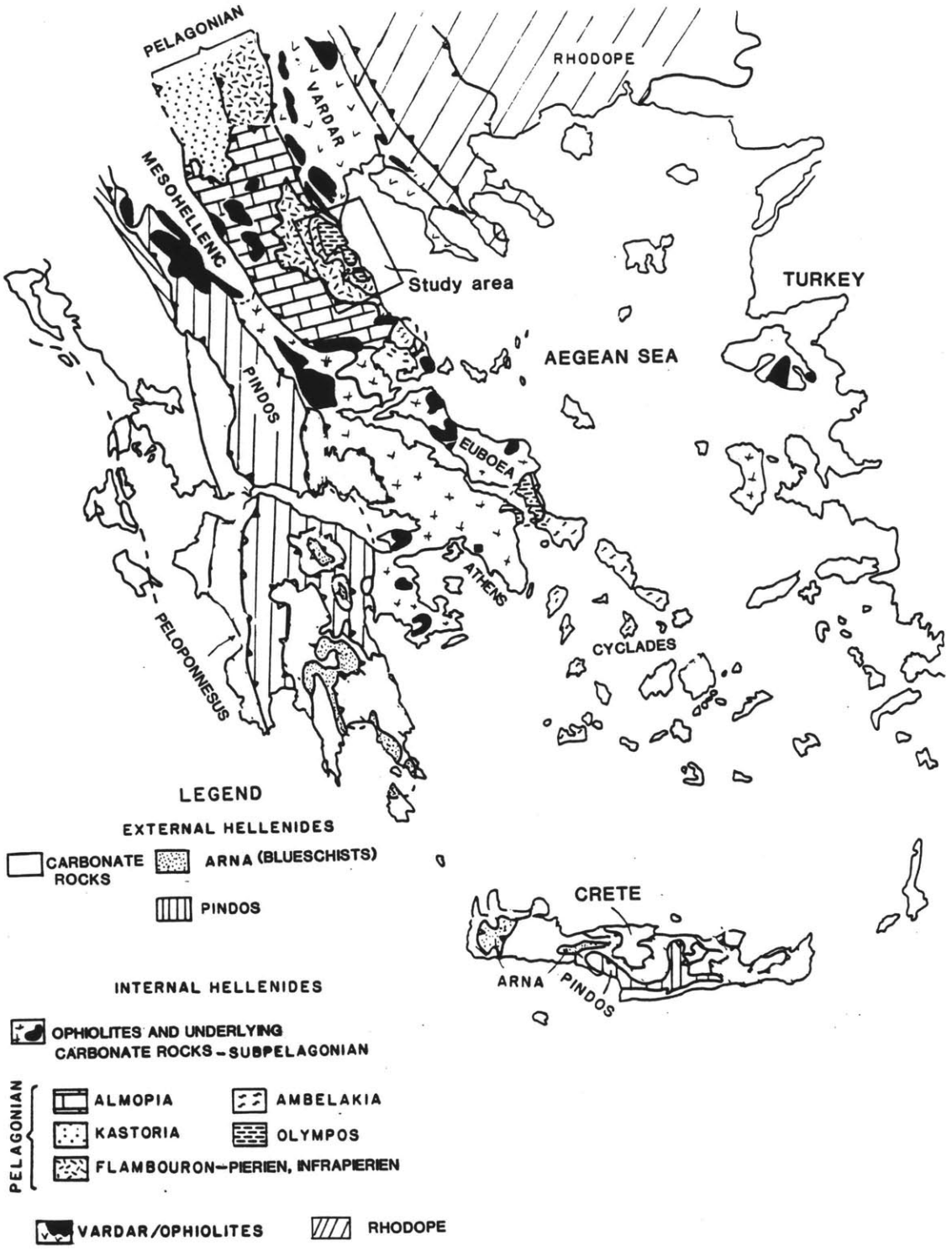

Figure 1.1 Tectonic map of Greece, modified from Papanikolaou (1984a) and Jacobshagen et al (1978). The location of the study area in the Mt. Olympos region is indicated.

the metamorphic rocks of the internal Hellenides. A cross section through part of the Alpine orogen is exposed as a series of thrust sheets with higher-grade, early-deformed metamorphic nappes on top, and progressively lower-grade metamorphic nappes deformed at later times towards the base of the structural succession. The lower parts of the nappe sequence record A-type subduction of continental basement and cover rocks that was accompanied by deformation and metamorphism under high pressure-low temperature conditions. Subsequent exhumation of the thick section of metamorphic nappes has provided the opportunity to study a large part of the long history of deformation and metamorphism in the Hellenides.

The Olympos region is somewhat unusual in that it contains continental basement rocks that were subducted to blueschist-facies conditions and subsequently exhumed without being overprinted by higher temperature metamorphic assemblages. The long history of deformation preserved in these rocks is in part due to the lack of overprinting, and thus a detailed study of the deformational and metamorphic history provides insight into the processes involved in continental collision, subduction, and the uplift and preservation of blueschists.

Some of the general questions that can be addressed by a detailed study of an A-type subduction zone include the following: 1) How deep can continental crust be subducted; how much of it disappears and how much of it is incorporated into the orogen? 2) How does the crust deform during A-type subduction and what are the pressure-temperature conditions during deformation? 3) If subducted crust is incorporated into the mountain belt, how does it become exposed at the surface?

The principal purpose of this thesis is to use a variety of techniques, including field mapping, geochronology, and metamorphic petrology, to obtain a better understanding of the mechanical and thermal evolution of an A-type subduction zone. Secondly, the structural analysis places kinematic constraints on the structural evolution of this part of the Hellenides that will contribute toward a better reconstruction of the paleogeography of the region. Thirdly, by determining a detailed chronology of the sequence of orogenic events, I am able to recognize not only the episodic deformation related to Eocene A-type subduction, but also the effects of Miocene and younger back-arc extension that have been superimposed on the compressional structures. Because recognition of the significance of major extensional structures that occur within the Hellenides is only beginning, I hope

that this study will serve as an impetus for reexamination of the interplay between thrust tectonics and back-arc extension in the continental Hellenides.

Organization

This thesis is written in part as "thesis-format" chapters and in part as papers that will be submitted for publication. This chapter will present background material on the geologic setting of the Hellenides and the Mt. Olympos region. Chapter 2 details the tectonostratigraphy of the study area, describes the lithologies mapped on Plate 1, and discusses the implications of these data for the paleogeography of this part of the Hellenides. Chapter 2 also includes an appendix containing geochemical analyses of meta-igneous rocks. Because the geochemical study is incomplete at this time, I have included preliminary interpretations and conclusions only as they pertain to the paleogeography of the Olympos region, and have presented the data in the appendix without interpretation in order that the interested reader may draw his or her own conclusions. Chapters 3 and 4 are written in publication format, and as such the introductory sections of these chapters repeat much of the background material contained in this chapter. Chapter 3, entitled "Structural Evolution of Subducted Continental Crust: Mt. Olympos Region, N.E. Greece" will be submitted as a paper coauthored by B.C. Burchfiel. Chapter 4, "Temperature-Time History of Subducted Continental Crust, Mt. Olympos Region, N.E. Greece" is coauthored by D.R. Lux and B.C. Burchfiel. An abbreviated version of Chapter 4, entitled "Age and Tectonic Significance of Metamorphic Events in the Mt. Olympos Region, Greece", by E.R. Schermer, D.R. Lux, and B.C. Burchfiel, has been accepted for publication in the Bulletin of the Geological Society of Greece. Chapter 5, "Metamorphic Petrology and P-T history of the Mt. Olympos region" is written in thesis-style as the present study is largely descriptive; further work is needed before the complexities of the metamorphic evolution can be resolved to a point where a coherent analysis can emerge. Chapter 6 summarizes the conclusions of the previous chapters and attempts to place these conclusions in a broader tectonic framework with speculation as to why A-type subduction occurred and why its effects are preserved in the Mt. Olympos region.

Methods

Approximately ten months were spent during the three summers of 1984-1986 mapping the area of Plate 1. Although Mt. Olympos itself, the highest peak in Greece (2911 m), is very rugged, access to the flanks of the range is afforded by

numerous dirt roads, and new roads are built each year by logging companies. The elevation within the study area ranges from less than 300 m to greater than 2000 m above sea level. While exposure is very good at higher elevations and on the western and southern flanks of the mountain, thick pine forest and brush are present on the northern and eastern flanks; road cuts provide the majority of outcrops in these areas, particularly in the ophiolitic rocks.

Mapping was done at a scale of 1:25,000 on base maps enlarged from the 1:50,000 sheets (contour interval 20 m) provided by the Institute for Geological and Mining Exploration (ΙΓΜΕ) of Greece in Athens.

There does not appear to be any native wildlife left in the Olympos region; although rumors of wolves and snakes abound, goats, sheep, dogs, and cows constitute the majority of the animal life. Several small villages on the flanks of Mt. Olympos, in the valleys to the west, south, and east provided ouzo, fresh feta cheese, and much entertainment. The weather was generally excellent.

Geological Framework of the Mt. Olympos Region

The Hellenides form part of the more southern of the two branches of the eastern Alpine system. This southern branch extends NW from Greece into Yugoslavia, where it is termed the Dinarides, and then bends westward in Austria and merges with the Eastern and Southern Alps. The northern branch of the system consists of the double-looped Carpathian-Balkan chain (Figure 1.2). As summarized by Burchfiel (1980), the eastern Alpine orogen consists of a number of fragments of continental crust that were assembled from late Jurassic to Miocene time during closing of the Mesozoic Tethyan ocean basins that existed between Africa and Europe. The interactions between two of these fragments, Rhodope, in northeasternmost Greece, and Apulia, constituting most of western and central mainland Greece, were responsible for the deformation in the Hellenides (Figure 1.2).

Geologic setting of the Internal Hellenides

The principal tectonic subdivisions of the Hellenides are shown in Figure 1.1. Aubouin (1959) originally interpreted these "isopic zones" in terms of geosynclinal theory. It is now recognized that the Hellenides consists of various thrust nappes of continental and oceanic provenance that belong to the continental parts of either the European plate, the Apulian plate (African promontory), or to the intervening oceanic lithosphere that was present during early stages of Alpine convergence.

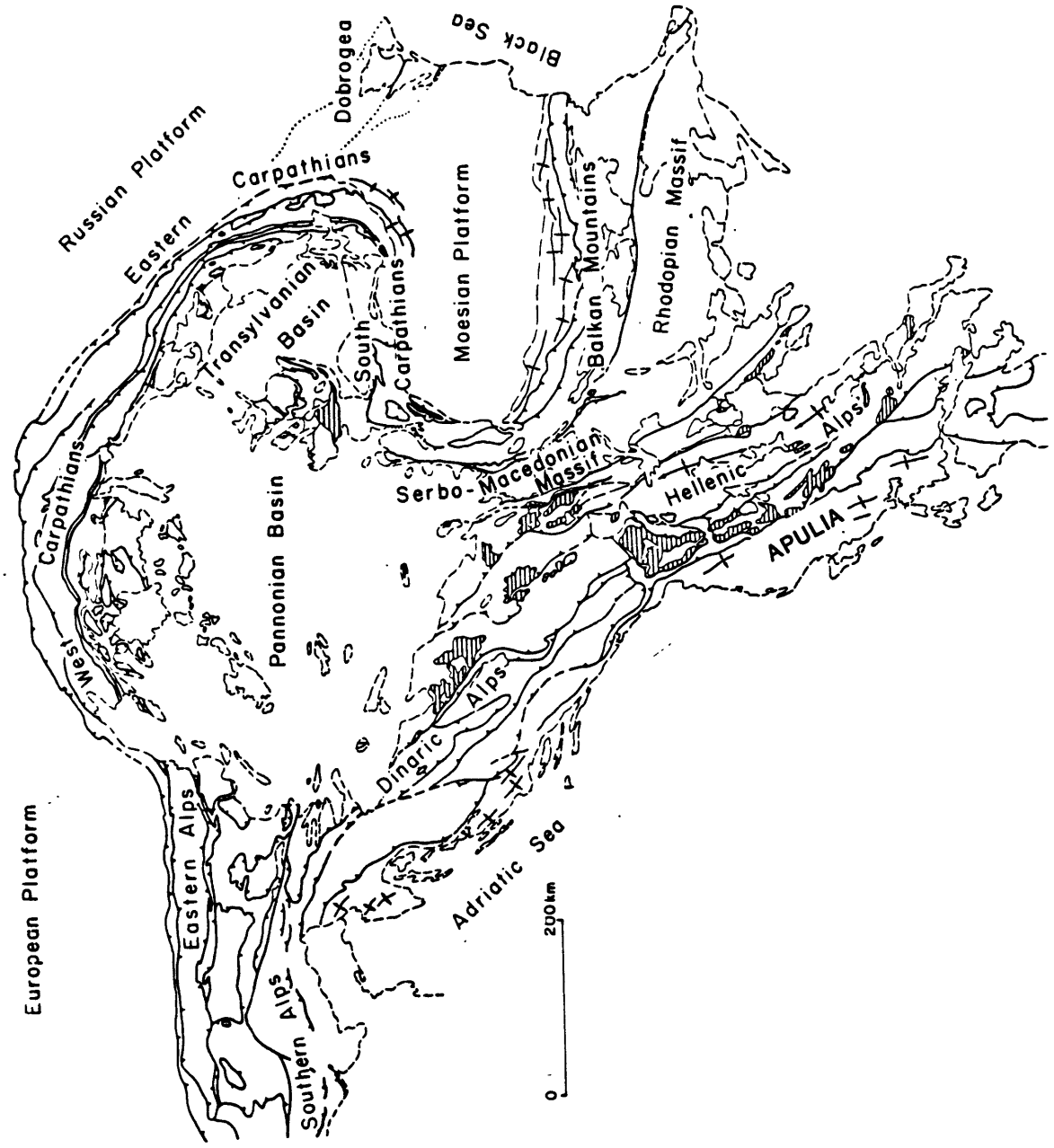

Figure 1.2 Tectonic and geologic setting of the Hellenides within the Eastern Alpine mountain system. From Royden et al (1984). Ruled pattern indicates ophiolites.

Eastern Greece consists dominantly of Precambrian to Paleozoic metamorphic rocks of the Rhodope and Serbo-Macedonian massifs (Fig. 1.2). These continental basement and cover rocks have been subjected to several periods of deformation and metamorphism, including Alpine tectonism, and were interpreted by Burchfiel (1980) as a microcontinental fragment that collided with the European plate during the Early Cretaceous. On the western boundary of the Rhodope fragment, the circum-Rhodope belt contains Triassic to Early Jurassic deep marine sediments, thick acid to intermediate metaigneous rocks, and ophiolites. The Vardar zone is dominated by ophiolitic rocks and extends northward into the inner part of the Dinarides in Yugoslavia (Fig. 1.1, 1.2). This zone is thought to be a main suture between the continental fragments of the Pelagonian zone to the west and Rhodope to the east, but the original size of the oceanic basin or basins is uncertain (compare Burchfiel, 1980; Jacobshagen et al, 1978, and Vergely, 1984). Calc-alkaline volcanic rocks of Late Jurassic age and Paleocene-Eocene age may be evidence of subduction of a sufficient length of ocean floor to generate a volcanic arc (a few hundred kms; for example see Mercier, 1968; Burchfiel, 1980).

Ophiolites that may have originated in the Vardar ocean basin (or basins) are now present >150 km to the west in the Subpelagonian zone (Fig. 1.1). There is considerable disagreement on whether all these ophiolites were derived by westward obduction from the Vardar zone or whether an additional oceanic basin, now represented only by Triassic-Maestrichtian pelagic sedimentary rocks of the Pindos zone (with no known basement), existed to the west of the Pelagonian zone (e.g. see Jacobshagen et al, 1978; Smith, 1971). Ophiolites from a Pindos ocean would have been thrust eastward onto the Pelagonian margin and westward onto the Apulian plate. In such a scenario the Pelagonian zone would have been a microcontinental fragment during the Jurassic and Cretaceous (e.g. Mountrakis, 1986).

The age of first emplacement of ophiolitic rocks is known to be latest Jurassic to Early Cretaceous (pre-Albian) in the Vardar zone because Tithonian sedimentary rocks contain ophiolitic debris and Albian limestone overlaps the thrusts in the Vardar zone (Mercier, 1968; Mercier et al, 1975). However, subsequent shortening has reactivated many of these thrust faults so that ophiolites rest on sedimentary rocks as young as Eocene in the Pindos zone.

The term "Pelagonian zone" is used here in the same sense as Aubouin (1959) and Mountrakis (1984) to include metamorphic rocks between the basal

thrust of the Vardar zone to the east and the Subpelagonian zone to the west (Fig. 1.1); this includes pre-Alpine rocks as well as their Mesozoic carbonate cover called "Pelagonian zone (s.s.)" by Celet and Ferrière (1978) and Papanikolaou (1981). The structural succession in the Olympos region of the Pelagonian zone consists of four principal structural units, including from top to bottom (Fig. 1.3): 1) dismembered ophiolitic rocks and coherent late Jurassic ophiolite suites; 2) deformed greenschist and blueschist facies Paleozoic continental basement gneisses and granites overlain by Permo-Triassic metasediments and metavolcanic rocks, and Triassic and Jurassic platform limestone and dolomite (Infrapierien, Pierien units, Fig. 1.3; Flambouron, Kastoria, and Almopia units of Papanikolaou, 1984a; Fig. 1.1); 3) blueschist-facies continental margin carbonate rocks, quartzo–feldspathic sediments, and basic to intermediate volcanic rocks (Ambelakia unit of Schmitt, 1983; Figs. 1.1,1.3); 4) parautochthonous Triassic to Eocene neritic carbonate rocks and Eocene flysch, metamorphosed at very low-grade. The lowest unit, the Olympos unit, is exposed in a tectonic window in the Mt. Olympos region, the area of this study (Figs. 1.1, 1.3). This unit consists of carbonate platform rocks and was originally thought to be part of the external Hellenides as it was apparently not deformed until post-middle Eocene time (Godfriaux, 1968; Fleury and Godfriaux, 1974). However, recent work by Schmitt (1983) has shown that Lower Jurassic to upper Lower Cretaceous rocks are missing from the sequence; thus the paleogeographic position of the Olympos platform is uncertain.

Blueschist facies metamorphic rocks of the Pelagonian zone extend from Mt. Olympos in the north through the Cyclades Islands and eastward into Turkey (in part denoted by the Ambelakia unit on Fig. 1.1). In general these rocks comprise marble, calcschist, metapelite, metatuff, and metabasalt (Durr et al, 1978; Blake et al, 1981; Papanikolaou, 1978,1984b). Ophiolitic melange is locally associated with the blueschists, however, the ophiolitic rocks are generally <u>not</u> blueschist-grade, and thus must have been emplaced after metamorphism. K-Ar and Rb-Sr ages of white mica and glaucophane from the blueschists range from Late Cretaceous (~80Ma) to late Oligocene (25-29Ma); (Blake et al, 1981; Ferriere, 1982).

Pelagonian zone rocks are thrust westward over deep-water sediments of the Pindos zone. Thrusting progressed westward from the internal Hellenides in Cretaceous-Eocene time with imbrication of non-metamorphic Triassic-Tertiary carbonate platform rocks of the external Hellenides during the Oligocene, Miocene, and Pliocene (Aubouin, 1959; Jacobshagen et al, 1978; Papanikolaou, 1984b).

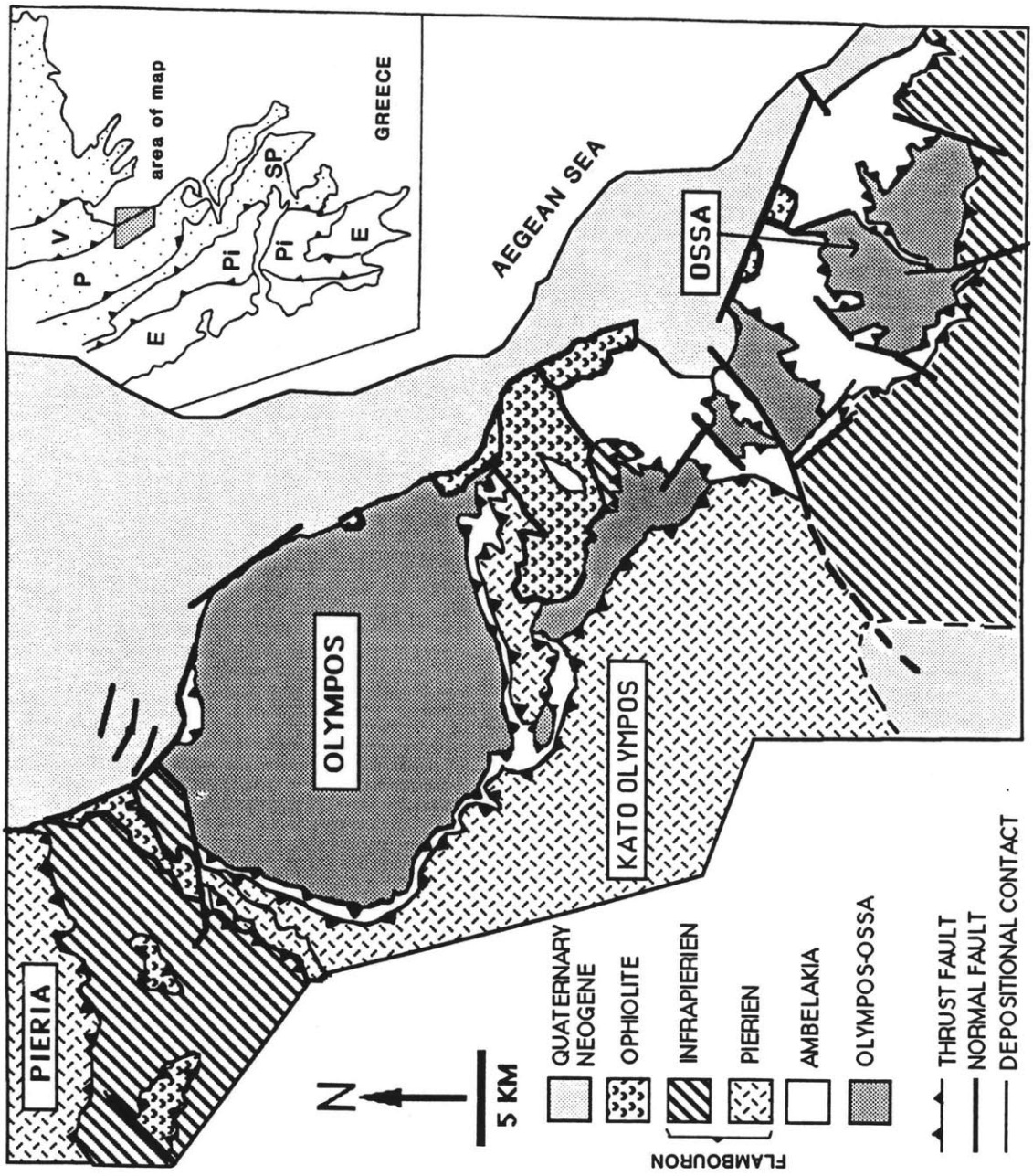

Figure 1.3 Generalized geologic map of the Mt. Olympos region, showing principal structural units. Inset: V: Vardar zone; P: Pelagonian zone; Pi: Pindos zone; Sp: SubPelagonian zone; E: External Hellenides. Internal Hellenides are indicated by dot pattern.

Part of the sedimentary cover of the external Hellenides was subducted and metamorphosed to blueschist facies during the Miocene (Arna unit, Fig. 1.1); this event has been interpreted as intra-continental subduction by Thiébault and Triboulet (1984). Concurrent with compressional deformation, extension and subsidence of the Mesohellenic trough occurred during the Oligocene and Miocene (Papanikolaou, 1988). Opening of the Aegean back-arc basin and formation of the present-day plate boundary system began at ~10-13 Ma (Angelier, 1978).

Previous work

After the initial discovery and description of the Olympos window (Godfriaux,1962, 1968), several workers have studied various aspects of the geology of this region. Godfriaux (1977), Dérycke and Godfriaux (1976) and Godfriaux and Pichon (1979) recognized the presence of blueschists in a thin thrust sheet between granitic gneisses and the carbonate rocks, and proposed SW-directed movement of the thrust sheets above the Olympos unit. In a detailed structural study of the western margin of the window, Barton (1975a,b; 1976) proposed that the metamorphic nappes moved to the NE over the carbonate rocks. He used the Rb-Sr whole-rock method on phyllonites from the thrust zone to determine the age of thrusting as Eocene. Nance (1981), Yarwood and Aftalion(1976), and Yarwood and Dixon (1979) studied the Infrapierien and Pierien rocks to the NW of Mt. Olympos and in the Pieria mountains (Fig. 1.3). They recognized Cretaceous metamorphic and deformational events in addition to the Tertiary events. Yarwood and Dixon (1979) documented southward displacement of Pierien over Infrapierien rocks, and postulated NE-directed thrusting of the imbricated basement stack over the Olympos unit, although without direct structural evidence. Schmitt (1983) conducted a detailed study of the stratigraphy of the Olympos unit. She discovered that the Olympos platform sequence, previously thought to contain a continuous sequence of Triassic to Eocene rocks, contained a hiatus, wherein uppermost Triassic to upper Lower Cretaceous rocks were missing, thus rendering the correlation with external Hellenide units less certain. Schmitt (1983) also studied structural and metamorphic features of the overlying metamorphic nappes in a large area around the Olympos window and proposed SE-directed movement of these nappes over the Olympos unit. The tectonostratigraphic nomenclature proposed in Schmitt (1983) is adopted here with some modifications (Chapter 2).

Because the Olympos unit is thought to be a window into the external Hellenides, the structural and metamorphic history of both the window rocks and the overlying nappes has important implications for the paleogeography and tectonic evolution of the Hellenides. The Cretaceous to mid-Tertiary deformational history recorded in the study area spans much of the Alpine orogeny in the Hellenides, and the lithologies present span the transition from the internal to the external part of the orogen. Noting that the workers cited above concluded three entirely different tectonic scenarios from studies of the same rocks, and in an attempt to resolve some of the controversy concerning the tectonic evolution of this important part of the Hellenides, this study focuses on the structural and metamorphic aspects of the Alpine deformation. In particular, I have examined the faults surrounding the Olympos window, and the detailed relation between metamorphic and deformational events in the different structural units. Radiometric dating of many of the events provides additional new constraints on the deformational and metamorphic evolution of the Mt. Olympos region.

Chapter Two: TECTONOSTRATIGRAPHY OF THE MT. OLYMPOS REGION

INTRODUCTION

The structural succession of the Pelagonian zone in the Olympos region consists of four principal fault-bounded structural units, including from bottom to top: 1) The Olympos unit comprises parautochthonous, very low-grade Triassic to Eocene neritic carbonate rocks and Eocene flysch. 2) The Ambelakia unit includes blueschist-facies continental margin carbonate rocks, quartzo–feldspathic sedimentary rocks, and basic to intermediate volcanic rocks. 3) The Pierien and Infrapierien units consist of imbricate thrust sheets of deformed greenschist and blueschist facies Paleozoic continental basement gneisses and granite that are overlain by Permo-Triassic metasediments and metavolcanic rocks and Triassic and Jurassic platform limestone and dolomite. 4) The ophiolite unit consists of mafic and ultramafic rocks in coherent thrust sheets and in serpentinite matrix melange that also contains blocks of marble and mica schist . These units are overlain by Neogene and Quaternary conglomerate on the flanks of the range. Figure 2.1 is a generalized geologic map showing the location of all the units; Figure 2.2 is a composite tectonostratigraphic section; and Figure 2.3 compares the subdivisions and nomenclature used in this study with that of other workers in this region.

The lithologies of each unit are described in detail below. Because all of the units except the lowest are complexly deformed and metamorphosed, the deformational and metamorphic characteristics are as much distinguishing features of each unit as are the lithologic types. Therefore, a brief description of the metamorphic assemblages and micro-and mesostructures is presented here, while details of the petrologic and structural evolution are given in subsequent chapters. The tectonostratigraphy will be discussed in terms of the paleogeographic setting of the units and their relative positions prior to Alpine deformation.

OLYMPOS UNIT

Introduction

The Olympos unit consists of Triassic to Eocene platform carbonate rocks and Eocene flysch that constitute the main massif of Mt. Olympos. Godfriaux (1968) was the first to study these rocks in detail. He established that the limestone sequence extended from Norien to Eocene, and that the overlying crystalline rocks were in thrust fault contact with the Olympos unit. Further work by Schmitt (1981a,b 1982, 1983) refined the stratigraphy of the carbonate rocks and flysch. The age designations on Plate 1 are based on the stratigraphy of Schmitt (1983).

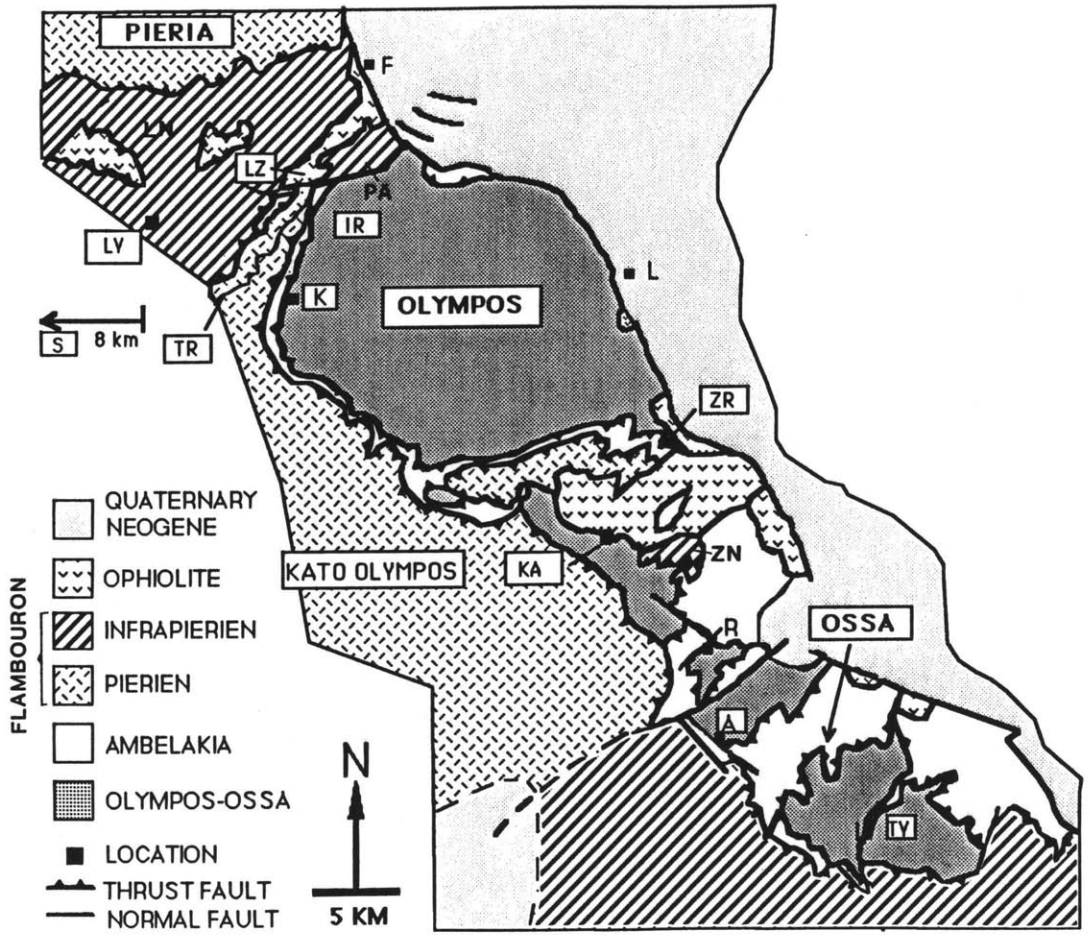

Figure 2.1. Generalized geologic map of the Olympos region showing localities mentioned in the text. Abbreviations: A=Ambelakia; F=Fotina; IR=Itamos river; K=Kokkinopilos; KA=Kallipevki; L=Litochoro; LV=Livadi village; LN=Livadi nappe LZ=Lizadiko ridge; PA=Paleambela nappe; R=Rapsani; S=Sarandoporou; TR=Trohalos ridge; TV=Tesseres Vrises; ZN=Ziliana nappe; ZR=Ziliana river.

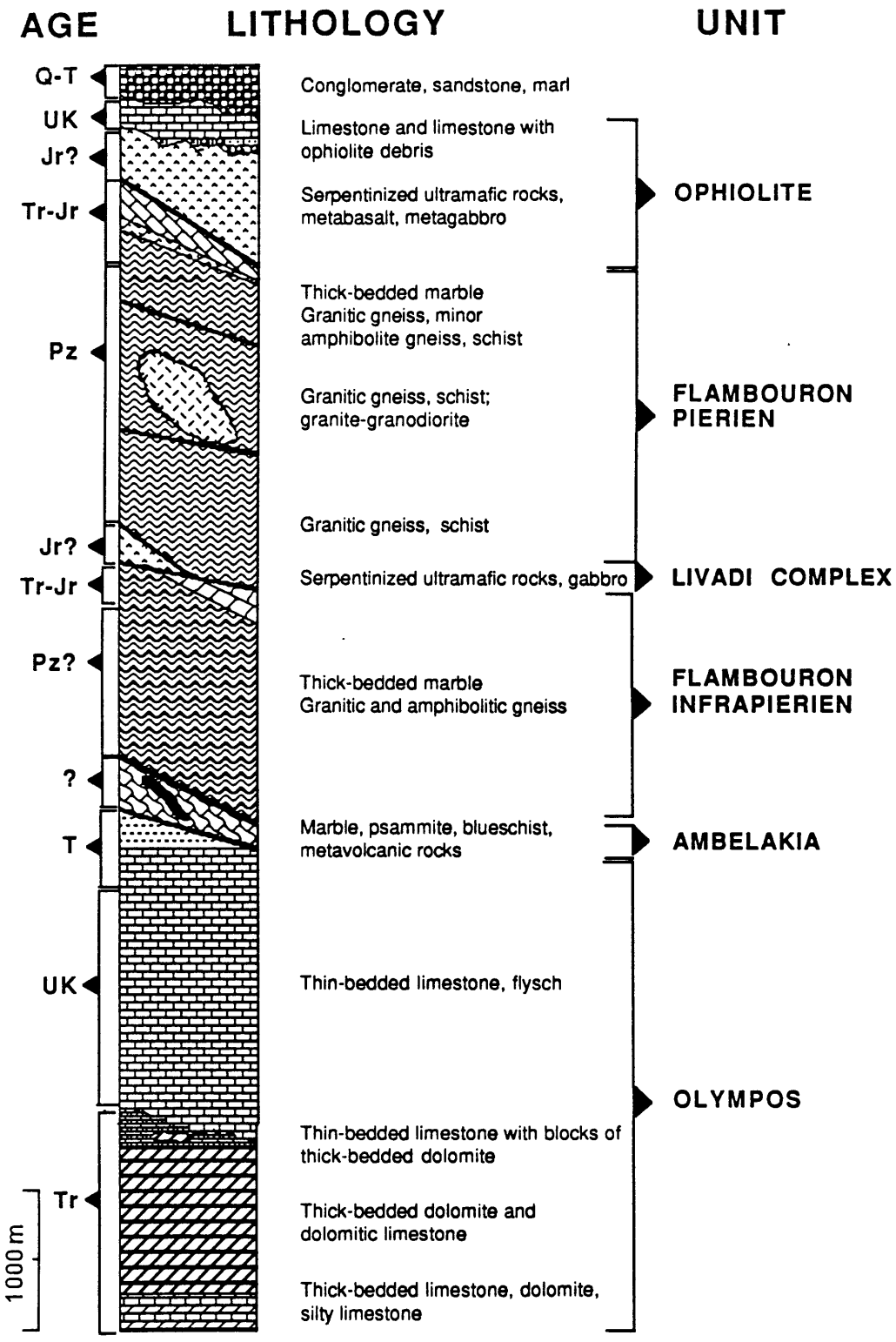

Figure 2. 2. Tectonostratigraphic column for the Olympos region. As thicknesses are variable due to deformation, all thicknesses are approximate. Heavy lines indicate fault contacts between units.

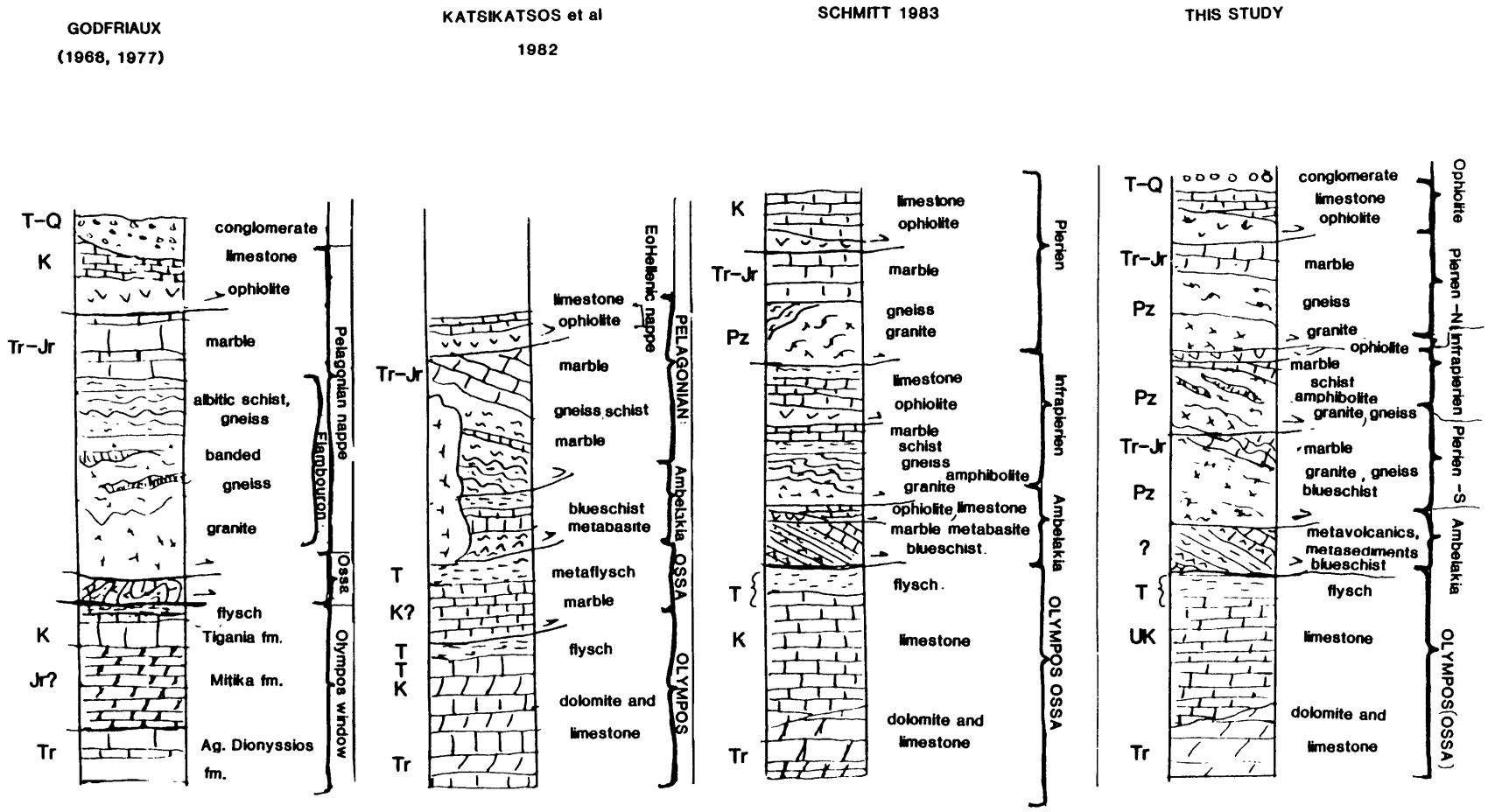

Figure 2.3. Comparison of nomenclature for tectonostratigraphic units in the Olympos region.

Carbonate rocks

As described by Schmitt, (1983), the Triassic rocks of the Olympos unit crop out in the eastern portion of the Olympos massif. The oldest exposed rocks consist of 250-270 meters of black to dark grey thick-bedded limestone, dolomite, silty limestone, and limestone with argillaceous intercalations up to 30 cm thick. These rocks are dated as Anisian and Ladinian by conodonts (Schmitt, 1983). Upper Triassic rocks comprise a very thick (~1150-1200 meters) section of dark grey thick-bedded dolomite and dolomitic limestone that are dated as Carnian and Norien by ammonites, gastropods, conodonts, and foraminifera (Godfriaux, 1968; Schmitt, 1983). The Upper Triassic strata are overlain by an undated sequence up to 230 meters thick of thin-bedded limestone containing slump structures and large blocks of thick-bedded dolomite apparently derived from the Upper Triassic rocks below. This sequence is overlain unconformably by Cretaceous to Eocene limestone.

Although Godfriaux (1968) interpreted the Olympos carbonate sequence to be continuous from Triassic to Eocene, more detailed work by Schmitt (1983) revealed an angular unconformity between the Upper Triassic rocks and overlying upper Lower Cretaceous rocks. While the rocks for 200 m above the unconformity are not precisely dated, they exhibit angular discordance with the underlying sequence and appear to be overlain conformably by the Cretaceous to Eocene carbonate sequence.

The Cretaceous to Eocene rocks in the Olympos area consist of thin- to thick-bedded calcareous turbidites containing slump structures, load structures, cross bedding, graded bedding, and reworked fossils and fossil fragments (Godfriaux, 1968; Schmitt, 1983). Due to structural complexity, it is difficult to estimate the thickness; however the complete sequence is apparently >2000 m thick (Schmitt, 1983). The rocks are dominantly light to medium grey limestone with local siliceous or dolomitic layers and lenses. Schmitt (1983) described some facies containing hard-ground and other evidence of emergence, and interpreted the alternation of turbiditic facies with shallower-water facies as evidence that Cretaceous to Eocene sedimentation occurred on the border of an unstable platform. Although fossils are rare, the sequence has been dated as Albian-Cenomanian at the base and Ypresian-Lutetian at the top by the presence of foraminifera (Godfriaux, 1968). Rudists of indeterminate age are also present (Schmitt, 1983). Intercalations of argillite, calcareous argillite, feldspathic greywacke, and calcareous sandstone up to 2 m thick are present at the top of the

limestone sequence where the contact is gradational over ~10-15 m into the Eocene flysch.

Schmitt (1983) correlated the undated sequence of carbonate rocks that crop out in the Kato Olympos and Ossa areas (Plate 1; Figure 2.1) with the Cretaceous-Eocene sequence of Mt. Olympos. The similarity of facies and the presence of depositional contacts with the overlying Paleocene-Eocene flysch, dated in Ossa (Dérycke and Godfriaux, 1978), supports this interpretation.

Flysch

The Eocene flysch consists of interbedded feldspathic greywacke and argillite which crop out predominantly in the Itamos Valley on the northern flank of Mt. Olympos (Plate 1). The flysch also crops out in a thin band on the western and southern flanks just below the thrust fault which bounds the top of the Olympos unit, and in tightly folded bands and fault slivers in Kato Olympos and Ossa.

The sandstone and siltstone weather yellow to medium brown and the argillite weathers black to dark brown. In the coarse- to medium-grained sandstones, beds are commonly 5-10 cm thick; however a large part of the unit consists of siltstone and fine- to medium-grained sandstone interlayered with 1-5 cm-thick layers of argillite (Fig. 2.4). In some areas, the poorly sorted greywacke is interbedded with moderately well-sorted coarse-grained arkosic arenite. Local conglomeratic beds are also present, containing pebbles up to 1 cm in diameter. Lenses and beds of limestone and calcareous siltstone up to 3-5 m thick are locally present. Detrital materials include coarse-grained quartz, plagioclase, and K-feldspar clasts, muscovite grains up to 2 mm long, hornblende, sphene, zircon, epidote, garnet, and a variety of lithic fragments. The lithic fragments are generally altered to chlorite-phengite-pumpellyite, but locally they can be identified as mafic volcanic rock, mafic and felsic plutonic rock, quartzofeldspathic schist and gneiss, chlorite-epidote schist, and amphibolite. Sub-rounded to sub-angular grains and pebbles are cemented by both quartz and calcite cement, but the matrix is more commonly clay-rich, recrystallized to phyllite. In the Ossa region the flysch is similar in composition, but appears to contain more abundant calcareous sandstone and siltstone, limestone with conglomeratic intervals, and several coarse pebble conglomerate layers. The clastic rocks of the flysch have not been directly dated in the Olympos region, however, limestone horizons at the base of the flysch contain middle Eocene nummulites (Godfriaux, 1968; Schmitt, 1983). Derycke and

Godfriaux (1978) reported the presence of Paleocene-Eocene microfossils in presumably correlative flysch of the Ossa region.

The thickness of the flysch is unknown because of the presence of several fold phases. The contact with the overlying Ambelakia unit is everywhere a fault and the structural thickness varies from <50 m to >1000 m. On the northern, western, and southern flanks of Mt. Olympos, in Kato Olympos, and in Ossa the contact is a tightly folded thrust fault; however, the contact has also locally been cut by younger normal faults.

The depositional setting of the flysch is indicated by 1) its presence on top of the shallow-water carbonate platform, 2) the abundance of quartzofeldspathic debris and lithic fragments derived from a plutonic and metamorphic area and 3) its generally fine-grained nature, with interbedded sandstone and argillite. Although most sedimentary structures have been obliterated by metamorphism and deformation, the rhythmic alternation of sandy and shaley layers and local conglomeratic and calcareous beds suggests turbidite deposition on a foundered carbonate platform.

Metamorphism and Deformation

The carbonate rocks of the Olympos unit are recrystallized, although sedimentary structures and fossils are generally well preserved. Near thrust faults and within folds the limestone and dolomite are recrystallized to fine- to medium-grained marble, occasionally containing micaceous laminae, and the calcareous sandstone and argillite contain a brown-weathering chlorite + phengite foliation. A well-developed mylonitic foliation and lineation is present near the thrust fault contact with the Ambelakia and Pierien units.

The flysch contains a moderately well-developed foliation consisting of quartz + albite + phengite + chlorite ± pumpellyite in the sandstones and calcite + phengite + chlorite + quartz + albite in the calcareous siltstones. We have also identified rare sodic amphibole (crossite) present as subhedral to euhedral grains (Chapter 5). Schmitt (1983) has also reported the presence of lawsonite, generally occurring within pebbles in the flysch.

The metamorphic assemblage of the Ossa flysch is similar to that in the Olympos region and consists of quartz + albite + phengite + chlorite ± lawsonite. Two metamorphic fabrics have been identified, both apparently are formed by phengite and chlorite.

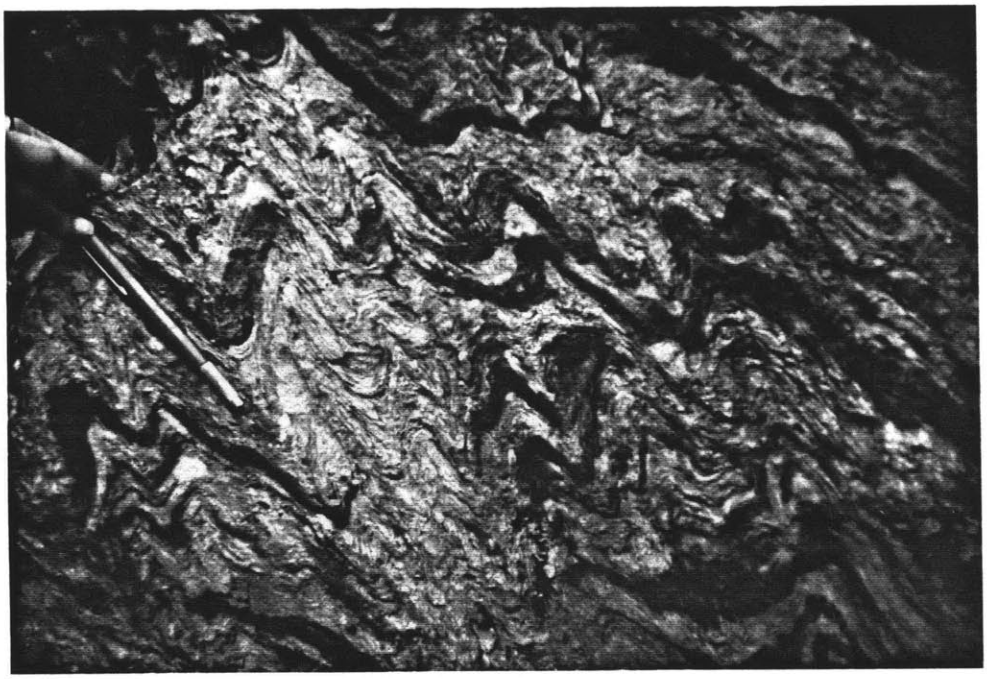

Figure 2.4 Photograph of outcrop of Eocene flysch of the Olympos unit, showing thinly-intercalated argillite (dark) and quartzofeldspathic siltstone and sandstone (light) layers.

AMBELAKIA UNIT

Introduction

The Ambelakia unit consists of a wide variety of metasedimentary and metavolcanic rocks that are multiply deformed and metamorphosed, and have no known basement. The definition of the Ambelakia unit in the Olympos-Ossa region has been controversial, as different authors have used different criteria to include or exclude rocks from this unit. Because many of the contacts between different lithologies are apparently tectonic, we have defined the Ambelakia unit on the basis of a combination of metamorphic and structural criteria as well as lithologic type. We have included blueschist-facies metavolcanic and metasedimentary rocks, but have excluded rocks that are not blueschist grade where they are in fault contact. Thus, we exclude the Ossa flysch (included by Godfriaux, 1977; Godfriaux and Pichon, 1979; Katsikatsos et al, 1982), and serpentinite and associated mafic volcanic and plutonic rocks (included by Blake et al, 1981; Schmitt, 1983; Vergely, 1984) because, even though similar bulk compositions may exist in the Ambelakia unit, the excluded rocks do not show the same blueschist-facies mineral assemblages and appear to have experienced a different structural and metamorphic history.

Godfriaux and Pichon (1979), and Vergely, (1984) combined the carbonate rocks and overlying lawsonite-bearing flysch of Ossa with higher-grade blueschist facies metabasalts and metasedimentary rocks in a unit called the Ossa unit which was thought to lie structurally above the Olympos unit. The distinction of the Ambelakia and Ossa units depends in part on conflicting interpretations of a sequence of rocks in the Tesseres Vrises region of Ossa. This sequence includes metabasalts, tuffaceous limestone, calcareous tuff, thin-bedded limestone and rare chert that are apparently interlayered with thick-bedded limestone that underlies the main part of Ossa Mt. It is unclear whether these rocks are a sliver of the Ambelakia unit, in fault contact, or whether they are in depositional contact and thus an integral part of the Ossa carbonate sequence. The metabasalts clearly metamorphosed the underlying thin-bedded limestone, and tuffs are depositionally interbedded with overlying limestone, however, Schmitt (1983) has mapped a folded thrust fault between two limestone units both above and below the basalt sequence. Because of the relatively poor exposure in the area and the small scale of Schmitt's map, we have been unable to confirm a fault contact. However, the metabasaltic rocks and associated metasediments throughout the Ossa region seem to be higher-grade and more strongly deformed than the Ossa carbonates

and flysch, even where bulk compositions are apparently similar. Thus, we have adopted Schmitt's definition, and included the carbonates and flysch in a "parautochthonous" unit, the Olympos-Ossa unit, (here termed the Olympos unit) and included the basalts and schistose metasediments in the Ambelakia unit.

The definition used here differs from that of other workers (Vergely, 1984; Katsikatsos et al, 1982; Migiros 1985; Papanikolaou, 1984a) who included *all* rocks containing blueschist-facies assemblages, regardless of protolith type, in the Ambelakia unit (or Kriovrissi-Kallipevki unit of Migiros, 1985). We exclude the blueschist-grade granitic to granodioritic gneiss of Kato Olympos which is clearly in fault contact with underlying metasedimentary rocks and belongs with the Pierien unit. We have also excluded quartzofeldspathic rocks that have only greenschist-facies assemblages and are in fault contact with blueschist facies rocks. Other greenschists that are interlayered on a small scale with blueschists are included; these rocks do not contain blueschist-facies assemblages because of their bulk composition (e.g. Brown 1974). Table 2.1 and Figure 2.3 present a summary of the different interpretations of the tectonostratigraphy of the Olympos region. Because most of the individual lithologies are too thin and discontinuous to depict on Plate 1, we have divided the Ambelakia unit into three lithologic groups: arkosic and calcareous metasandstone and schist, meta-argillite, and metagreywacke (acs on Plate 1); banded marbles, minor calcareous schist, and dolomitic breccia (am on Plate 1); and mica schists, metatuffs, and metabasalts (as on Plate 1). Each lithology is described in more detail below.

The protolith age of most of the rocks in the Ambelakia unit is unknown, and the tectonic complexity in the study area prevents estimation of the original thickness. Schmitt (1981a) reported Early Cretaceous to Cenomanian fossils from a banded marble of the Ambelakia unit on the northern flank of Mt. Olympos. $^{40}Ar/^{39}Ar$ data presented by Schermer et al, (in press) indicate that some of the schists could be Cretaceous or older.

"Type section" description

Near the town of Ambelakia, in the Ossa mountains, the Ambelakia unit is exposed as a series of interlayered marble, schist, and metabasaltic rocks. Although the rocks are complexly folded and imbricated, the marbles, calcschists, and arkosic greywackes appear to represent the lower part of the sequence, whereas interlayered metavolcanic flows and tuffs, tuffaceous marble, and quartzofeldspathic gneisses and schists appear to represent the upper part.

Table 2.1

Comparison of subdivision of high P/low T rocks in the Olympos region

Study	Unit name	Lithologies			
		Ossa lmst, flysch	Metabasites, schist, marble	Granitic rocks, SW Olympos	Oph.
Godfriaux 1977		Ossa	X	X	X
Katsikat-sos, et al, 1982	Ossa Ambelakia	X	X	X	X
Schmitt, 1983	Olymp/Ossa Ambelakia Pierien	X	X	X	X
Vergely, 1984	Ossa Ambelakia	X	X		X
Papani-kolaou, 1984a	Ambelakia		X	X	X
Katsikat-sos, Migir-os, 1987	Olymp/Ossa Meta-ophiolite	X Ambelakia		X	X X
This study	 Ambelakia Pierien	Olymp/Ossa	X X	X	

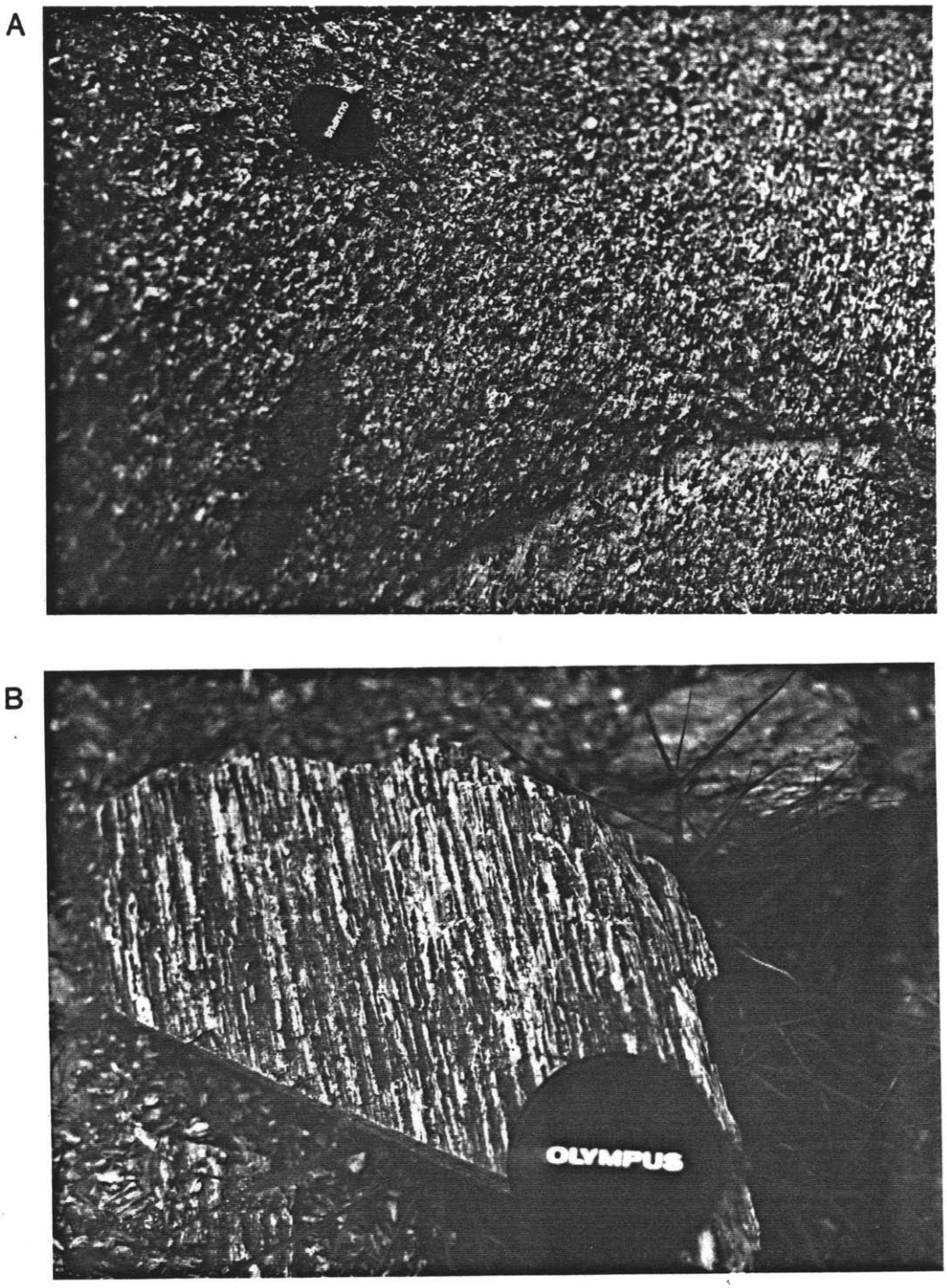

Figure 2.5 Photographs of granitic to granodioritic rocks from the southern margin of Mt. Olympos. A shows an outcrop of slightly foliated granodiorite from ~3 km structurally above the thrust at the base of the Pierien unit (Sparmou thrust). The dark minerals are biotite and hornblende. Note the rounded mafic inclusion, fairly common in the granitic basement at high structural levels, is preserved here. B show a sample of the same lithology from ~1 km above the Sparmou thrust; this sample is strongly foliated and lineated, although the mineralogy is essentially unchanged.

Metasediments

Metapelites and metapsammites

Yellow-weathering feldspathic greywacke and phyllite that strongly resemble the Paleocene-Eocene flysch are observed at the base of the calc-schists and marbles described below. Similar rocks occur as layers 0.3-1 m thick within the calc-schist and marble sequence. By themselves, these rocks are difficult to distinguish from the flysch. Conglomerate layers are present, containing quartz, feldspar and limestone pebbles 2-4 cm in diameter. Boudins of limestone and coarse feldspathic sandstone are enclosed in a phyllitic matrix. The phyllitic horizons contain a foliation defined by chlorite + phengite + pumpellyite + lawsonite ± glaucophane ± graphite. Locally, gradational contacts between the metapsammites and marbles are visible.

Marbles and calc-schists

Carbonate rocks occur as light grey to medium blue-grey well-foliated marble, with local interlayers of white chert and cream-colored dolomitic layers and boudins 0.3-5 cm thick. The marbles commonly crop out as resistant ledges composed of platy layers 1-10 cm thick. Green and greenish-blue micaceous laminae are present near the transitions to interbedded clastic rocks. The cherty, dolomitic, and chlorite-rich layers contain at least two generations of isoclinal folds and associated foliations that are considered a characteristic feature which allows distinction of marbles of the Ambelakia unit from those of the Olympos unit. Calcareous schists are silvery blue- to black-weathering phyllites and schists, containing abundant chlorite, phengite, and common graphite. Quartz, albite, crossite, sphene, and rare lawsonite(?) are also present in the calc-schists and within the phyllitic laminae in marbles.

Pink dolomitic breccia

A distinctive pink to cream-colored resistant, knobby-weathering dolomitic breccia is locally present intercalated within the metasedimentary and metavolcanic rocks of the Ambelakia unit. This rock is pink on fresh surface, and contains angular clasts of dolomite and red chert ranging from a few millimeters to a few centimeters in size in a dolomitic matrix. Porphyroclasts of feldspar and quartz are present. Everywhere I have seen the contact relationships (3 areas), the dolomite appears to be in tectonic contact parallel to the foliation in the enclosing schists and is well-foliated with phengite and epidote aligned in the foliation plane. However Schmitt (1983) interpreted the dolomite as having been deposited disconformably on top of ophiolitic rocks thrust over the Ambelakia schists,

although she admitted that this interpretation was compiled from several scattered outcrops of serpentinite, schist, and dolomite.

Mica schists

Green, blue, and silver-colored mica schists and gneisses are a common component of the Ambelakia unit. These rocks have no relict sedimentary or volcanic structures, thus their protolith is uncertain. Nevertheless, a wide range of relict minerals such as plagioclase, augite, hornblende, muscovite, K-feldspar, sphene, and zircon seem to indicate a mixed volcanic and terrigenous source area. In some schists the relict material is entirely volcanogenic; these may have been tuffs or volcaniclastic sediments prior to metamorphism. Marble occurs locally as boudins within the schists, and calcareous schist, feldspathic metasandstone and mica-chlorite schists are interlayered on a scale of 10 cm to a few meters; thus some of the schists are likely to have a sedimentary protolith.

Grain size in the schists ranges from fine-grained phyllite to coarse schist and banded gneiss, in which quartzofeldspathic and mafic layering alternate on the scale of 1-2 cm. In medium- to coarse-grained mica schists relict euhedral augites up to 5 mm long occur as augen. Two metamorphic foliations are present. The earlier fabric appears to consist of quartz + albite + phengite + epidote ± chlorite ± actinolite. A later fabric is defined by quartz + albite + phengite + chlorite + pumpellyite + glaucophane ± actinolite ± lawsonite. The latest metamorphic assemblage consists of poorly oriented to unoriented chlorite + pumpellyite ± stilpnomelane ± prehnite is commonly present. Sphene, apatite, rutile, calcite, and Fe-oxides are ubiquitous accessory phases.

Metavolcanic rocks

Metavolcanic rocks are relatively rare in the Ambelakia unit as a whole, but locally, as in the Tesseres Vrises region, comprise as much as 50% of the sequence. In this region, ~30-40 m of altered basaltic to andesitic lavas and tuffaceous schists are interbedded with ~50-60 m of thin-to medium-bedded limestone, tuffaceous limestone, and minor chert and calcareous phyllite. Near the village of Ambelakia, a group of lava flows ~10 m thick occurs interbedded with calc-schist and mica schist containing coarse relict augite grains.

Relict phenocrysts in the metavolcanic rocks include euhedral to subhedral plagioclase laths, augite, and hornblende, and rare altered and fractured olivine. Plagioclase grains are commonly recrystallized to albite and lawsonite. Augite grains are surrounded by sodic amphibole, actinolite, and chlorite. A well-

developed foliation is defined by albite + epidote + actinolite + chlorite + phengite + glaucophane. This foliation is folded and overgrown by a second foliation composed of chlorite + phengite + glaucophane ± lawsonite. However, textural relations are very complex, and consistent first- and second-phase metamorphic assemblages are difficult to determine. In several cases however, glaucophane clearly grew after actinolite and epidote. Late, unoriented pumpellyite, chlorite ± prehnite ± stilpnomelane fills cracks and vugs and cross-cut the earlier metamorphic and mylonitic fabric. Details of the petrographic and petrologic relations of the metabasites of the Ambelakia unit are discussed elsewhere (Chapter 5).

Ambelakia rocks in other parts of Olympos-Ossa region

In the heavily forested region on the eastern flank of Ossa, Schmitt(1983) and Katsikatsos and Migiros (1987) have mapped a large area underlain by Ambelakia unit lithologies. While I have only done reconnaissance mapping in that area, most of the unit seems to be composed of quartzofeldspathic gneisses containing quartz + K-feldspar + albite + phengite ± chlorite, associated with minor metabasites.

In the Kato Olympos region and on the western and southern flanks of Mt. Olympos, metabasalts and glaucophane-chlorite-phengite schists are rare. On the margins of the Olympos window, the lower marble-calcschist-metagraywacke part of the Ambelakia unit is the only portion exposed in the thin (<200 m) tightly folded and imbricated sequence. It is important to note, however, that a characteristic structural sequence ~150 m thick composed of 1) metasandstone and calcareous sandstone and phyllite; 2) strongly foliated and lineated light grey marble and marble with thin banded chert; and 3) marble with blue-green chlorite-phengite laminae interbedded with thin layers of calcareous crossite-chlorite-phengite schist and cherty marble can be followed in the hanging wall of the Olympos thrust from north of Kokkinopilos southward and eastward around the Olympos window to to the Ziliana river (Fig. 2.1; Plate 1). This association of glaucophane-bearing metasedimentary rocks with marble is characteristic of the Ambelakia unit, although these rocks have been variously mapped as Olympos unit (Gonnoi sheet, Migiros, 1985; Godfriaux 1968), Ambelakia unit (Kondariotissa sheet, Latsoudas, 1985); or both (Schmitt, 1983). A thin (<20 m) well-developed mylonite zone is present at the base of this sequence that is interpreted to be related to the underlying Olympos thrust although all rocks of the Ambelakia unit in this area could be considered as protomylonites. Another, thicker (>50-100 m in Pierien rocks) mylonite zone is

present at the overlying thrust contact against Pierien gneisses, although the mylonitic fabrics are most evident in the strongly sheared gneisses.

FLAMBOURON CONTINENTAL BASEMENT UNITS

Introduction and previous work

Schists and gneisses belonging to the Paleozoic Pelagonian basement are exposed in thrust sheets throughout the Olympos region. Originally designated as one unit, the "Flambouron gneiss" or "Pelagonian allochthon" by Godfriaux (1968), subsequent workers (Nance, 1977. 1981; Yarwood, 1978; Schmitt, 1983) have refined the structural and stratigraphic details. Papanikolaou (1984a) separated the cover sequence of marbles and overthrust ophiolitic rocks (Almopia unit) from the basement rocks (Flambouron unit). We adopt the terminology of Schmitt (1983), who recognized that the basement and cover sequences could be divided into at least two distinct associations: 1) a fairly homogenous granitic to granodioritic gneiss overlain by a thin sequence of metaclastic rocks and marbles, the Pierien unit, after the excellent outcrops in the Pieria mountains north of Olympos; and 2) minor granitic rocks overlain by interlayered metavolcanic and metasedimentary rocks, termed the Infrapierien unit. Nevertheless, we retain the name "Flambouron" as a group heading to indicate that these two units are similar in many ways and probably represent different parts of the same continental fragment. In the Pieria mountains, Pierien rocks are thrust above Infrapierien rocks, but further south, Infrapierien rocks are found both above and below Pierien rocks (Fig. 2.1). However, Schmitt (1983) considers the Infrapierien unit to always underlie Pierien thrust sheets.

Pierien unit

Introduction

The Pierien unit is divided into three lithologic associations: 1) Pre?-Carboniferous gneisses and Carboniferous granitic to granodioritic rocks; 2) mica schists, feldspar augen schists, and minor metavolcanic rocks; and 3) marble.

Pre?Carboniferous gneisses, granites and granodiorites

The dominant rock type in the Pierien unit is white-to light brown-weathering, coarse- to medium-grained granitic augen gneiss. Feldspar augen average ~1 cm in diameter, but range from ~2 mm to >2 cm in diameter. The gneisses are composed of quartz + orthoclase + albite + phengite or muscovite, with minor epidote, chlorite, sphene, allanite, and zircon. Rare garnets with abundant

inclusions provide evidence of an early metamorphic history, however, a later foliation and subsequent mylonitic fabric have essentially obliterated the earlier fabric and mineral assemblage. Weakly-foliated coarse-grained biotite granite and biotite-hornblende granodiorite and fine-grained aplitic dikes occur within the Pierien basement. Some of the quartzofeldspathic gneisses may be older than the intrusive rocks, as contacts locally appear transitional and irregular. However, subsequent deformation and metamorphism has produced a relatively uniform granitic gneiss so it is difficult to know whether the poorly-foliated rocks are simply less-strained equivalents of the gneisses, or whether the granite intruded a previously-foliated metamorphic complex. Variably-foliated rocks become more strongly mylonitic and contain a well-developed foliation and lineation toward the thrust faults above the Infrapierien and Ambelakia units (Figure 2.5). Quartz is dynamically recrystallized; feldspars are more brittley deformed and are present as augen with recrystallized tails. Mylonitization is intense within ~100m of the basal thrust fault, but structurally higher rocks are variably mylonitized, with high strain zones a few meters thick throughout most of the crystalline sheet.

On Plate 1 the granitic and gneissic rocks have been divided into three sub-units: relatively weakly-foliated granite and granodiorite (fgr); granitic gneiss (fgg) and granitic gneiss with minor amphibolite gneiss intercalations (fg1).

The structurally lowest part of the Pierien unit in the Kato Olympos region merits special attention because of its unusual mineral assemblage. Apparently derived from an alkaline granitic protolith, these rocks consist of quartz + K-feldspar + albite + phengite + riebeckite + acmite ± epidote ± allanite with coarse K-feldspar augen. Schists which may represent metasedimentary inclusions within the granitic rocks contain the assemblage quartz + albite + phengite + epidote + winchite-barroisite. While the assemblage riebeckite + acmite is not diagnostic of P-T conditions, the extremely high Si content of the phengite indicates minimum pressures of 6-8 kb (Massone and Schreyer, 1987; Chapter 5).

Papanikolaou and Stojanov (1983) have reported possible Precambrian marble intercalations within the Pierien basement in more northerly parts of the Pelagonian zone. In the Olympos region, thin marbles intercalated within the gneisses are only observed near the transition to the overlying thick-bedded Triassic-Jurassic marbles.

A

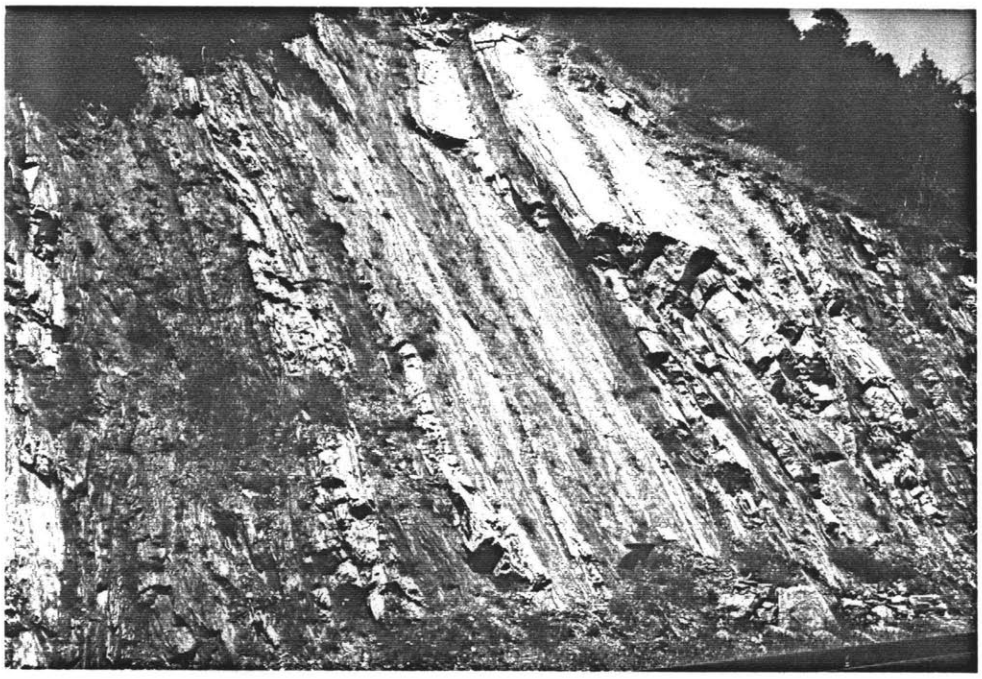

B

Figure 2.6 Photograph of alternating quartzofeldspathic and amphibolitic layers in the Infrapierien gneiss. A: Thin alternations (centimeters thick) occur within a larger-scale alternation of the two compositions, forming the intersection lineation on the outcrop surface. Note clipboard in lower center of photo for scale. B: Meter-scale alternation of amphibolite schist and granitic gneiss. Hammer handle in lower left of photo is 30 cm long.

Overlying metasedimentary rocks

Mica schists, augen schists, amphibolites

A thin (<300 m) sequence of metasedimentary and metavolcanic rocks disconformably overlies the basement orthogneisses. The sequence is present at Trohalos ridge NW of Mt. Olympos, in Kato Olympos ~10 km west of Rapsani, and in the Sarandoporou region (Figure 2.1; Plate 1). At Trohalos and Kato Olympos the granitic gneiss, with minor amphibolitic gneiss intercalations, is overlain by <50 m of thinly interbedded chlorite schist, crossite-phengite schist, plagioclase augen-amphibolite schist, and minor calcareous mica schist.

In the area north of Sarandoporou foliated hornblende-biotite granite is apparently overlain disconformably by 100-600 m of chlorite schist, pelitic schist and phyllite, quartzite, and graphitic schist. The lowest part of the sequence consists of grey-green-weathering chlorite schists composed of plagioclase + quartz + chlorite + muscovite, with minor zoisite, tourmaline, and sphene. These are overlain by an alternating sequence of metapelite, quartzite, and graphitic schist.

Metapelites consist of strongly weathered brown and rusty schists and phyllites that contain quartz + biotite + muscovite + plagioclase + garnet + magnetite. Tourmaline is a minor but ubiquitous accessory phase. Biotite is commonly altered to chlorite, and garnet appears to have several stages of growth, displaying complicated zoning and inclusion geometries.

Quartzites weather white to silver and contain varying amounts of muscovite and magnetite. Magnetite commonly appears as coarse-grained porphyroblasts up to 1 cm in diameter and is apparently flattened in the foliation planes. Graphitic schist and phyllite contain graphite and quartz; other phases which may be present are too fine-grained to identify. The graphitic schist is more abundant upward near the contact with overlying Triassic-Jurassic marbles and locally, a transitional contact is present between the schists and overlying marbles. The contact with the underlying gneisses and schists is commonly tectonic, however, and results in the variable thicknesses of exposed metasedimentary rocks and marbles.

The metasedimentary and metavolcanic sequence seems to correlate with Lower-Middle Triassic rocks described by Papanikolaou and Zambetakis-Lekkas (1980) from the northwestern part of the Pelagonian zone, and by Mountrakis et al (1983) from along the western margin of the Pelagonian zone. However, the distinctive Ammonitico Rosso facies limestone described by these workers is not present in the Sarandoporou area.

The contact of the metasedimentary and metavolcanic sequence with the overlying marbles is commonly sheared. Nevertheless, in many locations throughout the study area, the metasedimentary sequence is more calcareous and contains marble lenses towards the top, and the contact appears gradational over ~5 m.

Marbles

The highest part of the sedimentary cover of the Pierien basement consists of white to light grey thick-bedded marble presumed to be Triassic-Jurassic in age. Fossils within the marbles have been locally dated in the Sarandoporou area and in Kato Olympos by Katsikatsos et al (1982), and Katsikatsos and Migiros (1987) as Ladinian and Carnian, however most of the outcrops in the Olympos region have not yielded fossils. The upper age limit for the marbles is by analogy with the northern Pelagonian zone, where Upper Jurassic fossils have been found beneath the overthrust ophiolite nappe.

Geochronology

$^{40}Ar/^{39}Ar$ data reported by Schermer et al (in press) are summarized briefly here; the reader is referred to that paper for details.

The granitic intrusions into the Pelagonian basement in the High Pieria region have been dated using U-Pb on zircons at 302±5 Ma (Yarwood and Aftalion 1976). $^{40}Ar/^{39}Ar$ dates of 293 and 291 Ma on hornblende and biotite from Pierien granodiorite from western Kato Olympos (Schermer et al, in press), are consistent with these ages, providing additional support for the correlation of the Pierien rocks in the Olympos region with those in the Pieria mountains.

$^{40}Ar/^{39}Ar$ ages on white micas from Pierien gneisses also indicate two distinct metamorphic events, one during Paleocene to early Eocene time, at 53-61 Ma, and the other during the late Eocene unit at 36-40 Ma (Schermer et al, in press). Yarwood and Dixon (1977), and Barton (1976) obtained Rb-Sr mica-whole rock ages of 125-116 Ma from Pierien gneisses, suggesting that there was an earlier metamorphic event. These data are consistent with the interpretation that the carbonate cover of the Pierien basement is no younger than Jurassic in age.

INFRAPIERIEN UNIT

Introduction

The Infrapierien unit contains a wide variety of metasedimentary and metaigneous rocks. The basement is more heterogeneous than that of the Pierien unit, while the cover sequence is similar. Within the study area, this unit is divided

into three thrust sheets, from north to south, the Livadi nappe, the Paleambela nappe, and the Ziliana nappe. The lithologies are broadly similar in the three nappes; however, the detailed tectonostratigraphic sequences are different in each nappe, probably as a result of either facies changes in the protoliths and/or later structural disruption. Within each thrust package of Infrapierien rocks, contacts between lithologies appear to be parallel to the metamorphic foliation. However, in the Livadi nappe, contacts between foliated granitic rocks (the Livadi granite-gneiss of Nance, 1977) and the surrounding pelitic and amphibolitic schists are somewhat irregular and may indicate that the granite intruded these rocks prior to the latest phase of metamorphism and deformation. The principal rock types of the Infrapierien unit include 1) biotite-muscovite granite gneiss (fg2 on Plate 1); 2) green chlorite-epidote-muscovite schist and feldspar augen schist (fgs, Paleambela nappe; Plate 1); 3) marble (TJm; Plate 1); and 4) quartzofeldspathic gneiss; intercalated with 5) amphibolite gneiss and schist (combined as fa2 (Livadi nappe) and fa3 (Ziliana nappe) on Plate 1).

Livadi granite-gneiss

Commonly strongly weathered and poorly exposed, the Livadi granite-gneiss (fg2, Plate 1) is composed of biotite-muscovite granite, with coarse orthoclase crystals up to 1 cm in diameter and minor hornblende. It is well-foliated, and the foliation-forming minerals include biotite, muscovite, and phengite. A weak lineation is formed by elongate feldspar augen. Barton (1975a) attempted to date this granite using the Rb-Sr whole-rock method, but could not obtain an isochron. Cretaceous metamorphic ages in rocks which apparently overlie the Livadi granite-gneiss indicate that it is older than ~119 Ma (Yarwood and Dixon, 1977; Schermer et al, 1988), and workers agree that it is probably part of the allochthonous Paleozoic basement of the Pelagonian zone.

Interbedded quartzofeldspathic and amphibolite gneisses

The majority of the Infrapierien unit in the Livadi nappe is composed of alternating quartzofeldspathic and amphibolitic gneisses (fa2, Plate 1). Individual layers of each composition are commonly 2-50 cm thick (Figure 2.6), but range up to several meters thick. The thicker quartzofeldspathic bands are usually granitic in composition, containing K-feldspar + plagioclase + quartz + muscovite + phengite ± epidote. The thinner bands contain mostly plagioclase and less quartz and muscovite. Amphibolites occur as micaceous schists containing actinolite or hornblende + plagioclase + phengite + quartz + epidote ± apatite ± sphene ±

garnet ± biotite ± Fe-oxides. There are also massive amphibolites composed of hornblende + plagioclase + biotite ± chlorite ± epidote ± blue-green amphibole ± garnet. Garnet occurs as anhedral porphyroblasts rimmed by chlorite + epidote + Fe-oxides and appears to be a relict phase from an earlier metamorphic event. Blue-green amphibole, epidote, and chlorite seem to be the latest stable phases, although they are irregularly developed throughout the area. The amphibolites are variably foliated: locally, massive amphibolites crop out in layers up to ~2m thick within dominantly amphibolitic gneiss up to ~50 m thick that contains feldspathic layers 1-2 cm thick. In contrast the thin amphibolite layers are well-foliated and lineated schists.

In the Infrapierien unit in the Kato Olympos region (Ziliana nappe, Fig. 2.1; fa3, Plate 1), thin quartzofeldpathic layers (1-5 cm thick) are subordinate to amphibolite schists.

Overlying metasedimentary rocks

Muscovite schist and augen schist seem to be more abundant near the top of the Infrapierien unit, below overlying marbles presumed to be Triassic-Jurassic in age. The schists occur in a thin sequence (<250 m) at the top of the Livadi nappe and are the dominant lithology of the Paleambela nappe. Although the contact between the underlying gneisses and the mica schists is only locally observed, it appears to be parallel to the lithologic layering, and quartzofeldspathic gneisses are interbedded with the mica schists, so the contact is interpreted to be either conformable or pre-metamorphic. These quartz-rich coarse schists are green, with muscovite porphyroblasts and K-feldspar porphyroblasts. Two generations of white mica are present, a coarse-grained (up to 3mm) porphyroblastic phengite, and a fine-grained (40-50μm) phengite within the foliation planes. Epidote and sphene are ubiquitous; blue-green amphibole, actinolite, stilpnomelane and chlorite are commonly present. Grain size varies in these rocks from fine schists with feldspar augen <2mm across, to gneisses with compositional layering 3-4mm thick and feldspars up to 1 cm.

A thin (15-20 m) calcareous schist and phyllite unit is locally present between the mica schists and overlying marbles. This is a grey-weathering fine-grained muscovite-calcite schist with minor epidote and sphene.

The schists contain at least two metamorphic foliations accompanied by isoclinal folds that occur as "floating hinges". The early metamorphism appears to be moderately high temperature epidote-amphibolite facies while the later

assemblage seems to represent either lower temperature or higher pressure blueschist-greenschist transition facies (see chapter 5 for more details).

Blueschists and Mn-rich schists

A distinctive blue- and purple schist unit occurs near the contact of the Infrapierien and Pierien rocks in the Paleotherveno area, and extends to the NE for ~5 kilometers (fbs, Plate 1). The contact with the gneisses and schists to the NW is unexposed, but the contact with the underlying marbles appears to be a thrust fault that is isoclinally folded and locally overturned. Schmitt (1983) includes these rocks in the Infrapierien unit to the NW, and for lack of evidence to the contrary we agree.

The blueschists are composed of quartz + albite + phengite + crossite + stilpnomelane, with minor sphene, apatite, magnetite and hematite. Crossite growth appears to have persisted throughout two phases of isoclinal folding and foliation formation, but seems to post-date earlier actinolite and/or hornblende growth.

The purple schists are apparently manganiferous quartz-rich metasediments. They occur as a 20 m thick highly sheared sequence of blue and purple mica schist, purple carbonate rock, calcareous sandstone, fine-pebble conglomerate, a siliceous rock that resembles chert, and dense Mn-ore rock. These have been interpreted by Schmitt (1983) as deep-water cherts and sandstones.

Marbles

White, thick-bedded marble (TJm on Plate 1) overlies the Infrapierien schists and gneisses in apparently conformable contact. The uppermost ~20m of the schists are interlayered with marble beds 3-6 cm thick, and on the NW slopes of Lizadiko ridge (Fig. 2.1; Plate 1), a band of white marble 15-25 m thick is present near the top of the gneiss unit (fm on Plate 1). The lowest ~10 m of the unit contains quartz, feldspar, and green phengite grains similar to the underlying schists; this grades up into pure marble. The contact is thus locally gradational, although in many areas it is sheared and appears to be a fault contact. No fossils have been obtained from the marble unit. Most workers in the region have attributed the marbles to the Triassic-Jurassic as they are similar to dated carbonate rocks throughout the region.

OPHIOLITE

Introduction

Rocks mapped as "ophiolite" in the Mt. Olympos region comprise a dismembered and incomplete ophiolitic sequence including serpentinized ultramafic rocks, gabbro, mafic volcanic rocks, and phyllitic sedimentary rocks. There are no exposures of a complete ophiolite sequence, and neither pillow lavas nor sheeted dikes have been found. Exposures of the ophiolitic rocks are usually poor; in a large part of the study area they occur as a serpentinite-matrix melange which includes blocks of marble, sandy phyllite, and schist in addition to the igneous rocks (Fig. 2.7; also see Fig. 3.10).

Due to disruption by subsequent deformation, there are probably no original ophiolite emplacement-related structures preserved in the Olympos region. No "amphibolitic sole" rocks have been reported as have been found associated with other Hellenic ophiolite bodies (Roddick et al, 1979; Spray and Roddick, 1980). In the northern part of the study area, the faults at the base of the ophiolitic sheets are interpreted to be thrust faults. However, most of the other exposures of ultramafic rocks are interpreted to have been emplaced into their present positions along normal faults rather than thrust faults (see Chapter 3).

Regional relations

The age of ophiolitic rocks in the Olympos region is unknown. However, as the majority of ophiolites in the internal Hellenides are known to be middle-late Jurassic (Spray et al, 1984), most workers agree that ophiolitic rocks in the Olympos region are of similar age. Another characteristic element associated with the Hellenic ophiolites is the presence of a latest Jurassic-Early Cretaceous overlap sequence composed of limestone containing abundant ophiolitic debris overlain by neritic limestone. This transgressive sequence constrains the initial emplacement of the ophiolites over the Pelagonian zone to pre-Albian time, however, in several areas, ophiolites were further imbricated and now rest on rocks as young as Eocene. In the Olympos region the limestone which overlies the ophiolite has been dated as Maestrichtian (Godfriaux and Pichon, 1979), so it is possible that ophiolite emplacement could have occurred in the Late Cretaceous.

Livadi ophiolite complex

Ophiolitic rocks in the Livadi area mapped by Nance (1977; 1981) as the "Livadi complex" are more structurally coherent than those in other places within the map area. The Livadi complex includes metadunite, metaharzburgite,

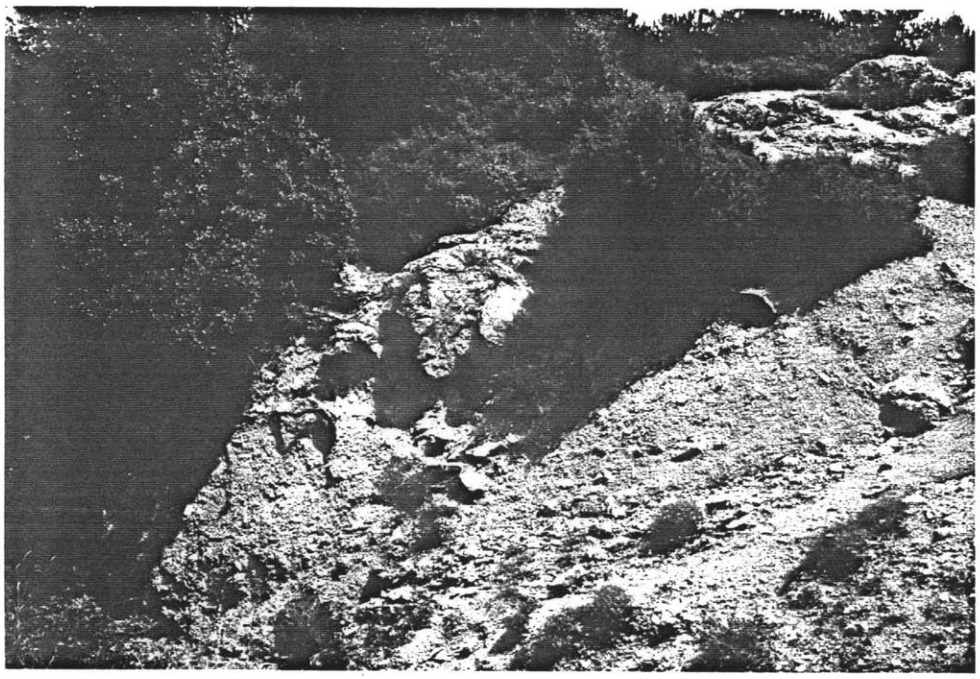

Figure 2.7 Marble boudins (near bushes on top of ridge) enclosed in serpentinite-matrix melange.

serpentinite, metalherzolite, and metagabbro. Nance (1981) recognized two metamorphic events in the Livadi complex, an early upper greenschist-lower amphibolite facies metamorphism, and a retrograde lower greenschist facies event. The Livadi complex is in thrust fault contact above Infrapierien gneisses, but is also overthrust by Pierien units north of Livadi.

The crystallization age of the Livadi complex is not known. Godfriaux (1968) believed the rocks were within, rather than structurally above, the gneisses, and assigned a tentative Paleozoic age to the complex. However, the recognition by Nance that the ophiolitic rocks were klippen allowed him to postulate a Mesozoic, possibly Jurassic age for the rocks. Nance (1981) assigned the early metamorphic event an Early Cretaceous age on the basis of correlation with a similar grade metamorphic event in Pierien granitic gneisses further north. However, he also reported that the thrust fault at the base of the Livadi complex cuts across the foliation in the Infrapierien gneisses which apparently formed during that metamorphic event. A thin (<20 m) mylonitic zone occurs in the Infrapierien gneisses at the base of at least one of the ophiolite klippen; Nance (1981) associates the greenschist-facies retrogression with the emplacement event. The Livadi complex is overthrust by Pierien and Infrapierien units.

The Livadi complex appears to be relatively unusual because of its high metamorphic grade; most other ophiolite bodies throughout Greece are either unmetamorphosed or contain only low greenschist-grade assemblages (Mercier, 1968; Zimmerman and Ross, 1976; Vergely, 1984).

Other ophiolitic rocks in the Olympos region

Ultramafic rocks

Ultramafic rocks generally crop out at the highest structural levels, and overlie mafic lithologies. They also occur as the matrix of a melange containing blocks of mafic and ultramafic rocks, marbles, and metasediments, and within high-angle shear zones cutting through the mafic rocks. Serpentinite is the most common lithology; partly-serpentinized peridotite, pyroxenite and dunite occur locally. These rocks are reddish brown weathering, and are blue, green, grey, and yellow-green on fresh surfaces. In addition to relict pyroxene, serpentine, chlorite, and minor talc are present. Small chromite bodies also occur within the serpentinites. Based on the absence of olivine, we infer that metamorphism occurred at greenschist grade or lower (Winkler, 1979). Mineral assemblages in associated mafic rocks are also consistent with greenschist facies metamorphism.

Mafic rocks

Mafic rocks associated with the ophiolite unit include metagabbro, metabasalt, and amphibolitic gneiss, schist, and phyllite. These rocks are generally brownish red-weathering and poorly exposed in blocky outcrops, particularly on the heavily forested eastern flank of the range. Gabbroic and basaltic rocks contain relict plagioclase, hornblende, and clinopyroxene. The original mineralogy is generally replaced by a greenschist facies assemblage consisting of actinolite + epidote + chlorite + zoisite ± sphene ± Fe-oxides. It is important to note that no blueschist-facies assemblages are present, even in rocks of basaltic bulk composition, in contrast to the metabasalts of the Ambelakia unit. The "ophiolitic" blueschists reported by Migiros (1985) and Katsikatsos et al (1982) appear to be in a tectonic unit that is below the ophiolitic rocks.

Carbonate and clastic rocks overlying(?) the ophiolite

Throughout the Hellenides, Upper Cretaceous neritic limestones were deposited unconformably on top of the ophiolites, indicating that the ophiolites were emplaced prior to Albian-Cenomanian time. In the study area, rocks that may represent this "Cretaceous transgression" are more commonly found in tectonic contact with serpentinite within melange zones. Godfriaux (1968) described conglomeratic limestone and marble containing clasts of serpentinite, chert, marble, and gneiss overlying ultramafic rocks in the northern Pierien mountains, in eastern Kato Olympos, and from southwest of Ossa. Foraminifera from these rocks are Maestrichtian.

A large area of ophiolitic melange occurs NW of Mt. Olympos on Lizadiko ridge, extending NE to Fotina (Fig. 2.1; Plate 1). The matrix of the melange is dominantly serpentinite, with blocks of marble, schist, and sandy phyllite ranging from a few meters to several tens of meters in length. Marble blocks commonly occur as elongate lozenges, subparallel to foliation in the serpentinite. These marbles commonly contain bluish-green micaceous laminae consisting of phengite + epidote + chlorite + sphene + quartz + graphite ± tremolite ± Fe-oxides. The foliation is associated with isoclinal folds, and is subsequently refolded. As folds within each marble block are at different orientations, it appears that the metamorphism and folding occurred prior to incorporation of the marble in the melange.

In some areas, as near the western edge of Lizadiko ridge, there is an apparently regular succession of serpentinite-mafic phyllite-calcareous schist-marble with schist laminae which may represent an essentially intact depositional

sequence of limestone over serpentinite. Contacts and lithologies are always sheared, and it is difficult to recognize ophiolitic debris in the mafic phyllite and calcareous schist due to their fine grain size. Abundant Fe-oxides and rare chloritized clasts may represent such debris.

The melange unit contains greenschist-facies blocks, and the serpentinite matrix may also be greenschist grade, although possibly metamorphosed during a different metamorphic event. Apparently, there are no blueschists within the melange.

NEOGENE AND QUATERNARY

Neogene and Quaternary conglomerates crop out dominantly on the eastern flank of the range. The conglomerates depositionally overlie the lower structural units and are in normal fault contact over serpentinite, schist, and marble.

The well-cemented conglomerates form relatively resistant yellow to light brown outcrops in the area between Fotina and Katerini, where they have been incised by the present drainages. However, much of the Neogene and Quaternary units are only loosely consolidated. Clasts range in size from pebbles to boulders, are well-rounded, and consist dominantly of limestone and marble, with additional clasts of gneiss, schist, mylonitic rocks, and serpentinite. However, the clast composition is variable, and in some areas gneissic and granitic clasts predominate over limestone. As this unit was not studied in detail, the distribution and range of facies within the conglomerate is not known. The matrix is dominantly sandy, and calcite forms an important part of the cement.

Fine-grained sandstone, clay, marl and marly limestone are locally interbedded with the conglomerate. Beds 1-10 cm thick of tan-white limestone occur interbedded with fine pebble and calcareous sandstone and siltstone layers. Large-scale cross-bedding is present in the sandstone.

Latsoudas (1985) reports the presence of ostracodes and gastropods of probable Pliocene age from these rocks. The division between Neogene and Quaternary in this study was made in part on the basis of the maps of Latsoudas (1985) and Godfriaux (1968), who do not discuss their criteria for distinguishing Neogene from Quaternary rocks. For this study, Quaternary rocks were mapped along the present drainages, and the uplifted, resistant conglomerates were mapped as Neogene; however, these age designations cannot be regarded as accurate.

GEOCHEMISTRY OF META-IGNEOUS ROCKS

Trace and major element geochemical analyses were performed on several of the metaigneous rocks from the Olympos-Ossa region in the hope of constraining the tectonic environment of the eruptive units. This study is still in progress, and the details of the geochemical data from these rocks will be presented elsewhere at a later date, so only a brief statement of the preliminary results and conclusions will be presented here to help constrain the paleogeographic interpretations discussed below. The geochemical data and plots of rare earth elements and incompatible trace elements are presented in Appendix A2.

The metamorphism and recrystallization that has affected the metavolcanic rocks has probably altered their major element composition. In particular, highly mobile elements such as Na, K, Ca were those used by Schmitt (1981b) to assign a tectonic environment to the volcanism in the Ambelakia unit. Although much controversy exists about the mobility of various trace elements during metamorphism, (e.g. Wood et al, 1979; Pearce and Norry, 1979; Hynes, 1980; Dungan et al, 1983), many workers agree that the rare earth elements (REE), Ti, Zr, Y, Ta, Nb, and Cr, if not immobile, are at least less mobile than major elements and Sr. Hellman et al (1979) discussed the behavior of REE during metamorphism and found both enrichments and depletions of the REE as a whole, as well as selective enrichment or depletion of light and heavy REE. In general, the arguments for a given interpretation of metamorphosed volcanic rocks must be based on the consistency among analyses, preferably from rocks of varying metamorphic grade, and other independent data, such as stratigraphic association.

Ambelakia unit

Trace and major element geochemical data were obtained on several of the metavolcanic rocks from the Ambelakia unit Schmitt (1981b) reported that these metavolcanics represented spilites, keratophyres, and orthokeratophyres, and that some of the mica schists were "greywackes" based on major element chemistry. She interpreted the chemical data to indicate that the basalts were erupted in an abyssal plain or oceanic island setting.

Trace Elements

Chondrite-normalized REE plots show that the metavolcanic rocks (two andesites and one basalt) are strongly light REE-enriched, and have negative Eu anomalies (Table A2.1; Fig. A2.1). "Spidergram" plots of chondrite-normalized incompatible trace elements (Thompson et al 1984) are remarkably similar to calc-

alkaline volcanic arc environments, with characteristic depletions (relative to REE) in Ta, P, Ti, Hf, and Zr (Table A2.1; Fig. A2.2). Contamination by continental crust also produces a pattern similar to that of arc volcanic rocks (Thompson et al, 1984; Taylor and McLennan, 1985; Gill, 1981).

Rb/Sr and Sm/Nd isotopes

Rb/Sr and Sm/Nd isotopes were analyzed in several samples from the Ambelakia unit (Table A2.2). Although it is necessary to know the age of the sample in order to determine the initial isotopic ratio, even when a maximum age of 250 Ma is assumed (other mafic-intermediate volcanic rocks in the Hellenides are no older than Permo-Triassic), the initial ratios of all the analyzed samples do not lie within the fields for MORB or ocean island basalt, but are similar to calc-alkaline arcs and continental crust. Minimum initial $^{87}Sr/^{86}Sr$ ratios of the metavolcanic rocks range from 0.7045-0.7060. Rb/Sr systematics are likely to have been affected by early Tertiary metamorphic events, indicated by mica-whole rock ages of ~60 Ma and 40 Ma in the mica schists, but enrichment of Nd relative to Sm in the metavolcanic rocks appears to be primary and results in the relatively low $^{143}Nd/^{144}Nd$ ratios of 0.5123-0.5127 (present-day; age-corrected values would be lower, and thus even more similar to arcs or continental crust).

Pierien and Infrapierien units

Trace and major element analyses of three orthogneisses and amphibolites from the Pierien and Infrapierien units are consistent with the hypothesis that they comprise the continental basement of the Pelagonian zone. The major element composition of the Pierien unit is predominantly granitic. REE and incompatible-element diagrams show strong LREE enrichment, as well as depletion of Ta, P, Ti, Hf, and Zr. The 295-Ma granodioritic rocks in the Kato Olympos region discussed above have initial $^{143}Nd/^{144}Nd=0.51215$. The Sr isotopes could have been reset during later Cretaceous and Tertiary metamorphic events, so the actual value of the initial ratio $^{87}Sr/^{86}Sr=0.7053$ could have no meaning, although it is consistent with the evidence from less-mobile elements. This signature is characteristic of continental crust and calc-alkaline arc volcanic rocks, however more data are needed to fully characterize the geochemistry of the igneous rocks from these units.

Ophiolite unit

Three samples of ophiolitic rock were analyzed for major and trace element geochemistry. Two foliated gabbros and one pyroxenite show very low concentrations of REE and other incompatible trace elements. The REE range from

slightly depleted to slightly enriched with respect to chondrites, and LREE are more depleted than HREE. Such flat to concave-downward patterns are characteristic of MORB and oceanic island basalts. Thus the trace element data, while limited, suggest the ophiolite was derived from an oceanic basin rather than an arc-related setting. This depleted trace element signature is in strong contrast to the three samples analyzed from the Ambelakia unit, which have LREE-enriched patterns and higher overall trace element abundances.

While we tentatively interpret these data to suggest that the Ambelakia volcanic rocks and the ophiolitic rocks were formed in distinctly different tectonic settings, more data are necessary to rule out the possibility that this difference is not controlled by metamorphic processes.

DISCUSSION: PALEOGEOGRAPHY OF THE OLYMPOS REGION

Olympos unit

The shallow-water Triassic to Eocene carbonate sequence of the Olympos unit has been recognized since the work of Godfriaux (1968) to represent a part of the external Hellenides exposed in a window beneath the metamorphic nappes. Because no important deformation occurred prior to Eocene time, the Olympos unit must have been far removed from the site(s) of Eohellenic ophiolite obduction in latest Jurassic to Early Cretaceous time. Schmitt (1983) states that the pre-Cretaceous deformation that resulted in the angular unconformity between Cretaceous and Triassic rocks included listric normal faulting but not folding, and occurred in an extensional environment. Subsequent Cretaceous to Eocene calcareous turbidite deposition appears to have occurred on the margin of the former carbonate platform. The abundant plutonic and metamorphic debris in the Eocene flysch could have been derived from the advancing thrust sheets composed of Pelagonian basement.

Many workers have correlated the Olympos unit with the Gavrovo-Tripolitza zone (Godfriaux, 1968; Fleury and Godfriaux, 1974; Bernoulli and Laubscher, 1972; Jacobshagen et al, 1978) and with the Parnassos zone (Godfriaux,1968) of the Hellenides. The Triassic and Cretaceous facies of Olympos are very similar to rocks of the Gavrovo-Tripolitza zone, with the exception that the latter contains a continuous carbonate sequence from Triassic to Eocene. The Parnassos sequence contains upper Jurassic bauxite deposits which may indicate that part of the platform was emergent (and thus possibly partially eroded) prior to Cretaceous time. Unfortunately, there are no well-constrained sequences in the external

Hellenides that can be correlated to the Olympos unit. Thus it is uncertain whether the pre-Alpine paleogeographic position of Olympos was west or east of the Pindos trough (or ocean) (e.g. Robertson and Dixon, 1984; Schmitt, 1983).

Ambelakia unit

The trace element geochemistry of volcanic rocks from the Ambelakia unit, while suggestive of an arc or continental setting for the Ambelakia volcanic rocks, is inconclusive due to the paucity of data and the complex metamorphic history. However, the hypothesis that the Ambelakia rocks formed in an arc or continental environment rather than an ocean-floor setting is consistent with both the limited trace element data and the tectonostratigraphy discussed above. The abundance of carbonate rocks, apparently of relatively shallow-water facies, and of metasediments containing abundant terrigenous debris, and the absence of true ophiolitic rocks that have undergone the same deformational and metamorphic history suggests that deposition occurred in a proximal continental margin environment. The origin of the volcanics is enigmatic however: if they were erupted in an arc setting, we would expect much more voluminous volcanic and volcaniclastic rocks. In addition, arc-related volcanism is rare throughout the Hellenic-Dinaric orogen except during late Jurassic time. It is possible that: 1) they were derived from a distant arc, 2) most of the volcanic rocks from the original arc were removed during thrusting events, or 3) there was a minor amount of volcanism on the Pelagonian continental margin, and the volcanic rocks were erupted through fairly thick continental crust, inheriting the trace element characteristics of the crust. The latter hypothesis is supported by the strong similarity between trace element patterns from the Pierien unit and the Ambelakia unit (Fig. A2.2).

Pierien and Infrapierien units

The Paleozoic age of the granitic and gneissic basement and the Mesozoic age for its shallow-water carbonate cover, in addition to the geochemical data from the basement rocks, are consistent with the interpretation that the Pierien and Infrapierien units formed part of the continental basement of the Pelagonian zone, and were subsequently deformed and metamorphosed during the Alpine orogeny. However, the pre-Alpine location of this continental fragment with respect to other units is uncertain. Some workers (e.g. Burchfiel, 1980; Ricou et al, 1984, 1986) interpret the Pelagonian zone to be the eastern margin of the Apulian plate, separated from the Rhodope and European plates by the Vardar ocean. In this

paleogeographic position, it was imbricated from east to west during closure of the Vardar ocean during latest Cretaceous time. Other workers interpret the Pelagonian fragment to have been derived from Rhodope, or to represent a separate microcontinent, with a Pindos ocean basin to its west and the Vardar ocean basin to its east (e.g. Smith and Woodcock, 1976; Jacobshagen et al, 1978; Smith et al, 1979; Dercourt et al, 1977, 1986; Barton, 1976; Vergely, 1984; Papanikolaou, 1984a). In this paleogeographic position, ophiolites from the Vardar ocean were emplaced toward the west, onto the Pelagonian zone, while those from the Pindos ocean moved both eastward over the Pelagonian, and westward over the more external units of the Hellenides.

Ophiolite units

Preliminary geochemical data indicate that the ophiolite unit formed in an oceanic basin rather than in an arc environment. Although its age is unknown, correlation with similar ophiolites in the Hellenides suggest an Upper Jurassic age; the ophiolite must be older than the Upper Cretaceous limestone which locally rests unconformably on the ultramafic rocks. The differing structural and metamorphic histories of the ophiolite and the underlying Ambelakia and Infrapierien units implies that the emplacement of the ophiolitic rocks in the Olympos-Ossa region was later than the Eocene blueschist-facies metamorphic event. However, a previous emplacement event over other units cannot be ruled out with the available data.

CONCLUSIONS

From the data presented above, it is evident that there are no ophiolites between the Olympos and Pierien units. Ophiolites are present only at the highest structural levels except where they have been imbricated between Infrapierien and Pierien rocks in the Pieria region. Structural evidence presented elsewhere (e.g. Schermer and Burchfiel, 1987; Chapter 3) indicates the direction of movement of metamorphic rocks over the Olympos platform was from the northeast towards the southwest. Because the ophiolites are at high structural levels, the oceanic basin from which they were derived must have lain to the northeast of the Pelagonian zone, and continental crust was continuous westward to the external Hellenides. Another implication of these data is that the Ambelakia unit was deposited on continental crust, and the presence of blueschist facies parageneses in the Ambelakia and Pierien units indicates that the continental basement and cover sequences were subducted to depths greater than 20 km during Eocene time.

Appendix A2: Geochemical data for samples from the Mt. Olympos region

Table A2.1 Major and Trace Element Analyses of Samples from the Mt. Olympos Region

Sample	86RA6a	86RA8c	86RA10a	86GO22	85GO20	85OL46	85OL43	85GO42	86OL2	84OL24c	85OL32	85OL50	86GO18	86RA22	86GO11	86LC2
Unit	AM	AM	AM	PI	PI	PI	PI	PI	CL	IP	IP	IP	OPH	OPH	OPH	OPH
XRF Analyses																
SiO2	49.96	54.05	57.4	59.22	59.41	72.04	71.91	68.46	76.36	52.94	73.07	64.87	49.19	47.75	50.20	47.76
TiO2	0.98	0.61	1.54	0.7	0.67	0.67	0.44	0.53	0.49	0.74	0.34	0.69	0.15	0.14	0.06	0.21
Al2O3	14.17	13.39	15.2	18.49	18.59	11.63	14.63	15.34	10.62	15.23	14.44	15.89	17.40	20.61	2.35	16.63
Fe2O3	11.13	8.89	9.66	6.04	6.02	5.49	2.13	3.12	2.96	9.85	2.41	4.81	6.12	5.88	7.39	7.03
MgO	7.84	7.78	1.91	2.77	2.9	1.49	0.74	1.70	1.77	7.22	1.11	2.17	9.28	7.28	18.83	10.05
CaO	7.55	7.77	4.08	5.35	5.04	0.3	0.63	0.58	1.38	5.95	0.63	4.39	14.42	13.67	17.25	15.02
Na2O	4.33	3.21	6.15	3.89	3.61	2.82	4.35	4.29	2.28	4.79	2.83	2.79	1.57	2.35	0.04	1.00
K2O	0.91	1.59	1.26	2.38	2.81	3.83	4.39	4.04	1.73	0.87	3.87	3.58	0.00	0.28	0.00	0.41
P2O5	0.2	0.11	0.49	0.2	0.18	0.12	0.1	0.14	0.06	0.05	0.11	0.19	0.02	0.02	0.01	0.01
LOI	2.62	2.46	1.91	3.4	4.09	2.07	1.72	1.45	2.75	1.89	2.00	4.75	2.48	2.93	1.48	2.58
total	99.69	99.85	99.6	102.46	103.69	100.46	101.04	99.65	100.40	99.54	100.81	104.12	100.60	100.91	97.60	100.71
Zr	119	80	287	178	143	165	169		107	36			11	9	8	10
Rb	10	22	18	72	98	105	166		50	23			0	0	0	6
Y	24	17	56	24	16	14	18		17	19			8	5	3	7
Th	0	2	6	8	14	30	30		6	3			2	0	3	0
Pb	2	1	0	6	9	3	14		6	2			0	0	0	5
Sr	191	309	161	757	684	36	78		22	82			56	82	3	211
Ba	169	253	263	1100	910	665	282		272	106			25	49	31	144
Cr	273	258	22	21	23	41	5		174	225			246	119	2435	245
Ni	9	32	5	0	0	0	0		36	66			83	65	138	71
Neutron Activation Analyses																
La	15.3		30.86	38.6	46.2					3.6			0.44	1.12	0.033	
Ce	36.8		76.3	75.6	86.6					9.1			1			
Nd	19.6		41.6	29.3	27.9					5.7			1			
Sm	4.56		9.63	5.64	4.6					1.9			0.511	0.253	0.075	
Eu	1.349		2.7	1.437	1.222					0.569			0.21	0.155	0.05	
Tb	0.72		1.62	0.69	0.45					0.48			0.19	0.07		
Yb	2.4		5.48	2	1.63					2.16			0.94	0.35	0.287	
Lu	0.35		0.828	0.296	0.246					0.339			0.127	0.068	0.041	
Rb	10		18	72	98					23			b.d.	b.d.	b.d.	
Cs	0.42		7	1.28	1.65					1.26			b.d.	b.d.	b.d.	
Hf	2.82		6.85	4.26	4.01					1.13			b.d.	b.d.	b.d.	
Th	1.99		5.12	8.57	11.07					0.68			b.d.	b.d.	b.d.	
Ta	0.26		0.57	0.71	0.5					0.06			0.15	b.d.	b.d.	

b.d. = below detection limit
XRF Analyses performed at the University of Kansas by J.D. Walker
Instrumental Neutron Activation Analyses performed at M.I.T.

AM = Ambelakia
OL = Olympos
PI = Pierien
IP = Infrapierien
OPH = Ophiolite

TABLE A2.2 Rb, Sr, Nd, and Sm Analyses for Samples from the Mt. Olympos Region

SAMPLE	Rb, ppm	Sr, ppm	87Rb/86Sr	87Sr/86Sr	Sm, ppm	Nd, ppm	147Sm/144Nd	143Nd/144Nd
85GO42 plag	5.38	47.14	0.334	0.71306				
whole rock	142.5	36.45	11.33	0.71880				
mica	348.0	8.86	114.40	0.77984				
85OL43 plag	68.3	54.72	3.62	0.71839				
whole rock	165.0	73.57	6.53	0.71941				
mica	531.7	53.23	29.00	0.73245				
85OL46 plag	6.60	21.13	0.905	0.71531				
whole rock	133.3	40.84	9.45	0.72151				
mica	325.3	30.59	30.87	0.73451				
85OL32 whole rock	153.3	179.50	2.47	0.74262				
mica	397.0	53.24	21.65	0.71614				
85OL50 whole rock	141.6	279.27	1.470	0.71406				
mica	335.0	82.89	11.72	0.72748				
86RA3 whole rock	49.0	66.70	2.71	0.71102				
86RA5b whole rock	72.6	133.34	1.58	0.70768				
86RA6a whole rock	16.1	204.50	0.228	0.70632	4.53	19.74	0.139	0.512474
Initial ratio if age = 150 Ma:				0.70583				0.512338
86RA8c whole rock	27.7	325.60	0.246	0.70599	3.26	14.13	0.139	0.512518
Initial ratio if age = 150 Ma:				0.70546				0.512371
86RA10a whole rock	25.0	169.10	0.43	0.705883*	9.53	41.10	0.140	0.512709
Initial ratio if age = 150 Ma:				0.70496				0.512571
86GO22 whole rock	79.8	778.87	0.297	0.70651	5.64	32.00	0.107	0.512361
Initial ratio (300 Ma)				0.70524				0.512172

87Sr/86Sr corrected for fractionation using 86Sr/88Sr =0.1194 and normalized to E&A SrCO3 =0.70800. Analytical precision <0.0005%
Rb/Sr reproducible to better than 1%

143Nd/144Nd corrected for fractionation using 146Nd/144Nd = 0.7219 and normalized to BCR-1 = 0.51264. Analytical precision <0.004%
Sm/Nd reproducible to better than 1%

* preliminary value; this sample had ~0.2 mV 87Rb (out of ~140 mV total) in the Sr run

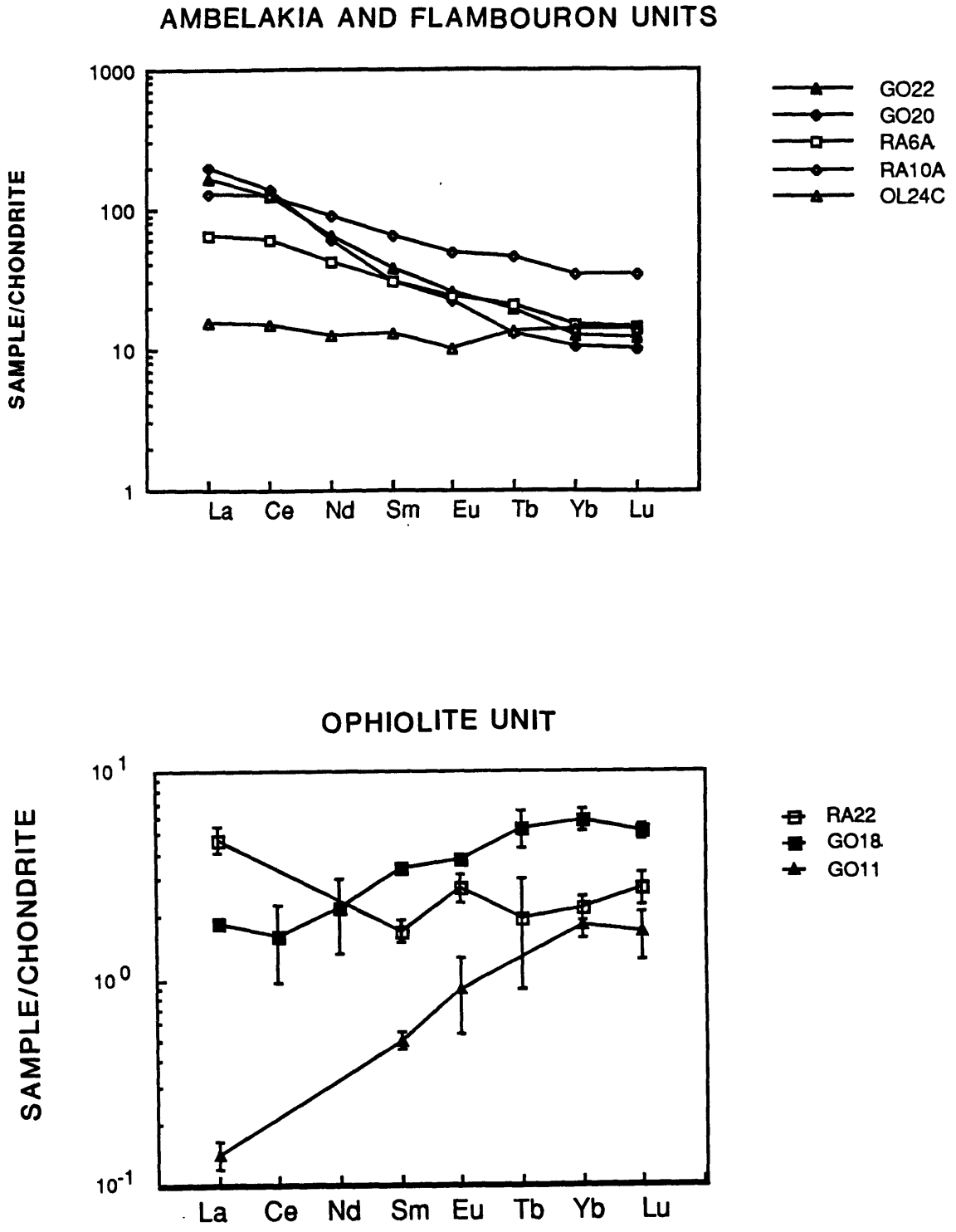

Figure A2.1 Chondrite-normalized rare earth element diagrams for A) the Ambelakia, Infrapierien, and Pierien units and B) the ophiolite unit

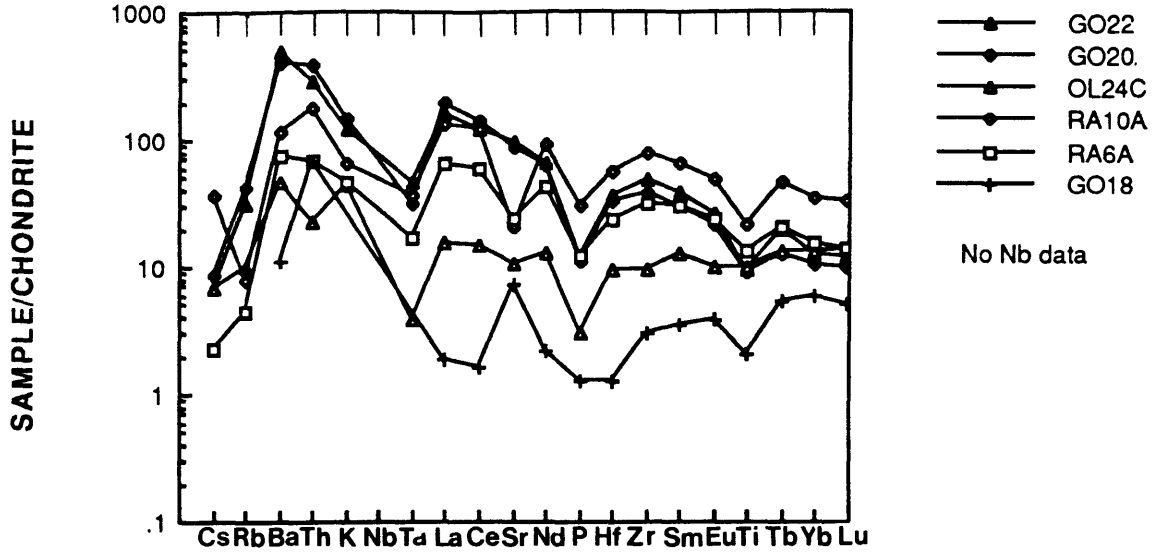

Figure A2.2 Plot of chondrite-normalized trace element abundances arranged in order of decreasing incompatibility from left to right, after Thompson et al (1984)

Chapter Three: STRUCTURAL EVOLUTION OF SUBDUCTED CONTINENTAL CRUST, MT. OLYMPOS REGION, GREECE

INTRODUCTION

During the Alpine orogeny in Greece, convergence between the Apulian plate and the European plate resulted in subduction of the western part of Paleotethyan and Neotethyan ocean floor and the subsequent collision of the two continents. Deformation began in latest Jurassic time with westward obduction of ophiolites from the Vardar ocean (e.g. Vergely, 1976; Mercier et al, 1975) and progressed both westward and eastward from the site of the future suture zone throughout the Cretaceous and Tertiary. Final closure of the ocean basin occurred in latest Cretaceous-Paleocene time (Smith, 1971; Burchfiel, 1980; Sengor and Yilmaz, 1981). In the internal, or eastern, Hellenides (Figure 3.1), deformation was accompanied by regional metamorphism and basement-involved thrust faulting during the early stages of the Alpine orogeny, whereas, in the external part of the orogen deformation formed a thin-skinned fold and thrust-belt of Eocene and younger age.

In the Mt. Olympos region, a cross section through the transition from the internal to external Hellenides exposes rocks deformed under low-grade to very low-grade metamorphic conditions in a series of thrust sheets with higher-grade, early-deformed metamorphic nappes on top, and progressively lower-grade metamorphic nappes deformed at later times towards the base of the structural succession. The lower parts of the nappe sequence record the subduction of continental basement and cover rocks accompanied by deformation and metamorphism under high pressure-low temperature conditions. Subsequent exhumation of the thick section of metamorphic nappes has provided the opportunity to study a large part of the deformational history of the Hellenides that began in Early Cretaceous time and has continued until the present. Through a detailed study of the geometry and evolution of structures in the nappe sequence, we can provide kinematic constraints on Alpine orogenic processes in the Hellenides. Combined with constraints on the thermal evolution of the crust during deformation afforded by Ar/Ar geochronology (Schermer et al, in press), a detailed picture of the tectonic history of this region is beginning to emerge.

The Olympos region is somewhat unusual in that it contains continental basement rocks that were subducted to HP/LT conditions and subsequently exhumed. The long history of deformation preserved in these rocks is in part due to these low temperatures (Schermer et al, in press), and thus the structural data

provide insight into the processes involved in continental collision, subduction, and the uplift and preservation of blueschists.

Geologic setting

The location of the Mt. Olympos region is shown in Figure 3.1. The Pelagonian zone (Aubouin, 1959), of which Mt. Olympos is a part, is a belt of metamorphic rocks that consists mainly of Paleozoic continental basement rocks overlain by Triassic-Jurassic marbles. To the west, Pelagonian rocks are thrust over unmetamorphosed Mesozoic carbonates and flysch of the external Hellenides, and to the east, they are overthrust by oceanic rocks of the Vardar zone (Mercier et al, 1975), the main oceanic terrane of the Dinaric-Hellenic Alps.

At Mt. Olympos, the platform carbonates of external Hellenides affinity are exposed in a window beneath a series of metamorphic nappes. This window, first discovered by Godfriaux (1968), contains flysch of middle Eocene age that was deposited on relatively undisturbed Triassic-Eocene carbonate platform rocks and thus is thought to represent a window through the Internal Hellenides into the External Hellenides. Because the youngest rocks are present in the lowest structural unit, all discussion of tectonostratigraphic units in this paper will proceed from top to bottom so that the structural evolution can be discussed in chronological order.

The structural sequence in most of the Pelagonian zone is similar to that described here for the Mt. Olympos region with the exception that the lowest unit is only rarely exposed. From top to bottom, this sequence comprises (Fig. 3.1): A) the ophiolite unit, consisting of probable late Jurassic ophiolitic igneous rocks overlain by Lower Cretaceous limestone in coherent thrust sheets and as serpentinite-matrix melange; B) the Infrapierien unit, consisting of blueschist-greenschist transition facies gneiss and schist overlain by probable Permo-Triassic metasediments and metavolcanic rocks followed by Triassic and Jurassic platform limestone and dolomite, and C) the Pierien unit, consisting of blueschist-facies Paleozoic granitic gneiss overlain by a thin metaclastic sequence and Triassic and Jurassic platform carbonate rocks; D) the Ambelakia unit that includes blueschist-facies continental margin carbonate rocks, quartzo–feldspathic sediments, and basic to intermediate volcanic rocks; and E) the Olympos unit, composed of parautochthonous, very low-grade Triassic and Lower Cretaceous to Eocene neritic carbonate rocks overlain by Eocene flysch.

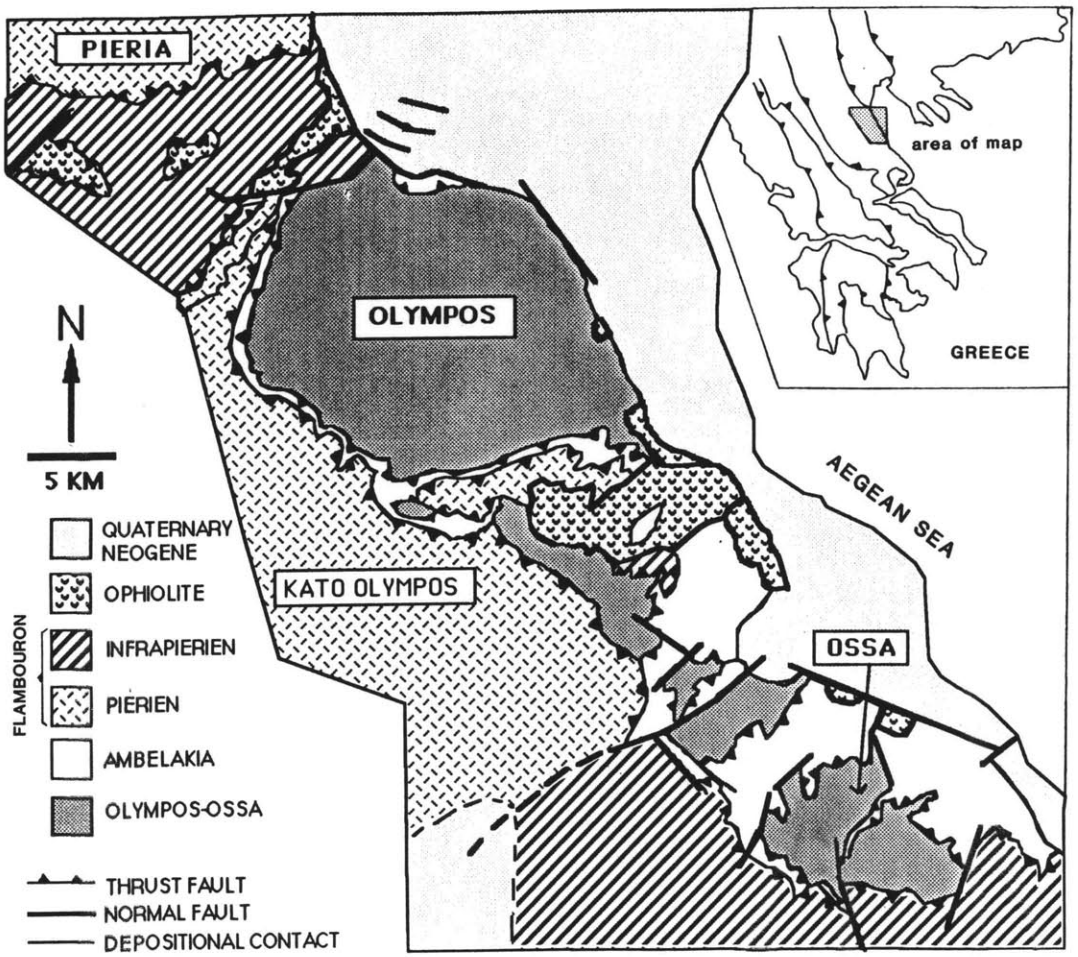

FIGURE 3.1. Generalized geologic map of the Mt. Olympos region, showing principal structural units and the location of Olympos within the Hellenides (inset). Inset: V: Vardar zone; P: Pelagonian zone; Pi: Pindos zone; Sp: SubPelagonian zone; E: External Hellenides. Internal Hellenides are indicated by dot pattern.

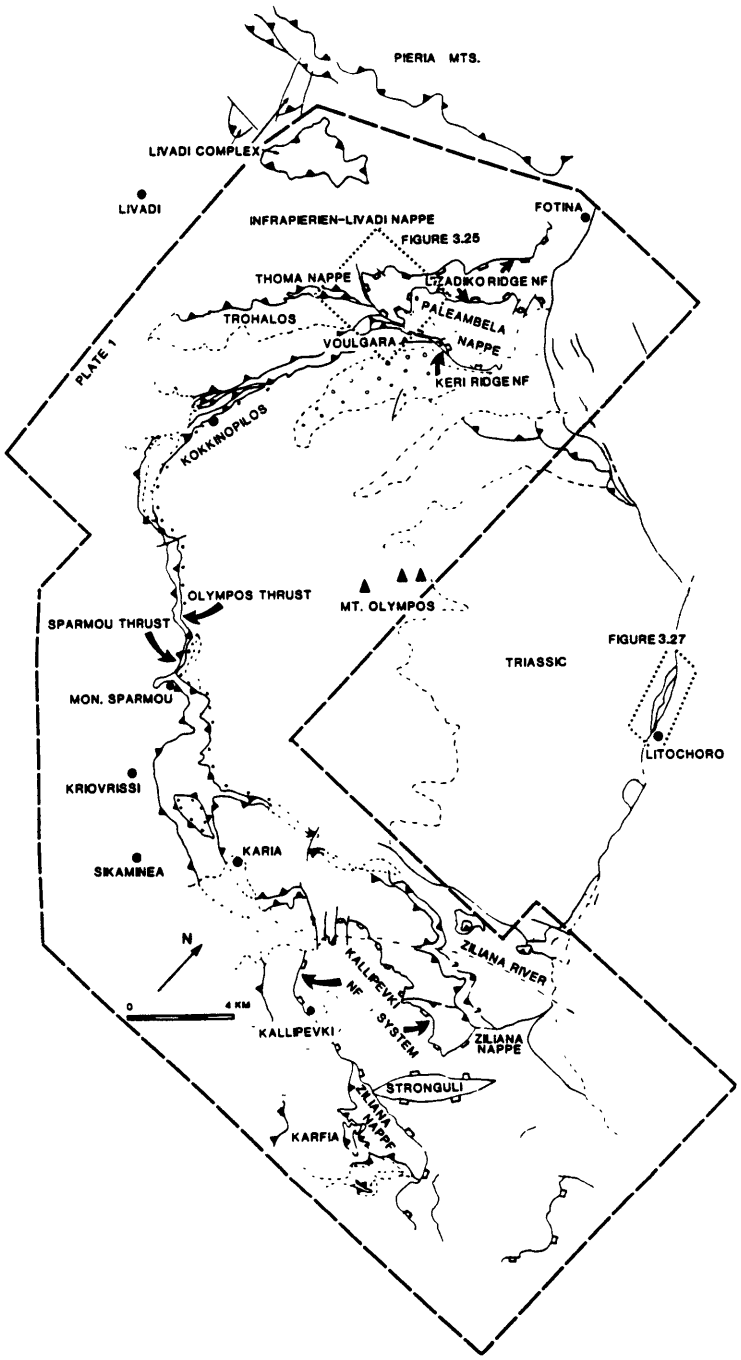

FIGURE 3.2. Locations of villages, geographic features, and major structural features discussed in the text. See Figure 1 and Plate 1 for geologic details; location of Plate 1 is indicated by dashed lines and the location of Figures 3.25 and 3.27 are indicated by dotted lines. Geologic contacts in the areas outside Plate 1 and Figure 3.27 are based on the work of Schmitt (1983). Units not shown on Figure 1 or Plate 1: The triangles in the center of the figure denote the summit of Mt. Olympos, "Triassic" indicates Triassic limestone and dolomite of the Olympos unit; open circles indicate Eocene flysch of the Olympos unit, dotted areas indicate Neogene and Quaternary sediments and sedimentary rocks.

The names of major structures in the study area and locations discussed in the text are shown in Figure 3.2. The Infrapierien and Pierien units are interpreted to be part of the same Pre-Alpine continental basement and cover sequence, and are commonly referred to by previous workers (e.g. Godfriaux, 1968; Papanikolaou, 1984a,b) and in this study as the Flambouron unit when it is not necessary to emphasize the distinctions between them. The Infrapierien unit is divided into three thrust sheets, from north to south, the Livadi nappe, the Paleambela nappe, and the Ziliana nappe (Fig. 3.2). The Pierien unit occurs in a thin thrust sheet (Thoma nappe) on the north flank of Trohalos ridge, and as a much larger (probably composite) sheet that crops out from Trohalos ridge in the north to the southern edge of the study area (Fig. 3.2). The Pierien unit occurs in thrust fault contact above the Ambelakia unit along the Sparmou thrust, and both the Pierien and Ambelakia units are in thrust fault contact above the Olympos unit along the Olympos thrust (Fig. 3.2). On the northern margin of the Olympos window, the Keri Ridge normal fault places Infrapierien rocks above rocks of the Olympos unit, and the Lizadiko Ridge normal fault juxtaposes serpentinite-matrix melange of the ophiolite unit against the Infrapierien unit (Fig. 3.2). In the Kato Olympos area, the Kallipevki normal fault system places the ophiolite unit against the Olympos, Ambelakia, Pierien, and Infrapierien units (Fig. 3.2).

Previous work

After the initial discovery of the Olympos window (Godfriaux 1968), several workers have studied various aspects of the geology of this region. Godfriaux (1977), Dérycke and Godfriaux (1976) and Godfriaux and Pichon (1979) recognized the presence of blueschists in a thin thrust sheet between granitic gneisses and the carbonate rocks, and postulated that the metamorphic rocks were transported to the SW over the carbonate platform. This model was based on correlation of Olympos unit rocks with similar sequences further west in the external Hellenides, but not on direct structural evidence. In a detailed structural study of the western margin of the window, Barton (1975, 1976) proposed that the metamorphic nappes moved to the NE over the carbonate rocks, and proposed an Eocene age of thrusting on the basis of Rb-Sr data on phyllonitic rocks above the Sparmou thrust (called the Olympos thrust by Barton; see below). Nance (1981), Yarwood and Aftalion(1976), and Yarwood and Dixon (1979) studied the Infrapierien and Pierien rocks in the Livadi region and in the Pieria mountains (Fig. 3.2). They recognized Cretaceous metamorphic and deformational events in

addition to the Tertiary events. Yarwood and Dixon, (1979) documented southward displacement of Pierien over Infrapierien rocks, and postulated NE-directed thrusting of the imbricated basement stack over the Olympos unit, although without direct structural evidence. Schmitt (1983) conducted a detailed study of the stratigraphy of the Olympos unit. She discovered that the Olympos platform sequence, previously thought to contain a continuous sequence of Triassic to Eocene rocks, contained a hiatus, wherein uppermost Triassic to upper Lower Cretaceous rocks were missing, thus rendering the correlation with external Hellenide units less certain. Schmitt also studied structural and metamorphic features of the overlying metamorphic nappes in a large area around the Olympos window; the tectonostratigraphic nomenclature proposed in her work is adopted here with some modifications (see chapter 2). Based on analysis of fold geometry, Schmitt proposed SE-vergent thrusting of metamorphic rocks over the Olympos platform. Vergely (1984) conducted a brief microstructural study on a few samples from the Olympos limestone and flysch and concluded that the nappe displacement was to the SW.

Purpose of this study

Because the Olympos unit is thought to be a window into the external Hellenides, the direction of overthrusting of the metamorphic nappes has important implications for the paleogeography and structural evolution of the Hellenides. In particular, it bears on the question of whether the Pelagonian basement unit was separated from the carbonate platform of the external Hellenides by an ocean basin, or whether all the units below the Jurassic ophiolite nappe were part of the same continental fragment (see Robertson and Dixon, 1983 for a review). Noting that the workers cited above concluded three entirely different tectonic scenarios from studies of the same rocks, and in an attempt to resolve some of the controversy concerning the tectonic evolution of this important part of the Hellenides, this study focuses on the kinematic aspects of the Alpine deformation. In particular, we have examined the faults surrounding the Olympos window, and the detailed relation between metamorphic and deformational events in the different structural units. Based on our field work and that of previous workers, we were able to separate pre-Alpine and distinct Alpine events and further refine the tectonostratigraphy. We were also able to date many of the events using Ar/Ar and Rb/Sr geochronology (Schermer et al, in press), and thus provide important new

constraints on the metamorphic and deformational evolution of the Mt. Olympos region.

Summary of events

We have recognized seven deformational and metamorphic events related to convergence between the Apulian and European plates during the Alpine orogeny. The relation between events D0 to D7 and internal deformation in each unit is indicated in Table 3.1. Paleozoic events that can not be differentiated in the study area are combined into D0. Events D1-D3 include thrust faulting, mylonitization, NE-SW trending isoclinal folds, and relatively high pressure-low temperature metamorphism of continental basement and margin rocks as they were imbricated from NE to SW and thrust over the Olympos carbonate platform. The three distinct events have been dated by Rb/Sr and 40Ar/39Ar as ~100 Ma, 53-57 Ma, and 36-40 Ma (Schermer et al, in press). Deformation related to thrust faulting was followed by further development of folds (D4, D6), and subsequent low- and high-angle normal faults (D5, D7), which were in part responsible for the uplift of the blueschists and the present-day geometry of the thrust faults. The youngest normal faults (D7) cut Neogene and Quaternary conglomerates, however Ar/Ar cooling ages indicate extension and uplift may have begun in early-middle Miocene time.

In this paper we describe the geometric and kinematic aspects of the structures associated with Alpine deformation and metamorphism in the Mt. Olympos region. The relative timing of events, constrained by cross-cutting relations observed in the field as well as by absolute age constraints (Schermer et al, in press) will be discussed in terms of the internal deformation within each unit and the juxtapositions of the different structural packages.

GEOMETRIC, CHRONOLOGIC, AND KINEMATIC CHARACTERISTICS OF THE DEFORMATION IN THE OLYMPOS REGION

In the study area, deformational phases were identified within each structural unit on the basis of geometric and kinematic characteristics and relative timing relationships with other structures. These phases were correlated between structural units and divided into events of regional significance generally separated from each other by a distinct change in either style, orientation, or grade of metamorphism. The events are numbered D0 to D7, and folds, fabrics, and metamorphic assemblages for a given event are numbered according to that regional chronology. For example, D3 produced F3 folds, S3 fabrics, and M3 mineral assemblages even though within a particular structural unit, this may have

Table 3.1: Summary of Deformational Events

UNIT / EVENT	OPHIOLITE	INFRAPIERIEN	PIERIEN	AMBELAKIA	OLYMPOS	NEOGENE and QUATERNARY
D7	high-angle normal faults	high-angle normal faults	high-angle normal faults	high-angle normal faults	high-angle normal faults	high-angle normal faults
D6		open SW folds	open SW folds	open SW folds	open SW folds	
D5 16-23 Ma	low-angle	low-angle normal faults	low-angle normal faults	low-angle normal faults	low-angle normal faults	normal faults
D4		open NW-SE folds	close-open NW-SE folds	close-open NW-SE folds	open NW-SE folds	
D3 36-42 Ma		folds; thrusting to SW	blueschist metamorphism isoclinal NE-SW folds; thrusting to SW	blueschist metamorphism isoclinal NE-SW folds; thrusting to SW	prehnite-pumpellyite metamorphism isoclinal NE-SW folds; thrusting to SW	isoclinal NE-SW
D2 51-64 Ma	? greenschist metamorphism	blue-green metamorphism folding folds; thrusting to SW	blueschist metamorphism isoclinal NE-SW folds; thrusting to SW	blueschist metamorphism isoclinal NE-SW folds; thrusting to SW	isoclinal NE-SW	
D1 ~100 Ma	? greenschist metamorphism folding	greenschist metamorphism, NE-SW folds SW or S thrusting	greenschist metamorphism, NE-SW folds SW or S thrusting	? blueschist metamorphism, folding		
D0		greenschist-amphibolite metamorphism, folding	greenschist-amphibolite metamorphism, folding			

been the first deformational or metamorphic phase. On Plate 1, minor fold phases reflect this overall regional chronology, but metamorphic fabrics are only distinguished where two distinct schistosities were observed in the outcrop; in general this distinction could only be made with the aid of thin sections. Structural data are presented on lower hemisphere equal area projections in Appendix A3.

D0: Pre-Alpine deformation and medium-grade metamorphism

We include in D0 all deformation and metamorphism that occurred prior to deformation related to imbrication of the Pierien and Infrapierien units in D1. Evidence for D0 is preserved rarely, and only in the Flambouron units (Infrapierien, Pierien). The majority of evidence for D0 comes from regions north and west of the study area, which were examined by Mercier(1968); Yarwood and Dixon (1979), Mountrakis et al (1983), Mountrakis (1984, 1986), and Papanikolaou (1984a,b). Carboniferous granitic rocks intruded and metamorphosed a pre-existing basement complex; however there are no distinct structures related to Paleozoic deformation visible in the study area. According to Nance (1981), the Livadi granite-gneiss (of unknown, but presumed Paleozoic age) near the town of Livadi (Fig. 3.2) intrudes an older metamorphic basement; however, both the granite and surrounding rocks were strongly deformed and metamorphosed during later events. Mountrakis (1986) reports that upper greenschist-facies metamorphic rocks are intruded by granite dated as 302 Ma (U-Pb) in the Pelagonian basement rocks of northern Macedonia. In several locations, these granitic rocks have experienced only partial loss of Ar since ~295 Ma, even though they were strongly deformed in late Mesozoic and Cenozoic time (Schermer et al, in press). In the Flambouron units, floating fold hinges and porphyroclasts contain an early, greenschist-amphibolite grade fabric and provide additional evidence that the early metamorphic history is locally preserved in these rocks. Permo-Triassic metasedimentary rocks and Triassic-Jurassic marbles rest unconformably on the older rocks throughout the Pelagonian zone (Mountrakis et al, 1983; Papanikolaou and Zambetakis-Lekkas, 1980; Katsikatsos et al, 1982), thus the available evidence suggests that the D0 deformation is pre-Permian, and thus pre-Alpine, in age.

D1: Early to middle Cretaceous folding and basement imbrication

D1 structures are well-developed in the Pierien and Infrapierien units, but probable D1 structures and metamorphic assemblages may also be present in the ophiolite and Ambelakia units. Because these structures are strongly overprinted

by younger deformation and metamorphism, geometric and kinematic data are limited in the study area. Structures assigned to D1 are shown in Figure 3.3A. In the Infrapierien and Pierien units, D1 is associated with juxtaposition of these two units (Figure 3.4). As discussed further below, deformation prior to D2 in the Ambelakia unit does not appear to be related spatially to D1 in the Flambouron units, and probably occurred when the Ambelakia unit was separated from the Flambouron units; however, we have designated this deformation D1 in order to distinguish it from later events. In the ophiolite unit, only the Livadi ophiolite complex (Fig. 3.2) contains structures that we attribute to D1 and that appear to be associated with D1 structures in the Flambouron units. Other ophiolite occurrences throughout the study area contain structures that may be D1 in age, but the present contacts below these ophiolites are the result of much younger deformation, so that we cannot constrain where or when the earlier metamorphism and deformation occurred.

Ophiolite unit

Igneous rocks of the ophiolite unit contain low-grade assemblages (epidote-amphibolite facies) associated with an irregularly-developed S1 foliation. F1 isoclinal folds have been observed only in thin section and are locally associated with an amphibole mineral lineation which has a highly variable trend.

Nance (1981) reported that the Livadi ultramafic complex (Livadi complex, Fig. 3.2) was metamorphosed under amphibolite facies conditions prior to its emplacement above the Infrapierien gneisses, and subsequently retrograded to greenschist facies, possibly during emplacement. He describes a recumbent, NE-vergent isoclinal fold within the ophiolitic rocks (defined on the basis of the forsterite content of olivines) that is also apparently cut by the thrust fault at the base of the ophiolite unit; however, reconnaissance work in the area NE of Livadi village indicates that gneisses up to 15-20 m below the thrust fault and ultramafic and mafic rocks above the thrust fault contain mylonitic foliations parallel to the thrust fault and NE-SW trending lineations (Fig. 3.2; plate 1) that we attribute to D1 based on the similarity in style and orientation to better-dated structures in the Infrapierien unit (see below).

Pierien and Infrapierien units

In the Paleambela area, Triassic-Jurassic marbles are folded with the underlying gneiss and mica schist along kilometer-scale, N20-35E-trending isoclinal, recumbent folds (Plate 2, sections A-A', B-B'). Although the outcrop is

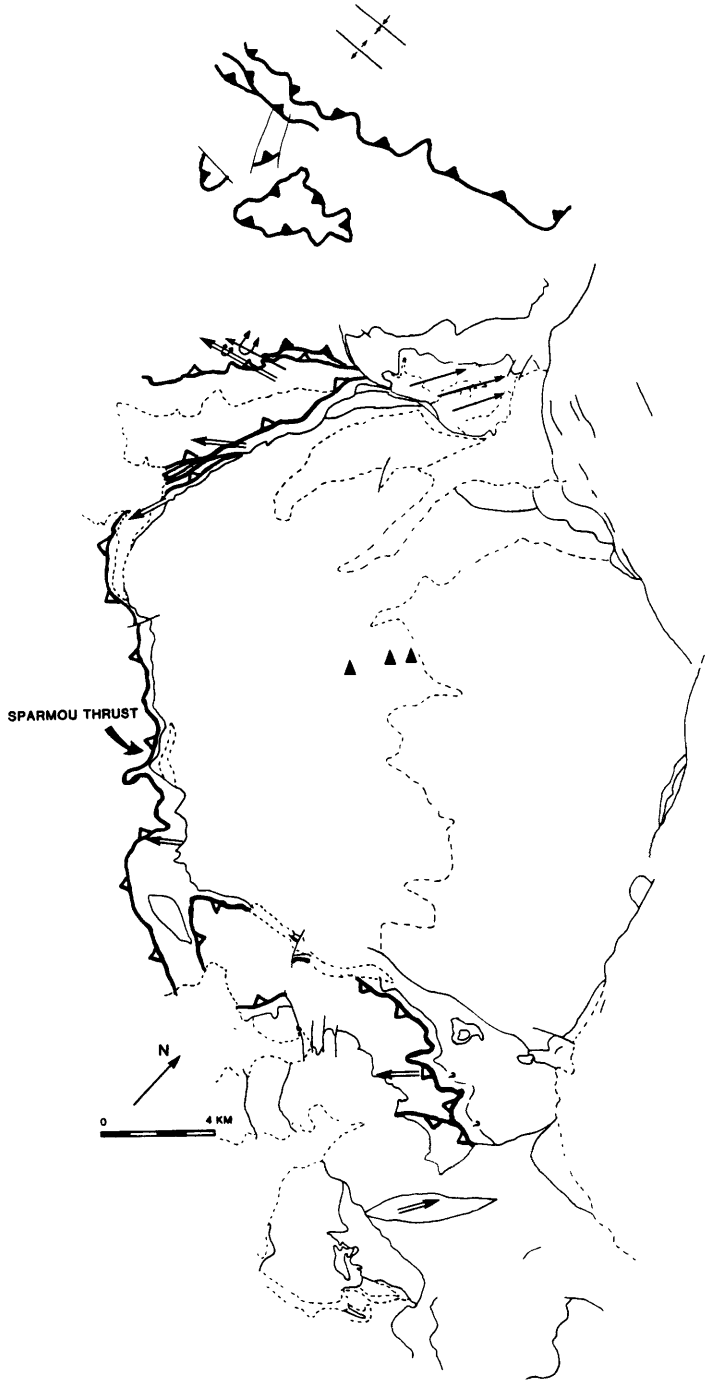

FIGURE 3.3. Tectonic maps of the Olympos region showing folds and faults for events D1-D7; all faults are shown by solid lines and all depositional contacts are shown by dashed lines. See Figs. 3.1 and 3.2 for lithologic unit designations and Plate 1 for detailed structural data. In A,B, and C, only the structures for designated deformational events are indicated by heavy lines. A: Structures developed during D1 and D2. D1 thrust faults are shown with closed barbs, F1 fold hinge traces are shown with single lines, D2 thrust faults are indicated by open barbs,the Sparmou thrust is labelled, and F2 hinge traces are indicated by double lines.

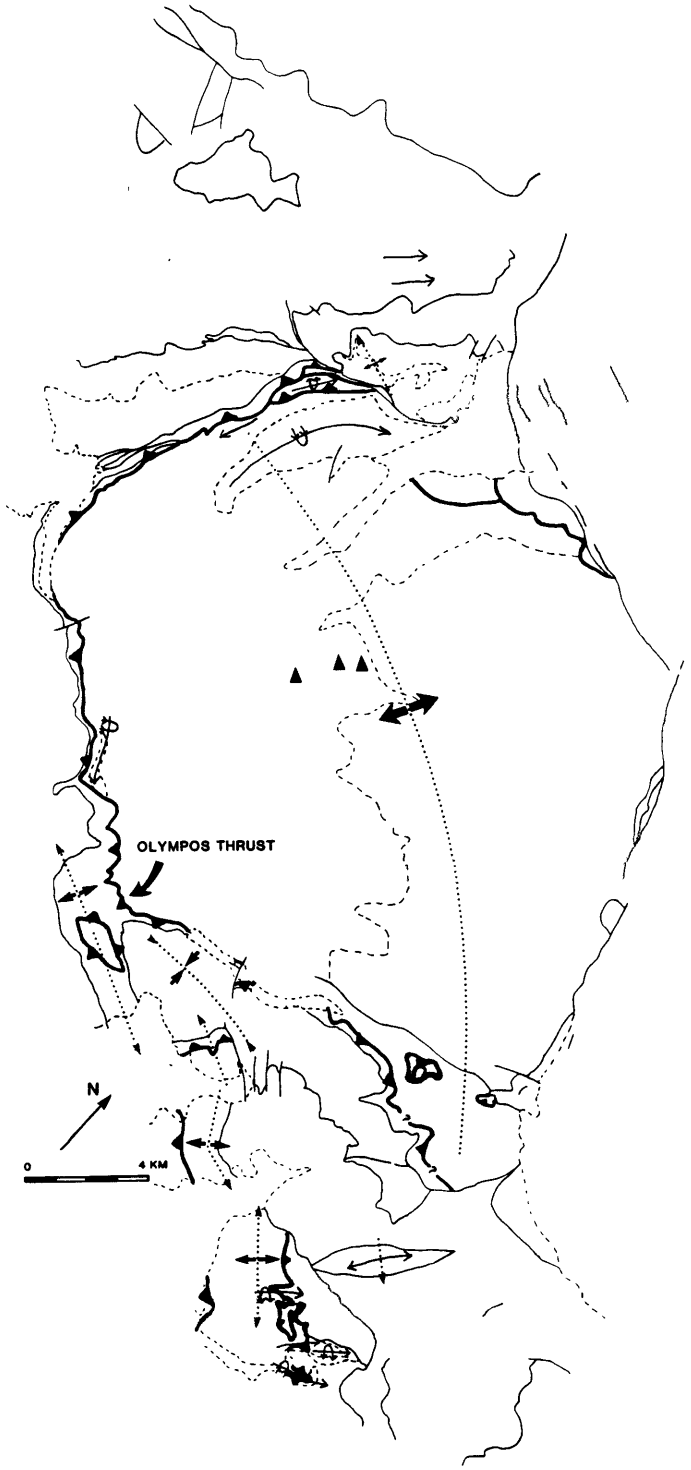

FIGURE 3.3B: Structures developed during D3 and D4. The Olympos thrust and other D3 thrusts are shown by closed barbs, F3 hinge traces are shown by solid lines, and F4 hinge traces are shown by dotted lines.

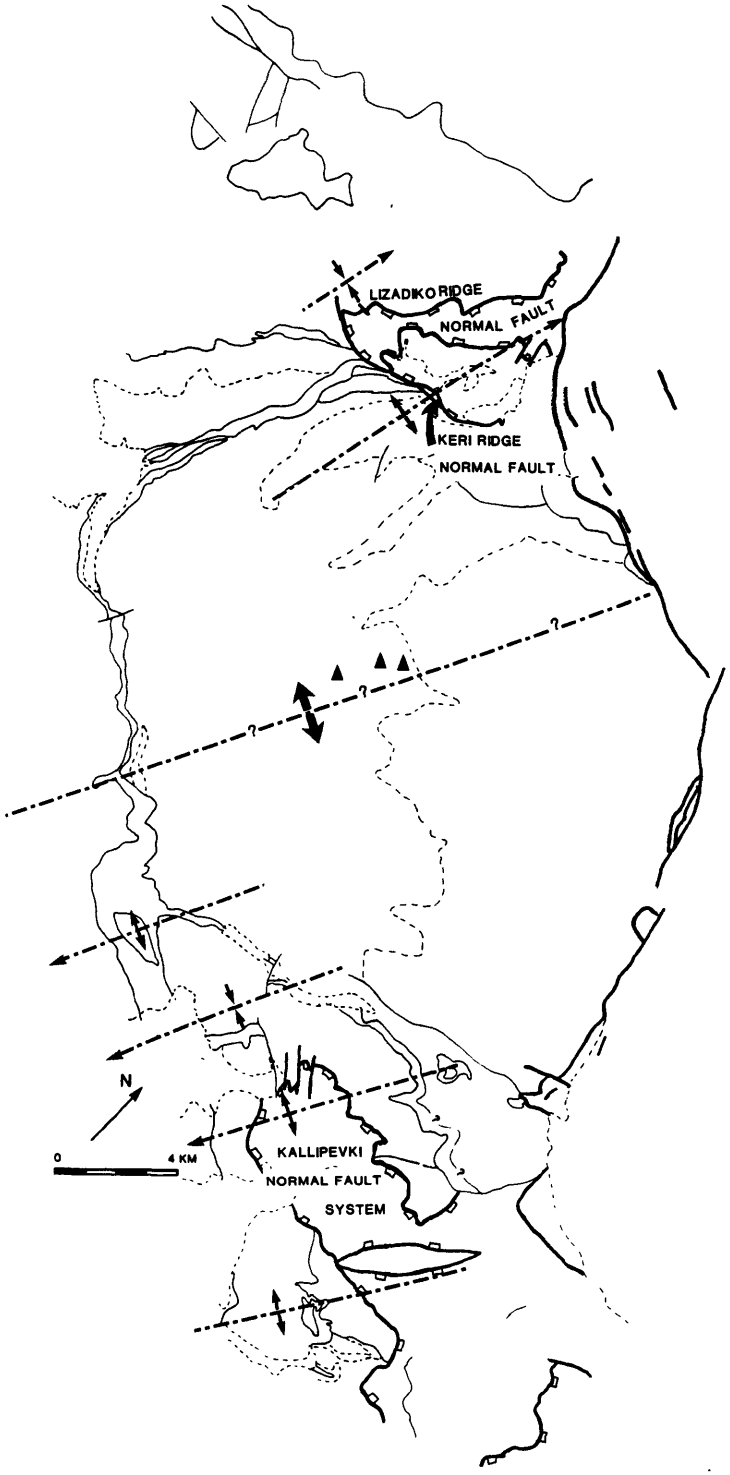

FIGURE 3.3C: Structures developed during D5, D6, and D7. D5 listric and low-angle normal faults are indicated with open boxes; D6 hinge traces are shown by dash-dot line.

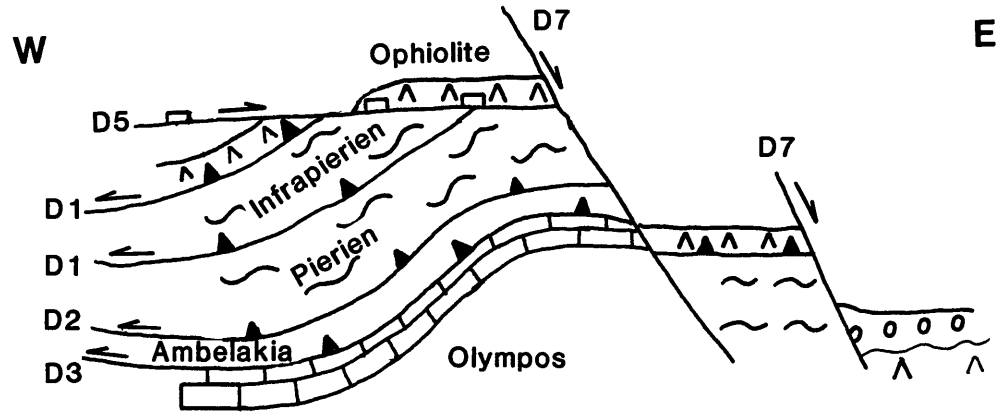

FIGURE 3.4. Diagram showing juxtaposition of tectonostratigraphic units in the Olympos region, and the age of faults between the units, as interpreted from structural and geochronologic data.

relatively poor in this area, these folds have been recognized on the basis of: 1) inverted stratigraphy both below and above the village of Paleambela; 2) small-scale recumbent folds visible in the calcareous schists and impure marble (cipolin) which mark the (locally inverted) depositional contact between the protoliths of the marbles and schists (Fig. A3.1; Fig. 3.5); and 3) parallelism of the dominant S1 greenschist-grade metamorphic fabric in the gneisses with the axial planes of the mesoscopic to map-scale folds in the marbles and gneisses, and the observation that this fabric is associated with microscopic isoclinal folds. F1 folds are characterized by extreme thinning in the limb regions. We were unable to determine the vergence of the largest scale fold trains; small-scale fold trains verge both NW and SE and are probably parasitic folds on larger structures.

In the Infrapierien unit, the Livadi nappe contains a well-developed compositional layering consisting of centimeter to meter-scale amphibolite and quartzofeldspathic gneiss segregations. A mineral lineation defined by amphiboles and elongate feldspar porphyroclasts shows a scattered trend because of later folding. Locally, F1 isoclinal folds are visible in mica schists (Fig. 3.6).

On the north flank of Trohalos ridge, amphibolitic gneisses of the Infrapierien (Livadi) unit occur in thrust contact above granitic gneisses of the Pierien unit (Thoma nappe). This thrust fault is associated with an S1 mylonitic fabric and S1 is also axial planar to large-scale F1 isoclinal folds (Plate 2, section D-D'). Locally, the thrust is involved in the F1 folds and is overturned, indicating that thrusting, mylonitization, and folding were part of a single progressive deformation. A well-developed quartz stretching lineation and feldspar porphyroclast elongation lineation within S1 trends S45-65 W, approximately parallel to the isoclinal fold axes (Fig. A3.2).

The Pierien unit contains a metamorphic compositional layering and variably-developed mylonitic fabric throughout the thrust sheet. This foliation generally dips NW to SW around most of the western and southern margins of the Olympos window, and locally an intersection lineation is present, that plunges from NW- to SW. The variation in plunge is due to overprinting by later structures.

In the Pieria mountains Yarwood and Dixon (1977) attribute ENE to E-trending mineral lineations and mylonitic schistosity to deformation within the Paleozoic Pierien granodioritic and metasedimentary rocks. Later E-W trending folds and intersection lineations in the underlying Infrapierien amphibolitic and quartzofeldspathic schists are thought to be related to emplacement of the Pierien

unit over the Infrapierien unit and the Livadi ultramafic complex (Yarwood and Dixon, 1977; Nance, 1981). These workers consider the thrusting to be due to a much younger deformational event, however this interpretation is contradicted by their own isotopic data (see below).

Ambelakia unit

In the Ambelakia unit, a pre-S2 greenschist- to blueschist-greenschist transition facies metamorphic foliation is visible as floating fold hinges on a mesoscopic to microscopic scale within the marbles and schists and is regarded as an S1 foliation (Fig. 3.7). A NE-SW trending intersection lineation is present, but the high strain related to F2 folds has strongly obscured geometric and kinematic characteristics of possible D1 structures as they may have been rotated into parallelism with D2 and D3 structures.

D1 relative timing

The timing of D1 events is not well-constrained in the study area due to overprinting by younger events. In the Pieria mountains to the north, and to the west in the Kamvounia mountains, where younger events are less penetrative, D1 structures in Flambouron rocks are associated with greenschist and amphibolite facies fabrics, in contrast to the blueschist-facies fabrics associated with younger events. On the flanks of Mt. Olympos we correlate structures formed during greenschist and higher grade metamorphism in the Pierien and Infrapierien units with D1 structures that are visible further west and northwest. Evidence presented by Yarwood and Dixon (1979) suggests that D1 may be polyphase; however, we cannot distinguish more than one distinct pre-D2 event in most of the study area.

Because the Paleozoic granitic rocks and their wall rocks and the overlying Triassic-Jurassic marbles are affected by structures attributed to D1, these events must be post-Jurassic. Similar grade M1 metamorphism in the Pierien and Infrapierien units, and in the ophiolitic rocks, thought to be Jurassic in age, in the Livadi area, may indicate that D1 is related to emplacement of the ophiolitic rocks on the continental margin. However, elsewhere in the study area, pre-emplacement structures within the ophiolite unit that may be equivalent in age and metamorphic grade to D1 are not associated with subsequent (D2-D4) structures that are similar to those of the underlying units. This suggests that, except in the Livadi area, "D1" in the ophiolite occurred in a location that was separated from that of the Flambouron and Livadi ophiolite units, and that the final ophiolite emplacement was a much younger event (see D5). The majority of occurrences of

FIGURE 3.5. Outcrop photograph of F1 fold in marble of the Infrapierien (Paleambela) unit. Note well-developed axial planar cleavage S1. Coin in photo is the same size as a nickel.

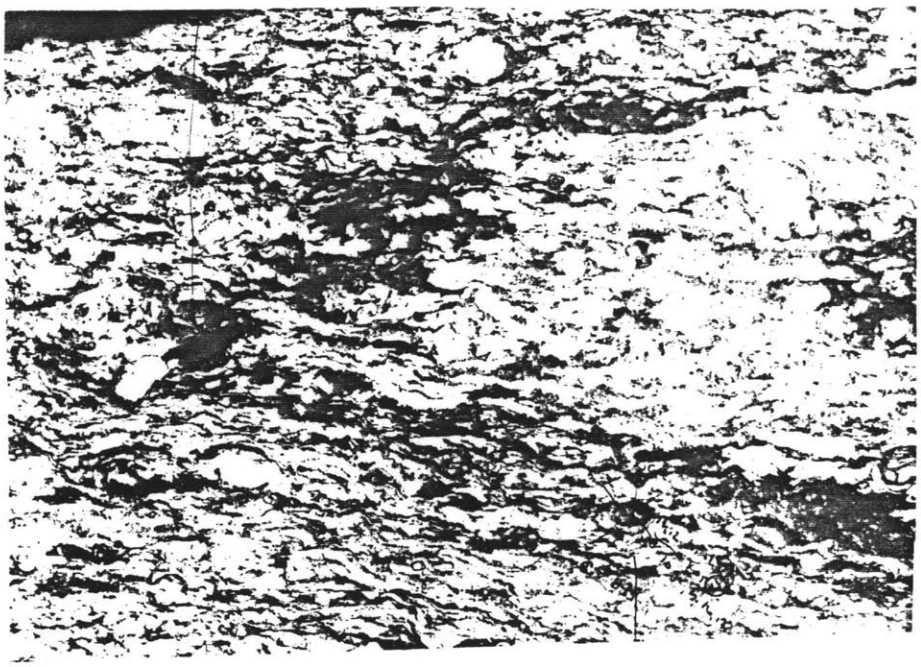

FIGURE 3.6. Photomicrograph of an F1 fold in a garnet-biotite-muscovite schist from south of Livadi village. Sample 85LI2a. Plane light, field of view ~2 cm long

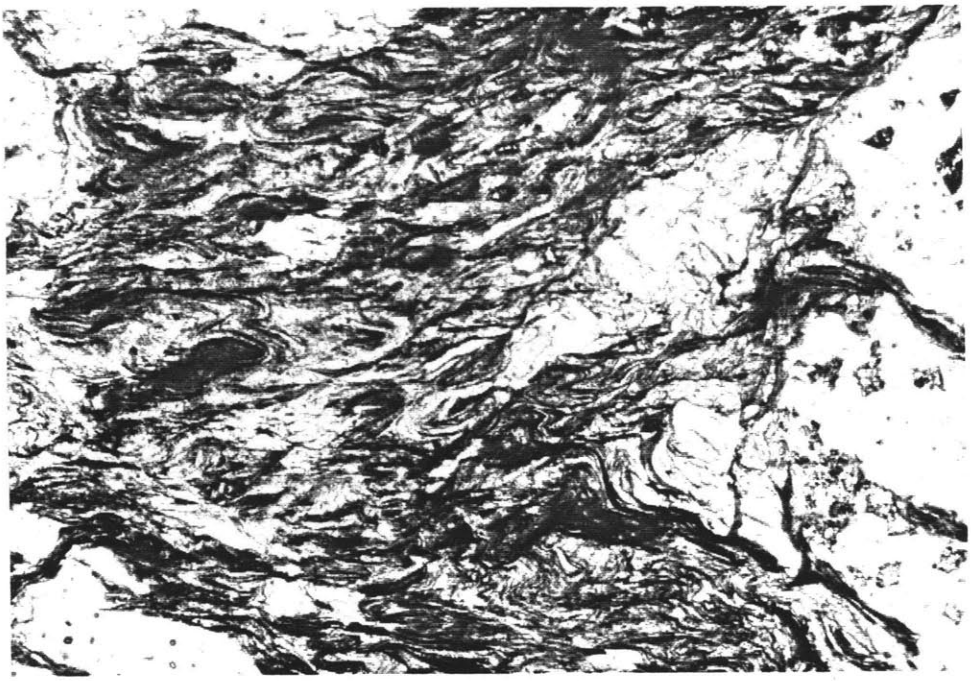

FIGURE 3.7. Photomicrograph of floating hinges of F2 folds in calcareous schist from the Ambelakia unit. F2 folds fold a foliation that contains Na-amphibole + chl + act. Plane light, field of view 4 mm.

ophiolitic rocks in the study area are serpentinite matrix melange containing blocks of metavolcanic rocks, marble, and mica schist; structures associated with the melange cut across the structural and metamorphic fabrics in the ultramafic and mafic rocks as well as the blocks in the melange, and thus must be related to a later event.

In the Flambouron units, D1 structures are clearly refolded by later folds and cut by the faults which juxtapose the units against the Ambelakia and Olympos units. The D1 gneissic fabric in the metagranitic and metaclastic rocks occurs several kilometers above D2 thrust faults and is cut by the mylonitic fabric associated with these thrust faults. For example, in the Trohalos area, the Sparmou and Olympos thrusts cut and transpose the fabric that is parallel to contacts between gneiss, amphibolite schist, and marble of the Pierien unit (Plate 1; Plate 2, sections C-C', D-D').

In the Ambelakia unit, we have no constraints on whether structures attributed to D1 may instead be an early phase of D2. The M1 metamorphic grade in the Flambouron units is upper greenschist to lower amphibolite facies; in the Ambelakia unit, M1 appears to be greenschist or blueschist-greenschist transition facies. In contrast, the M2 metamorphic grade is similar in both units, suggesting that the Ambelakia and Flambouron units were not juxtaposed until D2 (Figures 3.3, 3.4; Table 3.1).

Absolute timing constraints

Yarwood and Dixon (1977) obtained Rb-Sr internal isochron ages of 119±3 Ma and 116±5 Ma on deformed granitic rocks of the Pierien unit in the Pierien mountains and Barton (1976) obtained mica-whole rock ages of 124±4 and 123±11 Ma from mylonitic granites near Karia. Yarwood and Dixon (1977) also obtained an Rb-Sr internal isochron age of 101±2 Ma on augen schists from the Infrapierien (Livadi) unit, and interpreted the data to represent two distinct events, the first in Cretaceous time, and the second in post-Late Cretaceous time, interpreting the younger age as a maximum. Ar-Ar step-heating analysis of white micas from the Infrapierien (Livadi and Paleambela) unit yields Ar-Ar isotope correlation (isochron) ages of 98±2 and 100±2, supporting occurrence of one or more middle Cretaceous events (Schermer et al, in press).

D1 kinematics

Because of the sparse nature of the data on D1 structures in the study area, it is difficult to place independent kinematic constraints on this event. The parallelism

between F1 isoclines and mineral lineations, and the inconsistent vergence of F1 fold trains, suggests that these folds may have formed parallel to the transport direction (e.g. Hansen, 1971), which would then be along a NE-SW vector. Oriented samples were collected from mylonite zones within the Infrapierien (Livadi) and Pierien (Thoma) units and from rocks adjacent to the thrust fault contact between these two units as well as from rocks above and below the fault at the base of the Livadi ophiolite complex. While the stretching and mineral lineations in these samples generally trend NE-SW, the sense of shear, as determined by S-C fabrics, asymmetric augen structures and pressure shadows, and deformation lamellae in quartz (e.g. Lister and Snoke, 1984; Simpson and Schmid, 1983), is only moderately consistent. Of 18 samples that contain probable D1 lineations that were collected from the Infrapierien and Pierien units well above the Sparmou (D2) thrust, five have poorly-developed or ambiguous fabrics, two show NE shear sense, two show SE shear sense, and nine show SW-directed shear (Fig. 3.8). Figure 3.9 shows a moderately well-developed asymmetric fabric in a micaceous gneiss. Unfortunately, the oriented samples collected from the base of the Livadi ophiolite nappe yielded an ambiguous sense of shear, in part probably because the serpentinized rocks show a variable lineation and foliation direction, and the quartzofeldspathic rocks do not crop out abundantly in this area. One out of four samples yielded a SSW sense of shear while the other three contain poorly-developed and uninterpretable shear fabrics.

Although the sense of shear data do not conclusively demonstrate a SW direction of thrust emplacement, it will be argued below that a combination of structural, tectonostratigraphic, and geochronologic data constrain D1 thrust faults to have movement directions roughly similar to D2 and D3.

D2: latest Cretaceous to early Eocene blueschist-facies metamorphism and deformation

D2 deformation and blueschist-facies metamorphism affected the Pierien, Infrapierien, and Ambelakia units. Thrust faults and folds that we attribute to D2 deform the Flambouron and Ambelakia units under similar blueschist-facies metamorphic conditions, indicating that these units were juxtaposed at this time (Figs. 3.3, 3.4; Table 3.1). The ophiolitic rocks and the overlying carbonate cover may have experienced deformation and greenschist-facies metamorphism that was broadly coeval with D2 in the other units, however, the paleogeographic position of the ophiolite unit during this event is not well known. When compared with the continental units, the ophiolitic melange units exhibit significantly different

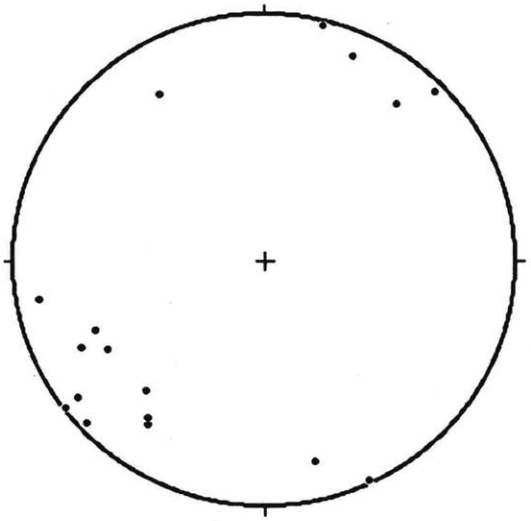

A

D1 mylonitic lineations

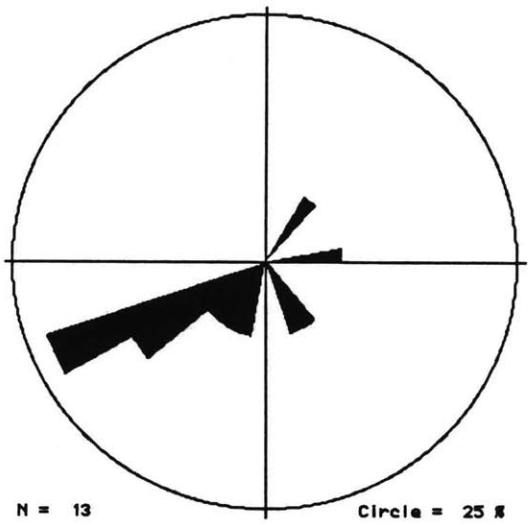

B

D1 sense of shear

FIGURE 3.8. A. Stereographic projection of stretching lineations from mylonites adjacent to D1 thrust faults. B. Rose diagram showing sense of shear as determined from microstructural analyses (see text for explanation).

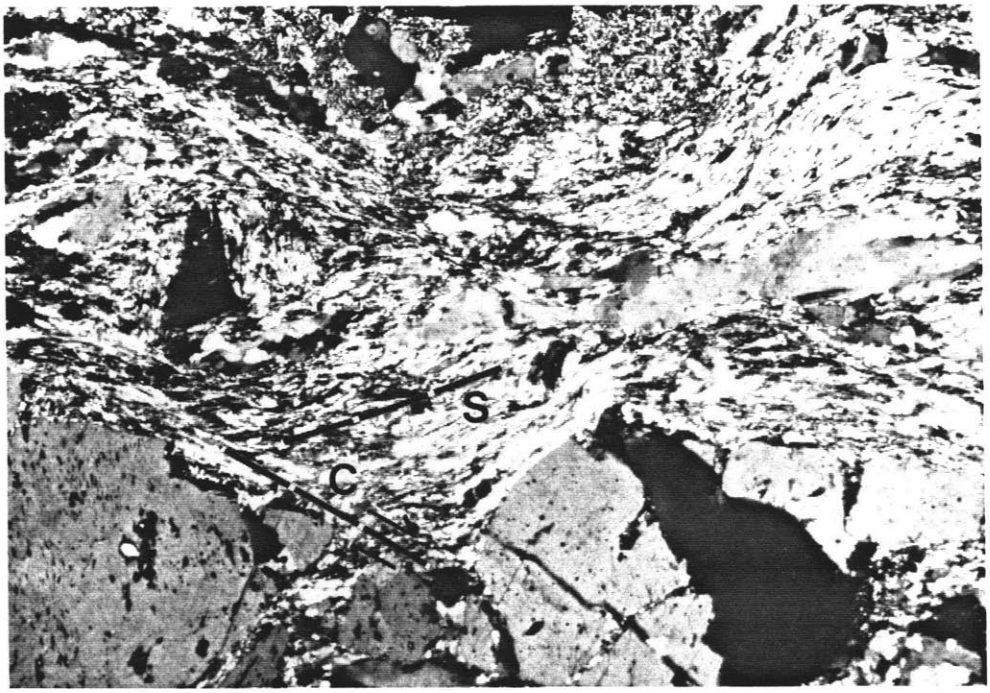

FIGURE 3.9 Photomicrograph of D1 S-C fabric in granitic gneiss from the Pierien unit Muscovite fish and quartz define S (~horizontal) and are dragged into C surfaces trending from upper right to lower left. Crossed nicols, field of view 4mm.

FIGURE 3.10. Isoclinally folded boudin of marble enclosed in sheared serpentinite. Knife in center of photo is 8cm long.

orientations of D2 structures and grade of M2 metamorphism, as well as a different deformational history between D2 and D5, thus we suspect that this part of the ophiolite nappe was widely separated from the Flambouron and Ambelakia units of the Olympos area during D2 deformation.

Ophiolite unit

Possible D2 structures occur in greenschist-facies calcareous schist and marble enclosed within the serpentinite-matrix melange of Lizadiko ridge. These consist of variably-oriented tight to isoclinal folds that fold the S1 foliation and contain a well-developed axial planar cleavage (Fig. 3.10). These folds have wavelengths from a few centimeters to several meters and are discordant to the foliation and folds in the surrounding ultramafic rocks. Igneous rocks of the ophiolite unit are commonly foliated, however the intensity of fabric development and the orientation of the foliation vary widely over short distances, so it is difficult to determine the large-scale geometric characteristics of this deformational phase. In some samples of the gabbroic and basaltic rocks two foliations are present that are interpreted to be S1 and S2 foliations. Both these foliations apparently formed under greenschist facies conditions. The second foliation is axial planar to tight folds that may be F2 folds. We have not identified structures correlative with D2 in ophiolitic rocks of the Livadi complex.

Infrapierien unit

D2 structures are irregularly developed in the Infrapierien unit. Perhaps because the internal stratigraphy of this unit is poorly known, we have recognized only a few large-scale isoclinal folds related to D2 within the Livadi and Ziliana thrust sheets (Fig. 3.3A). Small-scale isoclinal F2 folds are present in the Paleambela nappe. Many samples of Infrapierien gneiss, schist, and marble contain a NE-trending mineral lineation that is parallel to the axes of tight-to-isoclinal microfolds; these folds deform the S1 foliation and contain a variably-developed S2 axial planar foliation (Fig. 3.11). The mylonitic fabric associated with the thrust between the Livadi sheet and the Pierien marbles on Trohalos ridge (Plate 1, Fig.3.2) and the isoclinal folds that fold the thrust are attributed to D2. These folds plunge gently southwest and have axial planes sub-parallel to the thrust surface, (Plate 2, section E-E'). Small-scale tight-to isoclinal folds that are interpreted to be F2 folds are shown on Figure A3.3.

In Kato Olympos, amphibolite schists of the Ziliana nappe are folded about N50E-trending axes. The fold axes plunge gently both NE and SW, the vergence

FIGURE 3.11. A: F2 folds in marble with micaceous laminae, Infrapierien unit. The marble/schist laminae define S1, which is isoclinally folded about F2, with well-developed S2 cleavage. Knife at upper left is 8 cm long.

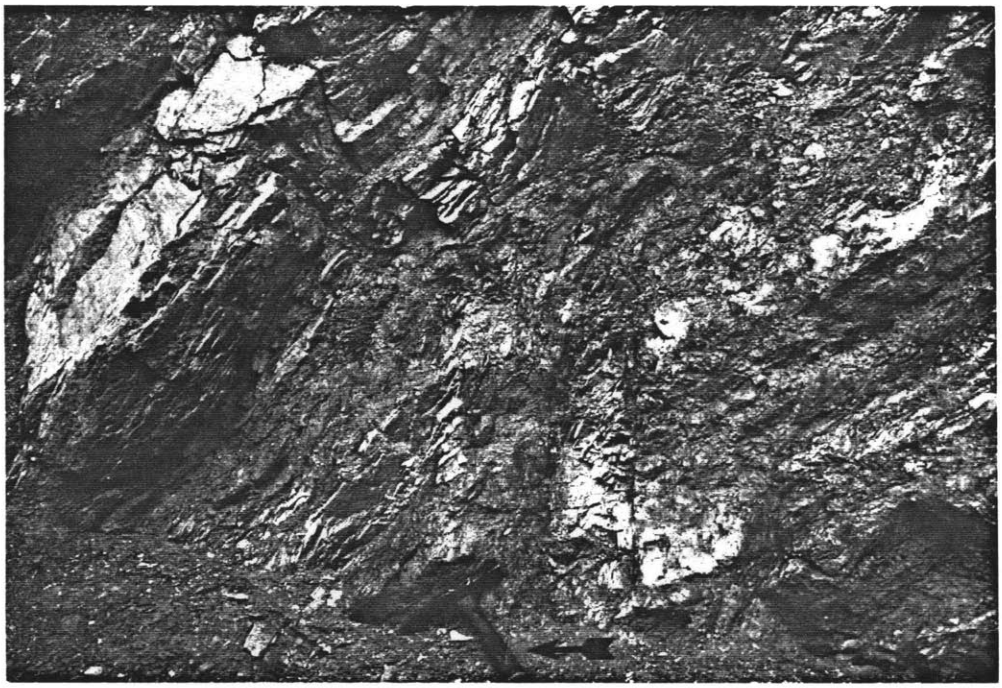

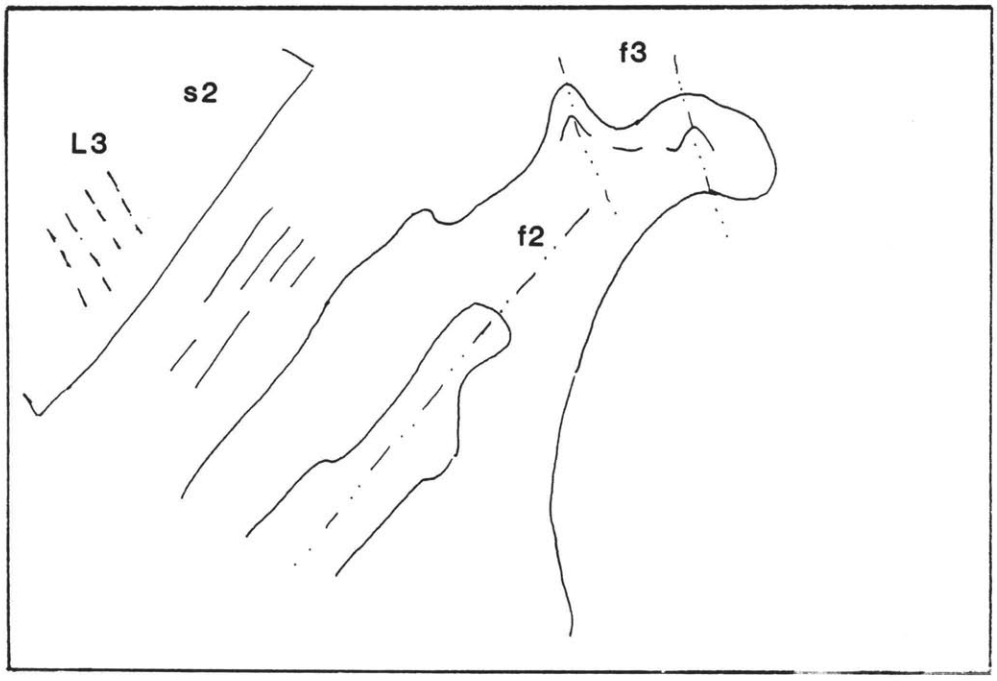

FIGURE 3.11B: F2 folds fold alternating granitic-amphibolitic layers in Infrapierien (Livadi) gneiss. Lineation on surface at left is intersection of F3 folds. Hammer handle is 30 cm long (arrow).

is dominantly NW, and axial planes commonly dip SE at ~35-60° (Plate 2, section I-I'). Amphiboles form a mineral lineation parallel to this fold axis and there is a well-developed axial planar cleavage.

In the Infrapierien units the D2 fabric is apparently associated with blueschist-greenschist transition facies metamorphism. M1 hornblende and actinolite are rimmed by a more sodic amphibole, and a relatively high-pressure phengite is contained in the S2 foliation plane with chlorite + epidote ± stilpnomelane (Schermer, in prep). However, M2 mineral assemblages are developed very irregularly throughout the Infrapierien unit. In the Paleambela nappe, no evidence of M2 phases was found, while in the Livadi nappe, the S2 fabric and M2 phase assemblages occur sporadically, though commonly in association with shear zones within the gneisses and near the contact with the underlying Triassic-Jurassic marbles on Trohalos ridge. In the Ziliana nappe all the samples examined appeared to contain M2 phases, yet M1 phases are only locally present and are difficult to recognize.

Pierien unit

The Pierien unit exhibits well-developed microstructures attributable to D2, however the homogeneous nature of the lithologies in this unit precludes recognition of large-scale structures except where the Sparmou thrust is affected. A well-developed mylonitic fabric is associated with blueschist-facies mineral assemblages in the granitic to granodioritic gneisses and mica schists in the area between Kokkinopilos and Kallipevki. Locally, F2 isoclinal folds are seen to fold the S1 fabric; transposition of S1 into S2 is nearly complete (Figure 3.12). Sodic amphibole and pyroxene (riebeckite-acmite) are aligned parallel to the stretching lineation defined by elongate quartz and feldspar grains that plunges S40-60W. This direction is also parallel to the fold axes of (F3) isoclinal microfolds that fold the S2 fabric (Figure 3.13). It is not known whether the entire Pierien thrust sheet in the Kato Olympos area is affected by D2 structures, as its entire outcrop area was not examined in this study. However, a transect through higher portions of the thrust sheet along the road south from Sikaminea (Fig. 3.2) revealed the presence of similar SW plunging lineations, blueschist facies mineral assemblages, and thin mylonite zones more than three km structurally above the Sparmou thrust, indicating that the Pierien unit in this area may be internally imbricated.

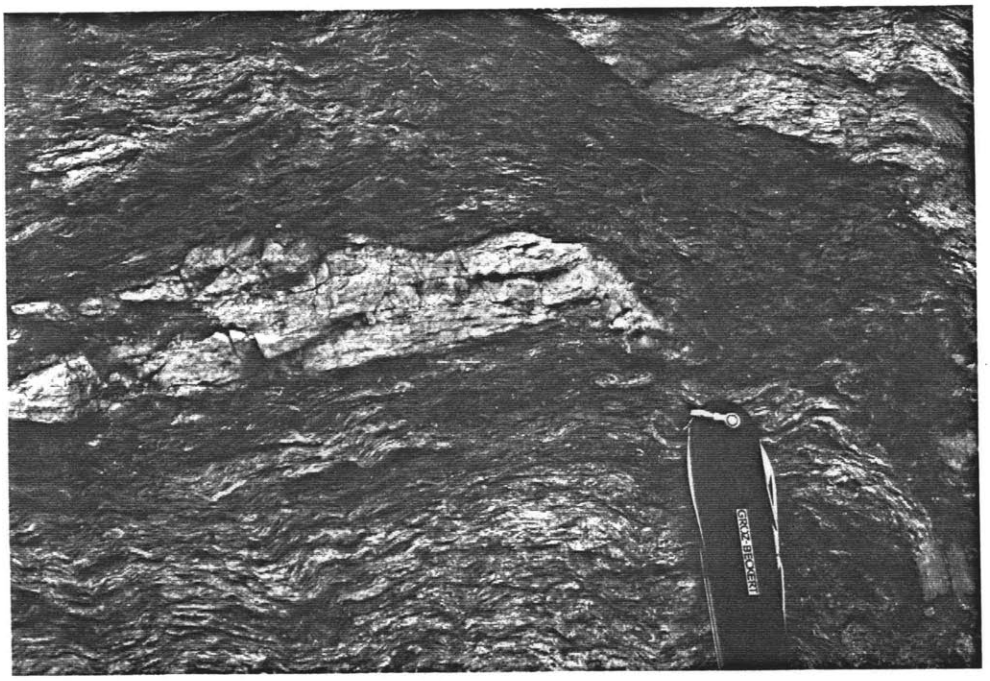

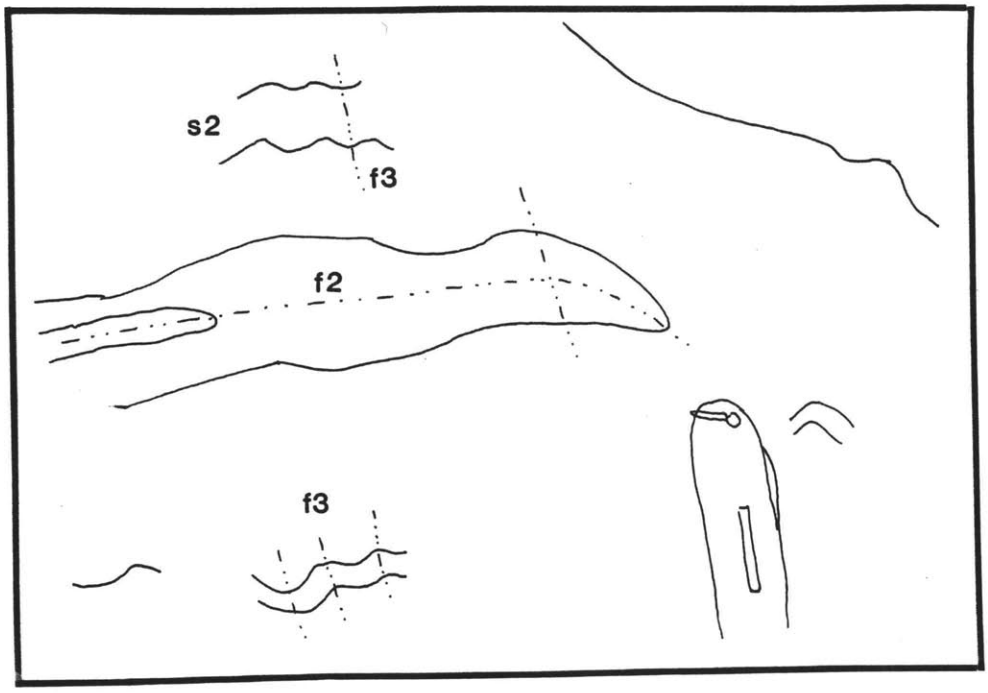

FIGURE 3.12. Isoclinal F2 fold in alternating blueschist and quartzofeldspathic gneiss of the Pierien unit. S2 mylonitic fabric developed parallel to the Sparmou thrust and was folded by later folds.

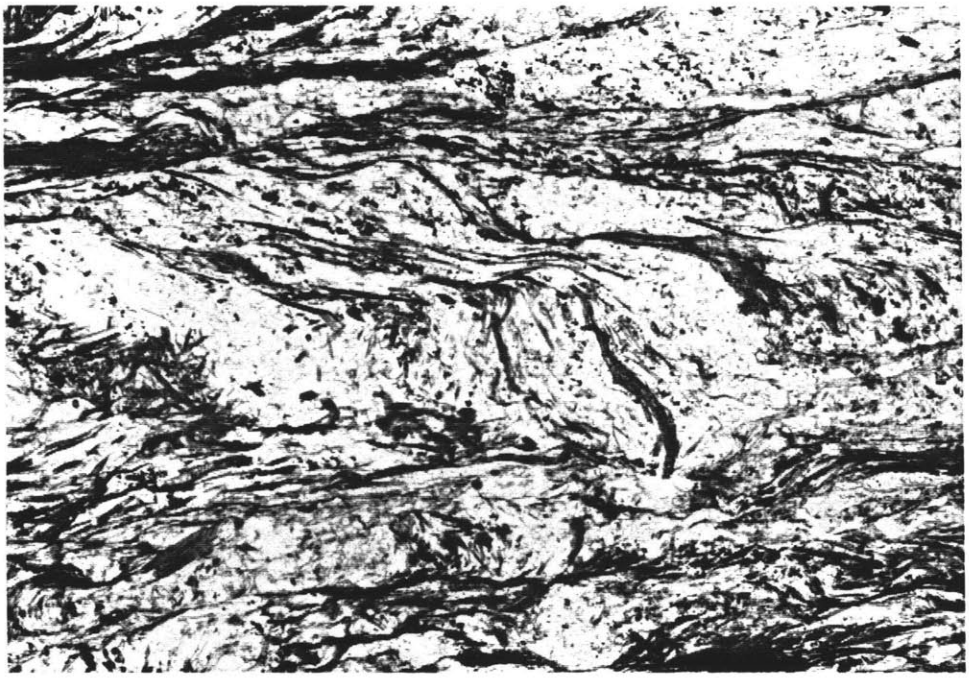

FIGURE 3.13. Photomicrograph of S2 fabric defined by phengite + riebeckite + acmite folded about F3 folds; S3 axial planear cleavage contains the same mineral assemblage. Riebeckite is dark, elongate mineral; acmite is lighter elongate mineral. Sample 85OL46. Plane light, field of view 4 mm.

Ambelakia unit

In the Ambelakia unit discrete small-scale structures associated with D2 are difficult to distinguish from those of D3 because they are generally parallel. The S1 fabric, outlined by cherty, dolomitic, and phyllitic layers in the marbles, and by the marble-schist compositional layering, is isoclinally folded about fold axes that generally trend NE, but scatter on the stereonet plot (Fig. A3.4a) due to later folding. A lineation is defined by mineral elongation in the schists and a calcite shape fabric in the marbles. This lineation is subparallel to F2 isoclinal fold axes (A3.4b).

The Sparmou thrust

The fault between the Pierien and Ambelakia units crops out over a large area, curving around from the northwestern to the southern to to the southeastern flanks of Mt. Olympos. This thrust fault is here named the Sparmou thrust after the excellent exposures in the area around Monastery Sparmou (Plate 1; Figs. 3.2, 3.3, 3.14). The Sparmou thrust was originally called the Olympos thrust (Godfriaux, 1968; Barton, 1975, 1976), when it was thought that the Ambelakia unit represented a more sheared equivalent or possibly different facies of the Olympos unit. However, with the recognition of blueschist-facies assemblages in this intermediate thrust sheet, Godfriaux, (1977) correlated it with similar rocks in the Ossa mountains further south called the Ossa unit. Arguments presented elsewhere (Chapter 2) and in Schmitt, (1983) support the correlation of this intermediate thrust sheet with the Ambelakia unit (which is thrust above the Ossa unit in the Ossa Mountains). Because the thrust fault below the Sparmou thrust contains the Olympos unit in the footwall, it is more properly named the Olympos thrust (discussed under D3 below).

The Sparmou thrust is associated with a well developed mylonite zone that is best-developed in the gneisses of the hanging wall and ranges in thickness from ~50-300 m, but strongly sheared rocks are present in thin parallel bands up to 1000 m above the thrust. A SW-plunging mylonitic lineation is commonly developed in both the hanging wall and the footwall, and structures related to non-coaxial shear parallel to the lineation are present both in outcrop (Fig. 3.15A) and in thin sections cut parallel to the mylonitic lineation (Fig. 3.15B). Quartz is dynamically recrystallized and occurs in various stages of recrystallization, including strained grains, grains with incipient and well-developed subgrains, ribbons, and aggregates of neoblasts (Fig. 3.15B). Local domains of strongly oriented crystallographic fabric are observed. Feldspars are commonly broken and

cracked; however, in some samples, incipient subgrains occur within the augen, and dynamically recrystallized grains occur along the perimeter of the augen, indicating the feldspars behaved ductiley during mylonitization (Fig. 3.16).

In the Kokkinopilos area, the Ambelakia unit and Pierien units are imbricated in a series of steeply west-dipping, anastomosing faults (Plate 1; Plate 2, section E-E'). F2 isoclinal folds also fold the Sparmou thrust east of Sparmou (Fig. 3.17) and in the Karfia ridge area, indicating that thrusting and folding were contemporaneous.

D2 relative timing

While many field relations indicate that, in general, D2 and D3 produced structures of similar style and orientation, cross-cutting relations can be distinguished at all scales. Constraints provided by Ar/Ar data also enable us to interpret these structures to be the result of two distinct structural events that occurred under similar P-T conditions.

Ophiolite unit

The local presence of two foliations in the igneous rocks of the ophiolite unit may indicate the overprinting of D1 structures by D2 (or younger events), however we were unable to define a general F2 phase in this unit. The principal difference between possible D2 structures in the ophiolite unit and those present in other units is that the former were clearly not formed under blueschist-facies conditions. Because the geometric and kinematic characteristics of D2 structures in the ophiolite unit have been obscured by later melange formation (D5?), we cannot correlate the structures on the basis of style. Some of the marbles and calcareous mica schists apparently depositionally overlie the ultramafic rocks (e.g. Lizadiko ridge, Plate 1; Plate 2 section C-C') and thus may be Upper Cretaceous in age (Maestrichtian; Godfriaux and Pichon, 1980); however, the carbonate rocks that overlap on ophiolites elsewhere in the internal Hellenides are Albian-Cenomanian (Mercier, 1968). Because these carbonate rocks are also greenschist-grade, the metamorphic event is constrained to be later in the Cretaceous or Tertiary, but its absolute age is unknown. Thus, we can not constrain whether this deformational event in the ophiolite unit belongs to D2 or younger events.

Infrapierien unit

In the Infrapierien unit, F2 folds clearly fold the earlier S1 fabric, and D2 faults cut across S1 and produce a mylonitic fabric parallel to S2. The thrust fault

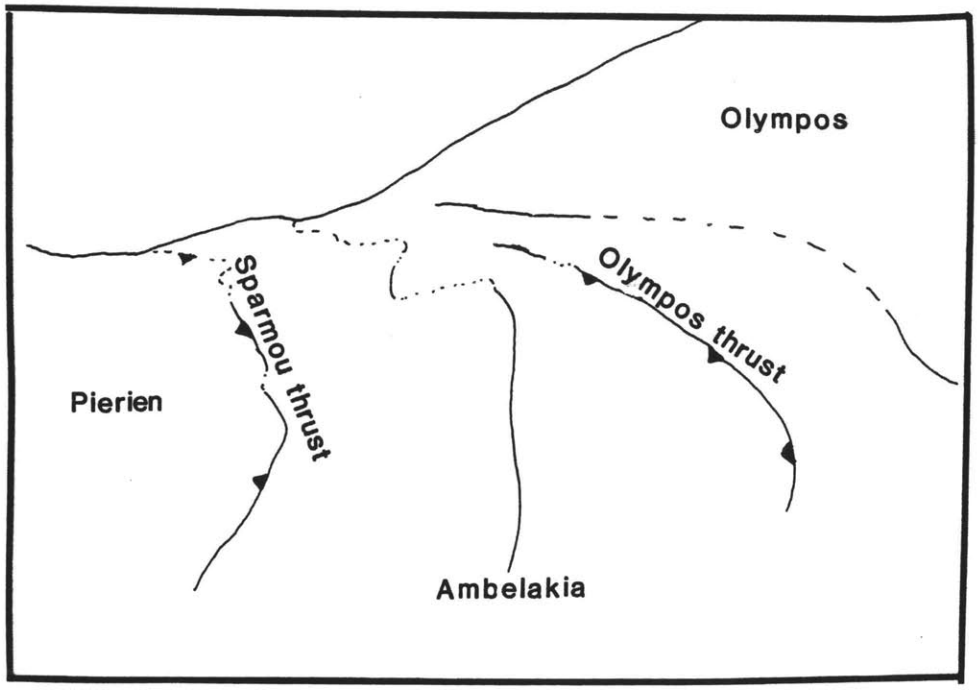

FIGURE 3.14. View of Olympos and Sparmou thrusts from southern margin of Olympos window, near Monastery Sparmou. View toward NW; thrusts dip to SW. In this area the Olympos thrust is located in a strongly mylonitic zone between flysch of the Olympos unit and calcareous greywacke of the Ambelakia unit (overlain by the marble which forms the ridge in the center of the photo). The Sparmou thrust is defined by the contact between mylonitic gneiss of the Pierien unit above, and marble of the Ambelakia unit below.

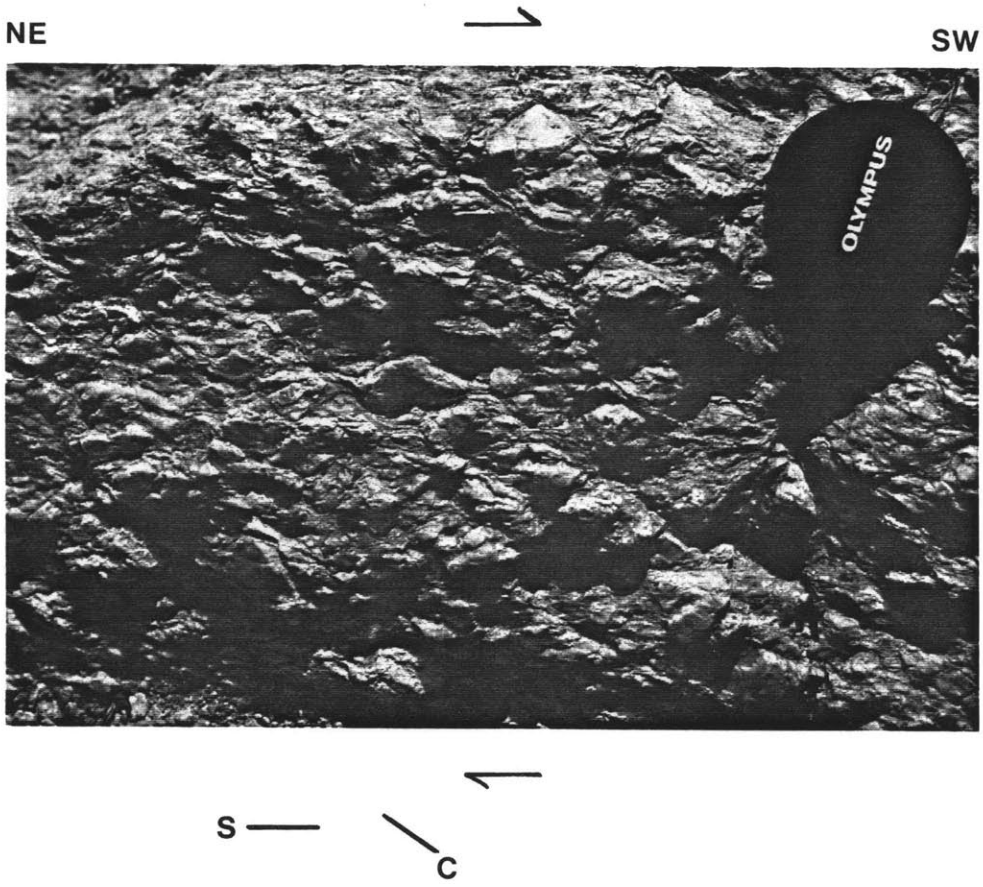

FIGURE 3.15. Sense of shear indicators along the Sparmou thrust. In both photos, SW is to right; sense of shear is top-to-SW. A: Outcrop of sample 85LI12 showing well-developed assymetric augen and S-C fabric.

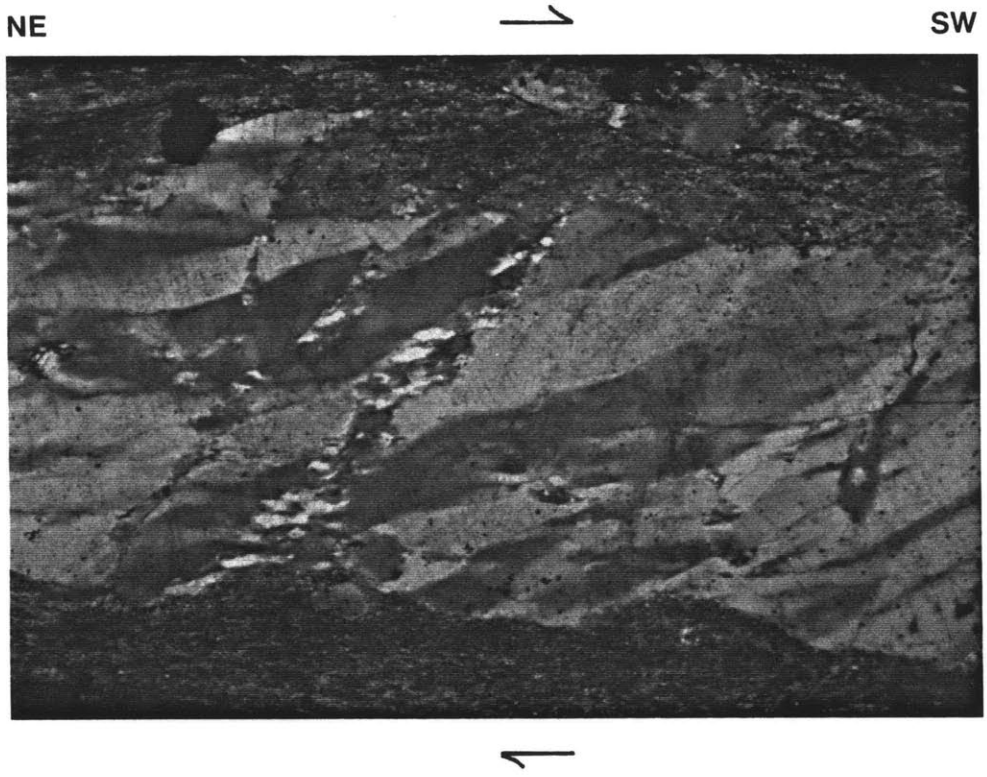

FIGURE 3.15B: Photomicrograph of quartz deformation textures in sample 85LI13. Coarse quartz grain in center has deformation bands inclined in the direction of shear, a tension crack with newly recrystallized quartz, and deformation bands within the small grains in the crack all give the same shear sense. C-planes are parallel to the long dimension of the photo. Field of view is 4 mm, crossed nicols with gypsum plate inserted.

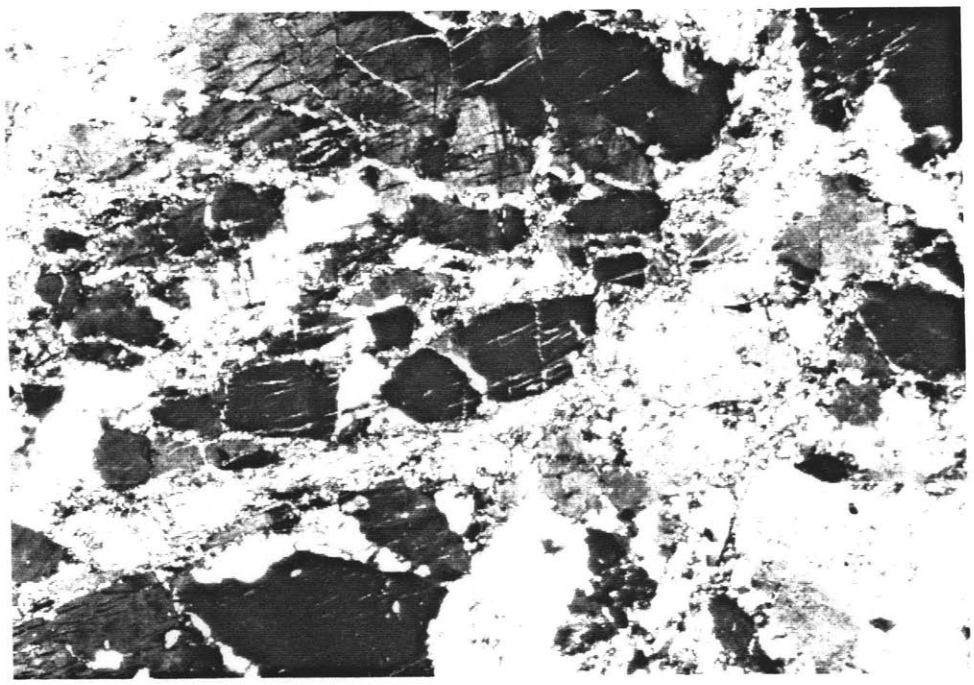

FIGURE 3.16. Photomicrograph of coarse K-feldspar augen in a mylonite from <30 m above the Sparmou thrust. This grain exhibits both brittle and ductile deformation features; part of the grain is cracked while part of it contains subgrains with serrate boundaries or surrounded by very-fine-grained neoblasts. Crossed nicols, field of view 4 mm.

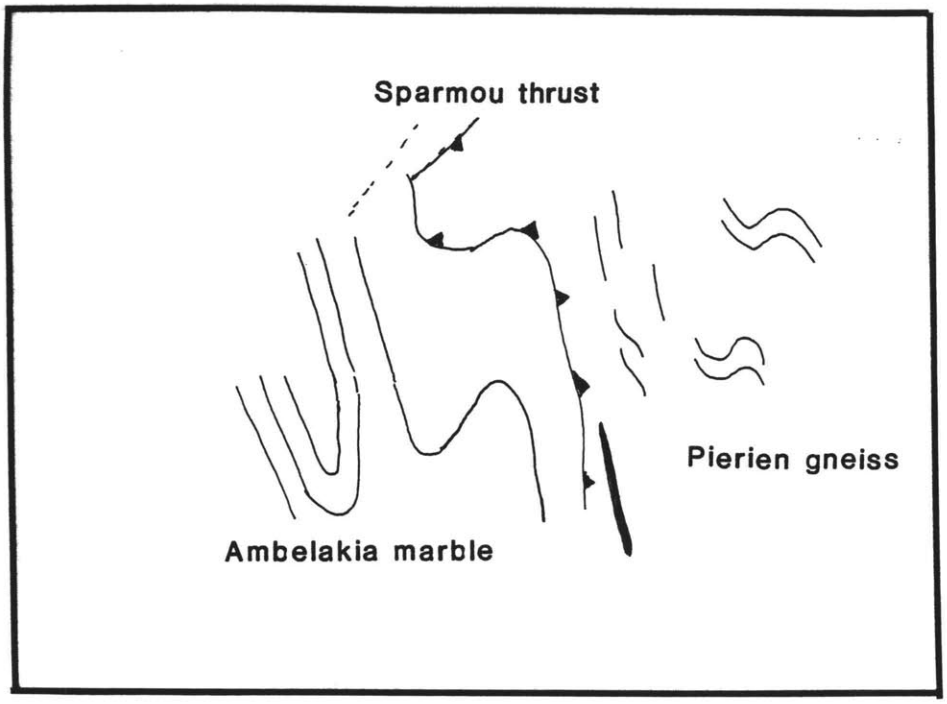

FIGURE 3.17. Photograph of the Sparmou thrust folded by F2, or possibly F3 fold. Axial planar surfaces and shear planes associated with folds such as this one are parallel to the mylonitic fabric associated with the Sparmou thrust. Pencil for scale.

between the Livadi sheet and the Pierien marbles appears to cut the D1 thrust fault between the Livadi nappe and the Pierien (Thoma) nappe, although the two surfaces are subparallel at the NE end of Trohalos ridge. Ar/Ar dating of white micas from mylonitic samples collected from <50 m above the D2 thrust fault indicates partial Ar loss from the white micas that is interpreted to reflect movement along this thrust fault at ~55-64 Ma, and white micas from a mica schist with well-developed S2 yielded a 63.3±1.7 Ma plateau age, thus constraining D2 in the Infrapierien unit to the latest Cretaceous to Paleocene time (Schermer et al, in press).

Pierien and Ambelakia units

As discussed above, D2 structures cut across, fold, and transpose the metamorphic layering that was developed during D1 and D0. In the Ambelakia unit, isoclinal F2 folds are coaxially refolded about isoclinal F3 folds, forming type 3 (Ramsay, 1967) interference patterns (Fig. 3.18).

Ar/Ar ages on several mica samples from near the Sparmou thrust are interpreted to represent the age of blueschist metamorphism and mylonitic fabric formation at 53-55 Ma. Pierien samples from >450 m above the thrust yielded slightly older ages, including one plateau at 61.7±0.8 Ma, so that blueschist metamorphism may have begun during Paleocene time, and continued during Eocene movement along the Sparmou thrust (Schermer et al, in press).

D2 kinematics

As discussed above, coherent kinematic data on D2 structures in the ophiolite unit are not well preserved. The lack of correlative D2 structures between the ophiolite melange and the Flambouron and Ambelakia units, and the different P-T conditions of deformation suggest that at least the Lizadiko ridge and Kallipevki parts of the ophiolite unit may have been widely separated from the other units during D2 deformation and metamorphism.

The mylonitic fabric associated with the Sparmou thrust contains variably developed shear-sense indicators. These include S/C fabrics, asymmetric feldspar augen and pressure shadows, and oblique elongate recrystallized quartz grains and subgrains. Although many samples contained ambiguous evidence for the shear direction (either no indicators or both up- and down-plunge senses), the majority of samples show a SW-directed sense of shear. Figure 3.19A shows a summary of all the samples collected and a rose diagram indicating the shear sense for D2 and D3 mylonites where it could be determined (27 out of 42

samples). The variation in trend from S30W to S70W is the result of later folding, which has not been removed in this diagram, but is not significant enough to change the quadrant in which the lineations plot on the rose diagram. Several samples were cut perpendicular to the lineation in order to confirm that the displacement direction was parallel to the lineation. In all cases, no dominant shear sense could be determined from the perpendicular sections. This observation suggests that the formation of NE-trending isoclinal folds does not reflect transport of thrust sheets perpendicular to the fold axes, as interpreted by Schmitt (1983), but instead reflects either rotation of the fold axes into the transport direction or initiation of the folds in this direction.

D3: Late Eocene SW-directed emplacement of metamorphic nappes over the Olympos carbonate platform

D3 structures are the first to affect the Olympos unit, and are also well-developed in the Ambelakia and Flambouron units. This event resulted in the juxtaposition of the blueschist and greenschist facies metamorphic rocks against the very low-grade Olympos carbonates and flysch along the Olympos thrust (Fig. 3.3B; Plate 1). The structures grouped in D3 appear to represent a complicated sequence of folding and thrust faulting; however, they are correlated and grouped together on the basis of similar style, kinematic significance, and age (both relative to D2 and absolute). We can distinguish three categories of close- to isoclinal folds on the basis of their ages relative to movement along the Olympos thrust: $F3_a$=pre-thrust folds; $F3_b$=syn-thrust folds, and $F3_c$=post thrust (but pre-F4) folds. All of these folds are subparallel, and we cannot group every fold observed in the field unequivocally into one or another of these categories.

Pierien and Infrapierien units

In the Pierien and Infrapierien units microscopic tight- to isoclinal $F3_b$ folds commonly fold the S2 fabric, and have an associated S3 axial planar foliation developed parallel to the Olympos thrust (Fig. 3.13). Mesoscopic F3 folds are indistinguishable from F2 folds, however the large-scale tight to isoclinal folds in the Kato Olympos region (Fig. 3.3B; Plate 2, section I-I') affect the Infrapierien, Ambelakia, and Olympos units together, and thus are interpreted to be $F3_c$ structures.

Ambelakia unit

A penetrative S3 mylonitic fabric occurs in the hanging wall of the Olympos thrust in the calcareous schist and marble of the Ambelakia unit. This foliation is parallel to the axial planes of refolded F2 isoclinal folds; the F3 fold axis is parallel to the mineral lineation in the schists and marbles (Fig. A3.4). Glaucophane, phengite, chlorite, and minor lawsonite are diagnostic blueschist facies minerals that occur parallel to the foliation planes (see Ch. 5 photos). Clasts within local pebbly layers in the calcareous flysch exhibit a strong flattening perpendicular to the foliation and elongation parallel to the mineral lineation. The limbs of F3 folds in the Ambelakia unit are commonly extremely thinned.

Olympos unit

In the Olympos unit, both the flysch and carbonate rocks contain an early $S3_a$ solution cleavage that is locally associated with isoclinal folds visible in thin section and outcrop as floating hinges (Fig. 3.20A). This cleavage is folded by small-scale tight- to isoclinal N50E trending $F3_b$ folds that plunge both NE and SW and generally have steeply NW-dipping axial planes (Fig. 3.20A). Mesoscopic $F3_b$ folds occur as parasitic folds to the map-scale overturned syncline in the flysch NE of Kokkinopilos (Plate 1, Fig. 3.3B; Fig. 3.20B). The hinge surface traces of F3 folds appear to wrap around the margin of the window following the trend of the thrust fault (Fig. 3.3B). Locally, $F3_b$ folds appear to be cut by the thrust fault, but the thrust is also folded by close- to tight $F3_c$ folds, for example on Voulgara ridge and in the Karfia ridge area (Plate 2, sections C-C' and I-I' respectively). Because the superposition of folding and faulting is not consistent, and the kinematic significance of both is apparently the same (see below), we interpret both the folds and the Olympos thrust to be D3 structures.

For >800 m structurally below the Olympos thrust, a stretching lineation formed by quartz and feldspar grains in the flysch and by a calcite shape fabric in the limestones is present. This lineation is oriented ~N50E, sub-parallel to the fold axes, although both stretching lineations and fold axes are dispersed by younger folding (Fig. A3.5). A well-developed mylonitic fabric $S3_b$ occurs in the thin sliver of flysch which crops out parallel to the Olympos thrust from the northern to the southeastern margin of the window. The mylonitic flysch contains asymmetric augen and pressure shadows; locally both S and C planes are developed (Fig. 3.21). There is strong flattening perpendicular to the schistosity and elongation parallel to the inferred transport direction. Prehnite-pumpellyite facies

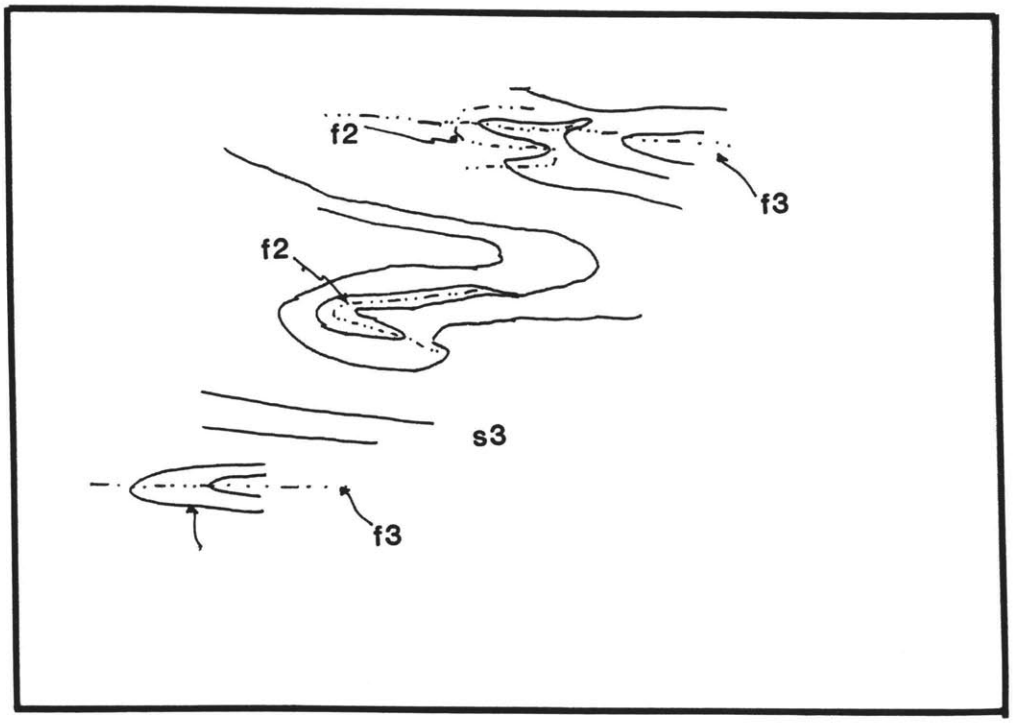

FIGURE 3.18. F2 isoclinal folds in cherty marble of the Ambelakia unit are coaxially refolded about F3 axes. The fold axes trend plunge 10-40, S40-60W, subparallel to the mylonitic lineation associated with the Olympos thrust.

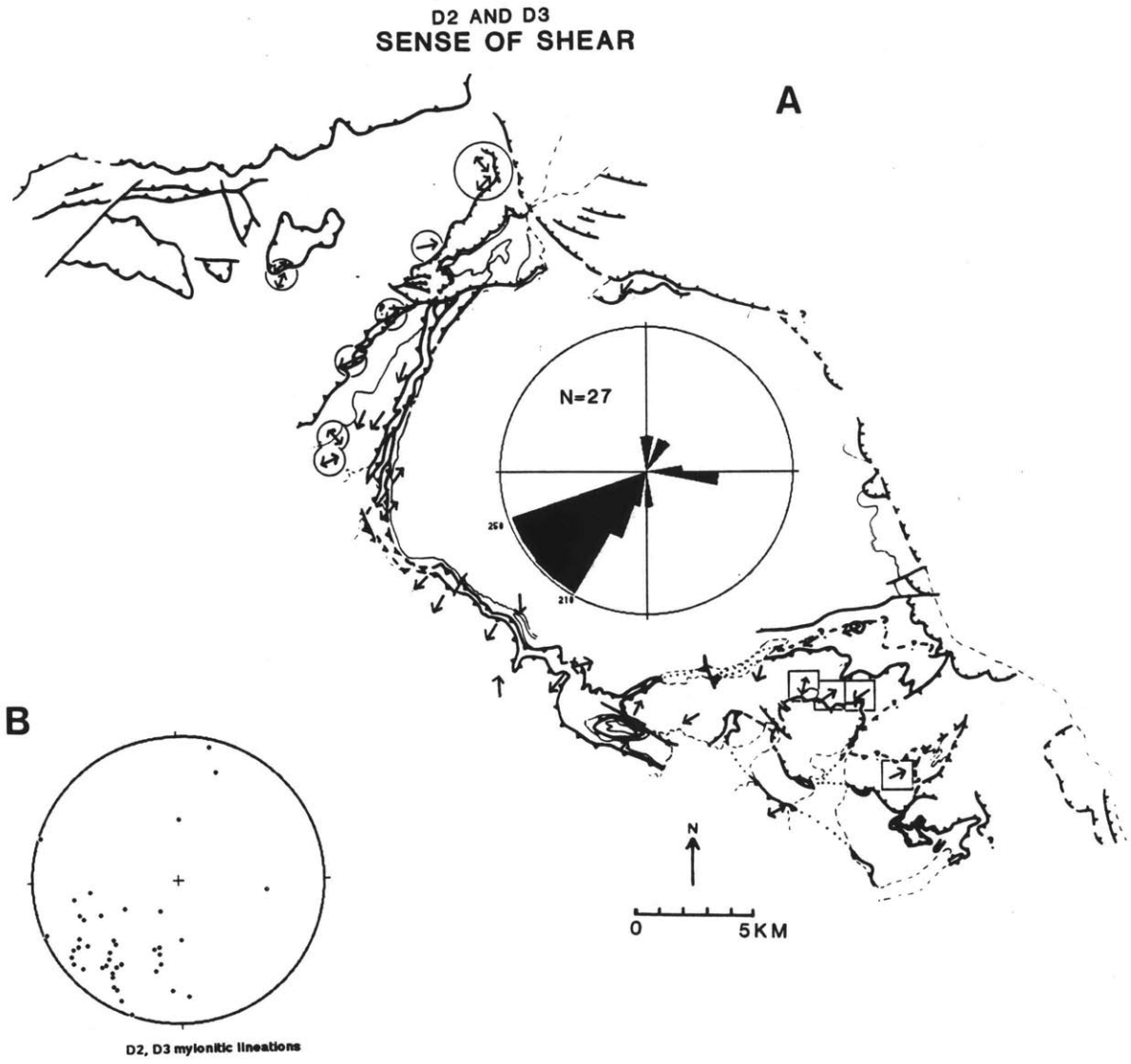

FIGURE 3.19. A. Map showing location of oriented samples used to determine sense of shear along major faults. Direction of arrow shows direction of shear sense, two-headed arrows indicate that microstructures were ambiguous. Samples thought to be related to D1 structures are circled; those thought to be related to D5 structures are enclosed in boxes; other samples are related to D2 and D3. If more than one sample was collected from an outcrop and all gave the same sense of shear, the average direction is plotted on the map. B: Lower hemisphere equal-area steronet plot of mylonitic lineations produced during D2 and D3.

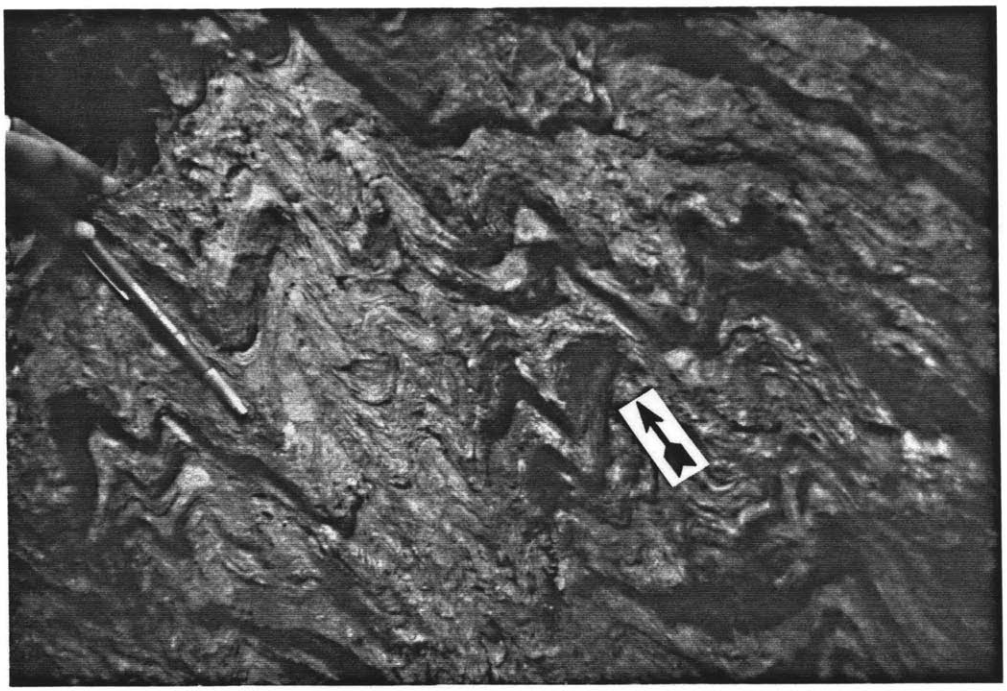

FIGURE 3.20. F3 folds in flysch of the Olympos unit. A. $F3_b$ folds with moderately well-developed spaced cleavage, in alternating argillite and fine sandstone and siltstone. Axial surfaces dip steeply NW. An $F3_a$ fold hinge is indicated by the arrow.

FIGURE 3.20B. $F3_c$ folds in micaceous flysch are more open than $F3_b$ folds and tend to have more rounded hinges and poorly-developed axial planar cleavage. Both folds trend NE-SW.

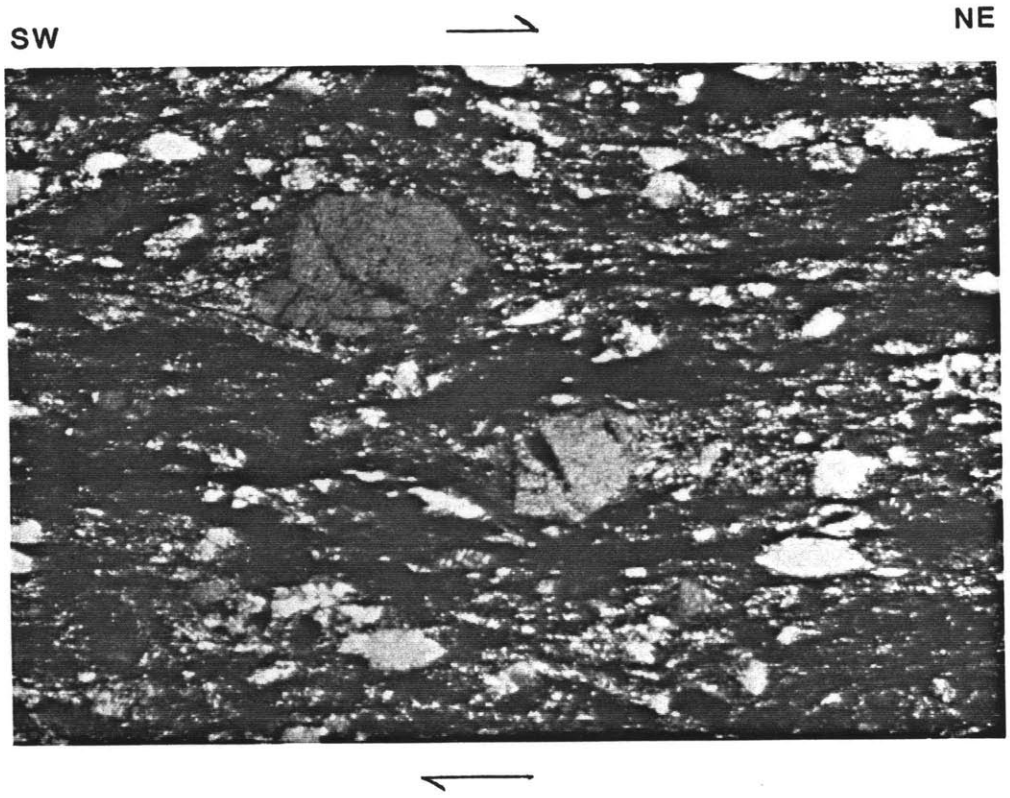

FIGURE 3.21 Photomicrograph of mylonitic fabric in Olympos flysch. Detrital grains are still visible, foliation is formed by phengite + chlorite + pumpellyite. Sample 86OL2 from the western limb of the large F4 antiform between Kriovrissi and Karia. Sense of shear is top-to-NE. Crossed nicols, field of view 4 mm.

metamorphism synchronous with mylonitization is indicated by the presence of phengite + chlorite + pumpellyite ± lawsonite in the foliation planes.

The Olympos Thrust

The Olympos thrust is defined by the mylonite zone which separates the Olympos unit from the Ambelakia unit. The Lutetian age of the rocks in the footwall constrain the age of deformation to post-middle Eocene time (Godfriaux, 1968; Schmitt, 1983). Within the shear zone, it is commonly difficult to distinguish the Ambelakia unit from the Olympos unit. The quartzofeldspathic flysch of the Olympos unit and the calcareous schist and psammite of the Ambelakia unit appear very similar when strongly deformed, and because neither rock type is resistant, the outcrop is generally poor along the contact zone. The Olympos crystalline limestones are generally darker-colored and less-well foliated than the Ambelakia marbles; the latter also commonly contain distinctive white cherty layers and/or greenish-blue phyllitic laminae. However, a band of platy, strongly foliated and lineated, medium-grey pure marble occurs between the two units on Voulgara ridge and in the area NW of Sparmou (indicated by KTl? on Plate 1). Although locally a mylonite zone separates this marble from the Ambelakia marble and a slightly(?) disturbed depositional contact with metasediments attributed to the flysch is present, in other locations (e.g west of Karia) it appears to be in depositional contact with calc-schists attributed to the Ambelakia unit. Due to the extreme strain and isoclinal folding in the thrust zone, we cannot tell whether the stratigraphy in these rocks might be inverted.

The most easily mapped contact occurs between the metaclastic rocks and the overlying cherty and/or platy marbles, so in the absence of more conclusive evidence for the location of the Olympos thrust, we have interpreted this contact as the thrust fault. However, where an unequivocal fault relationship is present within the zone of metaclastic rocks or between different marbles, we have located the thrust at such contacts (e.g. Fig. 3.14). In some cases it is only possible to note that the base of the platy marble seems to be in depositional contact with flysch, but near the Sparmou thrust, the (apparently same) marble band contains the chert and blueschist-grade phyllite layers characteristic of the Ambelakia unit, so that the thrust must lie somewhere within the mylonitic marble (e.g. see the area between Sparmou and Kokkinopilos Plate 1). In all cases however, the significance of the Ambelakia unit remains the same: it is a thin, highly deformed sliver of blueschist-

facies continental margin carbonate and clastic rocks that was thrust over the Olympos platform in post-middle Eocene time.

D3 relative timing

In the Pierien and Ambelakia units, D2 and D3 structures are commonly parallel and difficult to differentiate. Nevertheless, the Sparmou and the Olympos thrusts are distinct, and the Olympos thrust must be younger on the basis of stratigraphic and radiometric data. These two events could be thought of as a broadly continuous deformation that occurred under blueschist-facies conditions. In samples such as the one shown in Fig. 3.13, the S2 and S3 fabrics are not obviously two distinct fabrics but appear to be a composite fabric related to continued rotational strain. However, in other areas, D3 structures clearly overprint D2 structures, as discussed above for the Voulgara ridge area (section C-C') and in Kato Olympos (sections H-H', I-I'). North of Kokkinopilos, the Olympos thrust (D3) appears to cut the imbricated Sparmou thrust (Plate 2, section E-E'), and west of Kallipevki, the Olympos thrust cuts out the Ambelakia unit and the Sparmou thrust, juxtaposing the Olympos and Pierien units. In the Olympos unit, there is no unconformity between Cretaceous-Eocene limestone and Eocene flysch, thus deformation is constrained to be post-middle Eocene, and must postdate D2.

The abundant isotopic data cited above constrain the age of D2 to be greater than ~53 Ma and thus older than the flysch in the Olympos unit. The fossil data indicate that D3 must be younger than the Lutetian age (52-43.6 Ma on the DNAG time scale) of the flysch in the footwall of the Olympos thrust. The 36-42 Ma Ar loss ages obtained by Schermer et al, (in press) are thus interpreted to represent 1) the age of movement along the Olympos thrust and 2) the age of probable reactivation of D2 and local D1? thrust faults, including the Sparmou thrust and the thrust faults on the north flank of Trohalos ridge.

D3 kinematics

Because outcrops of the Olympos flysch are generally poor and commonly have variable attitudes due to small-scale folding, only a few oriented samples were suitable for kinematic analysis. The orientations of lineations in the flysch samples and the associated shear sense determined from the kinematic indicators discussed above are included in Figure 3.19, along with those in the Ambelakia unit and the Pierien gneisses. The data, while sparse, support the SW-directed sense of shear interpreted from the data on the Sparmou thrust. Note that the two

samples from a small klippe on the northern margin of the window also show a SW sense of movement.

Geometric and stratigraphic arguments provide additional evidence for the interpretation that displacement on the Olympos thrust was from NE to SW: The Sparmou thrust and the Olympos thrust are generally parallel, the latter thrust is always in a lower structural position, and movement along it is later than movement along the Sparmou thrust. This "piggy-back" geometry suggests that the Sparmou thrust was carried in the hanging wall of the Olympos thrust during continued convergence with the same movement sense as that of the Sparmou thrust. The lineations and isoclinal fold axes in both D2 and D3 are parallel, and the two thrusts are isoclinally folded together apparently during the same deformational event that was associated with movement along the Olympos thrust. In addition, the Olympos thrust always contains the Olympos unit in the footwall and either the Ambelakia or Pierien unit immediately above the thrust; if the Sparmou thrust were SW-directed and the Olympos thrust were NE-directed, we might expect to see the Ambelakia unit overthrust the Pierien unit. The Olympos thrust appears to ramp up from Triassic rocks on the SE and NE margins of the window to Cretaceous and Tertiary rocks on the western margin, consistent with the common observation that thrust faults ramp up (not down) in the direction of transport (Royse et al, 1975).

D4: NW-SE folding

Because the main phase of structural stacking of thrust sheets was completed during D3, events D4-D7 affected all the units (except the ophiolite--Table 1) together. D4 and younger events were not accompanied by metamorphism, although prehnite-pumpellyite facies assemblages may be late- to post-kinematic with respect to D4 (Chapter 5).

D4 is generally manifested by map scale NW-SE trending folds. These folds are best developed along the southwestern to western margin of the Olympos window, west of Karia and NW and SE of Kallipevki, where the Sparmou and Olympos thrusts are folded into a close to open upright antiform-synform pair (plate 2, sections G-G', H-H'-H"). Locally, the F4 folds are associated with an axial planar spaced cleavage that is best developed in calcareous schists and sandstones of the Ambelakia unit and the flysch of the Olympos unit. The relation between S4 and S3 produces and apparent NE-vergent megascopic shear sense on the SW limb of the large fold west of Karia (Fig. 3.22). The trend of F4 folds varies from approximately N75W to N40W, with moderate ~30° plunge to both NW and SE

(Fig. 3.3C, A3.6). The core of the Olympos window also appears to have been folded about F4 as L3 lineations form a bimodal distribution that is consistent with folding about an axis oriented 31, N46W (Fig A3.5). F4 folds are not strongly asymmetric, however the NE limb of the large-scale folds near Karia and Kallipefki is steeper (up to 90°) than the SW limb (Plate 2, section G-G'). In the Infrapierien units, F4 folds are observed as local NW-trending minor folds, and as open folds in the Paleambela area and along the road between Agios Dimitrios and Fotina (Figs. 3.2, 3.3C). A small SW-dipping reverse fault along the northeastern margin of the F4 fold east of Karia appears to be associated with slip along the folded surfaces; this fault has gouge and brittle shears associated with it. The fault cuts across the S3 mylonitic fabric in the gneiss, and thus is interpreted to be an F4 structure (section H-H').

D4 relative timing

D4 clearly postdates D3 thrusts and folds because the thrust faults are folded by F4 along the southwestern and southern margins of the Olympos window. The mylonitic fabric of the gneisses and phyllonites up to ~150 m above the Sparmou thrust is tightly folded by F4 folds (Fig. 3.23), indicating that the folding postdates mylonitization. The double plunge of the map scale folds in Karia and Kallipevki areas suggests that they are refolded about younger (F6) axes.

In the Infrapierien unit, interference patterns (Type 1 dome-and basin; Ramsay, 1967) between poorly-developed NW-trending (F4) and NE-trending (F6) folds do not clearly indicate which fold phase was formed first. By comparison with folds of similar geometry in the other units, we have correlated the local NW-trending folds with F4.

D4 kinematics

Small-scale F4 folds verge both NE and SW (Plate 1). On the southwestern margin of the Olympos window, the major folds are slightly northeast vergent, however, these folds could be thought of as parasitic folds on the SW limb of a broad antiform whose east limb has been faulted out along the eastern margin of the window (see D7), and thus would reflect the expected sense of shear for that limb (e.g. Fig. 3.22). Because the folds are relatively open, they probably do not represent folds parallel to transport direction as do F2 and F3 folds, but would be perpendicular to the continued NE-SW shortening that was responsible for D2 and D3. The less-penetrative nature of D4 structures indicates that deformation occurred at a relatively shallower level, and at lower temperatures than D2 and D3.

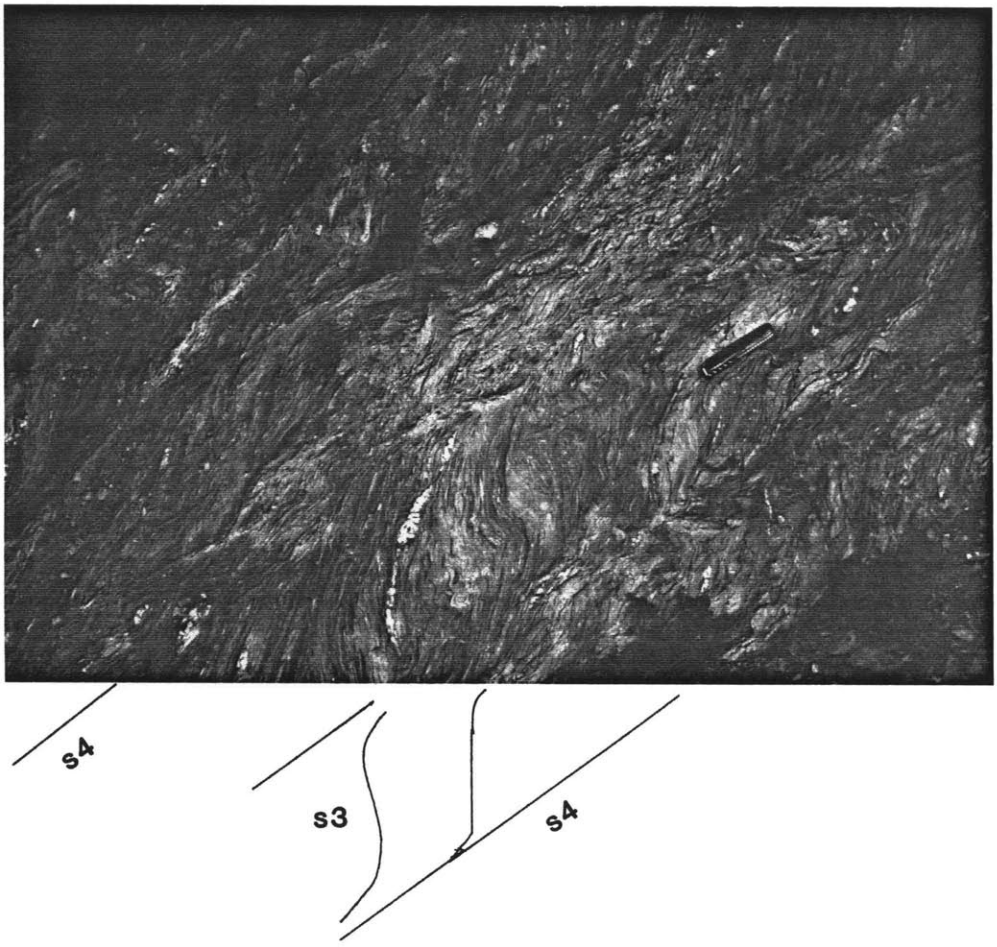

FIGURE 3.22. Large-scale shear fabric in Ambelakia unit metagraywackes from the same antiform as 3.21, showing top-to-NE sense of shear . However, S3, the mylonitic fabric associated with the Olympos thrust, is clearly cut by the S4 shear planes and folded by the F4 folds, indicating that the NE-vergence is not related to movement along the Olympos thrust.

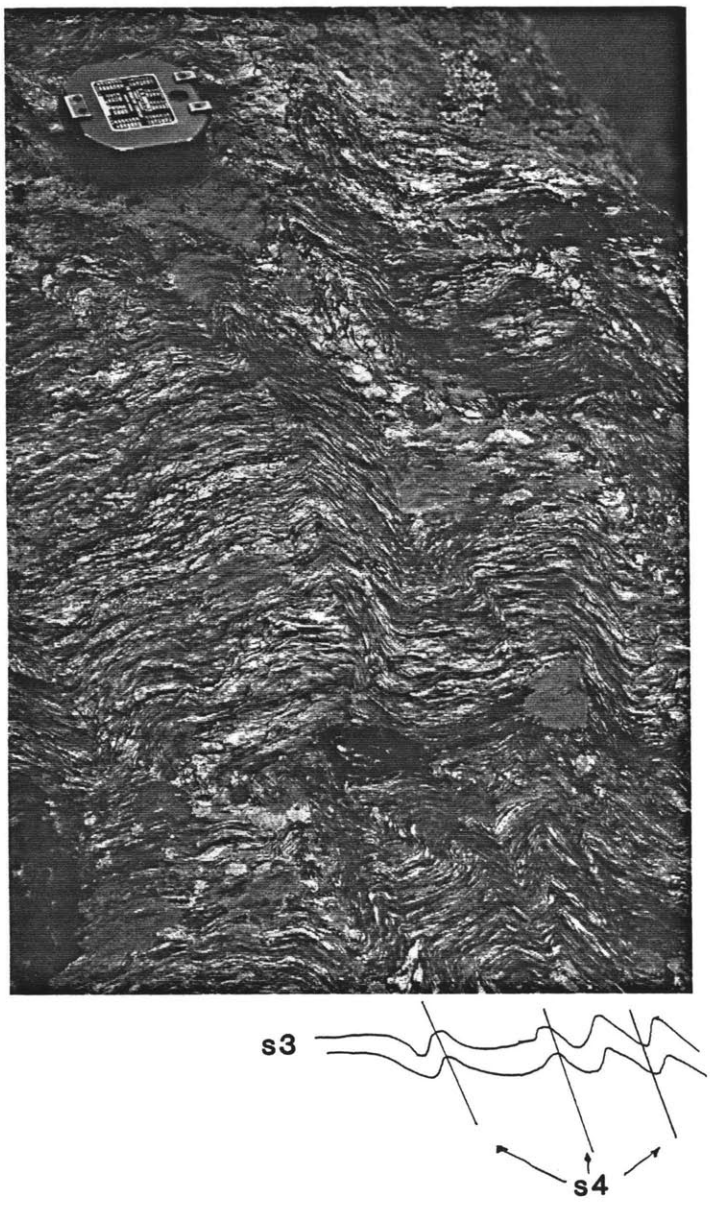

FIGURE 3.23. Folded mylonitic (S3) fabric in Pierien gneiss from the Kokkinopilos area. In this region, the Sparmou thrust is imbricated, some of the imbricate slices appears to be cut by the Olympos thrust. (Plates 1, 2).

The broad F4 fold that affects the entire Olympos window and surrounding rocks may be interpreted as a ramp anticline on a thrust below the Olympos unit. This lower thrust would have been contemporaneous with faults in the thrust belt west of the Olympos region.

F4 folds were interpreted by Barton (1975) to represent thrusting of the Flambouron unit towards the NE over the Olympos unit. He measured folds within the Olympos carbonate rocks and flysch as well as in the allochthonous gneisses in the Sparmou area. Using the technique of Hansen (1966), he determined that the thrust sheet was transported towards ~N45E above the Olympos carbonate rocks. The clear association of both large- and small-scale NW-trending folds that fold the mylonitic fabric in hanging wall and footwall of the Olympos thrust and the map-scale folds that fold the thrust and its associated F3 folds, indicates the post-thrusting nature of the folds that Barton interpreted to be related to movement along the Olympos thrust. In addition, apparently because of the small area of his study, Barton did not recognize the importance of F3 NE-trending folds in the flysch and allochthonous rocks; in the Sparmou area, these F3 folds have apparently been rotated to more northwesterly orientations by later folds (Fig. 3.3B).

D5: Low-angle normal faults

The fifth major deformational event in the Olympos region is interpreted to be movement along low-angle normal faults that juxtapose rocks of the ophiolite unit against the Olympos unit and the Flambouron and Ambelakia nappes. We interpret the Lizadiko Ridge and Keri Ridge faults and the Kallipevki fault system (fig. 3.2; Plate 1) to be normal faults based on the following evidence: 1) These faults are associated with brittle fabrics at microscopic and mesoscopic scales. The cataclastic nature of the deformation is observed to overprint earlier ductile (mylonitic) features (Fig. 3.24), and gouge or fault breccia is commonly present along the faults. In some places (e.g. the west end of Lizadiko ridge), the rocks above the base of the ophiolite unit are mixed in a thick (> 250 m) unit of serpentinized ultramafic rocks that resembles melange. 2) At the outcrop scale, the faults cut across the mylonitic and metamorphic fabrics in the footwall gneisses and schists and also commonly crosscut the shear foliation in the hanging wall serpentinites. 3)The map pattern of the faults indicates that they are discordant to the previously-formed thrust-related structural succession. This relationship is best observed at the northeast end of Trohalos ridge (or the southwest end of Lizadiko ridge) (Fig. 3.25; Plate 1), where, to the SW of the intersection of the Lizadiko Ridge

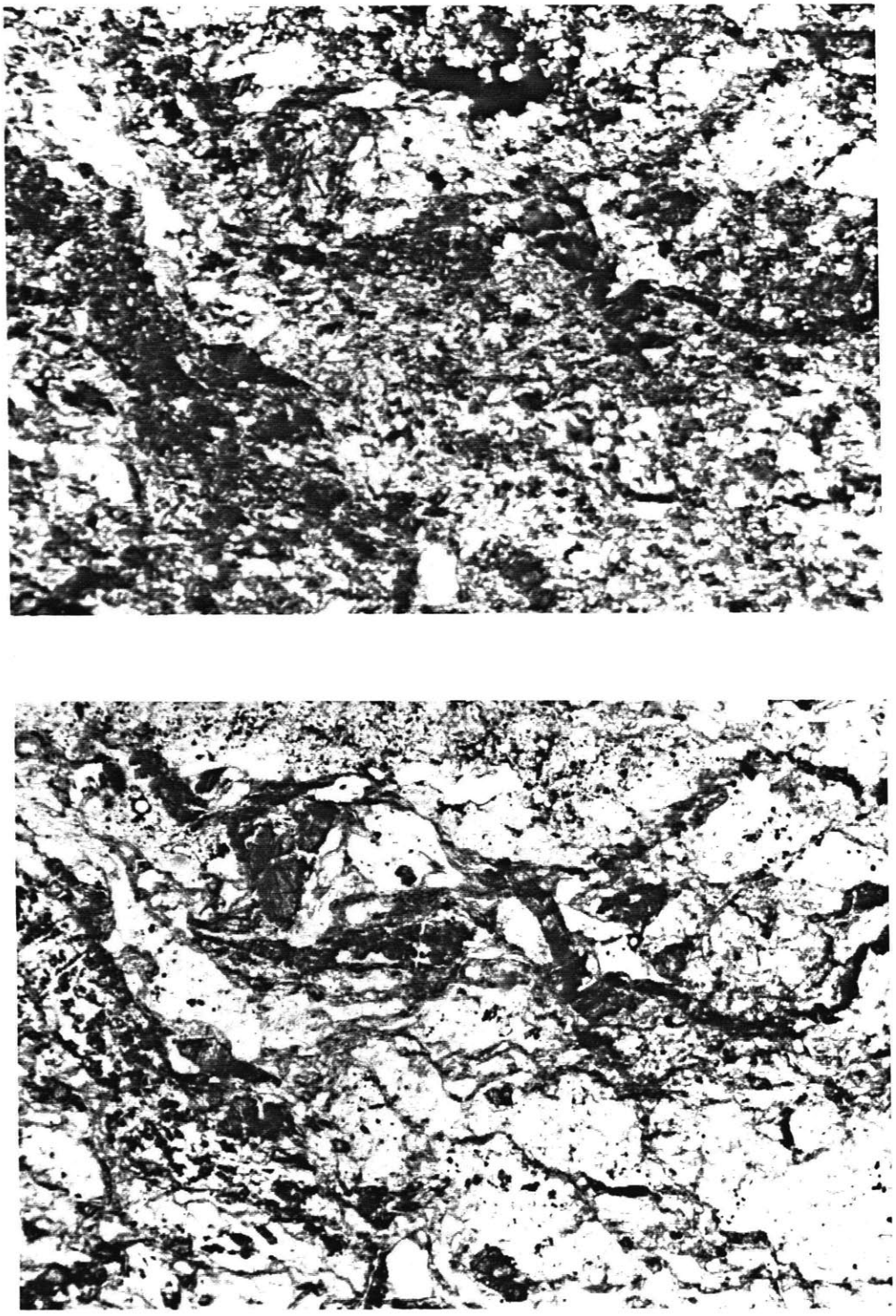

FIGURE 3.24. Photomicrograph, 4 mm across, of cataclastic texture in sample 86OL52, Infrapierien gneiss <10 m below the Lizadiko ridge normal fault. Top photo is in cross-polarized light, showing comminuted quartz texture in center of slide. Bottom photo is in plane light; dark grains are fractured epidote, light grains are quartz and feldspar.

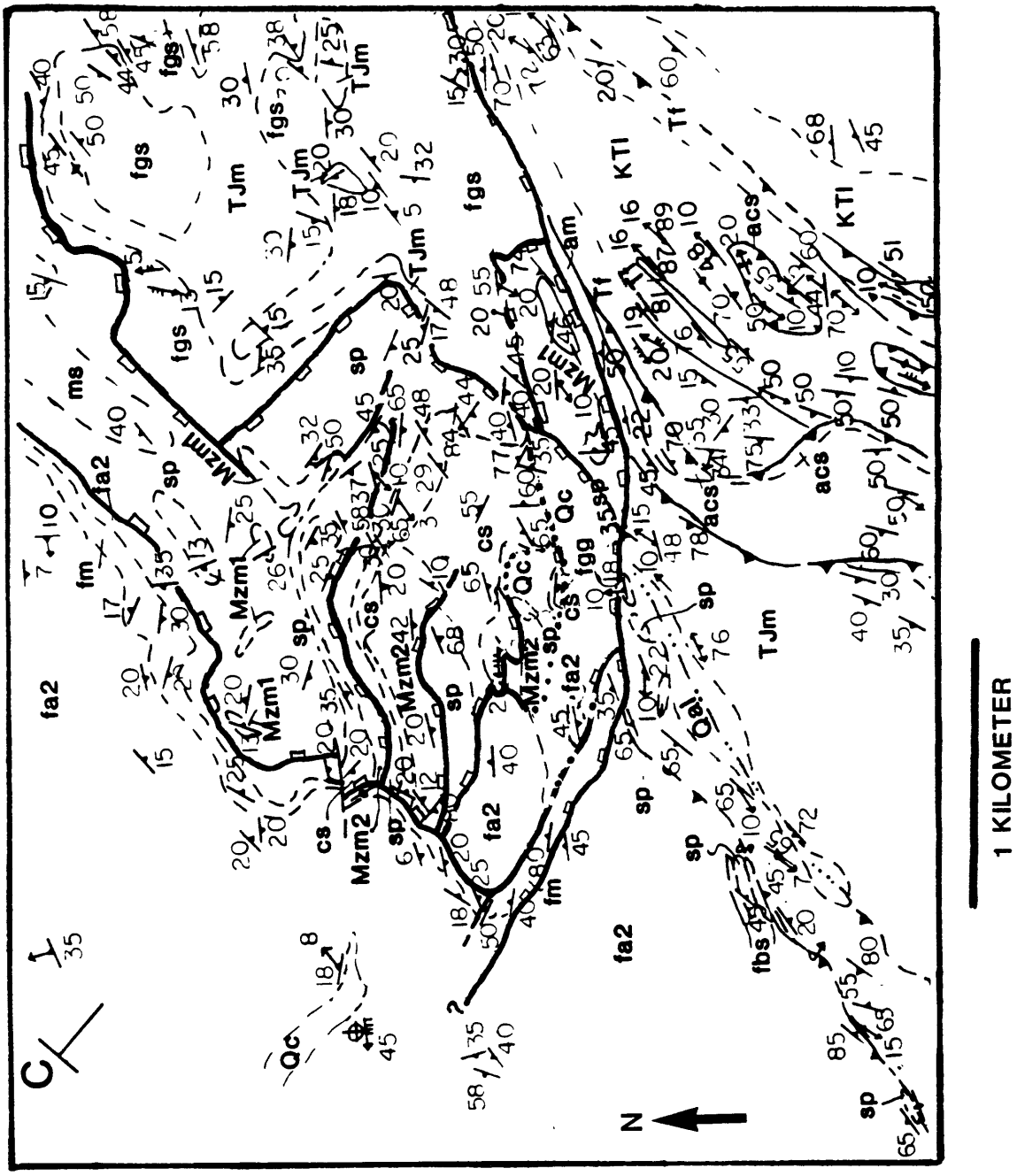

FIGURE 3.25. Map of the west end of Lizadiko ridge, shown at original mapped scale (1:25,000), with the Lizadiko ridge normal fault splays and imbricate normal faults in its upper plate shown in bold ink. "C" indicates NW end of section C-C' (Plate 2). Note that the sequence sp-cs-Mzm2 (serpentinite-calcareous schist-marble) dips SSW and is repeated by NNE-dipping normal faults that do not cut the basal low-angle fault except in one location, where the offset is minor.

and Keri Ridge faults with the Olympos and Sparmou thrusts, the entire thrust succession is intact, from the Olympos unit at the base to the Infrapierien and ophiolite unit (Livadi complex) at the top, whereas to the northeast, the fault below the ophiolite and Infrapierien (Paleambela) units cuts across the entire thrust stack. 4) The ophiolite unit contains only greenschist-facies rocks, whereas the footwall Pierien and Ambelakia units contain blueschist facies rocks. The age of this blueschist metamorphism is known to be latest Cretaceous to middle Eocene on the basis of Ar/Ar data (Schermer et al, in press), yet the age of ophiolite emplacement is considered by most workers (Nance, 1981; Barton, 1975; Katsikatsos et al, 1982; Schmitt, 1983; Vergely, 1984) to be pre-Eocene, possibly as old as Early Cretaceous in age. Thus if the ophiolite had been emplaced by thrust faulting prior to Eocene time, there should be some evidence that post-emplacement blueschist-facies metamorphism had affected the ophiolite unit.

The Lizadiko Ridge normal fault and the Keri Ridge normal fault both appear to have listric geometries. The southern parts of these faults are fairly high-angle (~60° or more), yet the map traces of these segments are strongly curved (Plate 1). It is possible that the apparent listric geometry is the result of two fault systems, an early low-angle one and a later high-angle one. Nevertheless, it can be demonstrated that, while there are high-angle normal faults that cut and displace the low-angle normal faults, the offset must be minor because rocks in the footwalls of the low-angle normal faults are not cut by major high-angle faults. For example, the Lizadiko Ridge fault follows the NE-trending trace of a thin band of marble and schist within the Infrapierien unit for ~3 km on the NW flank of the ridge. To the southwest towards Trohalos, however, three high-angle faults cause down to the NE apparent offset and SW tilting of a marble-schist-serpentinite sequence above the Lizadiko fault (section C-C'), but two of them do not cut the low-angle fault and the third causes an apparent offset of the marble in the footwall of <50 m (Fig. 3.25). On the NW flank of Lizadiko ridge, the two faults merge. This merging appears to be the result of a ~NNW trending ramp as the Keri ridge fault cuts downward to the NE, leaving the Lizadiko ridge fault in its hanging wall (Plate 2, sections A-A', B-B', F-F').

The Kallipevki normal fault system (Fig. 3.3C; Plate 1) has a geometry and apparent displacement direction broadly similar to that of the Lizadiko-Keri ridge system. In the Ziliana river area, high-angle normal faults with a total of ~500 m of down-to the-ENE vertical displacement offset the low-angle normal fault (section H-H'"). In cross-section, the low-angle normal fault is "scoop"-shaped, opening in

a northeastward direction (section I-I'), and east of Kallipevki, in a complicated and poorly exposed area (section J-J') tightly folded rocks of the Ambelakia unit are exposed in the footwall. In the hanging wall, vertical shear zones of serpentinized ultramafic rocks cut through the dominantly gabbroic and amphibolitic lithologies. Although outcrop is extremely poor and this area was not mapped in detail, these shear zones do not appear to cut the low-angle normal fault and extend into the footwall rocks.

It is worth noting that, although the geometry and nature of faults in the Strongguli Ridge area and further east (Fig. 3.2, Plate 1) is poorly constrained, the juxtaposition of rocks belonging to the ophiolite unit against various lower units, including the Ambelakia unit, implies that the area is probably affected by D5 and/or possibly D7 normal faults. In this part of Kato Olympos, even where there is outcrop, the rocks are extremely fine-grained and weathered, such that previous workers have mapped the same rocks as Olympos unit (Katsikatsos and Migiros, 1987) and as ophiolite unit (Schmitt, 1983). In thin section, many these rocks can be identified as epidote-chlorite schists, and epidote-amphibolite schist, and are clearly metamorphosed at least to low greenschist-grade and so cannot belong to the Olympos unit. However, it is not clear whether they are part of the Infrapierien (Ziliana) unit, the ophiolite unit, the Ambelakia unit, or some combination of the above. We have correlated the quartz-rich metasedimentary greenschists with the Infrapierien unit, the more massive amphibolite schists and featureless greenstones with the ophiolite unit, and, where blueschist mineral assemblages are visible in thin section, the Ambelakia unit (Plate 1).

D5 relative timing

The D5 normal faults clearly cut across the thrust fault contacts and folds associated with D1-D3. The absence of F4 structures in the Lizadiko ridge and Kallipevki areas of the ophiolite unit suggests that the normal faults also post-date D4. The melange structure within the ophiolitic unit on Lizadiko ridge is of uncertain age; however, the foliation in the serpentinite is locally parallel to the boundaries of individual marble blocks within the melange, but has no relation to the folds within the marble and schist blocks, and is highly variable from block to block. Thus the melange structure must post-date D1 and D2 folding and metamorphism, yet is unaffected by D3 and D4, therefore it could be associated with D5. The chaotic nature of the melange by definition precludes correlating this deformation with other, geometrically coherent, deformations on the basis of style.

The location of the structurally highest unit (the ophiolite) at topographically low positions NNW and SSE of the 3-km high Olympos window and the interpretation of both Lizadiko ridge and Kallipevki faults as low-angle normal faults suggests that if these normal faults were once part of the same system, they may have been folded about F6 axes (Fig. 3.3C). The broadly similar geometries and apparent displacement directions may be indicative of the once-continuous nature of these two fault systems. In addition, it is possible that the overall "dish" shape of the low-angle normal faults in NW-SE cross sections (e.g. C-C', I-I') is the result of F6 folds. On the other hand, these faults may have been originally listric. As discussed below, low-angle normal faults are locally cut by NW-trending high-angle normal faults, however, the down to the NE sense of displacement and the small magnitude of the apparent separation precludes these high-angle faults being solely responsible for the overall map pattern of the low-angle faults at the base of the ophiolite unit.

The available data are consistent with the interpretation that D5 normal faults are folded by F6 folds, however, we cannot prove this assertion because the D5 faults cannot be traced around the eastern margin of the Olympos window. The high-angle faults attributed to D7 are clearly <u>not</u> folded by F6 and thus must be younger. However, the open, upright, NE-plunging folds in the Keri Ridge-Paleambela area (attributed to F6) are cut by the Keri Ridge normal fault (Plate 2, section A-A'), thus at least some movement on the Keri Ridge normal fault postdates the formation of these F6 folds.

It is possible that events D5-D6 are broadly coeval. Ar/Ar data on potassium feldspar from samples below the low-angle normal fault segment of the Kallipevki normal fault system indicates rapid cooling of the metamorphic rocks began in early to middle Miocene time (~16-23 Ma; Schermer et al, in press). We interpret this cooling to reflect movement of the metamorphic rocks toward the surface and be related to the beginning of extension; however, D7 extensional structures clearly were active until recent time. The apparent contemporaneous development of compressional and extensional structures is discussed further below.

D5 kinematics

D5 fault surfaces are not exposed, so no slickenside or other similar kinematic data could be obtained. In the Lizadiko Ridge area, SSW tilting of fault blocks in the hanging wall suggests displacement of the hanging wall to the NNE. The NW orientation of the ramp in the Keri Ridge normal fault also is consistent with a NE

displacement direction. It is possible that the entire normal fault system has been rotated from its original orientation by F6 folds or by tilting due to D7 normal faults. Local drag folds associated with the high-angle normal faults in the area east of Karia (Plate 1; Plate 2, section H"-H"') indicate NE displacement similar to that of the normal faults on the northern margin of the window. It is also worth noting that the footwalls to the major low-angle normal faults of the Olympos region are relatively unaffected by the brittle deformation except within a few tens meters below the fault surfaces, possibly indicating that the footwall originated at a depth sufficient to allow ductile behavior in the early stages of movement on the low-angle normal faults.

D6: NE-SW open folds

The youngest folds are attributed to D6 deformation. These include open ~N40E-trending folds, and N-S and NE trending kinks that affect the Olympos, Ambelakia, and Flambouron units.

F6 folds are particularly well exposed on the east side of Karfia ridge south of Kallipevki village (Plate 2, section I-I'). In this region, the complicated outcrop pattern (Plate 1) is the result of the superposition of F2, F3, F4, and F6 folds (Fig. 3.3C). The elongate slivers of Olympos flysch and Ambelakia marble and schist are typically the result of F2 and F3 isoclinal folds; F4 and F6 folds produce an elongate dome-and basin pattern of the interfolded Olympos and Ambelakia rocks (Fig. 3.26). In this region symmetric, upright F6 folds plunge ~S40W and have a wavelength of 2-2.5 km. Folds of the same style and similar orientation (~30, S40W) but longer wavelength (>5 km) affect the F4 folds NW of Kallipefki and near Karia, and may also be partly responsible for the overall domal structure of the Olympos window. However, foliation and lineation orientations are scattered due to the superposition of several fold events, so it is difficult to constrain the orientation of possible F6 structures that affect the carbonate rocks of the Olympos window.

The Infrapierien units exposed north of the window also appear to be affected by open F6 folds, however, this is documented mainly by the scatter in earlier phase-folds and foliation directions, rather than by a coherent F6 fold axis. Nevertheless, as indicated on plate 2, sections A-A', and B-B', local F6 folds occur as open N30-50E trending folds with a wavelength of ~300-500 m.

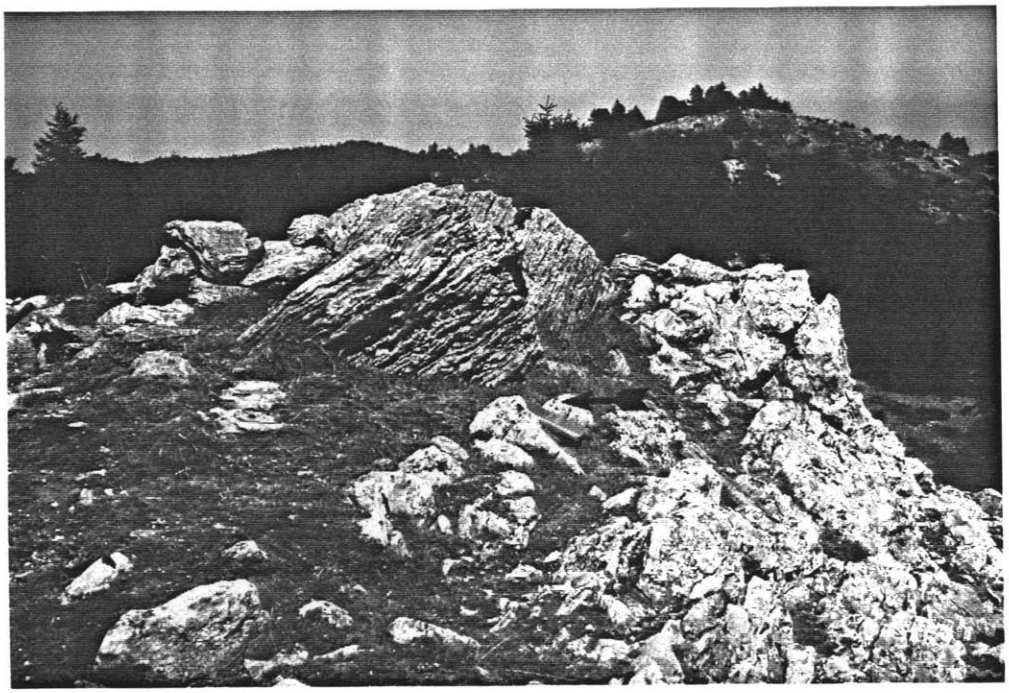

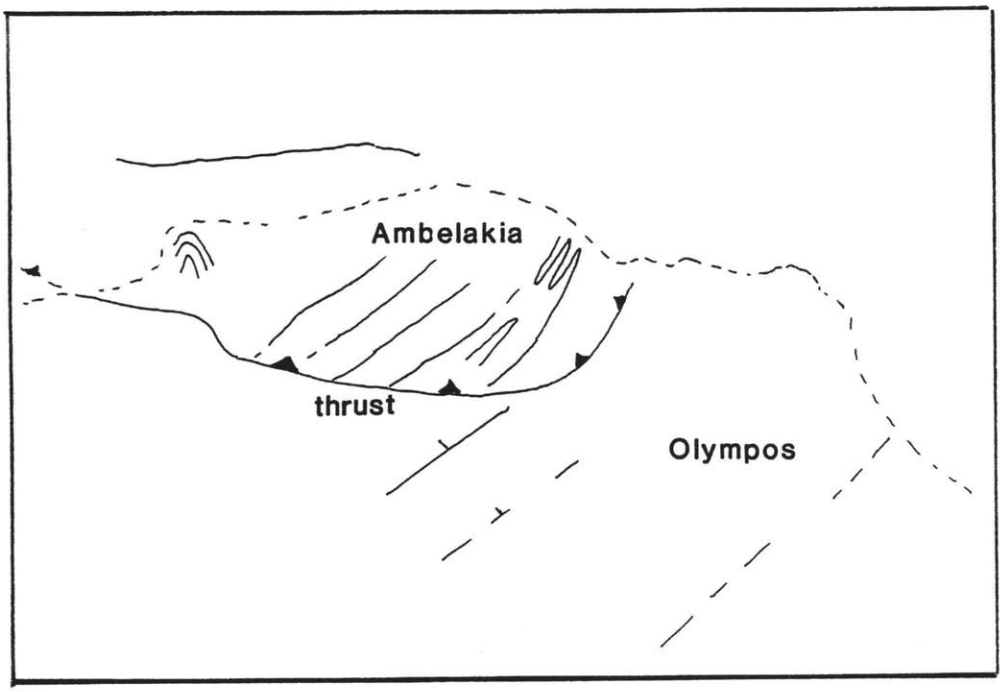

FIGURE 3.26. Small klippe of Ambelakia unit marbles thrust over the Olympos unit in the Karfia ridge area, Kato Olympos. Thrust fault is folded by F3, F4, and F6 folds which give a general dome-and basin type interference pattern to this region, with small klippen of thrust faults preserved where F4 synforms intersect F6 antiforms. View to NNW, oblique to F4 axis (NW); notebook in center of photo, on thrust contact, is 18 cm long (arrow).

D6 relative timing

The effect of SW-plunging D6 structures on NW-SE plunging F4 folds in the Kato Olympos region constrains the timing relationship of these fold phases. As discussed above, F4 structures are not well-developed on the northwestern margin of the Olympos window, so it is difficult to independently constrain the relative timing of F4 and F6 in this area. The folds are older than the high-angle normal faults related to D7 because folds attributed to F6 in the Keri ridge area (Plate 2, sections A-A', B-B') are truncated by high angle faults. While we have no absolute age information to tightly constrain the timing of D6, it is bracketed by the age (36-40Ma) of F3 structures which are folded, and Neogene conglomerates which do not appear to be folded.

D6 kinematics

The kinematic significance of D6 structures is somewhat enigmatic. If F6 folds are related to shortening, the shortening direction would be substantially different (NW-SE as opposed to NE-SW) than that recorded by D1-D4 events. The folds are broad, symmetric and upright, and show no vergence. The difference in scale of the D6 structures within the allochthonous rocks and the carbonate massif of the Olympos window may be due to the greater thickness and competence of the carbonate rocks relative to the flysch and thin thrust sheets of marble, schist, and gneiss in the Kato Olympos area, or it may reflect the possibility that the broad domal structure of the window is not the result of cross-folding. Instead, the dome could be the reflection of drag and uplift of the crust in the footwall of D7 normal faults along the eastern margin of Olympos. This possibility will be discussed in more detail below.

D7: High-angle normal faults

The final phase of deformation consists of high-angle NE- and E-dipping normal faults. These faults juxtapose ophiolitic rocks against Triassic limestone of the Olympos unit on the eastern margin of the window (Fig. 3.27; 3.3C); Plate 1). In contrast to the D5 low-angle normal faults, brittle deformation related to D7 normal faults extends well into the footwall rocks (>100 m locally) (3.28), and both hanging wall and footwall rocks are intensely brecciated and brittley sheared. Locally, gouge zones are >10 m thick. Fault scarps within Neogene and Quaternary conglomerates have been mapped in the Fotina area; the dips of 60° indicated for these faults on Plate 2 are probably minima because the dips are measured on the fault scarps which have been eroded (3.29). In general there are no marker beds

in the hanging walls and footwalls that we can use to estimate amounts of offset, but the scarps, such as the ones pictured in 3.29, range from 5-15 m high. Conglomerate in the hanging wall is locally tilted as much as 25° (Fig. 3.30) Although we have not mapped the surrounding area in detail, reconnaissance investigations indicate that similar faults occur on the eastern flank of the Pieria and Lower Pieria mountains to the north. D7 faults seem to be part of an important network of very young (and locally active) high-angle normal faults that bound the eastern flank of the mountains from the Yugoslavia border, along the western margin of the Vardar basin, south to the Ossa mountains, where they strike into the Gulf of Salonika.

D7 relative timing

D7 faults clearly cut D5 faults and D6 folds (Plate 2, sections F-F', H-H'''). The conglomerates and marls designated as Quaternary and Neogene are not precisely dated, however, the fact that scarps remain visible on these faults even in the relatively poorly consolidated marly rocks indicates they may be recently active faults.

D7 kinematics

None of the D7 faults that we examined contained visible polished surfaces or slickenside lineations, so it is difficult to know the displacement direction for these faults. The geometry of offset units in cross section requires some down-dip component of displacement, however we have no constraints on whether there may also be a strike-slip component. Schmitt (1983) characterized many of the high-angle faults in the Olympos region as strike-slip faults. Many of these faults on her map must have some component of normal displacement as they juxtapose units from different structural levels even where the contacts are essentially horizontal. Other faults do not appear to have offset that is visible at the 1:100,000 scale of her map. We could not confirm the presence of a major strike-slip faulting episode either on the basis of map-scale structures or minor folds and shear zones, however there may be some minor strike-slip faults that we have not recognized.

The overall tectonostratigraphic throw on the normal faults along the eastern flank of Mt. Olympos, though probably a cumulative displacement on D5 and D7 faults, may be as much as 6 km, the approximate thickness of the Flambouron and Ambelakia thrust sheets. It is important to note, however that if these blueschist-facies rocks were once at >20 km depth (Schermer, in prep), a good deal more cover has been removed than is evident here, as will be discussed further below.

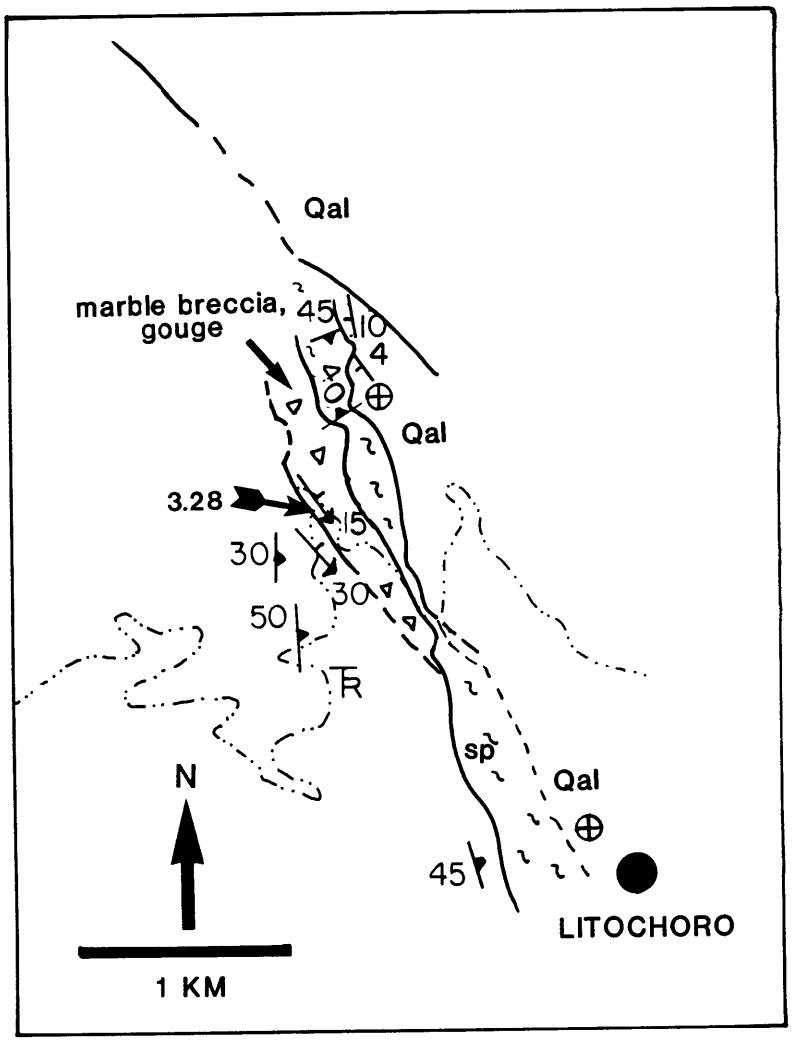

FIGURE 3.27. Map of the area near Litochoro showing D7 normal faults. Note that faults are high angle and cut both the serpentinite of the ophiolite unit (sp) and Quaternary alluvium (Qal). Qal is locally tilted and dips westward near the fault. Dash-dot line indicates road; arrow indicates location of photo in Fig. 3.28.

FIGURE 3.28. Brecciated limestone and dolomite of the Olympos unit on the eastern flank of Olympos, near Litochoro village. Carbonate rocks form the footwall to a high-angle normal fault with serpentinite melange in the hangingwall. Note abundant normal-sense offsets of limestone and dolomite layers. East is to left.

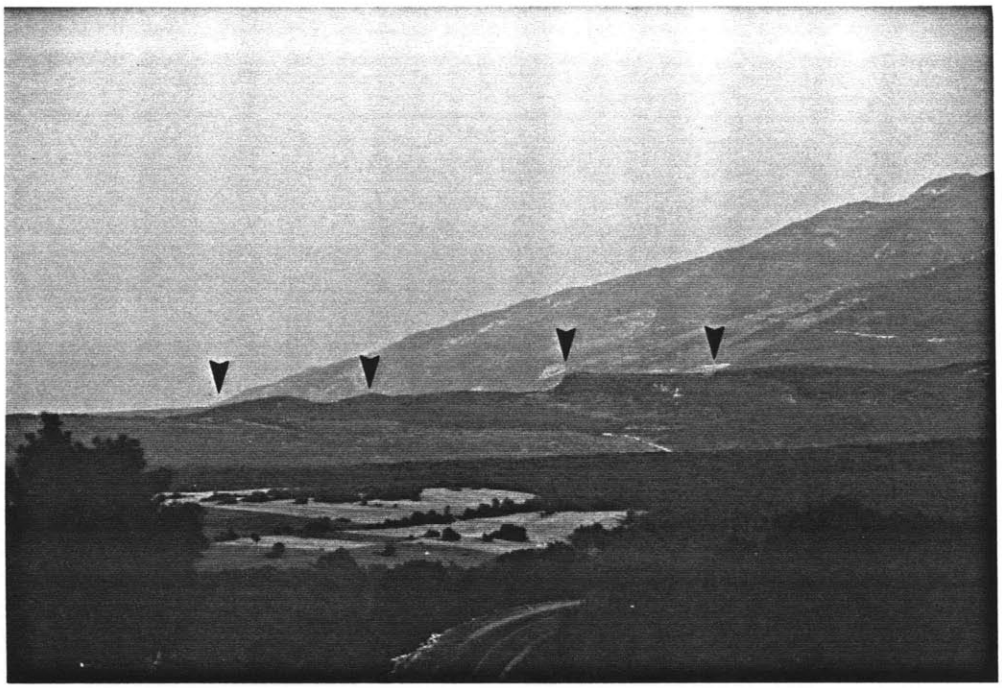

FIGURE 3.29. View to south from northern margin of Mt. Olympos along young normal fault scarps that cut Neogene and Quaternary conglomerate in the basin NE and E of the mountain range. Four scarps can be seen in this photo, indicated by arrows. Gentle slope in background is dip-slope of Olympos unit Triassic dolomite and limestone in the east limb of a broad fold.

FIGURE 3.30. Neogene conglomerate dipping 20° west towards the mountain front. View to N taken from east of the Lower Pieria mountains, ~5 km NE of Fotina village (Figure 3.2). Westward tilts of basin sediments are not uniform; some are flat, others dip eastward, but the presence of several fault scarps with apparent normal separation is indicative of extensional faulting throughout the eastern flank of the mountain range extending >100 km north and south from Mt. Olympos.

DISCUSSION

Summary of deformational events in the Mt. Olympos region

Alpine deformational events in the Mt. Olympos region overprinted earlier, probable Paleozoic deformational and metamorphic fabrics (D0). The D1 event was confined principally to deformation within, and imbrication of the Flambouron continental basement and carbonate cover rocks during lower Cretaceous time. It is also probable that ophiolitic rocks were thrust over continental margin rocks during the D1 event(s), however, there is no conclusive evidence in the study area that any of the present bounding faults below ophiolitic rocks were active during this period of deformation (except possibly beneath the Livadi complex). Basement-involved thrusting was associated with upper greenschist to lower amphibolite facies metamorphism, and may have been SW-directed. D2 and D3 produced isoclinal folds and mylonitic fabrics related to SW-directed thrusting of the Infrapierien and Pierien units over the Ambelakia unit, and of all three of these units over the Olympos unit. D2 deformation occurred under blueschist-greenschist transition facies conditions in the Infrapierien unit, and blueschist-facies conditions in the Pierien and Ambelakia units during latest Cretaceous to Early Eocene time. High pressure-low temperature conditions persisted during D3, and blueschist to prehnite-pumpellyite facies metamorphism affected the Ambelakia and Olympos units. D4 folds appear to be related to continued NE-SW compression and the propagation of thrusting towards the external Hellenides. Events D5-D7, including low- and high-angle normal faults and broad folds reflect the beginning of extension and uplift; these late events contributed to the exhumation of the blueschists from depths >20 km.

Regional implications of deformational events

Deformation in the Mt. Olympos region took place in the context of overall convergence between the Apulian and European plates and the closing of Tethyan ocean basins from late Jurassic to Tertiary time. There is considerable controversy over the number and location of ocean basins that may have been present in the Hellenides from Permian to Early Cretaceous time. Nevertheless, there is agreement that oceanic crust, whether in the form of small transtensional or arc-related basins or large tracts of ocean floor, existed between the external Hellenides and the European plate from Middle to Late Jurassic time. One set of workers considers the Vardar ocean to be the major ocean from which all the ophiolites were derived, and thus the Vardar zone would be the only true suture

zone in Greece (e.g. Bernoulli and Laubscher, 1972; Aubuoin et al, 1976; Burchfiel, 1980; Thiebault and Triboulet, 1984; Vergely, 1976, Mercier et al, 1975, Ricou et al, 1983). This hypothesis implies: 1) all the nappes east and north of (and structurally above) the external Hellenides, were emplaced from northeast to southwest; and 2) intracontinental, or "A-type" subduction (Bally, 1975) occurred in both the internal and the external Hellenides in Tertiary time. Other workers believe that two or three ocean basins existed; at least one (the Pindos ocean) lay to the west of the Pelagonian zone and separated it from the external Hellenides, and another (the Vardar ocean) lay to the east of the Pelagonian zone, and separated it from the European plate (e.g. Hynes et al, 1972; Smith et al, 1975, Barton, 1976). This latter hypothesis implies that 1) while some ophiolites were thrust westward onto the eastern Pelagonian margin, others were thrust both eastward onto the western Pelagonian margin and westward onto the external Hellenides and 2) high P, low T metamorphic rocks throughout the Hellenides represent "normal" oceanic (B-type) subduction, and each belt is associated with a suture zone between continental fragments. The detailed arguments for each hypothesis cannot be presented here; the reader is referred to the excellent summary in Robertson and Dixon (1984) for more information.

Constraints on the precise timing of closure of the ocean basin or basins due to microcontinental or continental collision are poor, but the following observations have led many workers to interpret the final closure of the ocean basin or basins in latest Cretaceous to Paleocene time (Mercier et al, 1975; Burchfiel, 1980; Vergely, 1984): Ophiolitic rocks in the Vardar zone are no younger than 160 Ma; associated granitic to gabbroic rocks that may be either subduction- or rift-related range from 150-163 Ma (Bebien et al, 1980; Spray et al, 1984). The youngest subduction-related volcanic rocks in Greece are Early Cretaceous in southern Greece, and Paleocene on the western margin of Rhodope.

Abundant evidence exists for the initial obduction of ophiolite rocks in latest Jurassic to Early Cretaceous (pre-Albian) time. This evidence includes the presence of flysch of Tithonian age in the Vardar zone, Barremian-Turonian age in the Pindos zone, and Albian age in south-central Greece that contains ophiolitic debris, and Albian-Cenomanian neritic limestone that was deposited unconformably on the ophiolite allochthons throughout the Hellenides. Obduction may have been diachronous, but it seems to have been completed by the end of the Early Cretaceous (Burchfiel, 1980). Several workers who favor a multiple ocean model for the Jurassic-Cretaceous period in Greece (e.g. Vergely, 1984)

relate each ophiolite obduction episode to a collision; others favor obduction onto the continental margin in the latest Jurassic, while the ocean basin was still open, followed by collision during late Cretaceous to early Tertiary time, as recorded by deformation in the Vardar and Pindos zones (e.g. Burchfiel, 1980; Zimmerman and Ross, 1976, 1979).

In the Olympos region, deformation was characterized by SW-vergent imbrication of the continental crust that continued episodically for more than 90 Ma, from Early Cretaceous to post Eocene time (D1 to D4) and was characterized by SW- (foreland-) directed basement-involved thrusting, and probably also by ophiolite obduction (D1 in the Livadi area). The main implications of the D1-D3 geometric and kinematic data presented above for the ocean-basin controversy are twofold: 1) obduction and imbrication may have occurred prior to final collision between the Pelagonian basement and Rhodope and 2) because the ophiolites rode "piggy-back" on top of the continental nappes and there was no oceanic terrane between Flambouron and Olympos unit rocks, the oceanic rocks must have been derived from the Vardar basin to the NE, and could not have come from a Pindos basin to the SW, as postulated by Barton (1976, 1979).

Intracontinental subduction

Initial (D1) basement-involved thrusting was followed by intracontinental blueschist-facies metamorphism during latest Cretaceous to early Tertiary time. High pressure-low temperature metamorphism began prior to emplacement of blueschist facies rocks on the carbonate platform, but similar pressure-temperature conditions persisted as imbrication of the Apulian margin proceeded from NE to SW. Within each major thrusting event D1, D2, and D3, there is an apparent sequential development of structures related to overall progressive simple shear, from 1) the formation of syn-metamorphic isoclinal folds and axial-planar schistosity to 2) thrusting associated with the formation of mylonitic foliation and stretching lineation to 3) folding of the thrust. Each of these stages appears to record not only the same sense of shear, but also a similar NE-SW orientation, suggesting that early-formed structures probably have been rotated into parallelism with progressive strain.

The relation between events D1-D4 and the presence of Oligocene and Miocene debris from the Pelagonian nappes in the Mesohellenic trough to the west (Brunn, 1956) seem to record the overall cooling, uplift, and erosion of the thrust belt as deformation progressed toward the foreland. Metamorphic conditions

progressed from blueschist-greenschist transition facies to blueschist to prehnite-pumpellyite facies with time and as lower structural levels were deformed. Continued compression and progression of deformation from the Olympos region toward the foreland is well-documented by the progressive younging of flysch and the age of the youngest rocks deformed in the various thrust sheets of the external Hellenides (e.g. Jacobshagen et al, 1978). Rocks of similar facies to the Olympos unit occur within these thrust sheets and the thrust faults project below the Olympos thrust. Thus we interpret the folding of the Olympos and Sparmou thrusts during the D4 event to be a ramp anticline on a thrust below the Olympos thrust. Similar relations have been proposed for the formation of basement culminations in the Scandinavian Caledonides (Hodges et al, 1982).

Deformation under HP/LT conditions began at ~60 Ma, and continued until <40 Ma. Even though temperatures were low (<400°C; see chapters 4,5), both the crystalline basement rocks and carbonates behaved ductiley. D4 and later events occurred at lower pressures and temperatures. Apparently the continued underthrusting of cool surface rocks maintained a relatively low geothermal gradient because the blueschists are not overprinted by greenschist facies assemblages (e.g. Rubie, 1984).

In the Mt. Olympos region, Alpine deformation involved subduction of the continental basement of the Pelagonian zone. Thrust sheets of the Paleozoic basement rock are relatively thin (<500m locally), and must have been detached from the lower crust. The upper parts of the basement may have been subducted to depths >20 km (see chapter 5), but were subsequently decompressed during thrusting above carbonate rocks of the Olympos unit, and uplifted and exhumed by the removal of tectonic overburden by normal faulting and erosion. Because the lower crustal portions of the Flambouron nappes are not exposed, and the crust here is only moderately thick (45-50 km; Makris, 1977; Geise et al, 1982), the lower parts of the continental crust may have been subducted into the mantle. Although it is traditionally assumed that continental crust is too buoyant to be subducted into the asthenosphere, calculations by Molnar and Gray (1979) indicate that, if the upper crust is detached from the lower crust, the negative bouyancy of the mantle part of the continental lithosphere is sufficient to subduct short (<30 km) lengths of continental crust. If the continent is attached to an oceanic plate being subducted, the gravitational body forces are sufficient to cause subduction of tens to hundreds of kilometers of the continental crust. Thus our estimate of ≥20 km depth reached by the Pelagonian crust is not unreasonable. In many collisional orogens, several

hundreds of kilometers of crustal shortening are inferred from geologic relations and require subduction of significant amounts of lower crust (e.g. Milnes, 1978; Burchfiel, 1980; Bally, 1981; Hodges et al, 1983).

Significance of D5 and D7 normal faulting

In addition to missing crustal material from below the basement thrust sheets, the present exposure of the blueschist facies rocks suggests that material is missing from above as well. Blueschist facies rocks metamorphosed at depths >20 km were underthrust by lower-grade rocks, but both low-angle and high-angle normal faults have also played an important role in the uplift and exhumation of the high pressure-low temperature rocks. The maximum apparent displacement that we can attribute to D5 and D7 normal faults is ~6 km, the approximate thickness of the exposed thrust sheets between the ophiolite unit and the Olympos unit. An unknown thickness of rocks could have been removed by erosion as clasts of Pelagonian metamorphic rocks are abundant in the Oligocene-Miocene MesoHellenic molasse basin west of the Olympos region. Nevertheless, the thickness of sediments in this basin cannot account for the apparent ~15 km discrepancy because the formation that contains abundant debris derived from the Pelagonian zone is only ~3 kilometers thick (Brunn, 1956; Papanikolaou et al, 1988).

We have been able to indirectly constrain the timing of the beginning of uplift of blueschist facies rocks to early to mid-Miocene time on the basis of cooling ages of potassium feldspars (Schermer et al, in press; chapter 4). Direct constraints from the age of faulted strata only bracket the timing of D5 low-angle normal faults to post Eocene, pre-Neogene time. It is clear, however, that normal faulting closely followed thrust faulting in the Olympos region, and may have been broadly contemporaneous with continued local folding (D6). In a regional context, D5 and D7 extensional deformation occurred while thrust faulting was still continuing to progress westward through the external Hellenides out to the present-day Hellenic trench.

The identification of low-angle normal faults occur at the base of the ophiolite unit in the Mt. Olympos region has important regional implications. Low-angle faults are commonly mapped as thrust faults in the absence of good kinematic indicators; there is still some controversy over whether low-angle normal faults actually initiate or are active at low angles (e.g. Wernicke, 1981; Miller et al, 1983; Jackson, 1987). We are just beginning to realize the significance and

characteristics of extensional deformation within convergent regimes (e.g. Royden and Burchfiel, 1987)]. The recognition of low-angle normal faults with significant displacement may require reexamination of contacts mapped as thrust faults throughout the Pelagonian zone and perhaps throughout the Hellenides.

High-angle normal faults similar to D7 faults extend along the western margin of the Vardar zone and bound the mountains of the eastern Pelagonian zone for several hundred kilometers along strike in Yugoslavia and Greece. The principal effect of this extensional deformation has been to uplift the mountains by at least three kilometers (the height of Mt. Olympos) with respect to the adjacent north Aegean basin. To the west of the Olympos region, a portion of the Larissa basin, filled with Neogene and Quaternary sediments, appears to be in normal fault contact on its western margin against carbonates that are equivalent to the Olympos unit, exposed in the Kranea window (Elassona and Deskati 1:50,000 sheets, 1988). As on the eastern margin of the Olympos window, faults on the eastern margin of the Kranea window juxtapose rocks of the ophiolite unit against the lowest structural unit (Olympos-equivalent). On the basis of mapped relations, we interpret these faults as normal faults that cut across the thrust faults between the Flambouron unit and the Olympos unit (1:50,000 sheets, op. cit; A. Sfeikos, personal communication, 1988).

Further to the west, the Mesohellenic basin (Figure 1) contains early Oligocene to middle Miocene strata that dip eastward into a high-angle normal fault that bounds the eastern margin of the basin. Subsidence of this basin may have in part been related to extension that occured in the upper part of the Eocene-Oligocene thrust belt and east of contemporaneous (Oligo-Miocene) thrusting in the external Hellenides (Papanikolaou et al, 1988).

The contemporaneous nature and parallelism of extensional and compressional structures in the Hellenides is a well known and engimatic problem in Mediteranean tectonics. This "back-arc" extension may be occuring as a result of the collapse of over-thickened crust (e.g. Dalmayrac and Molnar, 1981; Royden and Burchfiel, 1987) or in response to slab retreat processes such as those described by Royden (1987) for the Appenines and Royden and Burchfiel (in press) for the Alps and Carpathians. While our data do not provide dynamic constraints on the processes responsible for extension in northern mainland Greece, we can demonstrate that normal faulting rapidly followed thrusting, caused significant (probably >6 km) uplift of metamorphic rocks in the Olympos region, and was essentially antiparallel to the thrusting direction.

CONCLUSIONS

In conclusion, the detailed study of the geometric and kinematic aspects of deformation in the Mt. Olympos region provides the following constraints on the Alpine tectonic evolution of this part of the Hellenides: 1) Deformation occurred over a long period of time (>90 Ma) and was episodic, but produced consistent foreland-directed emplacement of thrust sheets throughout most of Cretaceous-Eocene time (D1-D4). 2) Deformation of the continental crust of the Pelagonian zone included basement-involved thrusting and continental subduction that may have begun before collision of the Apulian and European plates. 3) The present-day geometry of the metamorphic nappes is controlled by extensional tectonics, which was partly (but not solely) responsible for rapid uplift of the blueschist-facies rocks, and was synchronous with overall convergence in Hellenic arc.

APPENDIX A3

LOWER HEMISPHERE EQUAL AREA PROJECTIONS OF SELECTED STRUCTURAL DATA FROM THE MT. OLYMPOS REGION

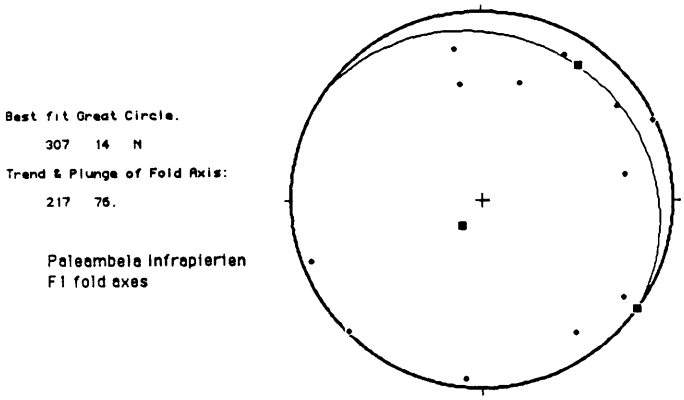

Figure A3.1

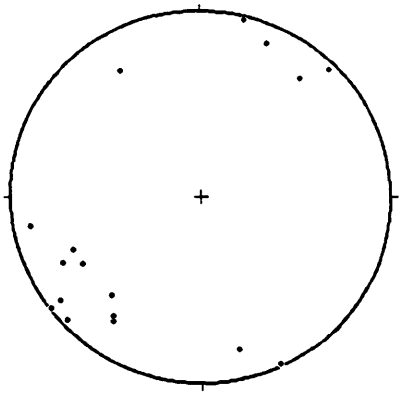

D1 mylonitic lineations

Figure A3.2

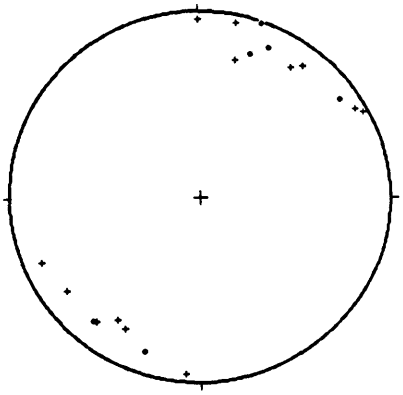

Figure A3.3

Figure A3.1. F1 isoclinal fold axes, Infrapierien-Paleambela unit.
Figure A3.2. Stretching lineations from Infrapierien-Livadi and Pierien-Thoma thrust sheets thought to be related to D1 thrusting.
Figure A3.3. F2 and F3 fold axes, Infrapierien unit

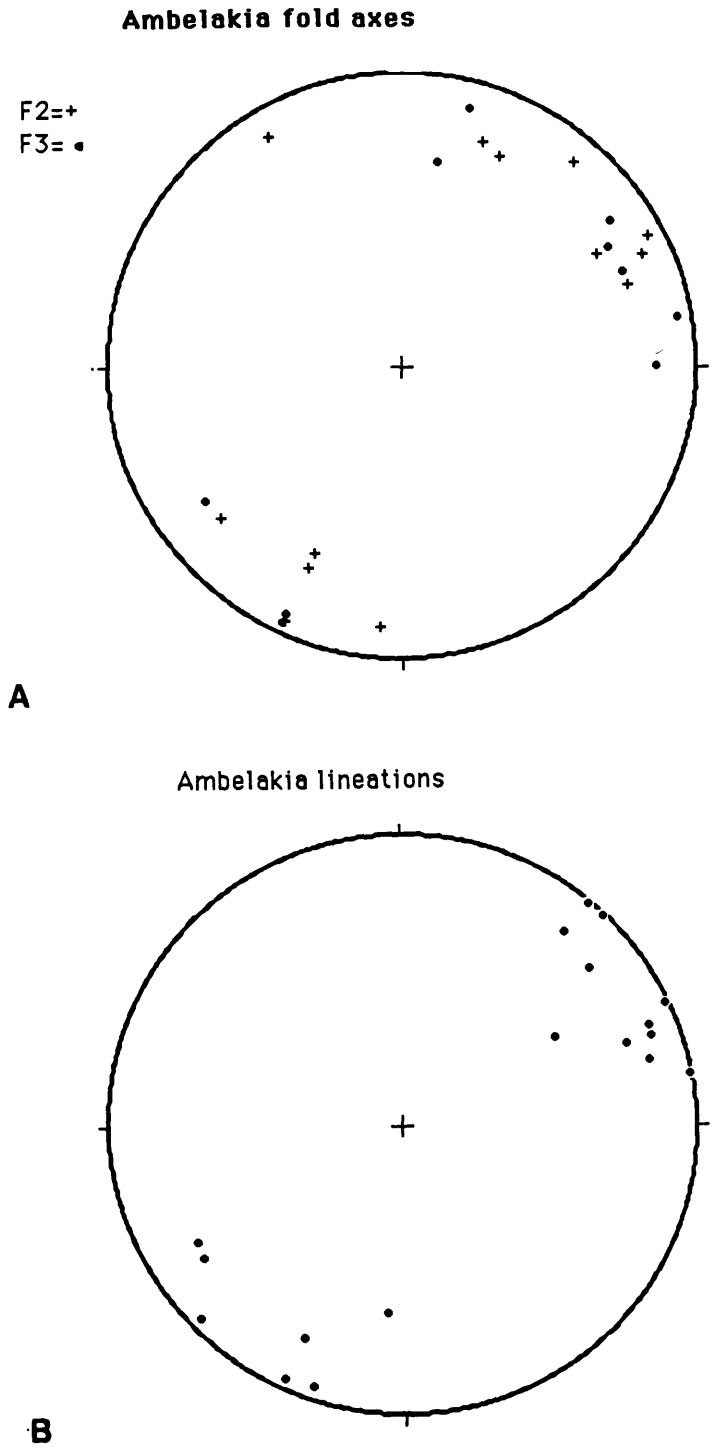

Figure A3.4. A: F2 fold axes, Ambelakia unit; B: L2 mineral lineations, Ambelakia unit

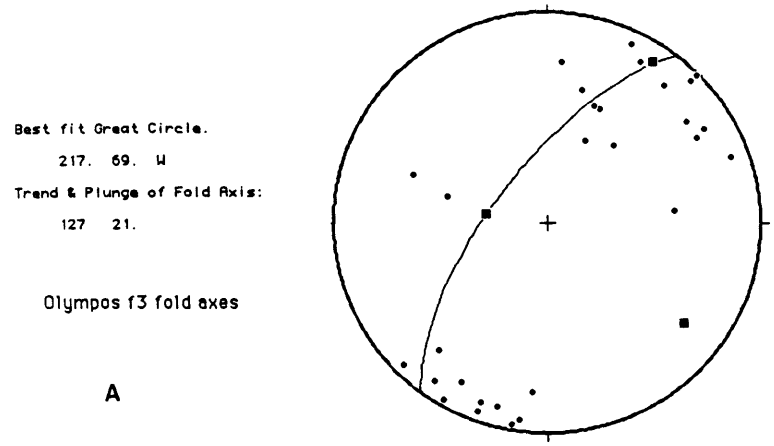

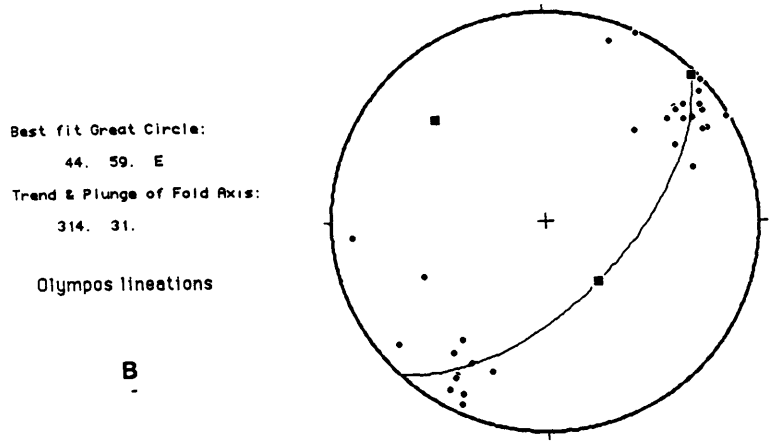

Figure A3.5

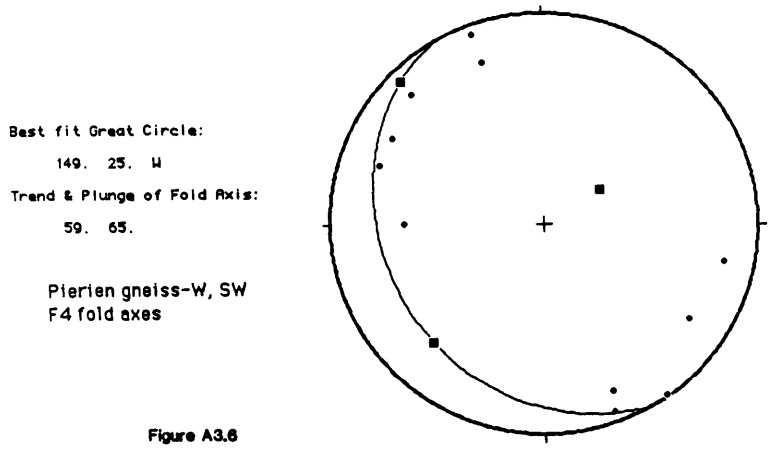

Figure A3.6

Figure A3.5. A) F3 fold axes and B) L3 mineral lineations, Olympos unit
Figure A3.6 F4 fold axes, Pierien unit.

Chapter Four: TEMPERATURE-TIME HISTORY OF SUBDUCTED CONTINENTAL CRUST, MT. OLYMPOS REGION, GREECE

INTRODUCTION

During the Alpine orogeny in Greece, the African plate collided with the European plate to form the Hellenic Alps. Deformation began in the internal (eastern) Hellenides with intrusion of middle Jurassic granites and obduction of middle Jurassic ophiolites in latest Jurassic time, and continued episodically through Cretaceous and Tertiary time as deformation progressed from east to west into the external Hellenides. In the Mt. Olympos region, continental basement and cover rocks were subducted, metamorphosed under high pressure – low temperature conditions, and thrust over carbonate platform strata. Due to the complex metamorphic and deformational history of the internal Hellenides, considerable controversy still exists as to the number, age, and regional significance of various deformation phases, and there is little agreement on the paleogeographic reconstruction of the region (see Robertson and Dixon, 1984 for a useful introduction to the many problems).

The peaks and high topography of Mt. Olympos (Fig. 4.1) are formed by carbonate rocks that are thought to correlate with the external Hellenides (Godfriaux, 1968; Fleury and Godfriaux, 1974) These rocks are exposed in a tectonic window through the metamorphic rocks of the internal Hellenides. The exposure of a thick structural cross-section through the orogen in this area provides the opportunity to study a large part of the long history of deformation and metamorphism in the Hellenides.

In this paper we present $^{40}Ar/^{39}Ar$ and Rb/Sr data from metamorphic rocks of the Olympos region of the internal Hellenides. We have combined the geochronologic study with detailed mapping and petrologic analysis in order to constrain the relations between deformation and metamorphism and to better interpret the tectonic significance of the geochronologic data (Schermer and Burchfiel, 1987; Schermer et al, 1988; in prep). Because abundant structural evidence exists for the rapid uplift of these blueschist facies rocks, we hoped that dating of minerals with different closure temperatures (Dodson, 1973) would also provide a low-temperature thermal history of the units as they were transported from high-pressure, low-temperature conditions to the surface.

The relatively low temperatures of metamorphism (~350-400°C) and the absence of overprinting by higher-T assemblages have resulted in the preservation of the long and complex thermal and structural history of the metamorphic rocks in this region. Diffusive-loss profiles in $^{40}Ar/^{39}Ar$ spectra from white mica and

microcline record evidence for pre-Alpine thermal events as well as several distinct phases of Alpine metamorphism and deformation.

Geologic setting of the Internal Hellenides

The Hellenides (Fig. 4.1) have been divided into internal and external parts. The internal, or eastern, portion was deformed and metamorphosed beginning in latest Jurassic to Early Cretaceous time. The external Hellenides consist dominantly of unmetamorphosed Triassic to Tertiary carbonate platform and basinal strata that were not deformed until post-Eocene time. Thrusting progressed westward from the internal Hellenides in Cretaceous-Eocene time, with imbrication of the external Hellenides during Oligocene to Pliocene time (Aubouin, 1959; Jacobshagen et al, 1978; Papanikolaou, 1984a). Concurrent with compressional deformation, extension and subsidence of the Mesohellenic trough occurred during the Oligocene and Miocene (Papanikolaou et al 1988). Opening of the Aegean back-arc basin and formation of the present-day plate boundary system began at ~10-13 Ma (Angelier, 1978).

Mt. Olympos, in northern Thessaly, (Fig. 4.1) appears beneath a large area of Paleozoic to Mesozoic metamorphic rocks termed the Pelagonian zone of the internal Hellenides (Aubouin, 1959). To the east of the Olympos region, the Vardar zone (Fig. 4.1) is dominated by ophiolitic rocks and extends northward into the inner part of the Dinarides in Yugoslavia. This zone is thought to be a main suture between the continental fragments of the Pelagonian zone (or the African promontory) to the west and Rhodope to the east, but the original size of the oceanic basin or basins is uncertain (compare Burchfiel, 1980; Jacobshagen et al, 1978, and Vergely, 1984). Other workers (e.g. Smith, 1971; Barton, 1976) believe that the ophiolites present throughout the internal Hellenides originated from more than one Jurassic ocean basin; a Vardar ocean to the east of the Pelagonian zone, and a Pindos ocean to the west. In such a scenario the Pelagonian zone would have been a microcontinental fragment, rather than a part of the Apulian (African) plate during the Jurassic and Cretaceous (e.g. Mountrakis, 1986).

In the Mt. Olympos region, (Fig. 4.2), the Pelagonian zone can be subdivided into four principal structural units, including from top to bottom (Figs. 4.2, 4.3): 1) dismembered ophiolitic rocks; 2) deformed greenschist and blueschist facies Paleozoic continental basement gneisses and granites overlain by Permo-Triassic metasediments and metavolcanic rocks, and Triassic and Jurassic platform limestone and dolomite (Pierien and Infrapierien units); 3) blueschist facies

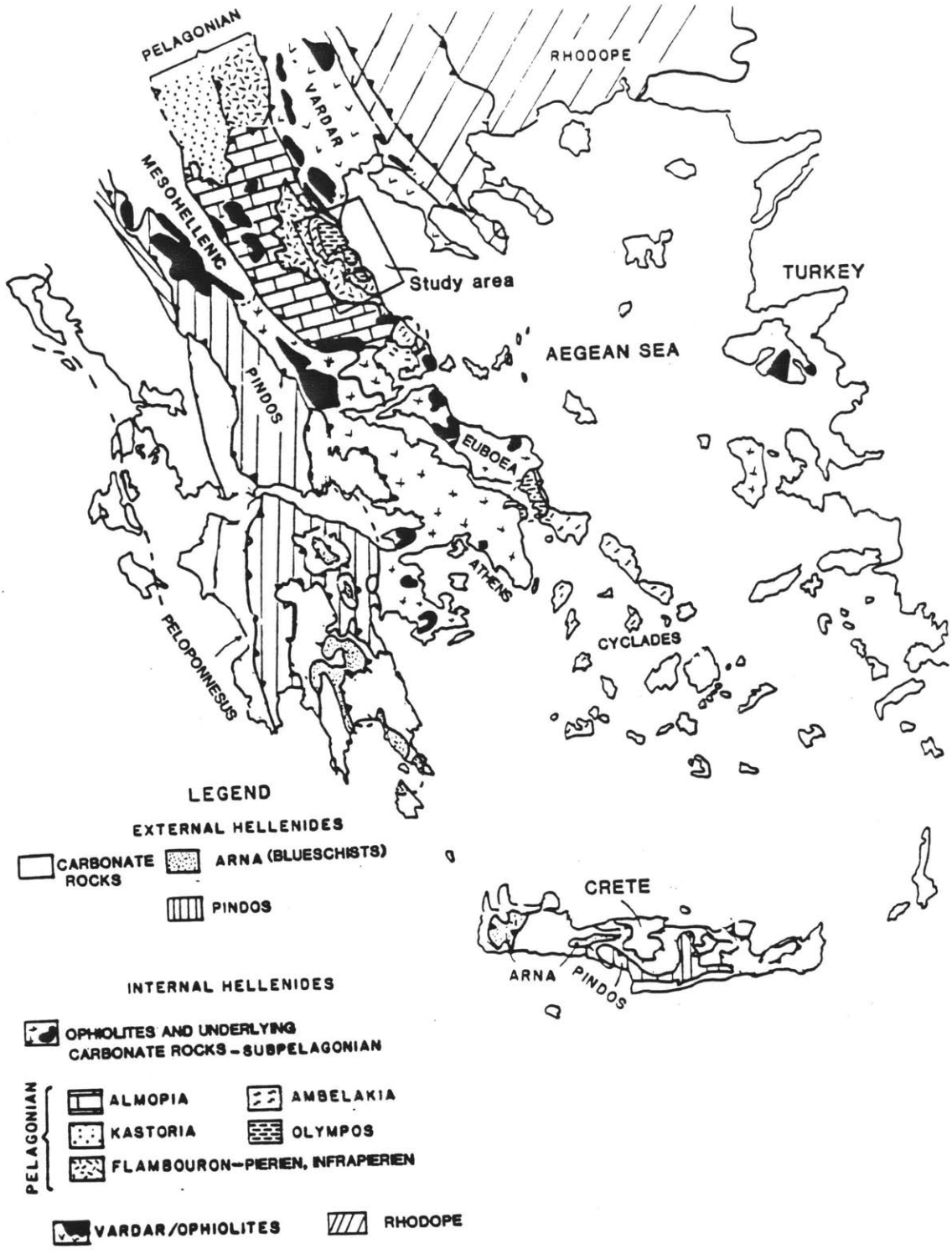

Figure 4.1: Tectonic map of Greece, modified from Papanikolaou (1984a), Jacobshagen et al (1978).

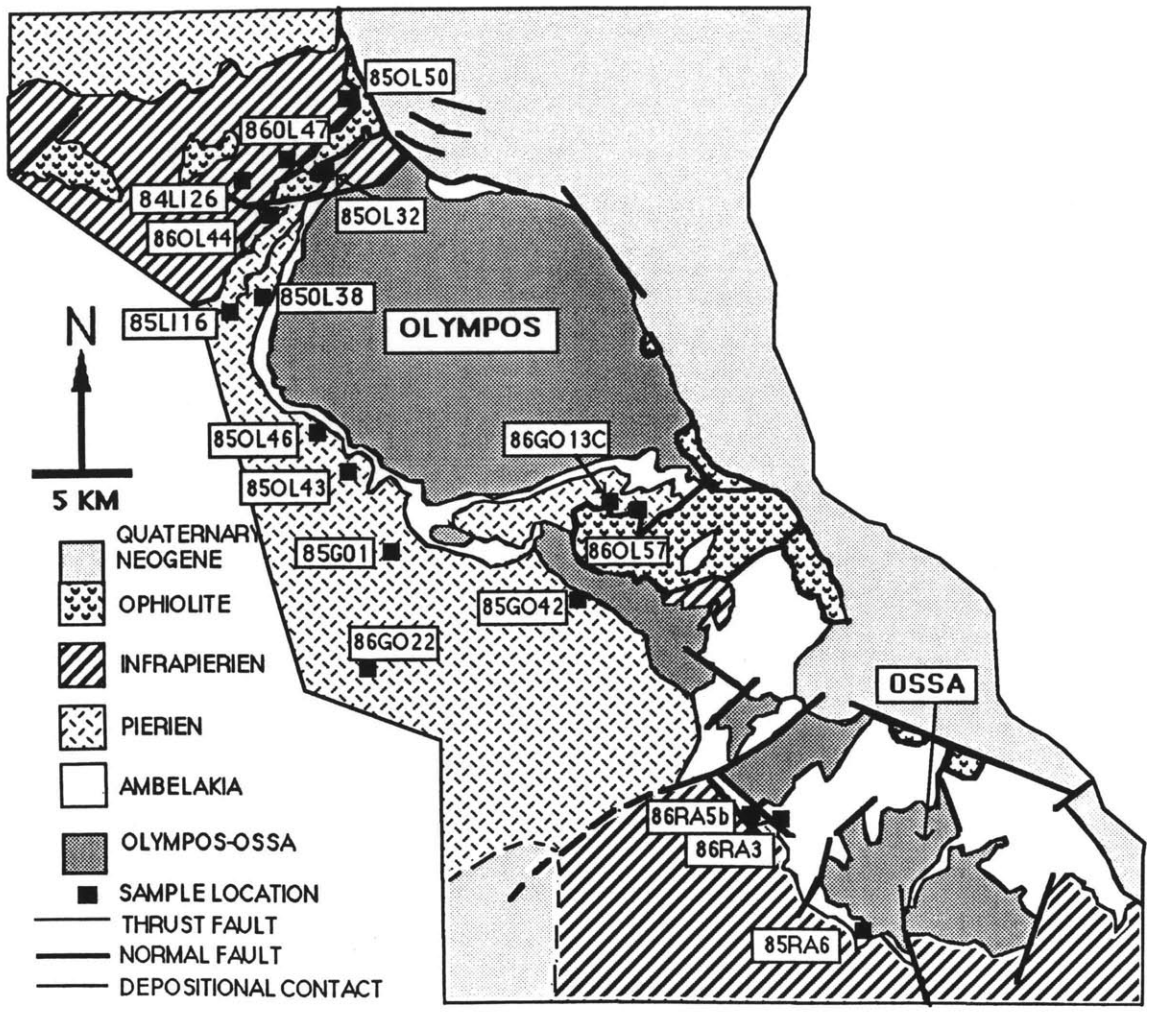

Figure 4.2: Simplified geologic map of the Olympos area, with locations of samples analyzed for Rb/Sr and $^{40}Ar/^{39}Ar$ dating. Mapping by the author on the flanks of Mt. Olympos , modified from Schmitt (1983) and Katsikatsos and Migiros (1987) in the Ossa mountains.

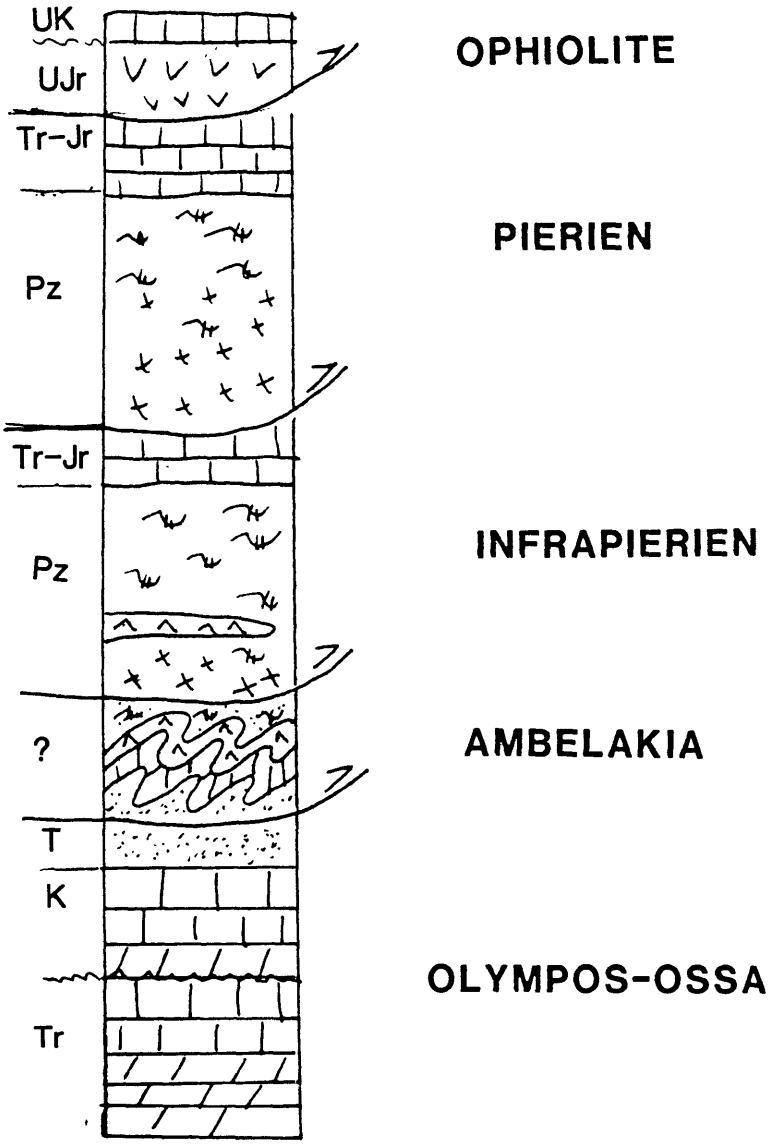

Figure 4.3: Schematic tectonostratigraphic section showing lithologies and terminology of the structural units in the Olympos region.

continental margin carbonate rocks, quartzo–feldspathic sediments, and mafic to intermediate volcanic rocks (Ambelakia unit); 4) parautochthonous Triassic to Eocene neritic carbonate rocks and Eocene flysch (Olympos unit).

The continental basement rocks (2) have been divided into the "Pierien" unit, consisting of dominantly granite and granitic gneiss, overlain by thick marble; and the "Infrapierien" unit, consisting of minor granite, intercalated quartzofeldspathic and amphibolitic gneiss, mica schist, and a thin marble cover (nomenclature modified from Schmitt, 1983). These units are imbricated so that Infrapierien rocks are found both above and below Pierien rocks. In the study area, low-grade metamorphic assemblages occur at four structural levels, with peak metamorphic T apparently decreasing from top to bottom: from A) greenschist and blueschist-greenschist transition facies in the northernmost Infrapierien unit; B) blueschist-facies (P>6-7 kb; Schermer, in prep) in the underlying Pierien unit to the south; C) blueschist-facies in the Ambelakia unit; to D) prehnite-pumpellyite facies in the Olympos unit (Fig. 4.2).

Detailed mapping and sample collecting in the Olympos area have provided insight into the structural and metamorphic evolution of the continental margin during subduction and collision. As reported in Schermer and Burchfiel (1987), and described in more detail elsewhere (Chapter 3), seven tectonic events have been recognized. At least two phases of thrusting and metamorphism within the Pierien and Infrapierien units occurred prior to their emplacement above the Ambelakia and Olympos units (D0, D1; Chapter 3). Emplacement of ophiolite nappes above the Pierien and Infrapierien units probably occurred during these phases. Thrusting was accompanied by isoclinal folding and greenschist-amphibolite facies and blueschist-greenschist transition facies metamorphism. Blueschist facies metamorphism of the Ambelakia and Pierien units was accompanied by two phases of folding and foliation formation, culminating in the southwest-vergent thrust emplacement of the Pierien unit above the Ambelakia unit (D2) and later emplacement of both units above the Olympos platform along the Olympos thrust (Godfriaux, 1968; D3). Movement on the Olympos thrust must be younger than the Lutetian flysch that occurs in its footwall. Two subsequent phases of tight to open folds have deformed the original thrust faults (D4,D6). The final phase of deformation includes several generations of normal faults (D5,D7) which cut through the sequence of thrust faults and place the highest structural units down to the east and northeast against the lowest structural units. Young normal

faults also cut Neogene and Quaternary alluvial deposits along the eastern flank of Mt. Olympos.

Previous geochronological studies

The age of first emplacement of ophiolitic rocks is known to be latest Jurassic to Early Cretaceous (pre-Albian) in the Vardar zone because Tithonian sedimentary rocks contain ophiolitic debris and Albian limestone overlaps the thrusts in the Vardar zone (Mercier, 1968; Mercier et al, 1975). However, subsequent shortening has reactivated many of these thrust faults so that ophiolites rest on sedimentary rocks as young as Eocene in the Pindos zone. Rb-Sr internal isochron ages (mica, epidote, plagioclase, whole-rock) of 119±3 and 116±5 Ma (Yarwood and Dixon, 1977) as well as an Rb-Sr mica-whole rock age of 124±4 Ma (Barton, 1976) on deformed granitic rocks of the Pierien unit indicate basement involvement during post-Jurassic thrusting. Yarwood and Dixon (1977) also obtained an isochron age on mica-epidote-plagioclase-whole rock of 101±2 Ma on augen schists from the underlying Infrapierien unit. They correlated the greenschist facies metamorphism and foliation formation with this later event and suggested that two distinct Cretaceous events may be interpreted from the data. Granitic intrusions into the Pierien basement have been dated at 302±5 Ma by U-Pb-zircon (Yarwood and Aftalion, 1976). The age of the blueschist metamorphism that affects both the Pierien and Ambelakia units is unknown; however, an Rb-Sr whole rock date of 39±1 Ma by Barton (1976) on phyllonites from the Olympos thrust zone has been interpreted as the age of metamorphism by several authors (Katsikatsos et al, 1982; Vergely, 1984) This age may instead represent the age of thrusting, inasmuch as the rocks are pervasively recrystallized and contain a mylonitic fabric that is parallel to the thrust fault. Dérycke and Godfriaux (1978) reported that the lawsonite-bearing flysch of the Olympos-Ossa unit in the Ossa mountains south of Olympos contains Paleocene fossils, implying that both metamorphism of the flysch, and thrusting of the basement units over the Olympos-Ossa unit are younger than Paleocene.

Blueschist facies metamorphic rocks of the Pelagonian zone extend from Mt. Olympos in the north through the Cyclades islands and eastward into Turkey. In general these rocks comprise marble, calcschist, metapelite, metatuff, and metabasalt (Durr et al, 1978; Blake et al, 1981; Papanikolaou, 1978,1984b; Okay and Ozgul, 1984). Ophiolitic melange is locally associated with the blueschists, however, these rocks are commonly unmetamorphosed or lower greenschist-

grade, and thus must have been emplaced after metamorphism. K-Ar and Rb-Sr ages of white mica and glaucophane from the blueschists range from Late Cretaceous (~80Ma) to late Oligocene (25-29Ma); (Altherr et al, 1977a, 1979; Blake et al, 1981; Ferriere, 1982; Henjes-Kunst and Kreuzer, 1982).

The Cycladic and Thessalian blueschists occur between two other belts of blueschist-facies rocks. In the Vardar zone, older (middle Jurassic, Baroz et al, 1987) blueschists are apparently present, although they were overprinted by greenschist facies metamorphism. To the west in the Peloponnesus, within the external Hellenides, younger (Miocene) blueschists are also present; these have been interpreted to reflect intracontinental subduction (Thiebault and Triboulet, 1984). Thus the subduction history of the Hellenides has been long and complex and involved both oceanic and continental crust.

Sample selection and analytical methods

Samples for geochronological analysis were collected from the different structural units in an effort to elucidate the complex history of metamorphism, thrusting, and normal faulting. We were unable to obtain separates of any minerals from the flysch of the Olympos unit or the ophiolite unit due to small sample size and extreme weathering. Samples were obtained from the Infrapierien, Pierien, and Ambelakia units. The majority of the samples are mica schists containing phengitic mica that is parallel to the schistosity. Granitic gneiss samples from the Pierien unit yielded both mica and K-feldspar separates, and one amphibolite from the Infrapierien unit was fresh enough to be sampled. Where possible, unweathered samples were obtained in the field; in all cases, any weathered edges were removed with a saw and samples were cleaned in distilled water prior to crushing.

Standard heavy liquid and magnetic separation techniques were used to separate phengite, potassium feldspar, biotite, and hornblende. Because of the extremely fine grain size (10-100μm) of the majority of the phengites from the blueschists, samples were also hand picked to ensure >99% purity. Nevertheless, in some cases, submicroscopic inclusions of sodic amphibole, sodic pyroxene, or epidote were probably present as volumetrically minor constituents. It is also possible that more than one composition of white mica was present in some samples, because many samples contain more than one metamorphic fabric. However, electron microprobe analyses presented in Schermer (in prep; Chapter 5) indicate that all of the white micas with the exception of samples 86GO22,

86OL44, and 86OL57, are phengitic, and that, while compositions vary between samples, the micas within each sample show a very limited compositional variation (with the exceptions noted above). Potassium feldspars are dominantly microcline, but partially exsolved K-feldspar is also present in in several samples. Samples (100 mg micas, 150-200 mg feldspar, 500 mg hornblende) were irradiated with two irradiation monitors, (interlaboratory standards, SB51-246.7 Ma, and IEH-180.9 Ma, by comparison with MMhb-1), for 72 hours in the Ford reactor at the University of Michigan. Incremental step heating analysis was performed at the University of Maine, Orono (supervised by Dr. Dan Lux), using a molybdenum crucible and radio frequency induction heating followed by gettering using Cu-CuO and Zr-Al getters and a molecular sieve desiccant. A Nuclide 6-60-SGA 1.25 m mass spectrometer was used for the isotopic analyses.

Ages and uncertainties (2σ) were calculated using equations given by Dalrymple et al (1981). Criteria for determining plateaus were from Fleck et al (1977) and Dalrymple and Lanphere (1969). Where several increments do not statistically define a plateau (using analytical errors) but are within 2σ error of each other (total error, including error in J-value) so that they overlap on the release spectra; a "near-plateau" age was calculated; the error on this near-plateau age reflects the spread of the increment ages. All ages discussed in this paper are calculated using the decay constants of Steiger and Jaeger (1979).

The assumption that non-radiogenic Ar is of atmospheric composition is tested by the use of a $^{39}Ar/^{40}Ar$-$^{36}Ar/^{40}Ar$ isochron plot (Roddick et al, 1980), where successive increments having a similar composition of extraneous (non-radiogenic) argon should lie on a mixing line between nonradiogenic Ar of $^{36}Ar/^{40}Ar$ ratio given by the x-intercept and radiogenic ^{40}Ar given by the y-intercept at a $^{39}Ar/^{40}Ar$ ratio corresponding to the true age of the increments. As discussed by Heizler and Harrison (1988), there may be more than one component of extraneous argon in a sample, each degassing over a particular temperature range, so that in order to obtain meaningful ages in the release spectra, each portion of the spectrum should be corrected for its corresponding isotopic composition of extraneous Ar. We have not corrected our spectra in this way, but in cases where the non-radiogenic component or components do not appear to have atmospheric composition, we have calculated an intercept age. Plots of K/Ca ratio as measured by $^{39}Ar/^{37}Ar$ are also shown where the ^{37}Ar peak was large enough to be measured accurately (it is often very small for Ca-poor

phases such as muscovite), and where the variation during the course of the step-heating experiment was significant.

Rb-Sr samples were analyzed in S.R. Hart's laboratory at M.I.T. Sample sizes for Rb and Sr analysis were typically 25-50 mg. Samples were digested in open beakers in an HF-$HClO_4$ mixture with spike solution, followed by dissolution in 6.2N HCl. Rb and Sr were analyzed by isotope dilution methods described in detail by Hart and Brooks (1977). Blanks averaged <300 pg/g for Sr and Rb and are negligible. Sr isotopic compositions were corrected for fractionation using $^{87}Sr/^{86}Sr = 0.1194$ and normalized to 0.7080 for E&A $SrCO_3$. Analytical precision for $^{87}Sr/^{86}Sr$ is <0.005%; Rb/Sr is reproducible to better than 1%.

RESULTS

Data are presented for each structural unit and discussed together in the following section. A brief summary of the metamorphic and structural characteristics of each unit is also given. Results of the Ar/Ar incremental heating analyses are presented in Table 4.1.

Ambelakia Unit

Three samples collected from the Ambelakia unit show varying degrees of recrystallization and deformation; however, all rocks contain a dominant S_2 foliation plane formed by phengitic micas. Sample 85RA6 was collected <10 m above the thrust fault that places Ambelakia schists above Ossa-Olympos unit metasedimentary rocks and contains a strong mylonitic fabric. Samples 86RA3 and 86RA5b were collected <300 m above the same thrust, however their precise structural position is uncertain as the thrust fault is tightly folded and poorly exposed in this area. Both samples show evidence of two metamorphic fabrics. The S_1 foliation is isoclinally folded and cut by S_2. Both foliations are formed by fine-grained phengites of similar composition (Chapter 5). Sodic amphibole prisms are present in both foliation planes and also as randomly oriented grains, and thus apparently grew throughout the deformation history. The presence of the assemblage glaucophane/crossite-phengite-Na-pyroxene-albite-quartz ± lawsonite ± chlorite constrains the P-T conditions of this unit to T ~250-350°C, P~6-8 kb (Godfriaux et al, 1988; Schermer, 1987; Chapter 5).

Step heating data from micas from the Ambelakia unit are shown in Figure 4.4. Sample 86RA5b shows a well-developed plateau at 39.6±0.9 Ma. The other two samples show complicated diffusive loss profiles yielding Oligocene ages for low-temperature steps and Cretaceous ages for high-temperature steps. An Ar

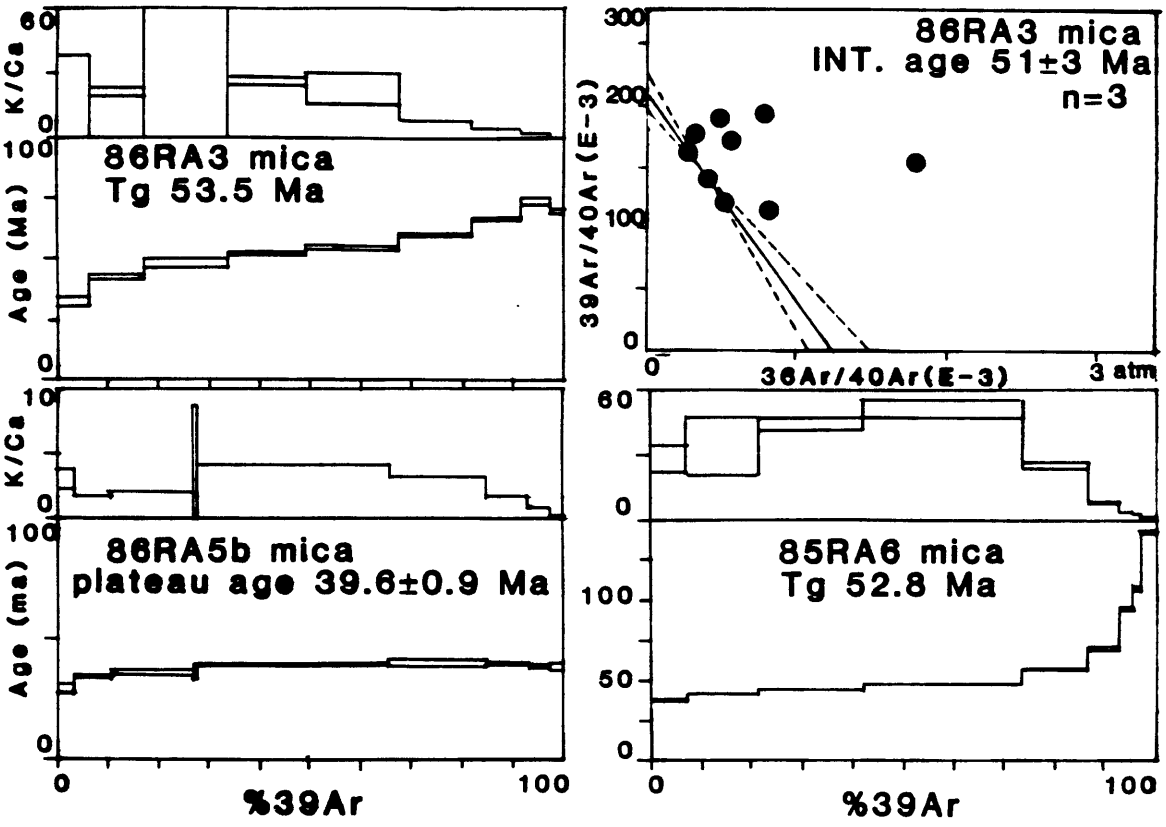

Figure 4.4: $^{40}Ar/^{39}Ar$ incremental release spectra and $^{39}Ar/^{40}Ar$-$^{36}Ar/^{40}Ar$ isochron plots for samples from the Ambelakia unit. See Figure 4.2 for sample locations.

isochron plot for sample 86RA3 (Fig. 4.4) indicates that the increments of gas released at high-temperatures do not plot on a line corresponding to atmospheric extraneous Ar; linear regression of these three steps gives an age of 51±4 Ma, in agreement with the total gas age of 53.5±1.1 Ma. Sample 85RA6 also has an early Eocene total gas age of 52.8±0.7 Ma, and the spectrum appears to level off at 44-55 Ma. However, during the high-temperature steps the K/Ca ratio drops sharply and the age increases, possibly indicating that an older mica of different composition is also present. There is no clear correlation of homogeneity of Ar composition with degree of recrystallization, as the apparently least-recrystallized sample, (86RA5b), shows the best-developed plateau, while the most thoroughly mylonitized rock, (85RA6), yields the most disturbed spectrum.

In summary, the three Ambelakia samples show at least two periods during which Ar sites were open to diffusion after their original Cretaceous or older crystallization age; once in early Eocene time, and again in late Eocene time.

Pierien Unit

Samples from the crystalline basement rocks of the Pierien unit have been divided into three groups based on structural level: 1) samples from 40-400 m above the basal thrust and from parallel mylonite zones higher in the thrust sheet; 2) metasedimentary and granitic rocks from >400 m above the thrust that are not strongly mylonitized; and 3) mylonitic gneisses 10-50 m below the normal faults which bound the upper part of the Pierien unit on the north and east sides of Mt. Olympos (Fig.4.2).

Samples from the mylonite zones in the lower part of the sheet, (85OL38, 85OL43, 85OL46, and 85GO42; Fig. 4.1), consist of mylonitized granitic to granodioritic gneiss, containing the mineral assemblages qtz-kspar-plag-phengite and qtz-plag-phengite-riebeckite-acmite as the latest stable assemblages. All samples are strongly foliated and contain a mylonitic fabric. Some samples show evidence of two metamorphic foliations; S_1 is isoclinally folded and transposed into S_2; however the same mineral assemblage is present in both fabrics. Quartz was dynamically recrystallized; feldspars are more brittley deformed and are present as augen with recrystallized tails. Mylonitization is intense within ~100 m of the basal thrust fault, but structurally higher rocks were variably mylonitized, with high strain apparently localized in zones a few meters thick throughout most of the crystalline sheet. The high phengite content of the micas indicates high pressure conditions of metamorphism, P>6-8 kb (Velde, 1967; Massonne and Schreyer, 1987);

however temperature conditions are poorly constrained. It will be argued below that temperatures probably did not exceed 350-400°C.

Incremental release profiles from these samples are shown in Figure 4.5. Sample 85OL46, a phengitic mica from ~45 m above the thrust fault, shows a gradient in age from 55 to 36 Ma that resembles a diffusive loss profile. Sample 85OL38, from ~310 m above the thrust fault has a similar pattern, with a near-plateau at 57±2 Ma, and a gradient down to 45 Ma in the low-temperature increments. In both samples, the final ~1% gas released is significantly older (middle Cretaceous) and could represent either excess argon incorporated into retentive sites, or another phase that has contaminated the sample. Phengite sample 85GO42, collected ~400 m above the thrust fault, shows a well developed plateau at 53.9 ± 0.8 Ma. Regression of these data on an isochron plot shows that the initial $^{36}Ar/^{40}Ar$ ratio was slightly different from atmospheric, giving a corrected age of 53.1±0.7 Ma. Phengite 85OL43, from a mylonite zone ~750 m above the thrust, shows a pattern similar to 85OL46 and 85OL38, with an age gradient from 56 to 40 Ma, and two small increments at high temperature with significantly older (middle Cretaceous and late Paleozoic) ages. Rb-Sr data from these samples reported by Schermer (1987) and shown in Table 4.2 and Figure 4.6, yield feldspar-whole rock-mica "errorchron" ages of 45±2, 40±2, and 39±4 Ma with increasing distance above the thrust fault, and mica-whole rock pair ages of 42±1 for all samples. The only potassium feldspar sample from near the thrust fault, 85OL38 (Fig. 4.5), shows a saddle-shaped argon release pattern, with a gradient from 50 Ma at high temperatures to a minimum of 28 Ma at low temperatures. The spectrum resembles a diffusive loss spectrum with a small component of superimposed excess argon (Harrison and McDougall, 1982).

In the second group of Pierien samples, 85GO1 and 85LI16 are blueschists from ~450 m and ~1200 m above the basal thrust of the Pierien unit. These samples are foliated, with phengite, blue amphibole, and epidote lying in the foliation planes, but do not contain the strong mylonitic fabric characteristic of the samples discussed above. Incremental release age spectra are shown in Figure 4.7. Sample 85GO1 shows a well-developed plateau at 61.7±0.8 Ma, with a gradient to 41 Ma at the lowest temperature step. Sample 85LI16 shows a continuous increase in age from 57-66 Ma for the first 95.5% gas released. The older ages in the high-temperature increments are associated with lower K/Ca ratios and thus may reflect degassing of another mineral, possibly sodic amphibole that is present as microscopic inclusions in the micas.

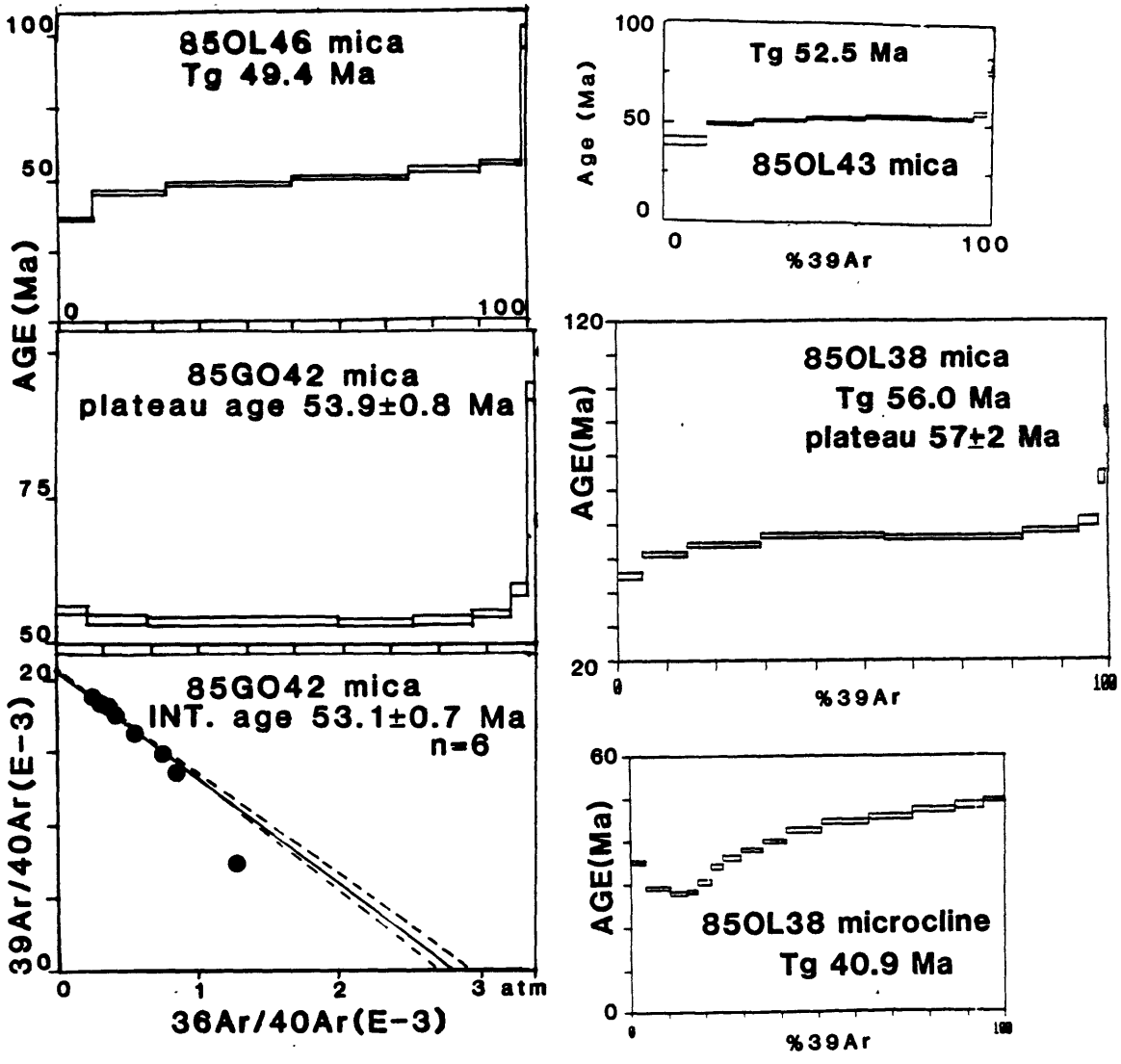

Figure 4.5: $^{40}Ar/^{39}Ar$ incremental release spectra and $^{39}Ar/^{40}Ar$-$^{36}Ar/^{40}Ar$ isochron plots for samples from the lower part of the Pierien unit. See Figure 4.2 for sample locations.

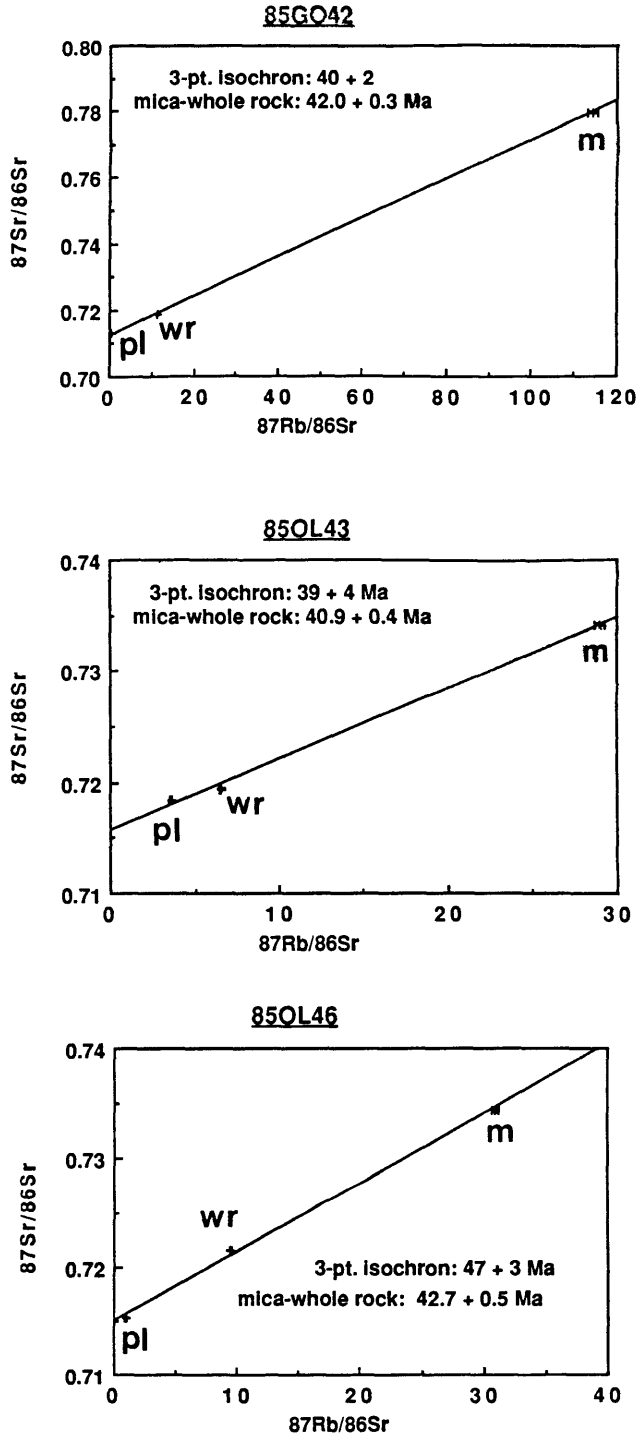

Figure 4.6: Rb/Sr isochron plots for samples from near the thrust fault at the base of the Pierien unit. Errors for 3-point isochrons were calculated using the method of York (1966); errors for 2-point isochrons reflect only the analytical uncertainty and not the degree of scatter about the line.

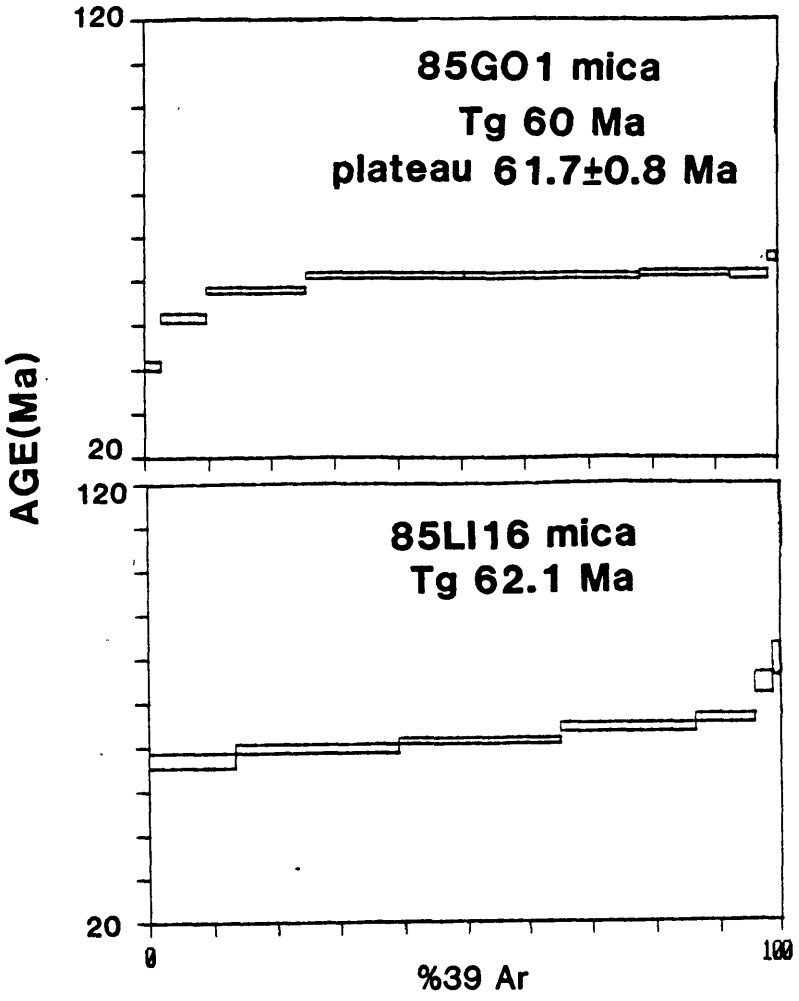

Figure 4.7: $^{40}Ar/^{39}Ar$ incremental release spectra and $^{39}Ar/^{40}Ar$-$^{36}Ar/^{40}Ar$ isochron plots for samples >400m above the basal thrust fault of the Pierien unit that contain blue amphibole and a weak mylonitic fabric; See Figure 4.2 for sample locations.

Samples 86GO22 and 86GO22a were collected from relatively weakly foliated granodiorite and granite from high levels within the Pierien unit (Fig. 4.2). Although the granodiorite is not strongly deformed at this locality, mylonitic fabrics are variably developed in rocks of similar lithology both above and below this level, and field relationships indicate it is part of the thrust sheet rather than a younger (post-Cretaceous, pre-Eocene) cross-cutting intrusive as interpreted by Katsikatsos et al (1982), and Davis and Migiros (1979) (Schermer and Burchfiel, 1987; in prep). Hornblende and biotite were separated from the main granodioritic body (86GO22), and potassium feldspar was separated from an aplitic dike which cuts the granodiorite (86GO22a). Similar dikes also cut more felsic parts of the igneous body and are foliated along with the host rocks in areas where deformation has been more severe.

The hornblende spectrum shown in Fig. 4.8a is disturbed, and shows a pattern characteristic of excess argon incorporation. Although the total gas age is 419 Ma and would be meaningless if the spectrum is dominated by excess Ar, the minimum (saddle) age of 295 Ma could represent a maximum age for closure of the hornblende to Ar diffusion. This is supported by the Ar-Ar isotope correlation plot, where regression of the last seven increments, representing 89% of the gas, gives an intercept age of 293±21 Ma. The biotite spectrum, while also disturbed, shows a similar age of 291±7 in its middle portion, with some indication of an argon loss event during or after the Late Cretaceous. The potassium feldspar shows a strong age gradient from 84 to 36 Ma, with minor excess argon indicated by the saddle shaped spectrum.

The third group of Pierien samples have experienced the most complicated structural history of any of the samples analyzed. In addition to containing mylonitic fabrics apparently related to thrusting, these samples also show a later, more brittle cataclastic fabric related to their proximity to normal faults. Samples 86OL57 and 86GO13c come from granitic gneiss <50 m below a low-angle normal fault that places ophiolitic rocks of the highest structural unit against a thin sliver of Pierien basement rocks which in turn overlies the Ambelakia units along a thrust fault. Samples 86OL44a and 44b are from near the intersection of a thrust between the Pierien and Infrapierien units and a large high-angle normal fault which places ophiolitic rocks against a variety of structurally lower units. The samples consist of quartz + microcline + plagioclase + phengite ± epidote. They also contain two generations of white mica, visible in thin section and hand sample as coarse-grained silver muscovite fish that are surrounded by later fine-grained green

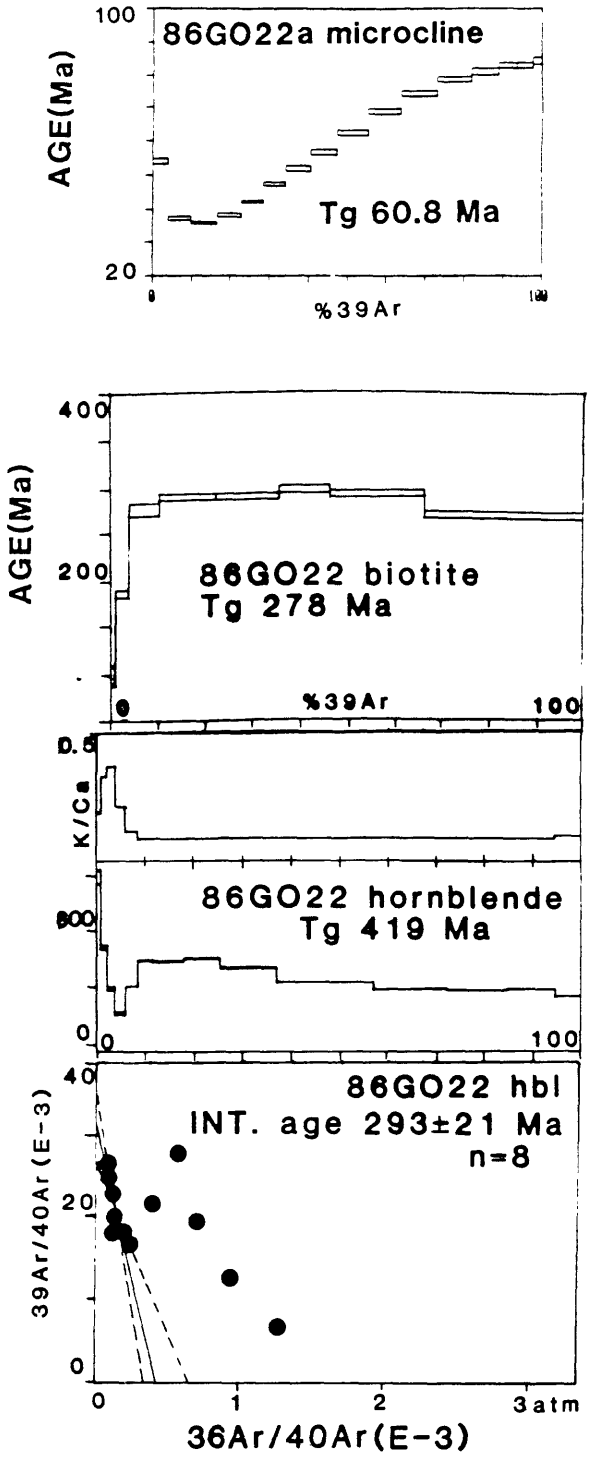

Figure 4.8: $^{40}Ar/^{39}Ar$ incremental release spectra and $^{39}Ar/^{40}Ar$-$^{36}Ar/^{40}Ar$ isochron plots for samples from upper parts of the Pierien unit: A) samples from granodioritic to granitic rocks in the upper part of the Pierien unit.

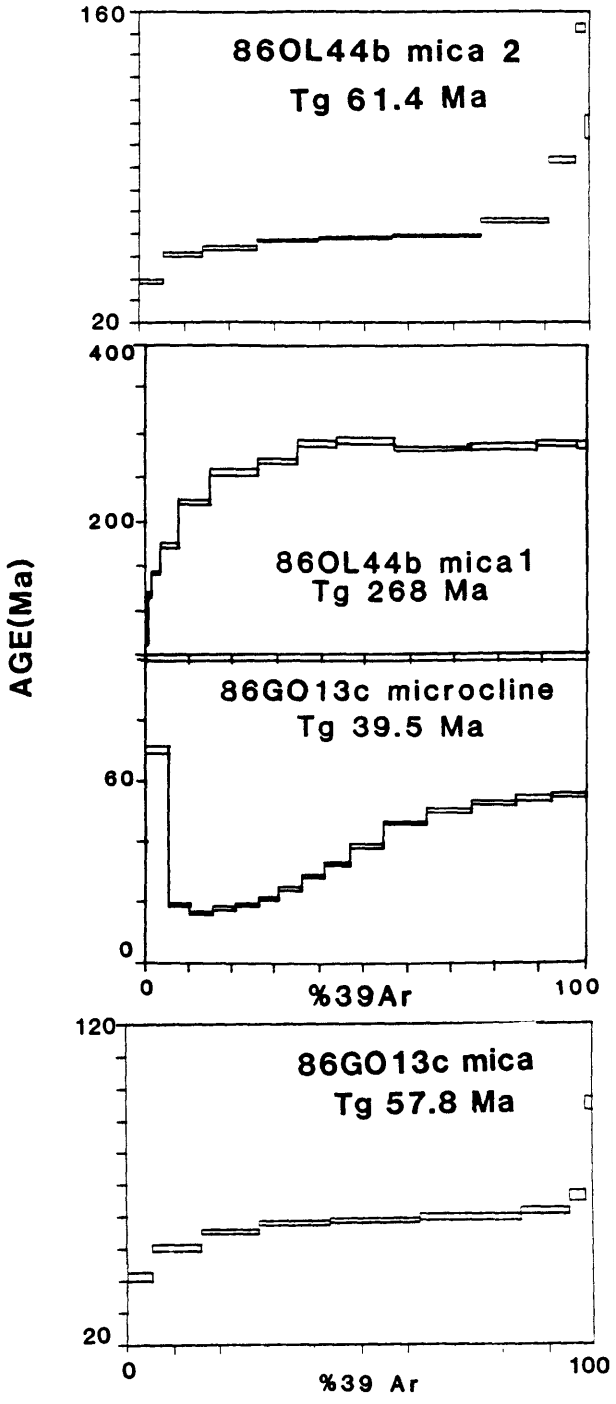

Figure 4.8b: Samples from the uppermost levels of Pierien gneiss below normal faults against ophiolitic rocks.

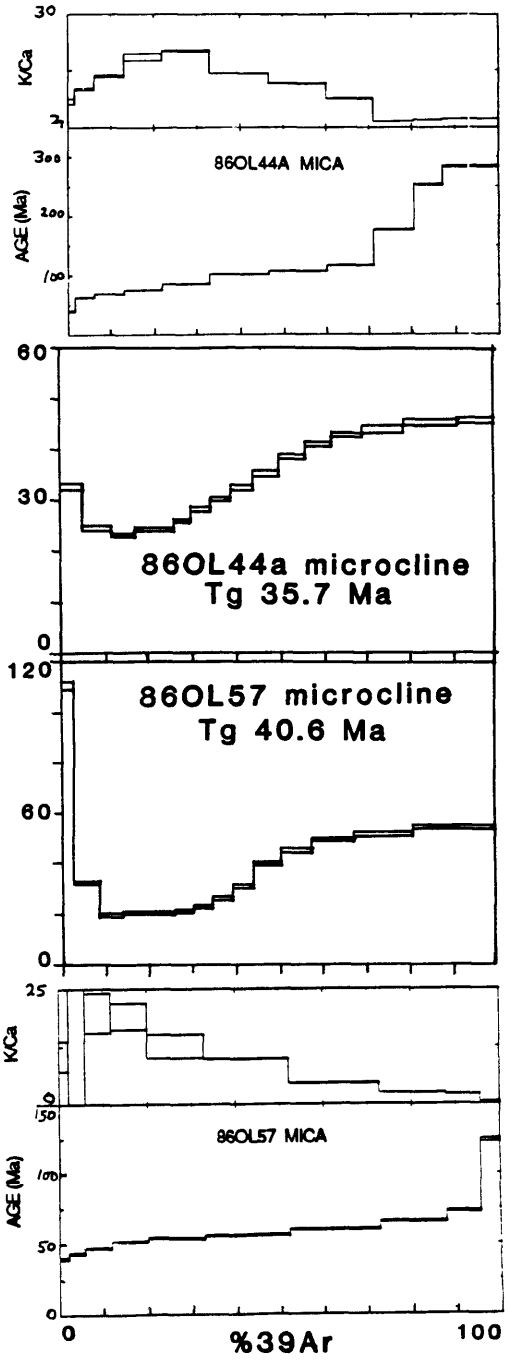

Figure 4.8b (continued).

phengites that parallel the mylonitic foliation. Fine-grained phengite dominates in sample 86OL44a; however it was impossible to obtain a clean separate from the crushed grains of the coarse mica and the contaminant may be >30% of the sample. 86OL44b-M1 consists of coarse (500-100 μm) muscovite, while 86OL44b-M2 is the fine-grained phengite, with perhaps ~2-5% contamination by the muscovite of sample M1.

Mica samples 86OL44a,b show complicated incremental release spectra indicated in Fig. 4.8b. Both 86OL44a and 86OL4b-M1 show evidence of preserving the original basement age, at 284 Ma and 290 Ma at the high temperature portion of the spectra, similar to the relatively undeformed samples discussed above. 86OL44b-M1 shows a smooth age gradient down to a poorly defined late Cretaceous-early Tertiary age, whereas OL44a appears to level off at Cretaceous ages in the middle steps, but was not closed to Ar loss until ~40 Ma. This spectrum may be the result of degassing of a mixture of the micas of the two different compositions noted above, as indicated by the K/Ca pattern. Sample 86OL44b-M2 also shows evidence of mixing of two different micas, however, this spectrum levels off at 56.8-58.7 Ma and shows a gradient down to 38 Ma. Apparently the two micas were thermally distinct during the degassing experiment and show distinct crystallization (or cooling) ages that are ~290 Ma and ~57 Ma, with final closure to Ar loss at ~ 38 Ma, consistent with the ages obtained on the cleaner mica separates discussed above.

The mica separate from 86OL57 also shows a complicated profile (Fig. 4.8b), with: evidence of a phase of middle Cretaceous age and low K/Ca ratio present in the high-temperature steps; ~60% of the gas in the 50-60 Ma range, though not forming a plateau; and a low temperature release indicative of final closure to Ar loss at 40 Ma. This sample also shows evidence of two generations of mica formation; one coarse-grained muscovite phase (~100-150μm), and a fine-grained phengitic phase. Although the coarse-grained phase appears to represent <2% of the separate, it may contain substantial amounts of ^{40}Ar. The mica sample 86GO13c shows a relatively simple age gradient interpreted to be a diffusive-loss profile, from a near-plateau of 59.5±3.6 Ma to 42 Ma. Again, the last ~5% gas released is significantly older.

The microcline spectra in Figure 4.8 are somewhat simpler than the mica release patterns. All three samples show saddle-shaped spectra, having high-temperature increments that level off to Eocene ages, and minimum ages in the Early Miocene. Sample 86OL44a appears to have the least excess Ar in low-

temperature steps, and also has the youngest high-temperature ages of the three samples.

In summary, samples from the Pierien unit show evidence for five distinct events of opening and closure to Ar diffusion: 1) late Paleozoic (~295 Ma) closure to diffusion in hornblende, biotite, and muscovite; 2) reopening to diffusion possibly in the Cretaceous, though poorly defined; 3) an event at 53-62 Ma; 4) another Eocene event at 36-40 Ma; and 5) a Miocene event at 16-23 Ma closure to Ar diffusion in potassium feldspar.

Infrapierien Unit.

Phengitic micas were separated from coarse mica schists from the Infrapierien unit (Schmitt, 1983) that were thrust above the Pierien gneisses (Fig. 4.2). This unit shows evidence of at least three periods of deformation and metamorphism. The first event produced isoclinal folds and S_1 foliation during amphibolite facies metamorphism. The second event formed tight folds with S_2 foliation, under blueschist-greenschist transition facies conditions. The third event developed an S_3 mylonitic fabric near thrust faults against the Pierien unit (Schermer and Burchfiel, 1987). S_2 and S_3 fabrics are overprinted by later cataclastic shears related to younger normal faults. Samples 85OL32 and 85OL50 are dominated by S_2 fabrics formed by coarse micas, blue-green amphibole, and epidote; 84LI26 contains the same mineral assemblage with more abundant amphibole but does not show evidence of a previous metamorphic foliation. Hornblende sample 86OL47 was collected from a massive amphibolite body enclosed within intercalated amphibolite gneiss and quartzofeldspathic gneiss that lie structurally below the mica schists. The mineral assemblage hornblende + plagioclase + biotite ± garnet indicates this rock experienced amphibolite facies metamorphism. Minor retrogression to greenschist facies (chlorite + epidote) is also evident.

Release profiles for the mica samples are shown in Fig. 4.9. Sample 85OL32 shows a pattern of diffusive loss, with high temperature increments that appear to level off at 98-99 Ma, and an initial increment at 56 Ma. The high-temperature data define an Ar-Ar isochron of 98±2 Ma. This is consistent with an Rb-Sr mica-whole rock age of 97±1 Ma (Fig. 4.10). The spectrum for sample 85OL50 is more complex, indicating a combination of Ar loss and excess argon incorporation. Nevertheless, the Ar-Ar isochron plot shows a good fit to the last five steps, resulting in an intercept age of 100±2 Ma, consistent with that of sample 85OL32. The Rb/Sr mica-whole rock age of this sample is 92±1 Ma (Fig. 4.10). Sample

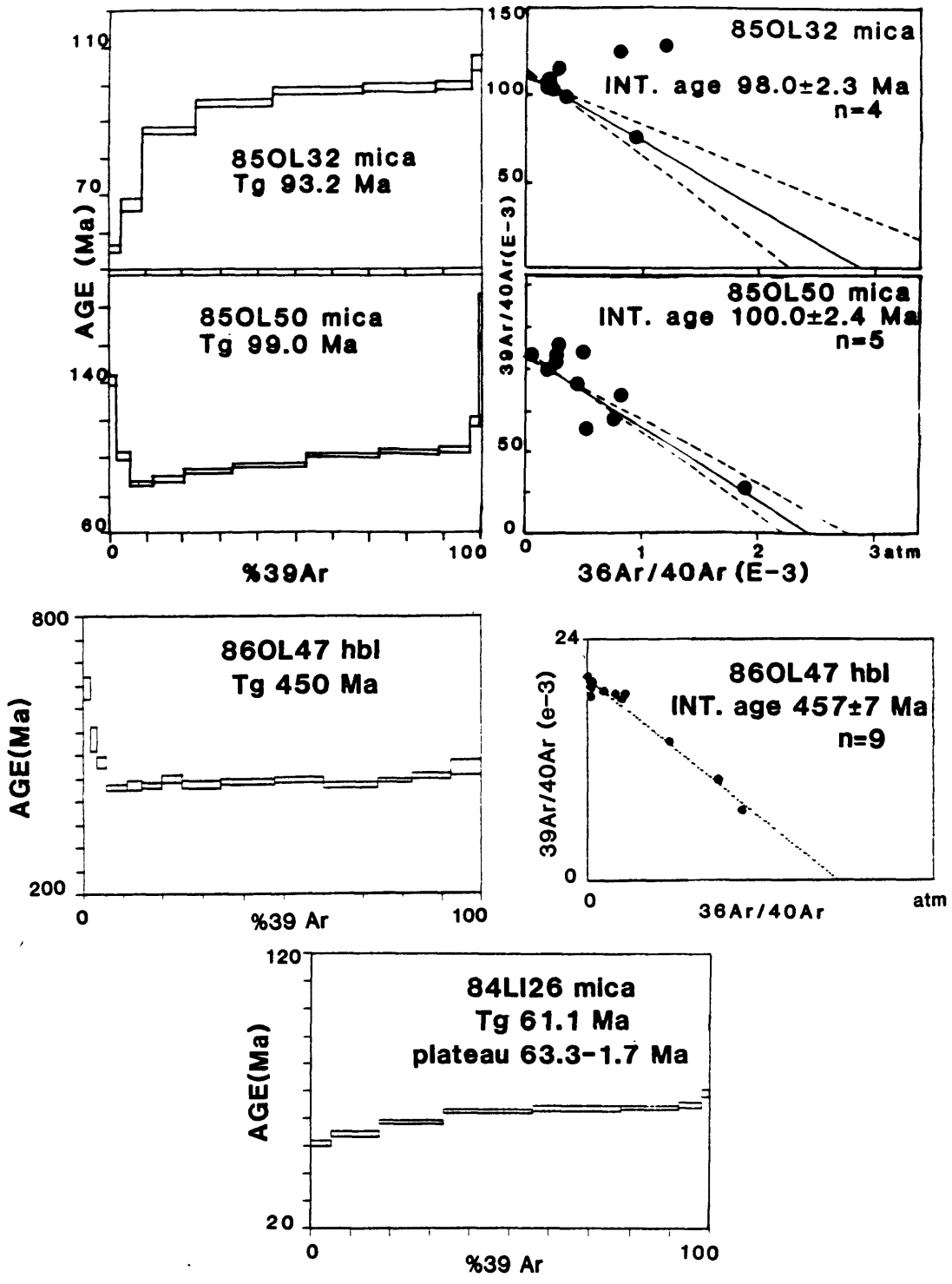

Figure 4.9: $^{40}Ar/^{39}Ar$ incremental release spectra and $^{39}Ar/^{40}Ar$-$^{36}Ar/^{40}Ar$ isochron plots for samples from the Infrapierien unit. See Figure 4.2 for sample locations.

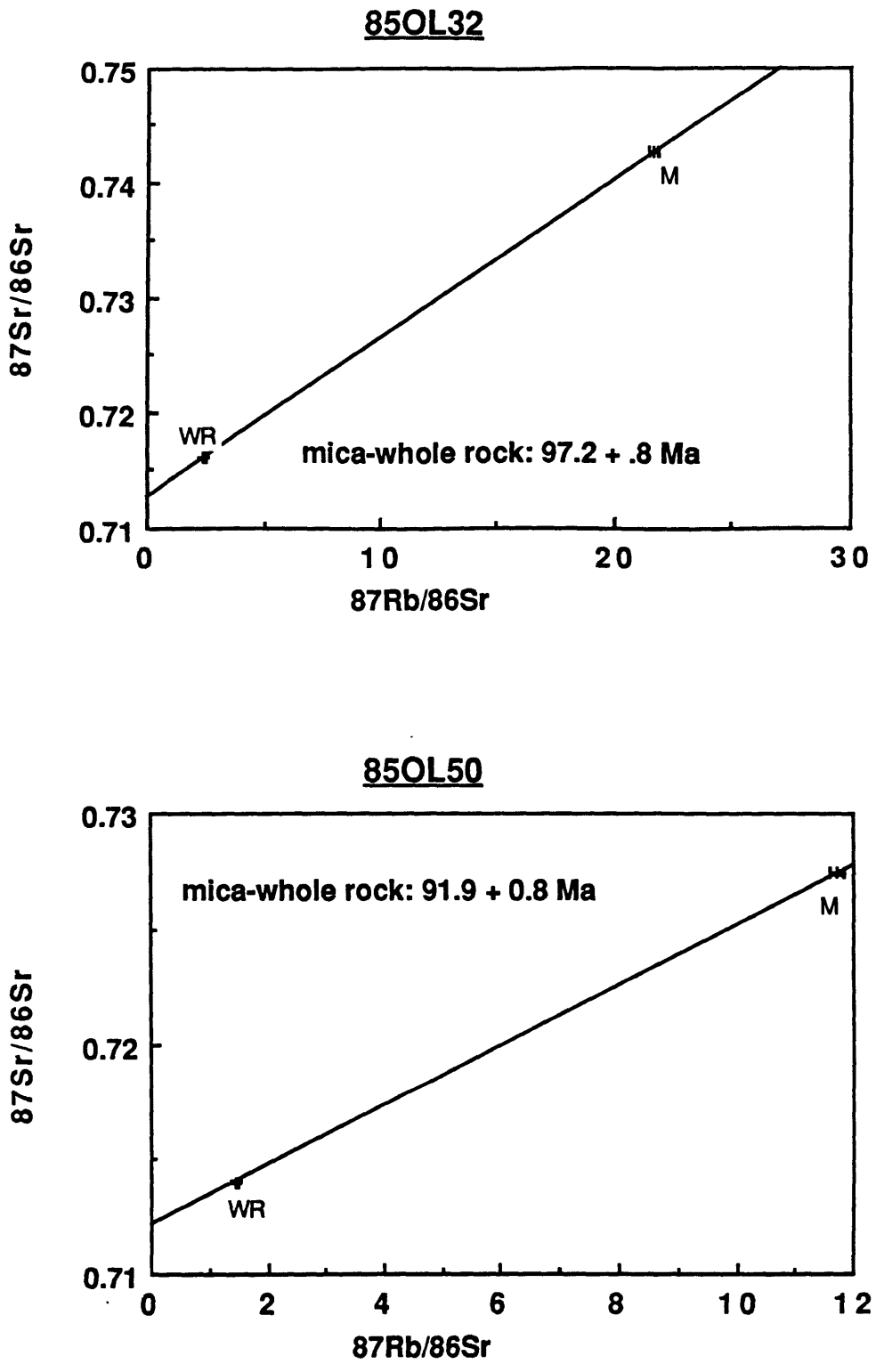

Figure 4.10: Rb/Sr isochron plots for mica-whole rock pairs from the Infrapierien unit. Errors reflect only the analytical uncertainty.

84LI26 exhibits an age gradient from a near-plateau at 63.3 ±1.7 Ma to final closure at ~50 Ma. The hornblende spectrum 86OL47 (Fig. 4.9) is characteristic of excess argon incorporation, but the fairly flat pattern for ~90% release and the approximate agreement between the total gas age (450±8), the "near-plateau" age of increments 4-10 (439±15) and the intercept age on the Ar-Ar isochron plot (457±7) may indicate that this early Paleozoic age is meaningful. However more hornblende samples are needed to ascertain whether this may only be a reflection of a pervasive excess argon component.

DISCUSSION

The complexity of the data presented above is in part a result of the long and complicated history of metamorphism and deformation in the Hellenic Alps. In the Mount Olympos region, much of the deformation and metamorphism occurred at relatively high-pressure, low-temperature conditions. The low temperatures resulted in incomplete resetting of micas and K-feldspars from earlier higher temperature crystallization events. As a result of the low temperatures of metamorphism, we can "see through" many of the younger events to the older events in the incremental heating spectra.

Nonetheless, there are several problems which must be addressed before we can interpret these data in terms of the temperature-time history of tectonism in the Mt. Olympos region. The discrepancy between Ar/Ar and Rb/Sr ages of samples from near the basal thrust of the Pierien unit is unexpected in light of published closure-temperature estimates for Ar (350±50°C) and Sr (500±50°C) in white mica (Purdy and Jaeger 1976; Wagner et al, 1977). We will discuss the potential effects of deformation, excess Ar, and Ar recoil in this context in order to determine whether the early Eocene thermal event recorded by the Ar/Ar data is "real".

We must also consider the origin of the age gradients exhibited by most of the spectra. The presence of the gradients is both problematic, in the sense that these are not easily interpretable spectra; and useful, in the sense that we can gain some insight into the nature of diffusion in phengitic micas and K-feldspar. The conclusion that these gradients are the result of episodic Ar loss that occurred during younger metamorphism and deformation has important implications for the thermal history of this region in that it constrains the temperatures to ~350°C or less during post-Cretaceous time. We can model the diffusion profiles to, in effect, obtain two ages from many samples, an intial crystallization or high-temperature metamorphic age, and the age of the resetting event.

We conclude with a summary of the temperature-time history of this part of the Pelagonian zone and discuss the implications of these results for the regional tectonics of the Alpine orogeny in Greece.

Closure temperatures and the discrepancy between Rb/Sr and Ar/Ar ages

The closure temperature, T_C of a mineral was defined by Dodson (1973) as the effective transition from open- to closed-system behavior in a geochronologic system where volume diffusion is the controlling process for the retention of radioactive daughter products. The principal variables that control the T_C of a mineral include the diffusion coefficient at a given temperature, the cooling rate, and the geometry and effective diffusion dimension of the mineral species (generally much smaller than the grain size).

Closure temperatures for hornblende, biotite, and microcline are estimated to be ~500-550°C, 300-325°C, and 100-150°C, respectively (Harrison, 1981;Harrison and McDougall, 1985; Harrison et al, 1982) at a cooling rate of 30°C/Ma. Slower cooling rates would decrease the closure temperatures, but do not have a strong effect.

The closure temperature for Sr diffusion in muscovite has been estimated at ~500°C (Wagner et al, 1977). The closure temperature for Ar diffusion in muscovite has been estimated to be ~350°C (Purdy and Jaeger 1976). These closure temperatures are based on empirical evidence from K-Ar and Rb-Sr studies; diffusion parameters for muscovite are poorly known. Although the closure temperature of phengitic mica is unknown, it is probably not significantly different from that of muscovite because the empirical studies included phengitic micas as well as muscovite.

The effect of deformation on closure temperature also is unknown, although we would expect that a reduction in grain size during mylonitization or cataclasis would cause Ar loss or rehomogenization in a mineral even at low temperatures. Deformation is though to have an important effect on the kinetics of metamorphic reactions, by enhancing diffusion through an increase in dislocation density, and through an increase in the surface area available for reaction by grain size reduction (Brodie and Rutter, 1985). Recrystallization results in Ar redistribution not only by volume diffusion within preexisting grains, but also by diffusion along grain boundaries and in the metamorphic fluid. Also, as discussed by Chopin and Maluski, (1980), there may be a difference in the effective T_C depending on whether the mineral is being "opened" by deformation, recrystallization, or an

increase in temperature, or "closed" by cooling from a higher temperature. White micas are known to crystallize at low temperatures during metamorphism and burial. Crystallization in a high stress regime below a temperature where diffusion is thermally activated would be expected to cause redistribution of K and Ar in response to stress-induced chemical potential gradients, and a decreased effective diffusion dimension; thus the effective T_C would be lower than that calculated using the equation developed by Dodson (1973) assuming average diffusion parameters.

The factors cited above may in part be the reason for the discrepancy between Ar and Sr dates of samples from near the basal thrust of the Pierien unit (Schermer, 1987). If the T_C for Sr is higher than that for Ar, we would expect older Sr ages, yet we find Ar ages on white micas (53-55 Ma) that are significantly older than Rb/Sr ages on the same minerals (42±1 Ma).

These mica samples are all from strongly mylonitic rocks, so deformation may have played an important role. In addition, the Sr ages may actually reflect an averaging of several diffusive loss events; one during early Eocene time, and another during late Eocene or younger time. While the step-heating profiles show these two events distinctly, the Rb/Sr age would be the equivalent of a total gas age, or K-Ar age of the sample.

The fact that the plagioclase-whole rock-phengite Rb/Sr data show "errorchrons" (deviation from the line that is in excess of analytical error) rather than isochrons is indicative of open-system behavior or lack of equilibration of the minerals during multiple episodes of deformation and metamorphism. The presence of syn- to late-kinematic calcite veins in clastic and carbonate rocks in the footwall of the thrust may indicate fluid flow which, due to high Ca (and thus possibly Sr) concentrations, reset the Sr isotopic composition during mylonitization.

Depletion of ^{39}Ar in the fine-grained phengites may have resulted from recoil of ^{39}Ar during irradiation. This would increase the $^{40}Ar/^{39}Ar$ ratio, and give a misleadingly old apparent age. As discussed by Hunecke and Smith (1976), the average ^{39}Ar recoil distance is ~0.1 μm, so fine-grained minerals are more strongly affected by recoil. The average distance between the cleavage planes of the micas in the samples in this study is ~10 μm, thus approximately 1% of the gas volume may have been depleted in ^{39}Ar; if all this Ar had been completely removed from the grain, the $^{40}Ar/^{39}Ar$ ratio and the age would be increased by 1%. If we assume the Rb/Sr age is correct at 42 Ma, a 1% increase is insufficient to explain the 50-54 Ma total gas ages. Even if the grains were 1μm thick, so that

recoil affected 10% of the gas volume, the age would only be increased to 46 Ma. Thus recoil does not seem to be the cause of the early Eocene mica ages.

Age gradients in white mica and microcline spectra

One of the most important results of this study is the observation that incomplete resetting of white mica and biotite ages in all structural units constrains the temperatures of metamorphism to T~350°C or less even where mineralogical constraints on temperatures are poor, such as in the Pierien unit. Samples such as 86OL44a,b and 86GO22 are the best examples of this, as they preserve even the crystallization age of the basement rocks as well as a later resetting event. Mica samples from near the basal thrust of the Pierien unit and from the Ambelakia unit are nearly completely reset from a possible Cretaceous age metamorphic event evidenced by the highest temperature gas fractions. However, the presence of two distinct Eocene ages in the micas and Eocene and Miocene ages in the microcline samples indicate that this part of the metamorphic and cooling history occurred at relatively low temperatures.

Three possibilities have been proposed for the origin of age gradients in the white mica and potassium feldspar spectra: mixing of two phases with different ages and/or closure temperatures (e.g. related to compositional differences; Wijbrans and McDougall, 1986); Ar loss by volume diffusion ("diffusive-loss") during a discrete heating event (Turner, 1968; Harrison and McDougall, 1980); or diffusive-loss during slow cooling (Harrison and McDougall, 1982). Wijbrans and McDougall (1986) interpret "upward convex" spectra in white micas from Naxos, Greece to be the result of mixing of earlier-formed high-pressure phengites with younger low-pressure muscovites. Because of the differences in age and degassing behavior of the two micas, a mixture results in a spectrum with a strong age gradient at low temperatures, a plateau at middle temperatures, and a decrease in age at the highest temperatures of the step-heating experiment. As discussed above, the composition of the white micas in this study varies very little in most samples, including those with strong age gradients (85OL43, 85OL46, 86OL44bM1). Samples that are known to be mixtures of older muscovite and younger phengite (e.g. 86OL57, 86GO13c, 86OL44a) display a double-stepped pattern (Fig. 4.8b) that seems to indicate that the two micas are thermally distinct as well as different in age. The constant composition of white mica in most samples and the smooth, increasing age gradients present in these samples leads us to rule

out mixing as a cause for the age gradients in the majority of the micas analyzed in this study.

The majority of the samples discussed above have Ar release patterns with age gradients that strongly resemble patterns produced by diffusive loss of argon during either slow cooling or an episodic heating event. Turner (1968) and Harrison and McDougall (1982) discuss the different incremental release patterns which would result from slow cooling and episodic heating. Although the profiles in themselves are not uniquely diagnostic, slow cooling profiles tend to have a smooth increase at low temperatures, plateaus at high temperatures and are convex upward, reflecting cooling at a rate of ~5°C/Ma or less, and a range of ~50°C over which diffusion gradually slows down in the mineral. Episodic loss curves can be linear at the low temperature end, depending on the diffusion geometry, and commonly do not preserve plateaus at the high temperature end of the spectrum. As indicated in the theoretical curves of Turner, (1968), calculated for diffusion in uniform spheres, the shape of the profile resulting from episodic loss depends strongly on the fraction of gas lost, and as the fraction of gas lost increases, more of the profile becomes linear at low temperatures. For the case of a lognormal size distribution of spheres, the spectrum flattens out in the low temperature range, such that the pattern is concave upward for large amounts of gas lost. If the amount of gas lost during the reheating event is small, the profile retains its true age over a large part of the spectrum, thus the original age is well constrained while the age of reheating is not constrained. However, if the amount of gas lost in the later event is large (>30%), the low-temperature end of the spectrum defines the age of the loss event while the high-temperature "plateau" grossly underestimates the original crystallization age.

Several problems exist in the interpretation of saddle-shaped potassium feldspar spectra. There are two different interpretations of the saddle shape: one that excess argon incorporated into weakly retentive sites is superimposed on a previously existing diffusive loss profile (Harrison and McDougall, 1982); the other that both low and high-temperature increments represent excess argon in different crystallographic sites superimposed on previously existing plateaus (Zeitler and Fitzgerald, 1986). With the first interpretation, the old ages at the high-temperature end of the spectrum would represent a maximum age of initial closure to argon loss, and the minimum could be projected to zero ^{39}Ar released as a maximum age for the episodic loss event. The excess argon incorporated could have increased the age of the spectrum as a whole, or may have only been incorporated

into weakly retentive sites on the surface of the grain, and would be released at low temperatures during the laboratory heating. Alternatively, Zeitler and Fitzgerald (1986) showed that in many cases, the minimum age in the saddle, which can be a plateau for a large proportion of the ^{39}Ar released, represents a geologically meaningful age, or at least a maximum age of the closure of K-feldspar to argon loss. The old ages shown by the high temperature gas released represent excess argon also on the surface of the grain, but in more retentive "anion" sites that do not release gas until high temperatures are reached, and in this case would have no geological significance.

We prefer the interpretation of excess argon superimposed on a diffusive loss profile for the following reasons: 1) The upper ages on all the microcline profiles do appear to have geological significance, by comparison with mica ages in the same samples and in nearby rocks from the same structural unit. 2) In all cases except 86OL57 and 86GO13c, the initial gas released is younger than the ages at the high temperature end of the spectrum, and the ages of gas fractions decrease to the minimum over the first ~10% of ^{39}Ar released, indicating the excess argon incorporated was either a small amount or had a $^{40}Ar/^{39}Ar$ composition similar to the radiogenic component and thus does not dominate the apparent ages over the whole spectrum. 3) The saddle portion of the curve is very narrow, and except in samples 86OL57 and 86GO13c, similarly young ages are recorded in <10% of the gas (compare with Zeitler and Fitzgerald, 1986). Thus we feel that we are justified in modelling the profiles as diffusive loss curves as discussed below.

The diffusive loss profiles in the microcline samples from the Mt. Olympos region are interpreted to be the result of thrust and normal faulting rather than slow cooling from the Eocene to the present. Evidence for this interpretation comes from detailed mapping and structural analysis as well as the release spectra (e.g. Schermer and Burchfiel, 1987; in prep.) Harrison and McDougall (1982) show that at a cooling rate of ≤5°C/Ma, the ~50°C range over which complete closure to Ar loss occurs in potassium feldspar is sufficient to set up age gradients within the grains. If we assume that the profiles have resulted from slow cooling, the high-temperature "upper age" would represent the time that diffusion of Ar in the sample began to slow down, and the minimum age would represent the time of complete closure to Ar loss. Thus if we take the maximum and minimum differences between the high-temperature "upper age" and the minimum age of the potassium feldspar samples analyzed, 40 Ma for sample 86GO13c, and 22 Ma for samples 85OL38 and 86OL44a, we obtain "cooling rates" of 1.25 and 2.3°C/Ma respectively,

assuming the temperature dropped 50°C during this interval. However, these extremely slow cooling rates during the Eocene-Miocene are contradicted by: 1) the complete overlap of phengite ages and "upper" potassium feldspar ages, suggesting that T decreased from ~350°C to ~150°C in a very short period of time during the early to late Eocene, (a cooling rate of ~28°C/Ma calculated for sample 85OL38 from 59 Ma to 52 Ma; a minimum average cooling rate for the Pierien unit of ~11°C/Ma could be calculated from the oldest mica plateau (~63 Ma, 85GO1) and the youngest microcline "upper" age (~45 Ma, 86OL44a)); and 2) the average cooling rate from ~15 Ma to the present is calculated to be ~10°C/Ma. Rocks containing the mica samples, metamorphosed at ~53-55 Ma, are thrust over fossiliferous middle Eocene flysch, so that two events within the Eocene are also required by the structural relations. In addition, the fact that a significant period of normal faulting and uplift has been documented in the field, and several of these samples were collected from immediately beneath normal faults, leads us to believe that the minimum ages of the feldspars indicates an episodic loss event during early to middle Miocene time.

We can model the diffusive Ar loss from each sample as a distinct outgassing event in order to obtain information about the original crystallization age (T0), the age of outgassing (T1), and the amount of gas lost during the outgassing event (F). Figure 4.11 shows model diffusive loss profiles that have been fit to the spectra of samples from the Pierien unit. For the model curves we have calculated the $^{40}Ar/^{39}Ar$ and age distribution after outgassing assuming a homogeneous distribution of ^{39}Ar, and assuming that diffusion of ^{40}Ar and ^{39}Ar occurs at similar rates in spheres of uniform size, the same assumptions adopted in Turner (1968). Zeitler and Fitzgerald (1986) have argued that the microstructural complexity of K-feldspar, with diffusion domains of various sizes and shapes, is best represented by a spherical model. However, diffusion in micas occurs primarily along cleavage planes and thus is properly represented by a cylindrical geometry. As discussed by Harrison (in prep), the differences between the two models are insignificant, particularly for the samples that have lost minor amounts of gas. We have iterated to find the range of values for F, the amount of gas lost, T0, the original crystallization age (or age of last homogenization of Ar isotopes), and T1, the age of the outgassing event, that fit the incremental release spectrum for each sample. In most cases this required allowing a variation of 50-60% in χ^2, the least-squares fit parameter, over the "best" fit represented by the minimum value of χ^2. Although we have produced model curves assuming only one outgassing event, the

geological evidence suggests that it is probable that some of the samples have experienced more than one Ar-loss event. Nonetheless, as discussed by Harrison (1985), it is nearly impossible to determine from the shape of a release spectrum whether a sample has undergone more than one outgassing event, so we would be unable to place constraints on F or T0 in such cases. This is important particularly in the case of the feldspars, which appear to have lost large amounts of gas. In cases where the first outgassing event results in loss of a minor amount of gas (<20%), the resulting profile after a second outgassing would still reflect the original crystallization age and modelling would only slightly overestimate the amount of gas lost during the second event. However, when more gas is lost in the first event, profiles from the second event would underestimate the true crystallization age and greatly overestimate the amount of gas lost during the second event (Harrison, 1985). Therefore, the modelled estimates of T0, the crystallization age, are minima, and the estimates of F, the amount of gas lost, are maxima.

The feldspar samples have generally lost >50% Ar since their original crystallization ages (Fig. 4.11a); and as expected, the constraints on T0 are poor, ranging from <100 to >300 Ma. The one feldspar sample which has lost only 31-48% gas, 85OL38, has a better-defined crystallization age of 52-57 Ma, in good agreement with its mica age of 57 Ma. The outgassing ages of samples 85OL38, 86GO22a, and 86OL44a fall in the early to middle Miocene, at 11-24 Ma, and may indicate that decompression and cooling related to normal faulting began at this time. The two samples from below the normal fault at the base of the ophiolite, 86OL57 and 86GO13c, have outgassing ages from 0-4 Ma. It is possible that uplift along this normal fault is this young, however, an alternative interpretation which would also explain these two spectra is that the diffusive loss curves do not approach the y axis linearly, as is the case for uniform spheres, but would level off in the initial increments if the spheres had a lognormal size distribution (Turner, 1968). Thus, we would have to use a more complicated diffusion model and attempt to fit the lower "saddle" portion of these spectra as well. Such a model would predict outgassing ages approximately equal to the saddle ages of 16 and 19 Ma, in better agreement with the other feldspar outgassing ages. The field, structural, and petrologic evidence that these samples have experienced more than one reheating event indicates that the range of F calculated is an overestimate of the amount of gas lost during the final outgassing event, and thus the T0 ages have essentially no geological significance for all but sample 85OL38.

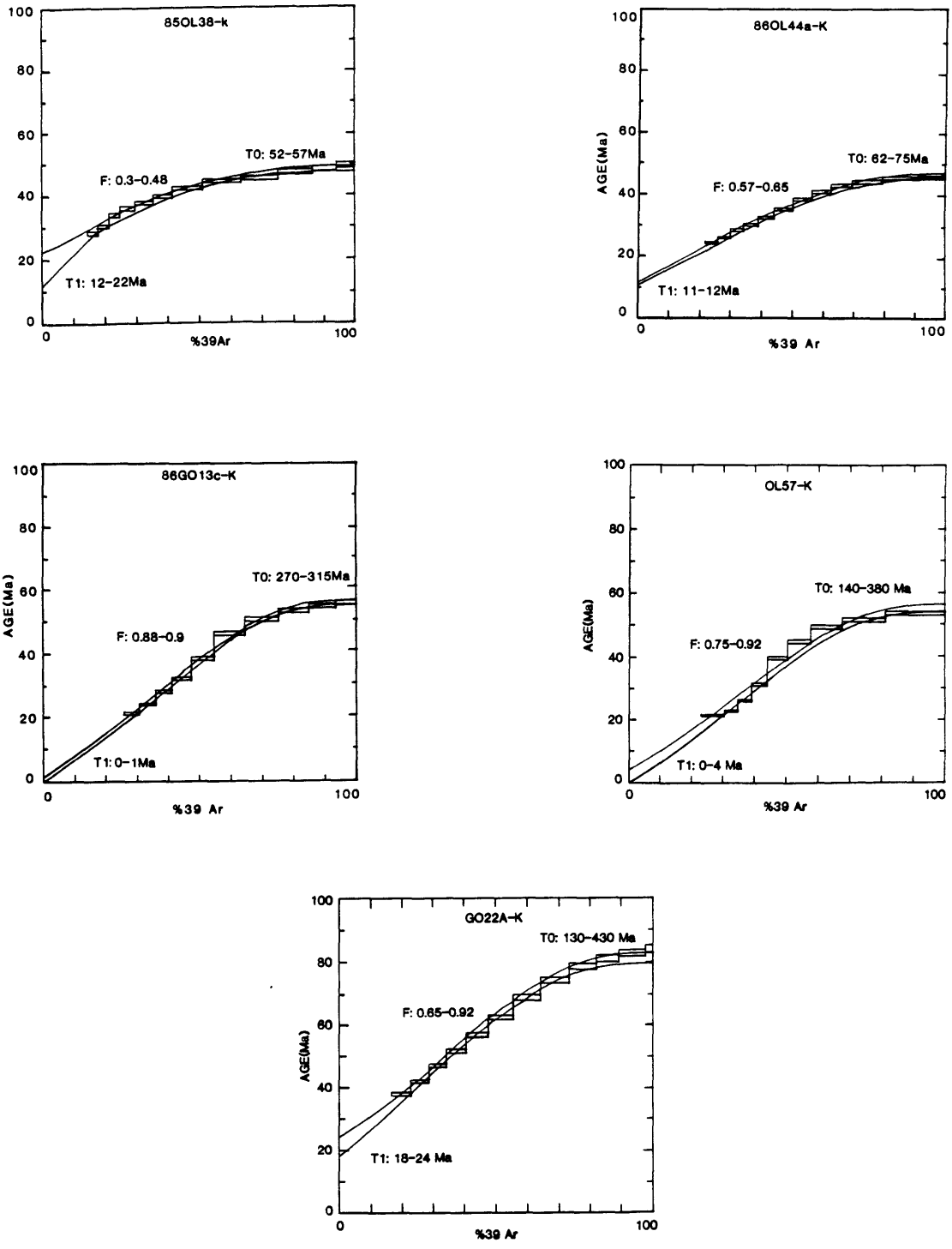

Figure 4.11a: Incremental release spectra from potassium feldspars analyzed in this study, with model diffusive loss curves indicating the possible ranges of T0, the original crystallization age, T1, the age of outgassing, and F, the amount of gas lost in the outgassing event. See text for details.

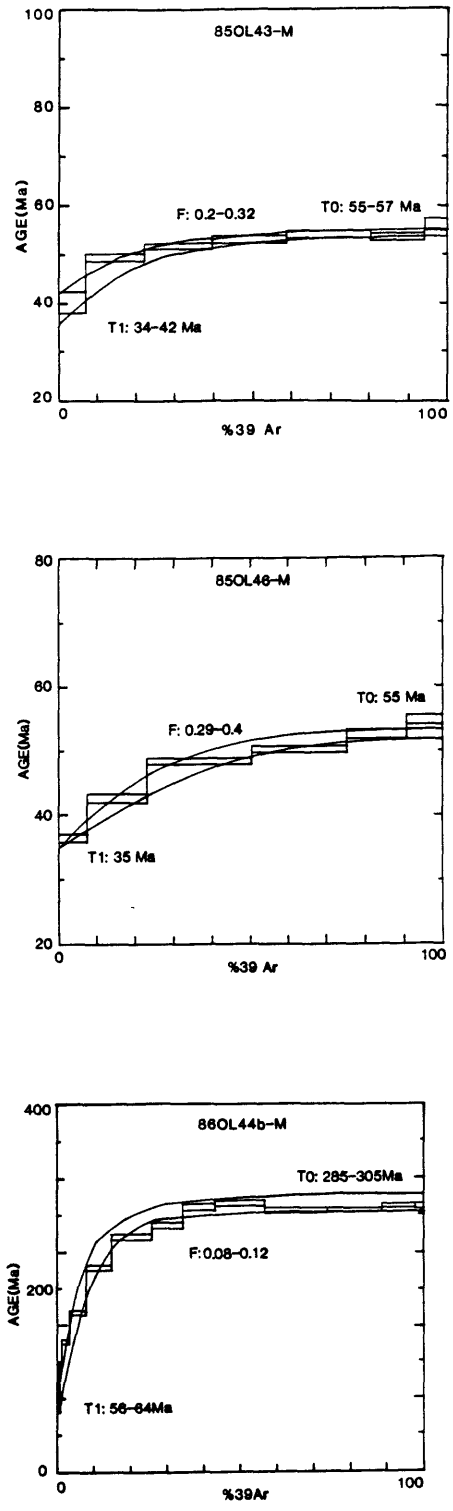

Figure 4.11b: Incremental release spectra from micas analyzed in this study, with model diffusive loss curves indicating the possible ranges of T0, the original crystallization age, T1, the age of outgassing, and F, the amount of gas lost in the outgassing event. See text for details.

The models of the white mica spectra indicate these samples have lost less gas than the feldspars, on the order of <10% for sample 86OL44b to as much as 35-40% for sample 85OL46 (Fig. 4.11b). The T0 age for sample 86OL44b is 285-300 Ma, in agreement with the biotite and hornblende ages from sample GO22 discussed above. This sample experienced an argon loss event in the Paleocene-Eocene, indicated by its T1 age of 56-64 Ma. At the same time micas 85OL43 and 85OL46, from closer to the basal thrust fault, were apparently essentially completely homogenized, along with 85GO42 which gives a plateau age related to this event. The later outgassing event which affected samples 85OL46 and 85OL43 appears to have occurred during late Eocene time, constrained by the T1 ages to 32-42 Ma. The results of the modelling add more support to the argument that the youngest structural events, which we interpret to be thrust faulting during late Eocene time and normal faulting during Miocene to Recent times, were low-temperature events.

Excess Argon

The composition of the extraneous argon component is highly variable in the samples studied. Most have $^{40}Ar/^{36}Ar$ compositions significantly greater than that of atmosphere (295.5). As discussed by Harrison and Heizler (1987) and Heizler and Harrison (1988), complex release spectra can often be resolved by examining successive increments that have the same component of extraneous argon which may differ compositionally from the extraneous argon in other increments. A notable example of this is the hornblende of sample 86GO22, which has a very complicated release spectrum. Regression of the last 8 increments gives an age of 293±20 Ma, within error of the minimum age in the spectrum, 295 Ma, and corresponds well with the zircon age of 302 Ma reported by Yarwood and Aftalion (1976) from granitic rocks of the same unit in a higher thrust sheet further to the north. Regression of increments 1-3 of this same sample gives an "errorchron" age of 276±67 Ma, within error of the better constrained intercept age; these two regressions indicate two different, non-atmospheric components of excess argon.

TEMPERATURE-TIME HISTORY OF THE PELAGONIAN ZONE DURING ALPINE OROGENESIS

While the individual release spectra studied seem to be complicated, a pattern of similar ages within and among the groups of samples has emerged. The samples which have plateaus or well-constrained isochrons: 86GO22 hornblende at 295 Ma, biotite at 290 Ma; 85OL32 at 100 Ma, 85GO1 at 62 Ma, 85GO42 at 53

Ma, and 86RA5b at 40 Ma, constrain the timing of four major deformational and metamorphic events in the history of the Pelagonian zone. The remaining samples show diffusive loss profiles, generally from one of these dates to a younger one, depending on the closure temperature of the mineral and in part on the proximity of the samples to major structures. The youngest ages recorded by potassium feldspar minima reflect a fifth event, the latest low-temperature "cooling" event that we interpret to be related to normal faulting and uplift of the metamorphic nappes. Figure 4.12 shows a schematic temperature-time history of the Pierien, Infrapierien, and Ambelakia units derived from consideration of the closure temperatures for various minerals and their ages.

Paleozoic

The oldest well-constrained event is recorded in the samples from the Pierien unit at ~295 Ma. As these ages come in part from relatively undeformed, unrecrystallized hornblende and biotite from the granitic basement terrane and correspond well to concordant zircon ages reported by Yarwood and Aftalion (1976); they are interpreted to represent the crystallization and cooling of the intrusive rocks. A rapid cooling rate of ~30°C/Ma after intrusion is indicated by the difference in zircon, hornblende, and biotite ages calculated from the differences in their closure temperatures: 700°C for zircon; 550°C for hornblende, and 300-325°C for biotite (Mattinson, 1978; Harrison, 1981; Harrison and McDougall, 1985) over a span of 12-14 Ma. The minor resetting of the biotite age during Cretaceous time, as shown by the initial 10% of gas released from this sample, indicates that temperatures in the Pierien unit did not exceed ~325 °C for any long period of time since the late Paleozoic. This observation is important to the interpretation of the conditions of later metamorphism and deformation, and to the tectonic setting of the Pierien unit during Alpine orogenesis. The granitic and gneissic rocks of the Pelagonian basement are overlain nonconformably by Permo-Triassic metasedimentary rocks (Katsikatsos et al, 1982) and Triassic-Jurassic marbles just to the west of the Olympos massif.

The granitic samples analyzed here were collected from an area mapped by Davis and Migiros (1979), and Katsikatsos et al (1982) as "recent" granites that intruded and metamorphosed a previously foliated gneiss complex. They considered the granites to be post-Late Cretaceous and pre-late Eocene. However, other workers (Godfriaux,1968; Schmitt, 1983; Vergely, 1984; Schermer, 1987; Chapter 2) include the granites in the the Paleozoic basement units. In addition to

the field relations noted above, the $^{40}Ar/^{39}Ar$ data indicate that the latter interpretation is correct.

The ~439-457 Ma age recorded by hornblende sample 86OL47 may represent the pre-Carboniferous basement of the Infrapierien unit that was unaffected either by granitic intrusion or the later metamorphism and deformation which affected the surrounding gneisses and mica schists. There are no dates on the granites from this particular unit, and they are not seen intruding the amphibolite at this locality. If this age is substantiated by further analyses, it would be one of the oldest age determinations reported from the Pelagonian basement. Marakis (1970, cited in Barton, 1975) dated biotites from granites in northern Macedonia using K-Ar and obtained a range from 461-465 Ma. However, more work is needed to rule out the possibility that the biotites, as well as the hornblende analyzed in this study, do not contain so much excess Ar that the crystallization ages are obscured.

Mesozoic

Regional stratigraphic relations suggest that ophiolite emplacement over Pelagonian zone rocks occurred during latest Jurassic to Early Cretaceous time, (Vergely, 1976; Mercier, et al, 1975). Unfortunately, there is no direct evidence of the age of ophiolite emplacement in the Olympos region. Limestone mapped as Maestrichtian by Godfriaux (1968) and Godfriaux et al (1979) is presumed to overlap the ophiolite and underlying rocks, however, most of the occurrences of ophiolitic rocks in the Olympos region have been disrupted by younger normal faults and the original thrust faults are no longer present.

The age of the greenschist facies or blueschist-greenschist transition facies metamorphism and deformation in the Infrapierien unit, which does have a preserved ophiolitic thrust nappe on top of it in the Livadi area (Fig. 4.2), is constrained by the mica ages of 98 and 100 Ma reported here; however, the metamorphic fabric in these samples is not known to be directly related to the basal ophiolitic thrust fault. We correlate these ages with D1 as described in Chapter 3. It is possible that the Rb-Sr ages of 119 and 116 Ma reported by Yarwood and Dixon (1977) from the Pierien unit in a higher thrust sheet are related to the ophiolite emplacement. The limited geochronologic data available from near the base of ophiolites and throughout the upper parts of the crystalline nappe stack prevent further constraints on the Cretaceous metamorphic history of this area, though Vergely (1984) has reported two major phases of ophiolite emplacement,

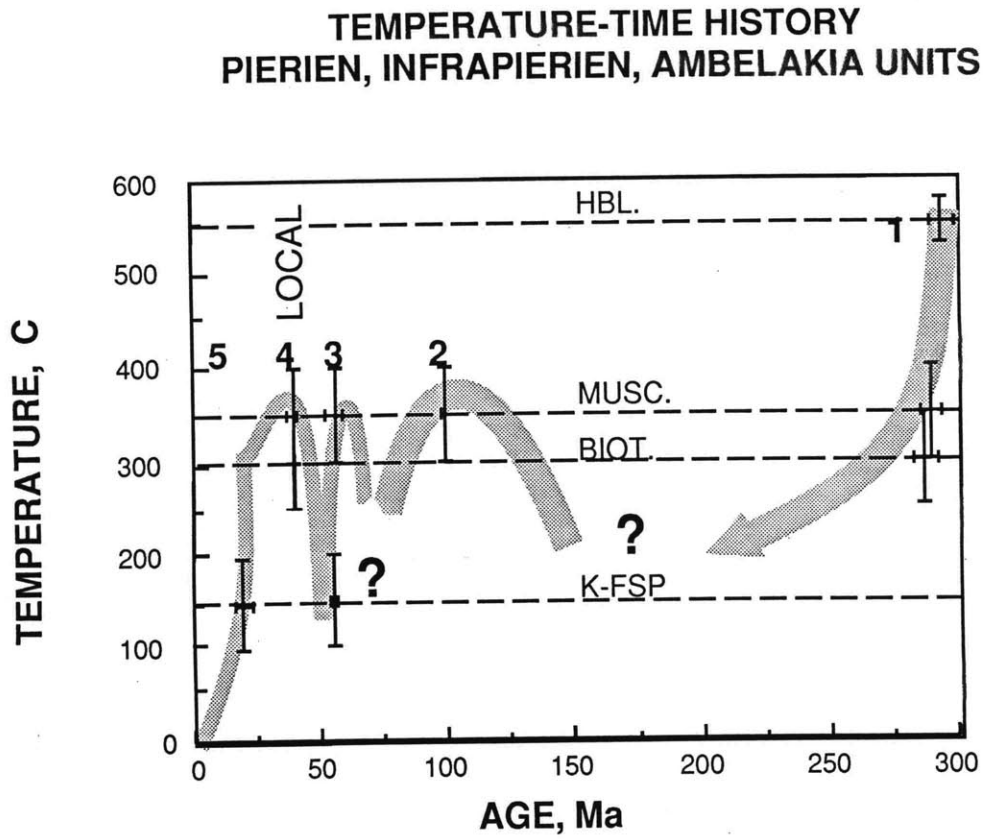

Figure 4.12: Schematic temperature-time history of the metamorphic rocks of the Olympos region, indicating ages of various mineral separates and their approximate closure temperatures. See text for details.

one during latest Jurassic time further to the north in the Vardar zone, and one during Early Cretaceous time in the Othrys areas of east-central Greece (Fig. 4.1). If the Ordovician hornblende age described above is valid, the amphibolite facies metamorphism that other workers have described as Cretaceous in age and possibly associated with ophiolite emplacement (e.g. Nance, 1981) or post-Carboniferous, pre-Triassic (Schmitt, 1983) is actually much older.

It is interesting that none of the samples collected from the upper parts of the Pierien unit record the Cretaceous event (microcline sample GO22a has probably experienced >70% Ar loss in younger events so that its Cretaceous upper age is meaningless). Samples from near the basal Pierien thrust fault have Cretaceous ages for the last 1-2% gas released, however it is not clear what mineral is degassing at these high temperatures or whether such ages could represent excess Ar or recoil effects. Nevertheless, the sample dated by Barton (1976) at 125 Ma by Rb-Sr contains a mylonitic fabric that he interprets to be early Cretaceous in age. It is possible that either any Cretaceous event was too local to cause open-system behavior of Ar in micas throughout the unit or that at least part of the Pierien unit was removed from the site of ophiolite emplacement and was not imbricated with the Infrapierien rocks until Tertiary time. More sampling throughout both units will be needed to test these hypotheses.

None of the Infrapierien micas that we have analyzed record pre-Cretaceous ages; thus it is probable that the mica grew during the Cretaceous metamorphic event, and/or that temperatures of greater than 350°C were achieved during that time. Preliminary study of the petrology of this unit suggests that the metamorphic temperatures were ~350°-500°C. Nevertheless, the rocks must have cooled fairly rapidly following metamorphism because samples 85OL32 and 85OL50 only record minor Ar loss during early Tertiary events. We cannot constrain the minimum temperatures reached by the Infrapierien unit between the Cretaceous and Tertiary events, as shown on Fig. 4.12. It is probable that the 63 Ma age of sample 84LI26 reflects new growth of micas related to Tertiary thrusting and high pressure-low temperature metamorphism as this sample only contains one metamorphic foliation; the Ar loss event experienced by the other two samples appears to coincide with this event.

Tertiary

Several distinct Tertiary events are evident from the Rb/Sr and the $^{40}Ar/^{39}Ar$ data and are summarized on the histogram of Figure 4.13. Major deformation and

metamorphism in the Olympos region occurred during Eocene time. Most of the blueschist-grade samples appear to record two events, one at 53-55 Ma and the other at 36-40 Ma. The earlier event is texturally associated with blueschist mineral formation, foliation formation, and isoclinal folding, and is correlated with the D2 event described above (Ch. 3). The younger event apparently records the age of thrusting of the blueschists of the Ambelakia and Pierien units over the Olympos-Ossa unit and the age of blueschist-facies metamorphism of the Olympos-Ossa unit, and is correlated with the D3 structural event. . The latter deformation and metamorphism are constrained by the age of fossiliferous flysch in the footwall to be post-Lutetian (50-44 Ma). Textural and mineralogic evidence recorded in the mylonitic rocks associated with the thrust fault indicates that the pressure-temperature conditions of thrusting were not very different from those of metamorphism. Phengites and sodic amphiboles of the first event are folded and sheared, but new phengites and amphiboles grew parallel to the mylonitic fabric and, based on microprobe analysis, have the same compositions.

Samples from >400 m away from the basal thrust fault (85GO1, 85LI16, 86GO13c, and 86OL57) apparently record slightly earlier blueschist facies metamorphism (~59-62 Ma) than the strongly mylonitized samples near the thrust fault. These samples also exhibit the later Eocene Ar loss event that we attribute to thrust emplacement above the Olympos unit, although the mylonitic fabric is not as well developed. The older ages of these high-level blueschists may reflect: 1) earlier cooling during an uplift event prior to thrusting or 2) subduction and blueschist metamorphism spanning the time from ≥62 Ma to <40 Ma. Samples at higher structural levels would be cooled before lower samples during an uplift event. It does not seem likely that the 53-55 Ma ages represent partial resetting of an earlier metamorphic age during thrusting at 36-40 Ma because sample 85GO42, with a plateau at 53.1±0.7 Ma and sample 85GO1, with a plateau at 61.7±0.8 Ma, are significantly different ages that apparently reflect a real variation in either cooling history or time of metamorphism. In addition, the diffusion modelling discussed above indicates only a small amount of Ar loss during the 36-40 Ma event, thus the model crystallization (T0) ages of 53-57 Ma are well constrained. We are uncertain whether these Paleocene to Eocene events were in fact distinct in time and space, or whether they could represent a protracted deformational event. Nevertheless, it is clear from petrologic and microstructural evidence that all of the fabrics were formed under high pressure-low temperature conditions.

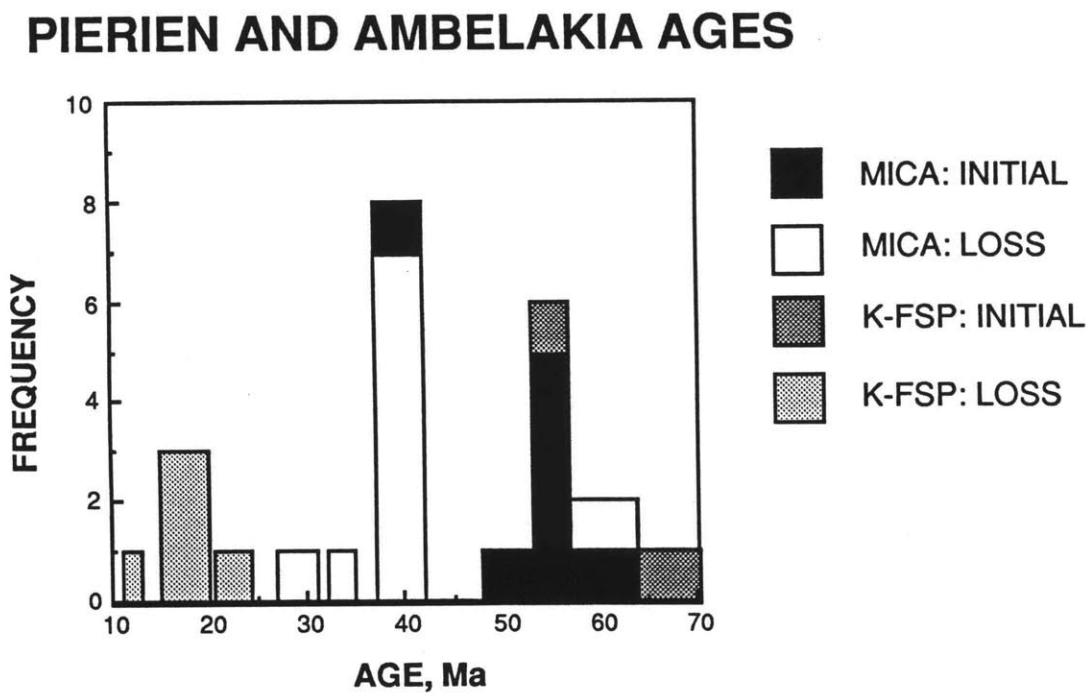

Figure 4.13: Histogram of Tertiary ages of mineral separates from the Pierien, Infrapierien, and Ambelakia units.

There is some suggestion in the data that the temperature decreased below the closure temperature for microcline (~150°C) between the early Eocene metamorphism and later Eocene thrusting (Fig. 4.12) Diffusion modelling of microcline sample 85OL38 indicates a crystallization age (T0) of 52-57 Ma and 30-48% gas loss during later events (Fig. 4.11). We can only distinguish the latest (Miocene) loss event; however, if we could account for all loss events, the actual T0 age would be greater than 52-57 Ma (Harrison, 1985). The phengite separate from this same sample shows a diffusive loss profile from 57±2 to 45±1 Ma. Thus it is possible that the sample cooled from ~350°C to below ~150°C over 0-7 Ma so that the K-feldspar began to retain Ar, but was later reset during the middle Eocene thrust faulting. The minimum cooling rate for this sample using the minimum T0 estimated above is calculated to be 28°C/Ma. The 36-40 Ma thrust event probably does not represent T>350°C for the entire Pierien thrust sheet; thus the thermal pulse shown on Fig. 4.12 between events 3 and 4 may not be real. Deformation-induced diffusion at lower temperatures, recrystallization of micas, and/or shear heating at the thrust (e.g Barton and England, 1979) are other possible causes for the Ar loss event exhibited by samples <1000 m above the thrust fault. Unfortunately, we are unable to accurately model the T0 ages of the other microcline samples because they have lost large amounts of Ar during post-crystallization metamorphism and deformation. More data are needed to confirm the early Eocene regional cooling suggested by the data from sample 85OL38 and from the discrepancy in metamorphic ages of samples 85GO1 and 85GO42.

It is clear from the $^{40}Ar/^{39}Ar$ and petrographic data that the Ambelakia and Pierien units were metamorphosed at approximately the same time and P-T conditions in the early Eocene, and thrust over the Olympos-Ossa carbonates during or after the middle Eocene. The later Eocene event also produced blueschist-facies assemblages in the Olympos flysch, but the metamorphic pressure and temperature may have been somewhat lower than in the early Eocene (Chapter 5). The lack of oceanic rocks in any of these three units implies that the subduction took place within the continental crust of the Pelagonian unit. The apparent metamorphic "inversion" of higher pressure rocks on lower pressure rocks supports the interpretation of the main fault between the blueschists and the Olympos platform as a thrust fault. Structural arguments developed in Chapter 3 and in Schermer and Burchfiel (1987) indicate that thrusting was SW-directed. Thus, we can envision the early Tertiary events as the subduction, imbrication and

obduction of the eastern margin of the Apulian plate (or a Pelagonian microplate) to have proceeded from NE to SW.

The present map pattern of the thrust nappes reflects severe disruption by younger normal faults such that, on the eastern margin of the Olympos massif, the contact between platform carbonates of the footwall and slivers of crystalline rocks and ophiolite in the hanging wall is not the original thrust fault (Schermer and Burchfiel, 1987). Several generations of normal faults are present which bring the highest structural units, the ophiolitic rocks, down on the lowest units. These faults cut out as much as 5-6 km of structural thickness. Some of the earlier faults are now low-angle normal faults (D5; chapter 3), whereas the majority of the younger normal faults are moderate- to high-angle, and cut Neogene and Quaternary alluvial deposits on the east side of the range (D7, chapter 3; Fig. 4.2). Although cross-cutting relations prove that the normal faults are younger than the thrust faults, it is uncertain when extensional tectonism in this area may have begun. The $^{40}Ar/^{39}Ar$ data on microclines provide constraints on the age of extension and uplift of the metamorphic rocks. The minimum ages evident in the microcline release patterns cluster around 16-23 Ma, although the diffusion modelling indicates some samples may not have been outgassed until much later times, possibly <0.5 Ma (Fig. 4.11). Several of the samples were collected from immediately beneath the normal faults, and cataclastic textures within them are clearly associated with these faults. Thus, we interpret these minimum ages to be the result of a low-temperature extensional deformation that occurred during the early to middle Miocene. Temperatures appear to have been high enough to partially reopen Ar diffusion in K-feldspar, with a T_C of ~150°C, but were insufficient to reset the mica ages. These normal faults appear to be partly responsible for the uplift of the blueschist facies rocks at a rate fast enough to avoid reheating by thermal relaxation (e.g. England and Richardson,1977; Draper and Bone, 1980).

Regionally, Neogene extension occurred within an overall compressional tectonic regime and was located between areas of oppositely-directed thrusting. During the early to middle Miocene, extension and subsidence occurred in the Mesohellenic trough to the west of the Pelagonian zone. To the east, the Aegean back-arc basin began to open at ~13 Ma (Angelier, 1978). Thus, during the time the Olympos platform and the overlying metamorphic rocks were being uplifted, cooled and tectonically denuded, the nearby areas on either side were also being extended and were subsiding. Further west, on the western margin of the Mesohellenic trough, southwest-vergent thrusting occurred throughout Miocene-

Holocene time, and north of the Aegean basin, Pliocene northeast-vergent thrusting affected parts of the Rhodope massif (Burchfiel, 1980; Papanikolaou, 1984b). As the extension and uplift of the metamorphic rocks in Greece has not yet been extensively studied, it will be important to gather additional data from other parts of the Pelagonian zone and from blueschists throughout Greece to confirm the early-middle Miocene uplift events presented here and their relation to compressional tectonics in the Hellenides.

CONCLUSIONS

Rb-Sr and $^{40}Ar/^{39}Ar$ ages from metamorphic rocks of the Pelagonian zone in the Mount Olympos region provide constraints on the ages of several metamorphic and deformational episodes, and the time-temperature history of this part of the metamorphic belt. The low temperature of metamorphism in these units has resulted in preservation of age gradients in the Ar release spectra. The samples in this study show that a wealth of information can be derived from $^{40}Ar/^{39}Ar$ dating of micas recrystallized at low temperatures, because the diffusive loss profiles can constrain both initial crystallization and younger metamorphic or deformational events which may easily be obscured by Rb/Sr mineral-whole rock dates.

Five deformational and metamorphic events have been recognized (Fig. 4.12): 1) the crystallization of granitic intrusions into the continental basement terrane at 302 Ma, and their cooling at ~30°C/Ma until ~290 Ma; 2) a greenschist to blueschist-greenschist transition facies metamorphism of continental thrust sheets at ~100 Ma, possibly associated with imbrication of the basement terrane in the Early Cretaceous (D1); 3) blueschist facies metamorphism of basement rocks of the Pierien unit and metasedimentary and metavolcanic rocks of the Ambelakia unit at 53-55 Ma, perhaps beginning in the Pierien unit before 62 Ma (D2); 4) underthrusting and subduction of the Olympos unit beneath the higher blueschist nappes at 36-40 Ma (D3); and 5) uplift and cooling below 100-150°C at 16-23 Ma, accompanied by normal faulting that has continued to the present (D5-D7).

Deformation in the Pelagonian zone occurred over a very long period of time (~90 Ma), and was episodic, involving subduction and imbrication of continental basement before, during, and after the collision of the Apulian and Eurasian plates and final closing of the Vardar ocean in latest Cretaceous time (Mercier et al, 1975; Burchfiel, 1980). Each succeeding imbrication of structurally lower units into the nappe stack appears to represent lower temperatures of metamorphism; pressures, while not well constrained, seem to either increase or be approximately constant

downward through the structural stack. Further work on the metamorphic petrology of these units is needed to constrain whether this apparent trend may represent the overall cooling of a subduction zone, as proposed by Cloos (1985) for oceanic subduction, here applied to an intracontinental subduction regime.

During the early to middle Tertiary, a fairly rapid cooling rate of ~10°C/Ma below metamorphic temperatures of ~350-400°C permitted preservation of the blueschist facies mineral assemblages as they were uplifted from depths of ~15-20 km.

ACKNOWLEDGEMENTS

This material is based upon work supported under a National Science Foundation Graduate Fellowship, a Grant-in-Aid of Research from Sigma Xi, and Geological Society of America research grant awarded to Schermer, and support from the Schlumberger Corporation to Burchfiel. We thank D. Papanikolaou for logistical support in Greece and helpful discussions. Reviews by Kip Hodges, Stan Hart, and Peter Crowley contributed significantly to the clarity of the manuscript.

TABLE 4.1

Temp °C	40Ar 39Ar	37Ar 39Ar	36Ar 39Ar	Moles 39Ar	39Ar %Total	%40Ar Rad	K/Ca	Age (Ma)
		85RA6-M		(E-14)				J = 0.006027
650	8.54	0.0174	0.0171	444.8	7.1	40.5	28.20	37.2 ± 0.8
800	4.84	0.0145	0.0032	870.1	13.9	79.6	33.91	41.4 ± 0.5
850	4.46	0.0112	0.0011	1302.5	20.9	91.8	43.95	44.0 ± 0.5
900	4.67	0.0096	0.0008	1968.6	31.5	94.1	50.96	47.2 ± 0.5
950	5.72	0.0197	0.0015	814.7	13.1	91.9	24.84	56.3 ± 0.7
1000	6.91	0.0634	0.0012	388.8	6.2	94.5	7.72	69.7 ± 1.2
1050	9.54	0.1493	0.0019	159.3	2.6	93.9	3.28	94.9 ± 1.1
1100	10.93	0.1919	0.0025	82.1	1.3	93.0	2.55	107.3 ± 1.7
FUSE	14.50	0.4800	0.0030	209.3	3.4	93.9	1.02	142.3 ± 1.6
TOTAL				6240.1	100.0			52.8 ± 0.7
		86RA3-M		(E-14)				J = 0.006009
650	6.410	0.0477	0.0115	471.0	6.3	46.6	10.27	32.06 ± 1.65
800	5.142	0.0228	0.0040	804.7	10.8	76.2	21.50	41.99 ± 0.95
850	5.237	0.0151	0.0026	1248.3	16.7	85.0	32.51	47.60 ± 2.01
900	5.851	0.0187	0.0033	1146.9	15.3	82.7	26.27	51.72 ± 0.68
950	5.643	0.0217	0.0018	1376.6	18.4	89.9	22.61	54.19 ± 0.66
1000	6.133	0.0616	0.0017	1078.1	14.4	91.2	7.95	59.64 ± 0.83
1050	7.128	0.1149	0.0030	707.8	9.5	87.3	4.26	66.24 ± 0.91
1100	8.242	0.2196	0.0044	432.1	5.8	84.0	2.23	73.56 ± 1.58
FUSE	8.658	0.7500	0.0073	210.2	2.8	75.3	0.65	69.39 ± 1.13
TOTAL				7475.7	100.0			53.48 ± 1.10
		86RA5B-M		(E-14)				J = 0.006001
650	8.661	0.1559	0.0200	214.6	3.2	31.4	3.14	29.20 ± 1.75
800	5.114	0.2886	0.0064	488.2	7.3	62.5	1.70	34.29 ± 0.62
850	4.154	0.2447	0.0027	1095.2	16.5	80.2	2.00	35.73 ± 0.79
900	3.471	0.2929	0.0007	44.9	0.7	94.0	1.67	35.01 ± 2.12
950	4.002	0.1193	0.0011	2536.6	38.1	91.2	4.11	39.10 ± 0.59
1000	4.103	0.1541	0.0013	1269.0	19.1	90.1	3.18	39.57 ± 1.19
1050	4.340	0.2953	0.0021	556.9	8.4	85.5	1.66	39.74 ± 0.68
1100	4.955	0.5938	0.0047	263.2	4.0	72.3	0.82	38.42 ± 0.79
FUSE	5.806	2.0727	0.0081	186.1	2.8	61.1	0.24	38.07 ± 1.39
TOTAL				6654.7	100.0			37.93 ± 0.82
PLATEAU AGE								39.6 ± 0.9

TABLE 4.1 (continued)

Temp °C	40Ar 39Ar	37Ar 39Ar	36Ar 39Ar	Moles 39Ar	39Ar %Total	%Ar40 Rad	K/Ca	Age (Ma)
	85OL38-M			(E-14)				J = 0.0051806
700	5.759	0.0227	0.0046	95.5	5.0	75.9	21.60	45.19 ± 0.99
825	5.816	0.0149	0.0027	177.5	9.3	85.6	32.80	51.39 ± 0.70
875	5.640	0.0107	0.0012	283.0	14.8	93.1	45.70	54.18 ± 0.77
925	5.770	0.0078	0.0007	481.0	25.1	95.8	62.60	56.97 ± 0.66
975	5.714	0.0099	0.0008	539.5	28.2	95.4	49.35	56.24 ± 0.76
1025	5.868	0.0396	0.0008	221.6	11.6	95.5	12.38	57.77 ± 0.71
1100	6.325	0.1339	0.0014	75.9	4.0	93.2	3.66	60.74 ± 1.09
1140	7.861	0.4724	0.0024	25.6	1.3	90.8	1.04	73.29 ± 1.76
FUSE	10.051	0.8937	0.0040	15.9	0.8	88.5	0.55	90.93 ± 2.99
TOTAL				1915.4	100.0			55.99 ± 0.78
PLATEAU AGE								56.99 ± 1.82
	85OL43-M			(E-14)				J = 0.006206
825	5.41	0.0282	0.00590	139.1	6.9	67.1	17.38	40.2 ± 2.3
905	5.55	0.0346	0.00353	306.9	15.3	80.6	14.16	49.4 ± 0.7
940	5.08	0.0047	0.00121	345.8	17.3	92.2	105.22	51.7 ± 0.5
975	5.06	0.0299	0.00069	382.6	19.1	95.2	16.41	53.1 ± 0.7
1000	5.10	0.0471	0.00052	434.8	21.7	96.3	10.40	54.2 ± 0.7
1025	5.21	0.0798	0.00113	274.2	13.7	93.0	6.14	53.4 ± 0.5
1050	5.78	0.1475	0.00223	85.4	4.3	88.1	3.32	56.2 ± 1.1
1075	8.75	0.4875	0.00472	25.9	1.3	84.1	1.00	80.6 ± 3.2
FUSE	27.26	3.1940	0.03978	9.5	0.5	57.7	0.15	168.4 ± 13.3
TOTAL				2004.2	100.0			52.7
	85GO42-M							J = 0.006179
825	6.65	0.0178	0.00515	136.0	6.6	76.6	27.47	55.9 ± 0.7
905	5.66	0.0000	0.00230	257.7	12.5	87.3	*	54.2 ± 0.8
940	5.49	0.0069	0.00184	826.2	39.9	89.4	71.12	53.9 ± 0.7
975	5.36	0.0000	0.00151	323.8	15.7	91.0	*	53.6 ± 0.7
1000	5.62	0.0000	0.00246	253.7	12.3	86.4	*	53.3 ± 0.7
1025	6.08	0.0162	0.00345	164.3	7.9	82.6	30.25	55.2 ± 0.7
1050	7.33	0.0136	0.00640	73.0	3.5	73.7	36.03	59.2 ± 1.5
FUSE	13.88	0.3252	0.01799	34.2	1.7	61.6	1.51	92.9 ± 1.5
TOTAL				2069.1	100.0			54.9
PLATEAU AGE								53.9 ± 0.8
	85OL46-M							J = 0.006193
825	4.32	0.0199	0.00336	141.8	7.5	76.2	24.62	36.4 ± 0.6
905	4.47	0.0271	0.00196	294.3	15.6	86.2	18.08	42.6 ± 0.7
940	4.78	0.0002	0.00117	513.6	27.2	91.9	2450.00	48.4 ± 0.5
975	4.97	0.0189	0.00128	470.1	24.9	91.7	25.90	50.2 ± 0.5
1000	5.32	0.0028	0.00172	290.7	15.4	89.7	177.09	52.5 ± 0.7
1025	5.84	0.0868	0.00281	154.6	8.2	85.2	5.64	54.7 ± 0.7
1050	11.68	0.0000	0.00898	6.2	0.3	77.0	*	97.8 ± 4.2
FUSE	20.67	0.5032	0.03267	16.3	0.9	53.3	0.97	119.1 ± 6.7
TOTAL				1887.6	100.0			49.0

* 37Ar below detection; Ca too low to measure

TABLE 4.1 (continued)

Temp °C	40Ar 39Ar	37Ar 39Ar	36Ar 39Ar	Moles 39Ar	39Ar %Total	%Ar40 Rad	K/Ca	Age (Ma)
	85G01-M			(E-14)				J = 0.005766
750	5.336	0.0153	0.0044	90.3	2.6	75.1	32.13	41.23 ± 0.99
850	5.900	0.0114	0.0028	243.4	7.0	85.4	43.10	51.64 ± 0.87
925	5.954	0.0074	0.0009	553.2	15.8	94.9	65.95	57.81 ± 0.69
1000	6.202	0.0032	0.0006	880.8	25.2	96.8	153.60	61.38 ± 0.95
1075	6.232	0.0042	0.0006	958.1	27.4	96.6	117.79	61.59 ± 0.72
1130	6.285	0.0115	0.0007	505.7	14.5	96.4	42.61	61.92 ± 0.69
1160	6.428	0.0350	0.0012	201.0	5.8	94.0	14.02	61.81 ± 1.00
1190	7.156	0.2848	0.0024	48.3	1.4	90.0	1.72	65.82 ± 1.10
FUSE	12.252	2.5036	0.0087	14.0	0.4	80.3	0.20	99.77 ± 5.75
TOTAL				3494.8	100.0			59.99 ± 0.83
PLATEAU AGE								61.67 ± 0.79
	85LI16-M							J = 0.005813
750	7.30	0.0143	0.0058	320.1	13.5	76.0	34.27	57.2 ± 1.6
850	6.33	0.0086	0.0018	615.6	25.9	90.9	57.11	59.4 ± 1.0
900	6.32	0.0088	0.0011	606.3	25.5	94.2	55.95	61.4 ± 0.7
950	6.56	0.0142	0.0010	502.4	21.2	94.9	34.48	64.1 ± 0.9
1000	6.91	0.0422	0.0015	225.2	9.5	93.2	11.60	66.2 ± 0.8
1050	8.18	0.2263	0.0032	71.4	3.0	88.3	2.17	74.2 ± 2.1
1130	9.27	0.6239	0.0051	22.4	0.9	83.9	0.79	79.7 ± 3.7
FUSE	14.96	1.8590	0.0135	10.9	0.5	74.0	0.26	112.7 ± 7.0
TOTAL				2374.2	100.0			62.1 ± 1.1
	85OL38-K							J = 0.006076
650	4.235	0.0005	0.0032	1146.6	3.9	76.7	960.78	35.25 ± 0.54
800	3.248	0.0010	0.0018	2000.8	6.8	82.5	512.66	29.13 ± 0.47
850	2.998	0.0013	0.0013	1269.8	4.3	85.8	389.18	27.99 ± 0.46
900	3.166	0.0026	0.0018	839.6	2.8	82.5	191.63	28.39 ± 0.57
950	3.224	0.0021	0.0013	1076.7	3.6	87.3	234.90	30.58 ± 0.43
1000	3.432	0.0031	0.0009	1017.5	3.4	91.6	158.49	34.12 ± 0.51
1050	3.602	0.0027	0.0008	1377.0	4.7	92.8	178.51	36.26 ± 0.52
1100	3.779	0.0027	0.0008	1723.8	5.8	92.6	182.02	37.94 ± 0.46
1130	3.953	0.0011	0.0008	1862.5	6.3	93.2	441.84	39.94 ± 0.49
1150	4.198	0.0007	0.0008	2855.4	9.6	93.7	735.74	42.63 ± 0.48
1170	4.390	0.0022	0.0008	3713.2	12.5	94.1	266.83	44.75 ± 0.55
1185	4.502	0.0020	0.0008	3464.2	11.7	93.8	248.73	45.72 ± 0.55
1200	4.671	0.0015	0.0009	3289.1	11.1	93.6	328.64	47.31 ± 0.54
1215	4.792	0.0033	0.0009	2230.3	7.5	93.5	150.50	48.48 ± 0.71
FUSE	4.960	0.0052	0.0011	1745.4	5.9	92.5	93.56	49.60 ± 0.58
TOTAL				29611.9	100.0			40.93 ± 0.53

TABLE 4.1 (continued)

Temp °C	40Ar 39Ar	37Ar 39Ar	36Ar 39Ar	Moles 39Ar	39Ar %Total	%Ar40 Rad	K/Ca	Age (Ma)
		86GO13C-M		(E-14)				J = 0 005818
700	4 804	0.0235	0.0027	128.1	5.7	82.9	20.87	41.31 ± 1.26
825	5.791	0.0177	0.0030	233.8	10.3	83.9	27.68	50.32 ± 1.03
875	5.825	0.0144	0.0014	280.5	12.4	92.2	33.93	55.52 ± 0.71
925	5.979	0.0238	0 0011	341.4	15.1	93.8	20.61	57.93 ± 0.67
975	6.029	0.0260	0.0011	433 2	19.1	94.2	18 84	58 67 ± 0.69
1025	6.185	0.0676	0.0013	488.9	21.6	93.3	7.25	59.57 ± 0.85
1100	6.413	0.1058	0.0013	236.6	10.4	93.4	4.63	61.79 ± 0.84
1140	7.099	0.1736	0 0022	83.3	3.7	90.6	2.82	66.26 ± 1.53
FUSE	10.043	0.5913	0.0024	40.2	1.8	93.0	0.83	95.47 ± 2.10
TOTAL				2266.0	100.0			57.78 ± 0.86
PLATEAU AGE								59 49 ± 3.64
		86G013C-K						J = 0.006063
650	7.317	0.0004	0.0024	1890.3	5 1	89.9	1338.80	70.52 ± 0.89
800	2.068	0.0008	0.0009	1829.7	4 9	85.4	593.94	19 20 ± 0 28
850	1.601	0.0004	0.0003	1966.9	5.3	93.2	1098.90	16.25 ± 0 22
900	1.716	0.0016	0.0002	1915.0	5.2	95.4	308.18	17.81 ± 0.22
950	1.822	0 0015	0 0002	1921.6	5.2	95.7	334.24	18.97 ± 0.23
1000	2.018	0.0012	0.0001	1816.1	4.9	96.3	399.35	21.12 ± 0.30
1050	2.312	0.0026	0.0002	1940.3	5.2	96.0	189.41	24.12 ± 0.29
1100	2.696	0.0016	0 0002	1948.6	5.3	96.2	307.23	28.14 ± 0.36
1130	3.102	0.0018	0 0003	2333.9	6.3	96.0	275.28	32.27 ± 0.38
1150	3 703	0.0008	0 0003	2691.7	7.3	96.4	597.56	38.64 ± 0.47
1170	4 458	0.0002	0.0004	3701.8	10.0	96.3	2620.32	46.36 ± 0.57
1185	4 884	0.0002	0.0005	3853.8	10.4	96.3	2450.00	50.74 ± 0.61
1200	5.146	0.0001	0.0005	3611.0	9.7	96.5	8249.16	53.52 ± 0.67
1215	5.229	0.0006	0.0005	3083.0	8.3	96.3	859.65	54.96 ± 0.70
FUSE	5.402	0.0004	0.0006	2538.1	6.9	96.1	1147.00	55.89 ± 0 65
TOTAL				37041.7	100.0			39.47 ± 0.49
		860L44A-M						J = 0 005992
650	7.11	0.0059	0 0013	208.3	1.6	52.7	8.36	40 0 ± 1.1
800	7.08	0.0430	0.0038	603.8	4.5	83.9	11.40	63.0 ± 0.8
850	6.94	0.0336	0.0014	924.0	6.9	93.5	14.58	68.8 ± 0.8
900	7.40	0.0255	0.0009	1177.2	8.8	96.1	19.22	75 3 ± 0 8
950	8.35	0.0237	0.0008	1475.4	11 0	96.9	20.71	85.4 ± 0 9
1000	9.93	0.0324	0.0008	1833.2	13.7	97.2	15.14	101.4 ± 1.1
1050	10.42	0 0384	0.0008	1811.6	13 5	97.6	12.75	106.7 ± 1.2
1088	11.36	0.0536	0.0008	1467.8	11.0	97.7	9.15	116 2 ± 1.3
1122	17.49	0 1410	0.0010	1256.1	9.4	98.1	3 48	176.6 ± 2.0
1140	25 46	0 1284	0 0011	892.5	6 7	98.6	3 82	252.8 ± 2.7
FUSE	28.80	0.1206	0.0013	1728.2	12.9	98.6	4 06	283 6 ± 3.1
TOTAL				13378.1	100.0			135 4 ± 1 5
		86OL44A-K						J = 0 00607
650	3.914	0.0013	0 0029	807.4	4.6	77.1	363.88	32.76 ± 0.58
800	2.836	0.0013	0.0019	1217.8	6.9	79.5	364.94	24.51 ± 0.38
850	2.295	0.0016	0.0005	957.2	5.4	91.8	304 35	22.93 ± 0.30
900	2.322	0.0024	0.0002	838.7	4.7	95.9	200.08	24.22 ± 0.27
950	2.321	0 0029	0.0002	699.0	4.0	95.9	170.79	24.20 ± 0.31
1000	2.453	0.0027	0.0002	741 8	4.2	96.8	178.25	25.81 ± 0.29
1050	2.690	0.0038	0.0002	755 8	4.3	96.2	130.15	28.12 ± 0.33
1100	2.872	0.0041	0.0003	844.9	4 8	95.8	119.77	29 88 ± 0.32
1130	3.125	0.0017	0.0004	924.5	5.2	95.0	296.54	32.21 ± 0.43
1150	3.368	0.0043	0.0004	1040.9	5 9	95.9	112.72	35.01 ± 0.47
1165	3.702	0.0042	0.0004	1098.1	6.2	95.6	115.32	38.35 ± 0.50
1180	3.947	0.0042	0.0005	1055.6	6.0	95.6	116.06	40.85 ± 0.46
1195	4.144	0.0028	0.0005	1247.0	7.0	95.6	174.81	42 89 ± 0.51
1210	4.261	0.0023	0.0006	1729.5	9.8	95.1	213.79	43.86 ± 0.53
1225	4.381	0.0017	0.0006	2125.7	12.0	95.2	285.55	45 09 ± 0.53
FUSE	4.431	0.0016	0 0007	1609.8	9.1	94.9	299.14	45.46 ± 0.51
TOTAL				17693 8	100.0			35.66 ± 0 88

TABLE 4.1 (continued)

Temp °C	40Ar 39Ar	37Ar 39Ar	36Ar 39Ar	Moles 39Ar	39Ar %Total	%Ar40 Rad	K/Ca	Age (Ma)
	86OL44B-M			(E-14)				J = 0 006023
650	31.43	0.0111	0.0846	51.4	0.4	20.3	44.19	68.1 ± 6.2
800	22.36	0.0095	0.0374	145.7	1.1	50.5	51.85	118.7 ± 2.2
850	17.38	0.0009	0.0127	260 5	2.0	78.2	564.06	141.9 ± 1.9
900	18.00	0.0040	0.0041	560.9	4 3	93.1	122.90	173.5 ± 2.1
950	22.42	0.0009	0.0019	938.5	7.1	97.3	560.00	222.7 ± 2 4
1000	25.78	0 0006	0.0013	1427.2	10.8	98.4	878.84	256.5 ± 2 8
1050	27.05	0 0023	0.0010	1150 8	8.7	98 8	216.62	269.1 ± 2.9
1088	29.16	0.0000	0.0010	1171.4	8.9	98.9	*	288.8 ± 3 3
1115	29.64	0.0007	0.0009	1777.9	13.5	99.0	753.85	293.6 ± 3 3
1135	28.82	0.0000	0.0009	2225.2	16.9	99.0	*	285 9 ± 3.1
1150	28.84	0.0028	0 0008	1954 1	14.8	99.0	172.78	286.3 ± 3.1
1170	29 27	0.0006	0.0009	1211.0	9.2	99.0	862 68	290.3 ± 3.1
FUSE	29 30	0.0142	0.0012	318.9	2.4	98.7	34.61	289.5 ± 2.9
TOTAL				13193.4	100.0			268.3 ± 5.9
	86OL44B-M2							J = 0.005825
750	6.74	0.0374	0.0102	149.1	5 1	54.8	13.11	38.4 ± 1.0
850	6.07	0.0247	0.0039	258.5	8.9	80.6	19.81	50.7 ± 0.7
900	5.76	0.0172	0.0018	343.8	11.9	90.2	28.53	53.8 ± 0.8
950	5.86	0.0145	0.0011	403.6	13.9	93.7	33.70	56 8 ± 0.7
1000	5.99	0.0516	0.0013	471.7	16.3	93.0	9.50	57 6 ± 0.7
1050	6.20	0.0805	0.0017	572.2	19 8	91.6	6 09	58.7 ± 0.9
1100	7.09	0.0573	0.0024	435.0	15.0	89.6	8.56	65.5 ± 0.9
1140	10 09	0 0997	0.0032	173.8	6.0	90.3	4.92	93.4 ± 1.1
1170	16.30	0 3534	0.0038	57.5	2.0	93.0	1.39	152.8 ± 1.9
FUSE	13.68	0.8455	0.0105	30.0	1 0	77.6	0 58	108.3 ± 5.0
TOTAL				2895.3	100 0			61.4 ± 0.9
	86OL57-M							J = 0.005974
650	7.56	0.0471	0.0129	205.5	2.1	49.3	10.41	39.7 ± 1 0
800	6.48	0.0317	0.0080	368.9	3.7	62.8	15.47	43 4 ± 0.9
850	5.32	0.0248	0.0029	585.6	5.9	83.1	19.77	47.1 ± 0.6
900	5.39	0.0257	0.0018	810.2	8.2	89.4	19.40	51.2 ± 0.8
950	5.54	0.0391	0.0015	1274 5	12.9	91.4	12.55	53 7 ± 0 8
1000	5.69	0.0501	0 0013	1900.5	19 3	92.6	9.78	55.9 ± 0.7
1050	6.07	0.1074	0.0013	2032.2	20.6	93.1	4.56	59.9 ± 0.8
1100	6.59	0.2030	0.0014	1487.1	15.1	93.5	2 41	65.2 ± 0.8
1130	7.50	0 2367	0.0021	763.0	7.7	91.6	2.07	72.6 ± 0.9
FUSE	13.05	1.0695	0 0040	438.7	4.4	91 4	0.46	124.3 ± 1.6
TOTAL				9866.3	100.0			60 5 ± 0.8
	86OL57-K							J = 0.006021
650	12.21	0.0007	0.0056	752.1	2 6	86 1	661.09	110.8 ± 1.4
800	3 73	0.0012	0.0023	1563.2	5.5	80.9	400.59	32.5 ± 0.4
850	2.14	0.0016	0.0010	1652.2	5.8	84.4	306.86	19 5 ± 0.3
900	2.15	0.0023	0.0008	1775.1	6.2	87.9	210.25	20.4 ± 0.4
950	2.14	0.0038	0.0007	1586.5	5.6	88 6	127.35	20.5 ± 0.3
1000	2.23	0.0026	0.0008	1276.4	4.5	88.4	185.73	21.2 ± 0.3
1050	2.39	0.0044	0 0009	1215.1	4.3	87.9	112.07	22.6 ± 0.3
1100	2 69	0.0040	0.0008	1236.5	4.4	89.5	121.80	25.9 ± 0.3
1130	3.16	0.0050	0 0008	1400 3	4.9	91.2	97 37	31.1 ± 0.4
1150	3.96	0.0043	0.0009	1830.8	6.4	92 4	113.69	39.4 ± 0 5
1170	4.48	0.0063	0.0010	2071.0	7.3	92 9	77.69	44.6 ± 0.6
1190	4.87	0 0033	0.0009	2786.7	9.8	94.1	148.98	49.1 ± 0.6
1210	5.12	0.0026	0.0010	3878.1	13.6	93.6	186.64	51 3 ± 0.6
FUSE	5.28	0 0020	0 0009	5389.0	19.0	94.4	242.38	53.4 ± 0.6
TOTAL				28413.0	100			40.6 ± 1.6

* 37Ar below detection; Ca too low to measure

TABLE 4.1 (continued)

Temp °C	40Ar 39Ar	37Ar 39Ar	36Ar 39Ar	Moles 39Ar	39Ar %Total	%Ar40 Rad	K/Ca	Age (Ma)
		86G022A-K		(E-14)				J = 0.006043
650	6.048	0.0062	0.0034	1001.6	3.8	82.9	79.30	53.87 ± 0.81
800	4.055	0.0080	0.0019	1608.6	6.1	85.1	61.46	37.25 ± 0.51
850	3.622	0.0062	0.0009	1736.0	6.6	91.6	79.19	35.82 ± 0.44
900	3.768	0.0060	0.0007	1653.5	6.2	93.6	81.67	38.05 ± 0.52
950	4.133	0.0067	0.0006	1540.8	5.8	94.6	72.68	42.13 ± 0.50
1000	4.629	0.0072	0.0007	1480.1	5.6	94.6	68.47	47.11 ± 0.57
1050	5.074	0.0071	0.0008	1683.2	6.4	94.8	69.60	51.68 ± 0.61
1100	5.542	0.0070	0.0008	1856.2	7.0	95.2	69.62	56.61 ± 0.67
1130	6.120	0.0065	0.0009	2093.9	7.9	95.0	75.15	62.26 ± 0.77
1145	6.741	0.0094	0.0009	2242.0	8.5	95.6	52.41	68.90 ± 0.80
1160	7.306	0.0049	0.0011	2430.2	9.2	95.1	99.14	74.17 ± 0.86
1175	7.698	0.0067	0.0010	2340.2	8.8	95.6	73.41	78.50 ± 0.93
1190	7.953	0.0080	0.0011	1896.5	7.2	95.5	61.33	80.94 ± 1.04
1200	8.345	0.0075	0.0019	1219.6	4.6	93.0	65.23	82.66 ± 0.99
1225	8.380	0.0129	0.0020	1042.4	3.9	92.6	37.93	82.68 ± 0.95
FUSE	8.637	0.0157	0.0024	661.8	2.5	91.2	31.13	83.94 ± 1.10
TOTAL				26486.6	100.0			60.81 ± 1.66
		86G022-B						J = 0.006042
650	28.35	0.1909	0.0645	73.3	0.9	32.7	2.57	98.3 ± 10.1
800	22.41	0.1044	0.0157	238.7	3.1	79.1	4.69	183.6 ± 3.0
850	30.03	0.0320	0.0087	495.0	6.4	91.4	15.30	276.7 ± 7.3
925	29.78	0.0145	0.0036	937.8	12.1	96.3	33.86	288.3 ± 3.6
975	29.64	0.0232	0.0026	1001.0	12.9	97.3	21.12	289.8 ± 3.1
1025	30.27	0.0691	0.0027	866.3	11.1	97.3	7.10	295.4 ± 3.1
1100	29.68	0.0772	0.0021	1570.6	20.2	97.9	6.35	291.7 ± 3.3
FUSE	27.00	0.0869	0.0015	2588.5	33.3	98.3	5.64	268.3 ± 2.9
TOTAL				7771.1	100.0			277.6 ± 3.5
		86G022H						J = 0.006041
750	147.90	2.5748	.1898	11.3	0.7	62.2	.1900	798.7 ± 25.1
825	80.47	1.4959	.0771	19.8	1.3	71.8	.3272	540.7 ± 6.0
875	50.59	1.3443	.0359	25.0	1.6	78.2	.3641	391.4 ± 5.0
940	35.66	2.3428	.0211	35.2	2.3	83.0	.2088	297.2 ± 3.6
975	46.12	4.2575	.0198	36.1	2.4	88.1	.1147	397.0 ± 2.9
1000	56.36	5.7274	.0172	43.4	2.9	91.9	.0852	492.8 ± 3.8
1025	54.46	5.6793	.0122	105.1	6.9	94.3	.0859	489.2 ± 3.4
1050	54.51	5.5426	.0095	113.3	7.5	95.7	.0880	496.1 ± 2.8
1075	50.28	5.3800	.0084	171.8	11.3	96.0	.0907	463.1 ± 3.2
1100	43.52	5.3196	.0066	301.6	19.9	96.6	.0918	409.6 ± 2.1
1025	40.45	5.2894	.0056	235.6	15.5	97.0	.0923	385.1 ± 2.1
1140	39.85	5.3501	.0053	180.4	11.9	97.2	.0912	380.7 ± 2.0
1160	40.31	5.3743	.0053	157.4	10.4	97.2	.0908	384.8 ± 2.5
1200	37.38	4.7795	.0049	82.0	5.4	97.2	.1022	359.3 ± 2.1
TOTAL				1518.1	100.0			418.88

TABLE 4.1 (continued)

Temp °C	40Ar 30Ar	37Ar 39Ar	36Ar 39Ar	Moles 39Ar	39Ar %Total	%Ar40 Rad	K/Ca	Age (Ma)
		84LI26-M		(E-14)				J = 0.005799
700	7.021	0.0198	0.0069	140.4	5.1	70.6	24.75	51.12 ± 0.95
825	5.900	0.0111	0.0020	336.3	12.2	89.2	44.22	54.23 ± 1.16
875	6.001	0.0073	0.0010	444.7	16.1	94.7	67.12	58.52 ± 0.73
925	6.339	0.0054	0.0007	617.0	22.4	96.0	90.41	62.56 ± 0.70
975	6.445	0.0091	0.0008	604.9	22.0	96.0	53.67	63.62 ± 0.73
1025	6.447	0.0198	0.0007	397.6	14.4	96.3	24.73	63.83 ± 0.75
1100	6.609	0.0507	0.0009	154.2	5.6	95.7	9.67	64.98 ± 0.87
1140	7.245	0.3252	0.0017	47.6	1.7	93.0	1.51	69.18 ± 1.19
FUSE	9.406	2.7928	0.0009	13.1	0.5	99.2	0.18	95.24 ± 2.56
TOTAL				2755.7	100.0			61.13 ± 0.82
PLATEAU AGE								63.34 ± 1.67
		85OL50-M						J = 0.006232
765	15.63	0.1843	0.00842	44.4	2.5	83.9	2.66	141.8 ± 2.3
825	12.29	0.1250	0.01016	60.2	3.4	75.3	3.92	101.2 ± 1.7
905	9.25	0.1005	0.00472	109.6	6.1	84.6	4.88	85.9 ± 1.0
940	8.86	0.0271	0.00249	155.9	8.7	91.3	18.08	88.7 ± 1.3
975	9.25	0.0136	0.00247	226.2	12.6	91.7	35.90	93.0 ± 1.0
1000	9.54	0.0002	0.00261	352.2	19.6	91.5	2450.00	95.5 ± 1.1
1025	9.30	0.3184	0.00040	349.1	19.5	98.6	1.54	100.2 ± 1.1
1050	9.97	0.0078	0.00195	293.5	16.4	93.8	63.06	102.2 ± 1.1
1075	11.01	0.0301	0.00511	153.3	8.5	85.9	16.28	103.4 ± 1.6
1100	14.08	0.1544	0.01083	40.0	2.2	77.1	3.17	118.1 ± 2.3
FUSE	36.33	1.3931	0.06874	10.3	0.6	44.3	0.35	172.6 ± 13.1
TOTAL				1794.7	100.0			99.0
		85OL32-M						J = 0.00622
825	7.89	0.0147	0.00952	63.7	3.3	63.9	33.44	55.7 ± 1.0
915	8.06	0.2306	0.00646	113.3	5.8	76.1	2.12	67.5 ± 1.5
975	8.75	0.0178	0.00244	274.2	14.0	91.3	27.53	87.5 ± 1.0
1000	9.27	0.0020	0.00181	400.0	20.5	93.8	244.63	95.0 ± 1.0
1025	9.47	0.0149	0.00159	473.0	24.2	94.6	32.89	97.9 ± 1.0
1050	9.56	0.0012	0.00162	385.3	19.7	94.6	411.76	98.7 ± 1.0
1075	10.20	0.0092	0.00366	190.5	9.8	89.0	53.47	99.1 ± 1.1
FUSE	13.46	0.2363	0.01282	53.4	2.7	71.7	2.07	105.2 ± 2.1
TOTAL				1953.5	100.0			93.2
		86OL47-H						J = 0.005745
750	140.39	7.281	0.2249	7.9	1.8	53.0	0.067	645.4 ± 23.8
825	99.32	7.515	0.1365	7.3	1.7	59.9	0.065	533.2 ± 26.2
875	72.11	10.713	0.0664	10.4	2.4	73.9	0.045	485.2 ± 12.6
937	54.63	15.027	0.0315	22.0	5.0	85.0	0.032	431.0 ± 6.1
975	54.67	16.177	0.0302	16.5	3.8	85.8	0.030	435.3 ± 9.4
1000	53.63	17.272	0.0282	21.2	4.8	86.8	0.028	432.7 ± 6.3
1025	53.20	17.048	0.0211	22.7	5.2	90.7	0.028	446.3 ± 8.1
1060	48.69	16.468	0.0100	41.0	9.4	96.5	0.029	435.7 ± 7.3
1100	51.35	16.226	0.0156	59.5	13.6	93.4	0.030	443.8 ± 5.9
1122	51.44	16.306	0.0154	53.0	12.1	93.5	0.030	445.0 ± 6.1
1140	50.10	16.502	0.0152	59.9	13.7	93.5	0.029	434.6 ± 5.1
1160	50.51	16.772	0.0132	39.1	8.9	94.8	0.029	443.2 ± 4.9
1190	51.86	16.544	0.0131	42.5	9.7	94.9	0.029	454.1 ± 5.4
FUSE	54.29	15.808	0.0137	33.6	7.7	94.7	0.031	471.7 ± 15.7
TOTAL				436.6	100.0			449.8 ± 7.7
PLATEAU AGE								438.5 ± 14.8

TABLE 4.2 Rb-Sr Analyses

SAMPLE	Rb, ppm	Sr, ppm	87Rb/86Sr	87Sr/86Sr
85GO42 plag	5.38	47.14	0.334	0.71306
whole rock	142.5	36.45	11.33	0.71880
mica	348.0	8.86	114.40	0.77984
85OL43 plag	68.3	54.72	3.62	0.71839
whole rock	165.0	73.57	6.53	0.71941
mica	531.7	53.23	29.00	0.73245
85OL46 plag	6.60	21.13	0.905	0.71531
whole rock	133.3	40.84	9.45	0.72151
mica	325.3	30.6	30.87	0.73451
85OL32 whole rock	153.3	179.50	2.47	0.74262
mica	397.0	53.24	21.65	0.71614
85OL50 whole rock	141.6	279.27	1.470	0.71406
mica	335.0	82.89	11.72	0.72748

87Sr/86Sr corrected for fractionation using 86Sr/88Sr =0.1194 and normalized to E&A $SrCO_3$ =0.70800. Analytical precision <0.005%
Rb/Sr reproducible to better than 1%

Chapter 5: METAMORPHIC PETROLOGY AND P-T HISTORY OF THE MT. OLYMPOS REGION

INTRODUCTION

The structural and tectonic history that has been outlined in the preceding chapters depends critically upon the interpretation and correlation of metamorphic and deformational events in the tectonostratigraphic units of the Olympos region. It is necessary, therefore, to elaborate on the bases for the interpretations of metamorphic facies and pressure-temperature conditions. The characteristic mineral assemblages for each metamorphic event in each structural unit will be described below, followed by a discussion of the pressure-temperature conditions of metamorphism.

Because of the complicated structural history and polymetamorphism in the Olympos region, it is difficult to determine which phases in a given sample were in equilibrium, and thus to provide unequivocal constraints on the metamorphic conditions. As discussed in Chapter 4, and further below, there is abundant evidence that metamorphism occurred at very low temperatures (<350-400°C for the major event). As a result of the low temperatures, rocks are only partially recrystallized; relict phases are ubiquitious, and textural disequilibrium is commonly visible. Nonetheless, one useful aspect is that the early metamorphic history of these rocks is can be observed in thin section, and while quantitative P-T constraints cannot be obtained, the mineral assemblages are at least indicative of the metamorphic facies. In part because of these difficulties however, as well as the lack of well-calibrated thermobarometers for high-pressure, low-temperature assemblages, I have limited the discussion to comparison with similar assemblages in metamorphic terranes where more extensive work has been able to better constrain the P-T conditions.

PETROGRAPHIC CHARACTERISTICS OF METAMORPHIC ASSEMBLAGES IN THE MT. OLYMPOS REGION

The lithologic and structural characteristics of tectonostratigraphic units in the Olympos region were discussed in Chapters 2 and 3. The structural units include, from bottom to top: the Olympos unit, the Ambelakia unit, the Pierien unit, the Infrapierien unit, and the Ophiolite unit.

Abundant evidence exists for polymetamorphism, thus the mineral assemblages and textural relations will be described with respect to four metamorphic events that are termed M1, M2, M3, and M4 in accordance with the terminology of Chapter 3: M1: greenschist-amphibolite facies; M2 and M3: blueschist-facies and blueschist-greenschist transition facies; M4: prehnite-

pumpellyite facies. M0 is not discussed in detail here as there is too little evidence to warrant any interpretation beyond that which has been made in Chapter 3, and this study is mainly concerned with deciphering Alpine-age events. Events M1-M3 are associated with different phases of foliation formation while M4 appears to be late- to post-tectonic with respect to the metamorphic fabrics. The M2 and M3 mineral assemblages are generally the same in each unit; however, radiometric data that indicate that two low-temperature metamorphic events occurred after M1 and the association of the assemblages with distinct structures requires the definition of two separate events. Events M1-M4 affected the Pierien and Infrapierien units, M2-M4 affected the Ambelakia unit, and M3-M4 affected the Olympos unit.

Because the tectonostratigraphy of each unit was described in chapter 2, the characteristic mineral assemblages for each metamorphic event will be dicussed in terms of the different bulk compositions present in the various units. Evidence for correlating each metamorphic event with the deformational events described in chapter 3 and the radiometric dates of chapter 4 will presented following the description of the metamorphism.

This section will focus on the petrographic characteristics and will be followed by a description of the mineral chemistry. Approximately 300 thin sections were examined to determine mineral assemblages and the relations between microstructures and metamorphic events. Locations of samples mentioned in the text are shown in Figure 5.1. Abbreviations used in the description of mineral assemblages are given in Table 5.1. Common mineral assemblages found within each unit are given in Table 5.2.

M1: Greenschist-Amphibolite facies metamorphism

Greenschist-amphibolite facies assemblages are present in the Pierien, Infrapierien, and ophiolite units. A possible pre-M2 greenschist or blueschist-greenschist transition facies metamorphism may also have affected the Ambelakia unit, but because the mineral assemblages are different in metabasites of the Ambelakia and ophiolite units, the event that is designated M1(?) in the Ambelakia unit may be a different age and/or occurred at a different location than in the other units.

Granitic rocks

The granitic augen gneiss of the Pierien and Infrapierien units contains the relict phases orthoclase, muscovite, allanite, and zircon. Rare garnet

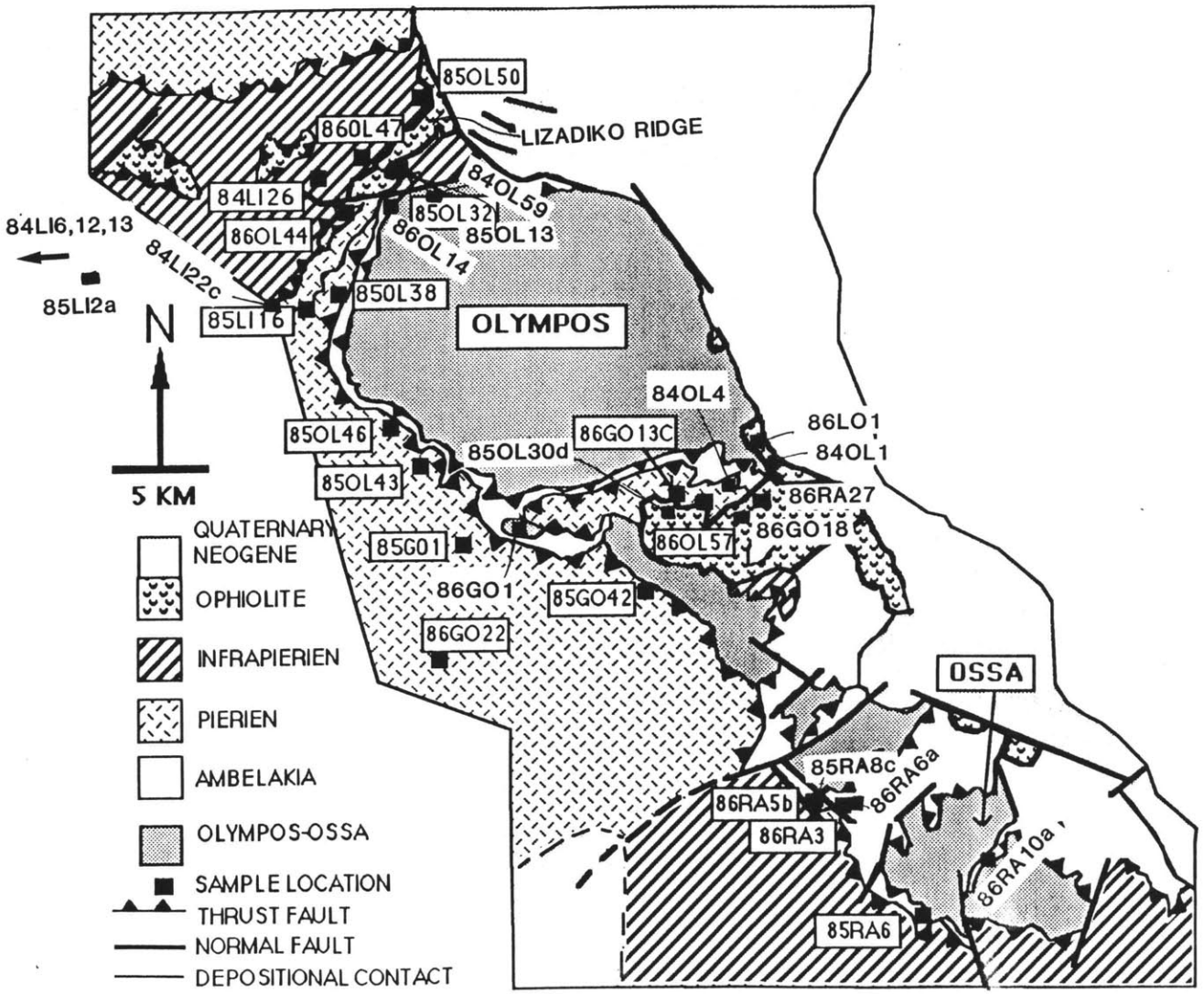

Figure 5.1: Generalized geologic map and locations of samples used in this study.

TABLE 5.1 Abbreviations of minerals used in the text

ab	albite
ac	acmite
act	actinolite
ap	apatite
bar	barroisite
bi	biotite
cc	calcite
chl	chlorite
cpx	clinopyroxene
ctd	chloritoid
cr	crossite
ep	epidote
ga	garnet
gl	glaucophane
hbl	hornblende
hm	hematite
ilm	ilmenite
ksp	K-feldspar
lm	laumonite
lw	lawsonite
mt	magnetite
mu	muscovite
par	paragonite
ph	phengite
plag	plagioclase
pp	pumpellyite
pr	prehnite
qtz	quartz
ri	riebeckite
rt	rutile
sp	serpentine minerals
sph	sphene
stilp	stilpnomelane
tr	tremolite
wn	winchite
wr	wairakite
zo	zoisite

Table 5.2 Representative mineral assemblages in the study area, divided by structural unit. X indicates a mineral is present; tr indicates trace quantities. (2) indicates 2 generations of a mineral are present in different sub-assemblages or 2 distinct compositions are present. M1 and M2 indicate different minerals that can be clearly associated with distinct metamorphic events. Rock type abbreviations: mb= metabasalt or metatuff; ms= metasediment; gg=granitic gneiss; cs=calc schist; am = amphibolite; um=ultramafic rock; mg=metagabbro. Na-Am indicates sodic amphibole (gl or cr); Ca-am indicates calcic or sodic-calcic amphibole (act, wn, barr); FeOx indicates iron oxides; other abbreviations as in Table 5.1 and in the last column of this table.

UNIT, SAMPLE#	ROCK		ASSEMBLAGE												
	TYPE	Na-Am	Ca-am	Na px	ph	chl	ep	pp	lw	cc	sph	stilp	FeOx	OTHER	abbreviations
OLYMPOS UNIT															
84OL59	MS	X	X		X			X	X					R	R: rutile
84LI20	MS				X			X							A: apatite
84LI19a	CS				X	X				X	X		H	A	M: magnetite
84OL48	MS				X	X		X		X					H : hematite
84OL18	MS				X	X		X					X		I: ilmenite
															G: graphite
AMBELAKIA UNIT															K: kspar
85RA8c	MB	X(M2)	X(2)		X	X	X(2)	X	X?		X		H		T: tourmaline
86RA5b	MB	X		X	X	M4	X	X			X	X	tr	A,I,R	S: sulfides
86RA6a	MB	X			tr	X	X	X	X		X		tr		C: chromite
86Ra10a	MB	X	X		X	tr	X	X	X		X	X	X	A,I	
86GO1	MS	X			X	X				X				GA	
86OL14	CS	X			X	X				X	X		X	A	
86OL30	CS	X	X		X	X		X(2?)	X		X			R	
86RA8C	MB	X(M2)	X(M1)			X(2)	X(2)	M4					x	I	
PIERIEN UNIT															
85LI16	MS	X			X	X	X				X	X	X		
85GO1	MB	X			X						X	X	tr	A,R	
85OL46	GG	X		X	X						X		X	A	
86OL44b	GG				X		tr							K	
85LI12	GG				X									A	
85GO42	GG	X(2)			X	late					X		M	A	
85OL43	GG				X		tr					X		A	
84OL4	MS		X		X		X				X		X		
84OL5b	MS	X			X	X	X(2)								
84OL31	MS		X		X								M		
85LI14	MS	X			X						X	X		A	
85LI15	MS	X			X		X	M4							
SAMPLE		Na-Am	Ca-am	Na px	pheng	chl	ep	pp	lw	cc	sph	stilp	FeOx	OTHER	abbreviations
INFRAPIERIEN															
84LI26	MS	X			X		X(2)				X		X		
85OL13	MS		X		X	M4	X (2)				X		X	bi(M1),A	
85OL32	MS				X		X				X				
85OL50	MS		X		X	M4	X			X	X			bi(M1),A	
85RA16a	MB		X		tr	X	X				X				
86OL47	AM		hbl(M1)			X(M2)	tr						M,S	bi,ga,A	plag not ab
86RA20	MB		X		X		X							A	
84OL24b	MB		X		X						X	X	X	R,A	
84OL24c	MB		act+hbl		X	X(2)	X				X		H	A	
84LI28	MB	X									X	X	X	A	
OPHIOLITE															
84OL1	MB		X			X	X				X		X	A	
85OL30d	UM		X			X	zo				X		X		
86LO1	MB		X			X	X				X		C		
86GO18	MG		X			late	zo								
86RA22	MG		X			X	X,zo							sp	
PELITIC SCHISTS		plag	ksp	mu	pheng	chl	ep	bi	ga	parag	ctd	sph	FeOx	OTHER	
84LI22c**	MS				X		X			X	X	X	X	A,R,I	
84LI6a**	MS			X		X			X					I,R,T	
84LI12a	MS	X		X		X	X		X	X		X	M	A,I,T	
84LI13**	MS			X		X			X	X	X			R,T	
85LI2a	MS	X	X	X				X	X						
ALL SAMPLES CONTAIN AB + QTZ UNLESS NOTED BY **															

porphyroclasts with abundant inclusions provide evidence of an early (M0) metamorphic history; however, a later foliation and mylonitic fabric have essentially obliterated the earlier fabric and mineral assemblage. The M1 assemblage in the granitic augen gneiss is interpreted to be qtz + pl + mu ± ep ± sph ± ilm. Epidote occurs as an apparently early phase, where it is anhedral, cracked, and deformed along the foliation planes (e.g. 85OL43; 86OL44b); it is not clear whether epidote was stable during the M0, M1, or both events. The degree of overprinting of this early metamorphism prevents correlation.with other metamorphic events in the study area; it may be pre-Alpine in age.

Pelites

In the area near Sarandoporou, ~12 km west of Mt. Olympos (Figure 5.1), a thrust sheet of the Pierien unit exposes pelitic schists at a high structural level that appear to have been unaffected by the blueschist metamorphism (M2-M3) documented for the Ambelakia and lower Pierien units. While I tentatively correlate the metamorphism in this thrust sheet to the M1 event; there are no direct radiometric age constraints. The metapelites contain the assemblage qtz + chl + mu + plag + ga + ilm + rt ± par ± ctd ± mt . Tourmaline is a minor but ubiquitous accessory phase. In some samples plagioclase is a minor component, and paragonite is present. In 84LI13, chloritoid is parallel to the foliation and is intergrown with chl + mu + par. In paragonite-bearing samples paragonite and muscovite are intergrown on a very small (~10-20μm layers) scale and are the dominant foliation-forming minerals. Chlorite seems to be an alteration product of biotite in some samples; however in others, it appears to be in textural equilibrium with garnet. Garnet appears to have multiple stages of growth, with an inclusion-free core, an inner rim with abundant inclusions (mainly qtz + ep), and an outer rim with no inclusions (Fig. 5.2). The qtz + mu + chl foliation wraps around the garnets, but in some samples, the garnets are strongly sheared, fractured, and flattened in the foliation plane surrounded by large pressure shadows of qtz + chl (Fig. 5.3). Thus the latest deformation, and latest mica growth, post-dates garnet crystallization.

In the Livadi area NW of Mt. Olympos (Fig. 5.1), pelitic schists are observed within an area of dominantly granitic gneiss in the Infrapierien unit. These schists contain the assemblages qtz + plag + mu + bi + ga + rt ± ilm ± ksp and qtz + plag + mu + bi ± rt ± ksp. Garnet occurs as subhedral grains in a well-foliated matrix of qtz + plag + mu + bi + ksp. Inclusions of quartz occur in the garnet, but the fine-grained

nature of both the garnet and the inclusions prohibits identification of other inclusion minerals. Biotite is locally oxidized or altered to chlorite, and the rims of biotite and garnet are partly altered to ep + phengite ± sph. These upper greenschist-amphibolite facies pelitic schists contain only rare evidence of overprinting by later metamorphic events, but by correlation with amphibolites in the Infrapierien unit, and with similar facies rocks in the Pierien unit, I attribute this metamorphism to the M1 event.

Metabasites

In the Ambelakia unit, relict phenocrysts in the metavolcanic rocks include euhedral to subhedral plagioclase laths, augite, and hornblende, and rare altered and fractured olivine. Augite grains are surrounded by sodic amphibole, actinolite, and chlorite in a clear reaction relation (Fig. 5.4). The earliest mineral assemblage (M1?) observed in the Ambelakia unit consists of qtz + ab + ph + ep ± chl ± act in the mica schists and ab + ep + act + chl + gl or cr ± ph in the metavolcanic rocks. Calcic amphibole cores in sodic amphibole may have been in equilibrium with this earliest assemblage (Fig. 5.5). In some samples the M1 assemblage is associated with a well-developed foliation, but in others, the earliest visible foliation appears to be associated with M2, and only the actinolite cores provide evidence for an earlier metamorphic event. Epidote occurs in contact with actinolite in the matrix parallel to the first (S1?) schistosity and also in rims and pressure shadows around relict clinopyroxene grains and is thus interpreted to be a M1 phase.

In the Infrapierien, Pierien, and ophiolite units, amphibolites occur as micaceous schists containing act or hbl + pl + ph + qtz + ep ± ap ± sph. There are also massive amphibolites in the Infrapierien unit composed of hbl + pl + bi ± chl ± ep ± gar ± Fe-oxides + pyrite. Garnet from Infrapierien amphibolite sample 86OL47 occurs as anhedral porphyroblasts with abundant cracks, and a well-defined reaction rim consisting mainly of ep and Fe oxides. Hornblende, biotite, and plagioclase form a moderately well-defined schistosity that wraps around the garnet grains. Clean, sharp contacts between hornblende, biotite, and plagioclase suggest that this assemblage is in equilibrium, while the garnet is a relict of an earlier metamorphic event (M0?) (Fig. 5.6).

Relict plagioclase, hornblende, and clinopyroxene are commonly present in metabasaltic and metagabbroic rocks of the ophiolite unit. The most common M1 assemblage consists of act + ep + chl + ab + zo ± sph ± Fe-oxides. Figure 5.7a shows relict ophitic texture and relatively little synkinematic metamorphic

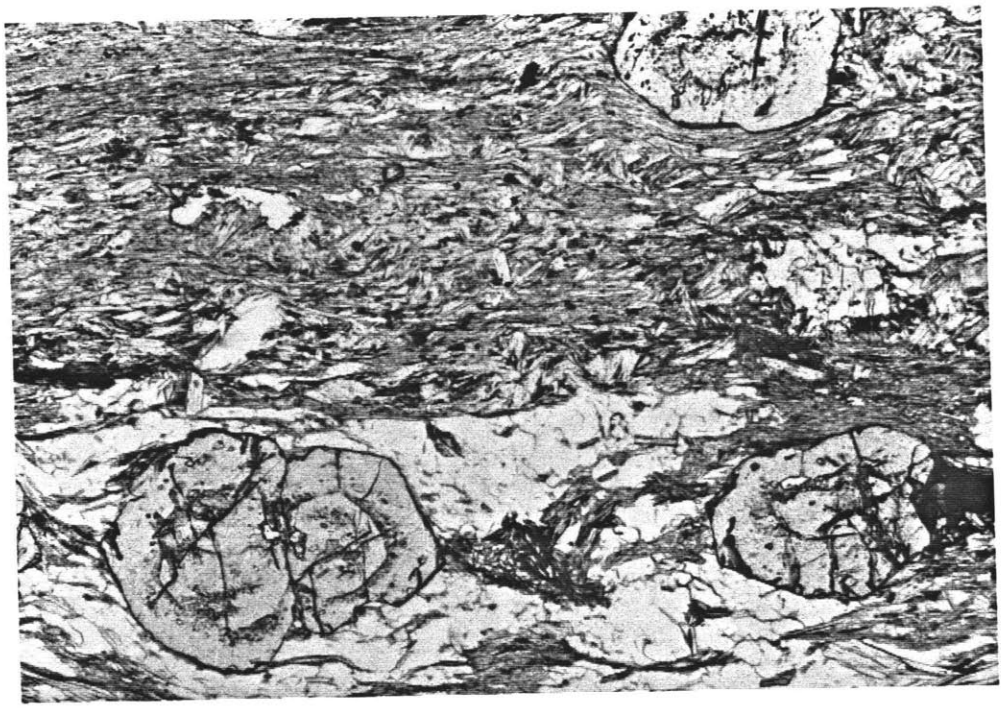

Figure 5.2: Photomicrograph of multiple growth zones in garnet from Pierien sample 84LI12a. Inner, rounded garnet is surrounded by a zone with many inclusions of qtz + ep that may represent a retrograde event which destabilized garnet; this is overgrown by subhedral to euhedral, inclusion - free garnet. Matrix phases include muscovite, paragonite, and chlorite. Plane light, 4 mm across.

Figure 5.3. Photomicrograph of garnet in Pierien sample 84LI6a. Garnet is fractured and sheared into foliation planes, and surrounded by pressure shadows of qtz + chl. Matrix phases are mu + chl; opaque minerals are ilmenite and rutile. Plane light ~13 mm across.

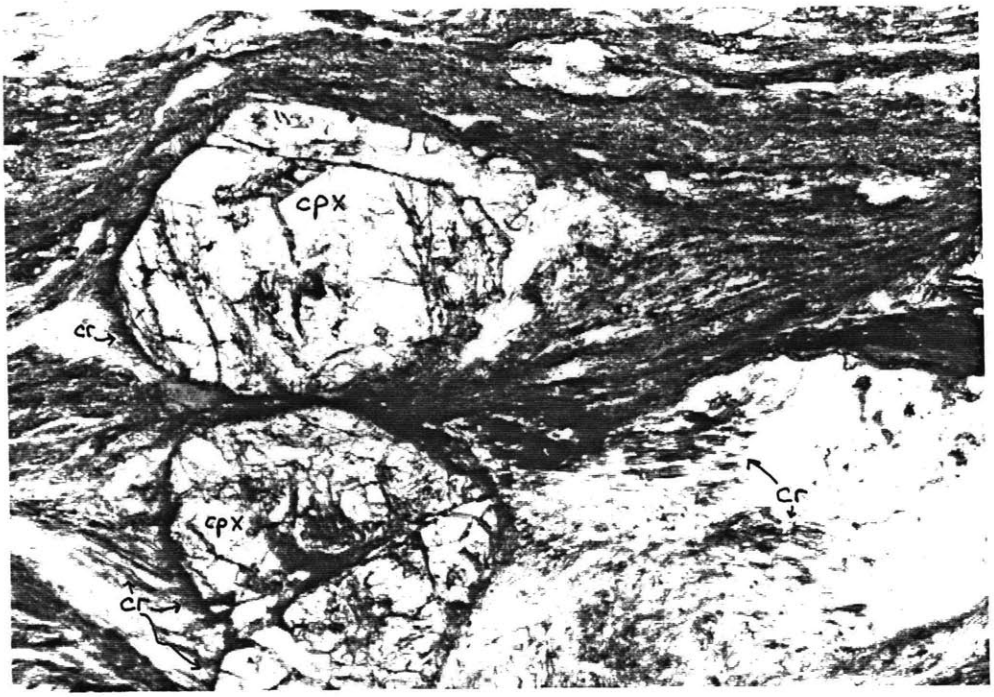

Figure 5.4: Photomicrograph of crossite growing on rims of relict augite phenocrysts, sample 86RA5b, Ambelakia unit. Cr grows in cracks in these grains and in pressure shadow of plagioclase grain in lower right corner of photo. Foliation-defining matrix phases are cr + ep + ph + pp. Plane light, scale 2 mm across.

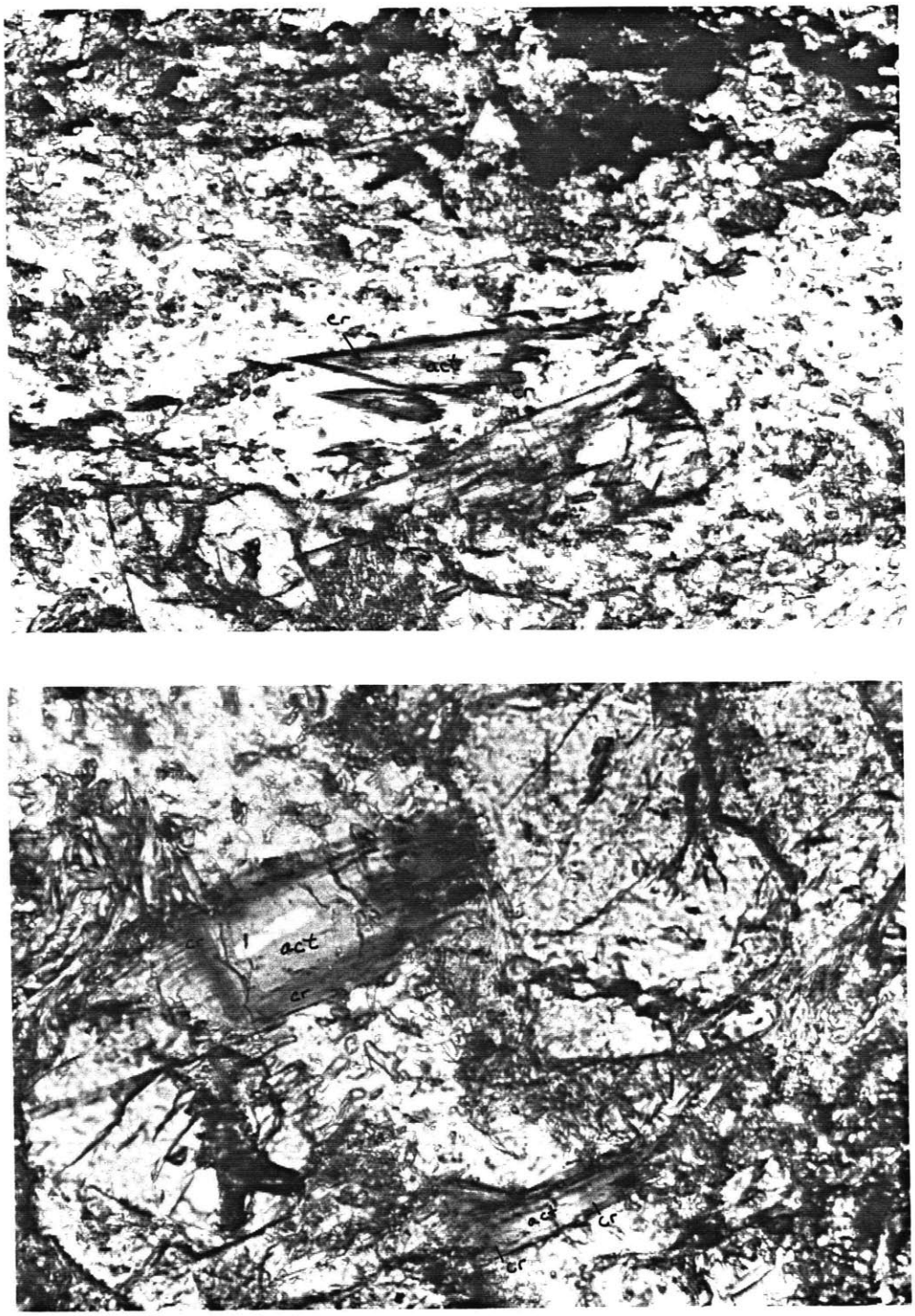

Figure 5.5: Photomicrograph of glaucophane rims on actinolite, sample 85RA8c, Ambelakia unit. Top: Scale 2mm across. Bottom: Scale 1mm across. Both photos in plane light.

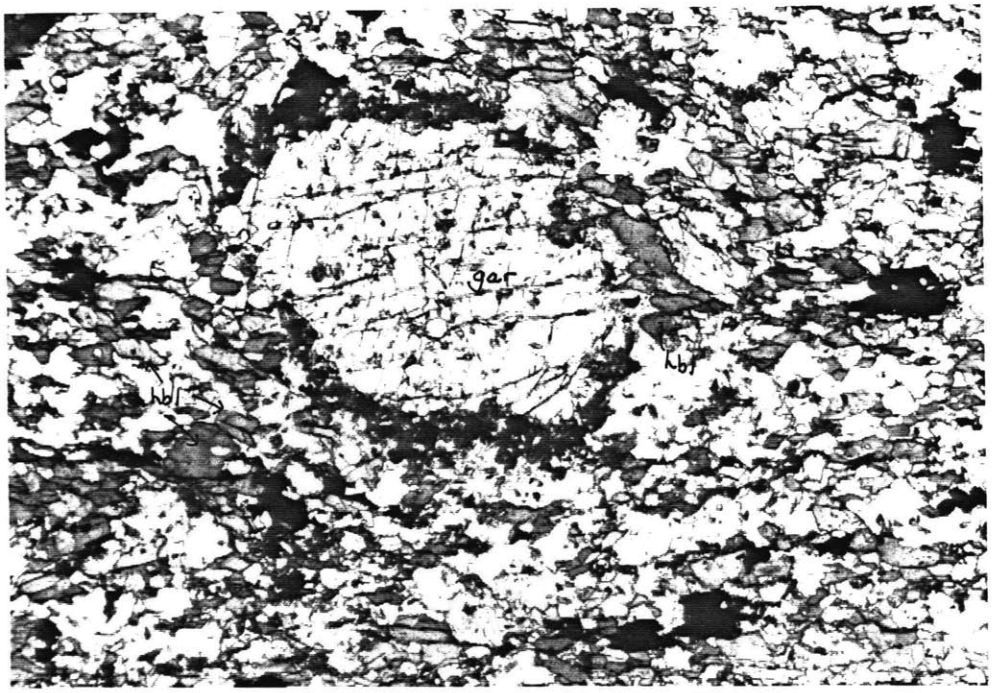

Figure 5.6: Photomicrograph of reaction rim around garnet of Infrapierien sample 86OL47. Garnet is surrounded by ep + chl + qtz + sph; matrix assemblage is plag + hbl + bi + Fe-oxides + pyrite. Plane light, 4 mm across.

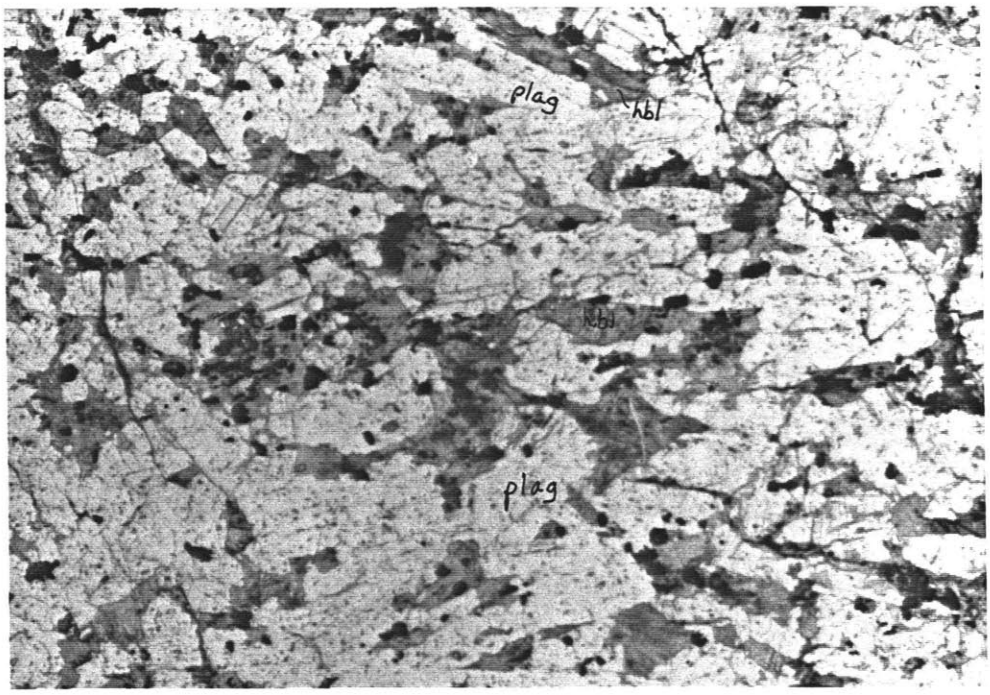

Figure 5.7: Textural relations in metabasalts of the ophiolite unit. A) Sample 84OL1, showing relatively undeformed relict plag + hbl (minor relict pyroxene not visible here). Actinolite, epidote, chlorite, and Fe-oxides overgrow the relict minerals and produce a weak foliation but plagioclase laths and interlocking texture with hbl is clearly visible.

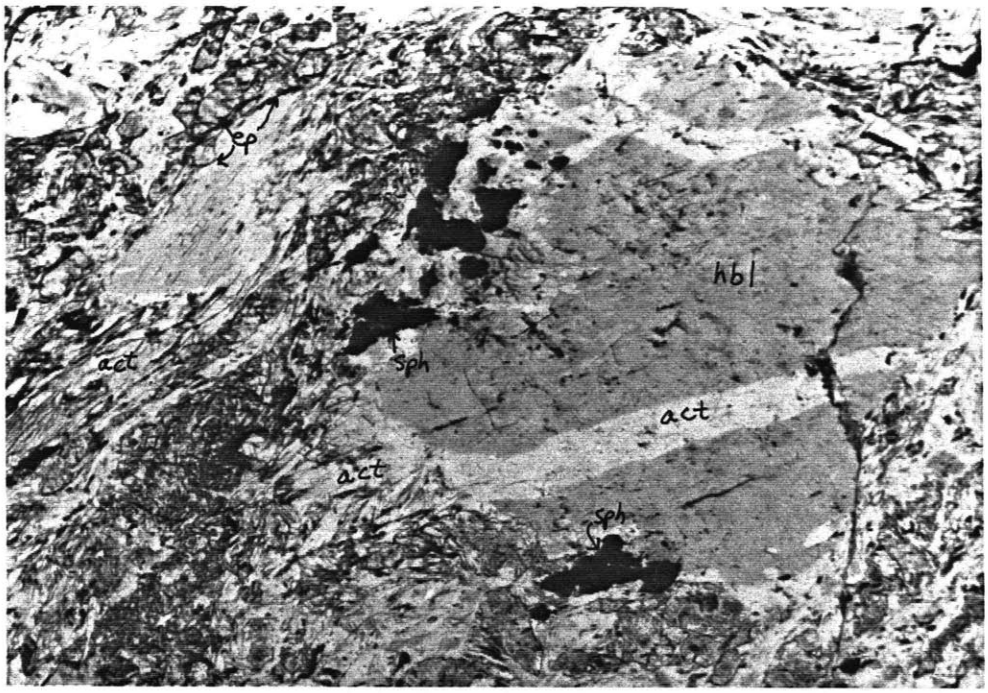

Figure 5.7B: Sample 86LO1 shows coarse hbl partially replaced by act (pale rims and stripes); dark minerals on rim are sphene. Well-developed foliation is visible in upper left, containing ep + chl +ab. Both photos in plane light, 4 mm across.

recrystallization, whereas Figure 5.7b, from a sample ~1 km away, shows a typical well-foliated metabasalt with relict hornblende rimmed by prismatic actinolite and a matrix of act + ab + chl + ep. Epidote commonly occurs as granular masses of coarse, anhedral grains as well as less abundant euhedral, prismatic grains. Zoisite also occurs as mats of extremely fine euhedral grains that replace plagioclase (saussuritization). Chlorite occurs as rims on hornblende and clinopyroxene, as pseudomorphs with epidote and sphene after clinopyroxene, and within micro-shear zones that cut the foliation. An isoclinally folded foliation is locally observed to be overgrown by a later foliation; however the mineral assemblages appear to be similar in both assemblages. Thus it is possible that the ophiolite unit also experienced a greenschist-facies M2 event.

Ultramafic rocks of the ophiolite unit commonly contain local relict pyroxene; however sp + chl ± talc is the dominant assemblage. A strong preferred orientation of serpentine and chlorite is present, but the orientation varies widely even at the thin-section scale, and shear bands cut across the fabric defined by phyllosilicates.

Carbonate rocks

Marbles within the ophiolitic melange of Lizadiko ridge (Fig 5.1) commonly contain bluish-green micaceous laminae consisting of ph + ep + chl + sph + qtz + graphite ± tremolite ± Fe-oxides. Because the metamorphic fabrics in the marbles are discordant to those in the enclosing serpentinite, and are interpreted to have formed prior to the incorporation of the marble blocks in the melange (Chapters 2,3), the metamorphic conditions experienced by the marbles may never have been reached by the ophiolite rocks themselves. Marble overlying the Pierien and Infrapierien basement rocks is commonly coarse-grained calcite marble with laminae containing ph + chl + sph ± ep. I have no petrographic or direct radiometric constraints on whether the marbles were metamorphosed during the M1 or later events, however it is unlikely that these Triassic-Jurassic marbles escaped the M1 metamorphism that affected the underlying basement.

M2 and M3: High P-Low T metamorphism

High pressure-low temperature assemblages occur in the Infrapierien, Pierien, Ambelakia, and Olympos units. In all but the Olympos unit, two deformational events can be correlated with the blue amphibole-bearing assemblages. Two metamorphic events are designated M2 and M3 by correlation with the deformational events discussed in chapter 3 and the Ar-loss events discussed in chapter 4. Nevertheless, in most samples there does not appear to be

a distinct change in the mineral assemblage from M2 to M3, so the petrographic characteristics of the two events will be described together. The Olympos unit experienced only the M3 event. The highest thrust sheets of the Pierien and Infrapierien units (e.g. in the Sarandoporou area and the Pieria Mountains; Fig. 5.1) do not appear to contain high pressure-low temperature assemblages, in contrast to the lower thrust sheets on the flanks of Mt. Olympos. Possible reasons for the absence of M2 and M3 assemblages at high structural levels will be discussed below.

Granitic rocks

The granitic augen gneiss contains the M2-M3 metamorphic assemblage qtz + ab + ph ± ep ± chl ± sph ± ilm. The quartz and albite are interpreted to be metamorphic phases because they commonly show evidence of dynamic recrystallization and occur as fine neoblasts parallel to the schistosity and surrounding K-feldspar augen. Because the mylonitic foliation that contains phengite (as opposed to M1 muscovite) is parallel to D2 and D3 structures, the mineral assemblage is attributed to M2 or M3 even though the assemblage is not diagnostic of the blueschist facies. The structurally lowest part of the Pierien unit in the Kato Olympos region merits special attention because of its unusual M2-M3 mineral assemblage. Apparently derived from an alkaline granitic protolith, these rocks consist of qtz + ksp + ab + ph + ri + ac ± ep with coarse relict K-feldspar and plagioclase augen and relict allanite and zircon (e.g. 85OL46, 85GO42, Table 5.2) Sodic amphibole occurs as very fine-grained needle-like grains aligned in the foliation and parallel to the mylonitic lineation (see Ch. 3). Green aegirine-jadeite occurs in sample 85OL46 as elongate grains parallel to the schistosity and intergrown with riebeckite. In most of the granitic rocks on the flanks of Mt. Olympos, white mica is the major foliation-forming phase and is parallel to the mylonitic fabric developed near the Sparmou and Olympos thrusts. Felsic mica schists consist of qtz + ab + ph ± ep ± sph and commonly contain relict feldspar augen. Based on petrographic observations, there does not appear to be any difference between M1, M2, and M3 assemblages in these felsic schists.

Pelites

The only pelitic rocks found in the lower thrust sheets of the Pierien unit consist of mica schists that crop out below the marble cover of the Pierien unit on Trohalos ridge. The sample analyzed (84LI22c) is quartz rich, and contains qtz + ctd + ph + par + ep + ilm + ap + rt + sph ± stilp. Plagioclase does not appear to be

present in this sample. Chloritoid occurs as post-kinematic radiating sprays that overgrow the foliation defined by qtz + ph + par.

Metabasites

In the metavolcanic rocks of the Ambelakia unit, the M1 foliation is folded and overgrown by a second foliation composed of chl + cr + ep + ph ± lw(?) (Table 5.2). The M2-M3 foliation in more micaceous metabasites (mica schists) is defined by qtz + ab + ph + chl + pp ± gl or cr± act ± lw. Calcic amphibole cores (M1?) have sodic rims (M2), but actinolite locally coexists with sodic amphibole in the later (M2 or M3) assemblage. Sodic amphibole occurs as relatively coarse grains (<2 mm wide) surrounding relict augite and as much finer grains intergrown with act + chl + ep in the matrix. Sodic amphibole apparently began growing early in the deformational history and continued to grow during two phases of foliation formation, at least the latest of which is associated with a mylonitic quartz fabric (Fig. 5.8). Fine-grained sodic pyroxene occurs as prismatic grains in contact with crossite and albite in a reaction rim around relict clinopyroxene. Because of the euhedral habit and its textural relation with the relict volcanic pyroxene, I interpret this to be metamorphic pyroxene. Epidote is also observed in contact with sodic amphibole, phengite, and actinolite in the S2 foliation. In many samples there appears to be two distinct habits of epidote in the matrix, one consisting of subhedral prismatic grains and the other of fine, granular anhedral grains. Fine-grained chlorite commonly occurs intergrown with epidote and phengite within the schistosity. Chlorite also occurs in cracks within and rims around relict augite grains. M2-M3 pumpellyite is intergrown with sodic and calcic amphiboles in the matrix foliation of metabasites, and occurs as rims on relict clinopyroxenes.

In the metabasites, lawsonite occurs as a very fine-grained replacement of plagioclase (Fig. 5.9), so it is difficult to determine which assemblage contains lawsonite in equilibrium. Sphene, apatite, rutile, calcite, and Fe-oxides are ubiquitous accessory phases that cannot be assigned to a particular phase of metamorphism, although they are commonly present in the foliation planes.

In the Pierien unit, schists which may represent metasedimentary inclusions within the granitic rocks and/or metasediments originally unconformably overlying the granitic rocks contain the assemblage qtz + ab + ph + ep + wn-bar (e.g 85GO1; 85LI16, Table 5.2). Chlorite is not abundant in the metabasites of the Pierien unit. Where present, it is generally extremely fine-grained and intergrown with phengite in mats parallel to the foliation.

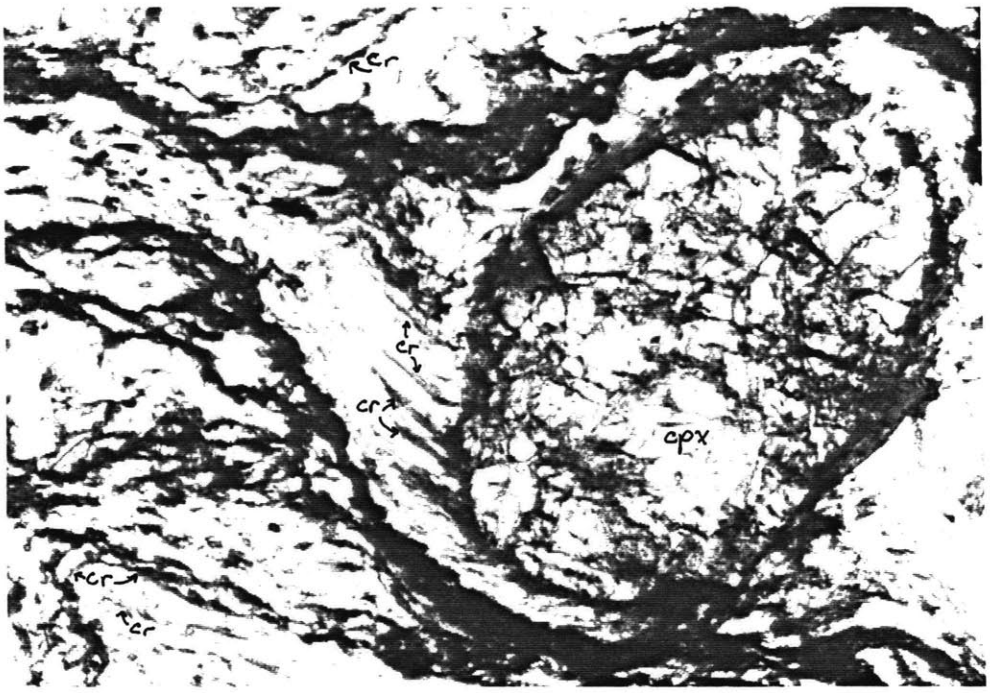

Figure 5.8: Photomicrogaph of crossite in foliation and rimming relict augite phenocryst, sample 86RA5b, Ambelakia unit. Note crossite grains occur in the pressure shadow of and are deformed with the rotated cpx porphyroclast, are parallel to the foliation, and are folded with the foliation (lower left corner of photo), indicating that sodic amphibole growth began early in the deformational history and continued growing throughout. Plane light, 2 mm across.

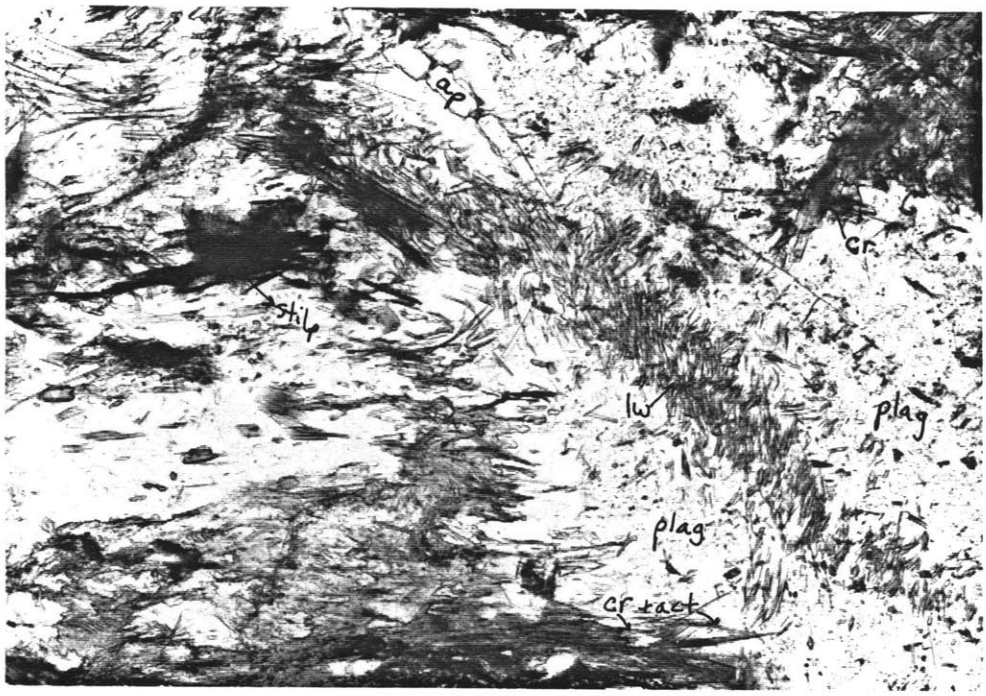

Figure 5.9: Photomicrograph of lawsonite growing in plagioclase grain, sample 86RA10a, Ambelakia unit. Plane light, scale 2 mm across.

In the Infrapierien unit the M2-M3 assemblages seem to represent somewhat higher temperature blueschist-greenschist transition facies (as opposed to blueschist-facies s.s.). In metabasites of the Infrapierien unit, blue-green amphibole, epidote, and chlorite seem to be the latest stable phases, and are interpreted to be M2 and/or M3 phases although they are irregularly developed throughout the area. In several amphibolite samples actinolite occurs as rims around hornblende and chlorite overgrows biotite, so it is possible that actinolite grew during both M1 and M2 metamorphism.

Blue-green (winchite-barroisite) amphiboles occur in the common mineral assemblage in the metabasites: qtz + ab + ph + ep + wn + stilp ± sph ± ap ± hem. Winchite growth appears to have persisted throughout isoclinal folding and foliation formation, but seems to post-date earlier (M1) act + ep and/or hbl + bi growth (Fig. 5.10) as it appear as rims around act. Because three amphiboles have not been observed in a single sample, I cannot constrain whether there was a progression from M1 hbl to M2 act to M3 blue-green amphibole, or whether actinolite was stable during all three events. Geochronologic data support the latter interpretation (samples 85OL32, 85OL50; chapter 4).

Epidote is abundant in the Infrapierien metabasites and occurs both as subhedral elongate grains that are major component of the matrix-defining foliation, (M2, M3) and as finer anhedral granular grains that appear to be in textural disequilibrium (M1?). Yellow, Fe-rich rims surround pale cores, and inclusions of plagioclase, sphene, and actinolite are present. In sample 84LI26, epidote occurs as inclusions within sodic amphibole. In several amphibolite samples (e.g. 86OL47, 86RA20), epidote overgrows biotite and/or hornblende. Zoisite is not abundant in the metabasites, however, it is a major component of some schists in the Infrapierien unit. Sample 86RA16a contains relatively coarse (~200 μm across) poikiloblastic epidote with inclusions of plagioclase, actinolite, and sphene.

Carbonate rocks

Limestone and dolomite of the Olympos unit are commonly recrystallized to fine- to medium-grained calcite and dolomite marble and marble with micaceous laminae. Aragonite has not been identified in the study area. The calcareous sandstone and argillite contain a foliation defined by cc + ph + qtz + chl + sph (Table 5.2). Calcareous schists of the Ambelakia unit also contain blue amphibole

(86GO1,86OL14, Table 5.2). No amphiboles have been identified in the calcareous schists of the Pierien and Infrapierien units.

Metagraywacke and meta-arkosic sandstone

The metasandstone and phyllite in the Olympos unit are of felsic, though variable, bulk composition (Table A2, sample 86OL2). The flysch contains qtz + ab + ph + chl ± pp ± lw in the sandstones and cc + ph + chl + qtz + ab in the calcareous siltstones. Sodic amphibole and actinolite have been observed in two samples of the flysch (Fig. 5.11), and probed in sample 84OL59 (Table 5.3). They form a minor component, and could be detrital; however, the grains are euhedral, not deformed by the flattening fabric, and do not have pitted or obviously weathered surfaces. These characteristics, in addition to the association of the amphiboles with a highly phengitic white mica (see below) leads us to interpret the amphiboles to be components of the metamorphic assemblage. Most of the flysch appears to have a bulk composition that is too felsic for the formation of abundant mafic phases other than minor chlorite and phengite, so the reason for the rare occurrence of amphibole may be related to bulk composition. Schmitt (1983) first reported the presence of lawsonite in the Olympos flysch, but there have been no previous reports of sodic amphibole. Chlorite occurs as very fine-grained mats intergrown with phengite in the foliation planes and as a retrogressive phase partially to completely replacing mineral assemblages in detrital metamorphic lithic grains.

The metamorphic assemblage of the flysch in the Ossa region is similar to that in the Olympos region; however lawsonite is more abundant and coarser-grained than in the Olympos flysch (Godfriaux and Pichon, 1979). Metasandstones of the Ambelakia unit also contain a similar assemblage with the exception that sodic amphibole is more abundant than in the Olympos flysch.

On the basis of fossil and radiometric age data, I correlate the blueschist facies metamorphism in the Olympos unit with M3, however the textural relations are ambiguous. Two metamorphic foliations have been identified, both are defined by phengite, chlorite and minor pumpellyite and are attributed to M3. The amphiboles are in contact with chl + qtz and chl + ph. However, because the occurrence of amphibole in the flysch is so rare, I cannot determine the textural relations between amphibole growth and formation of the foliation. In sample 84OL59, the amphibole prisms are at a high angle to the foliation direction. The metamorphic foliation is associated with flattening of detrital grains and solution

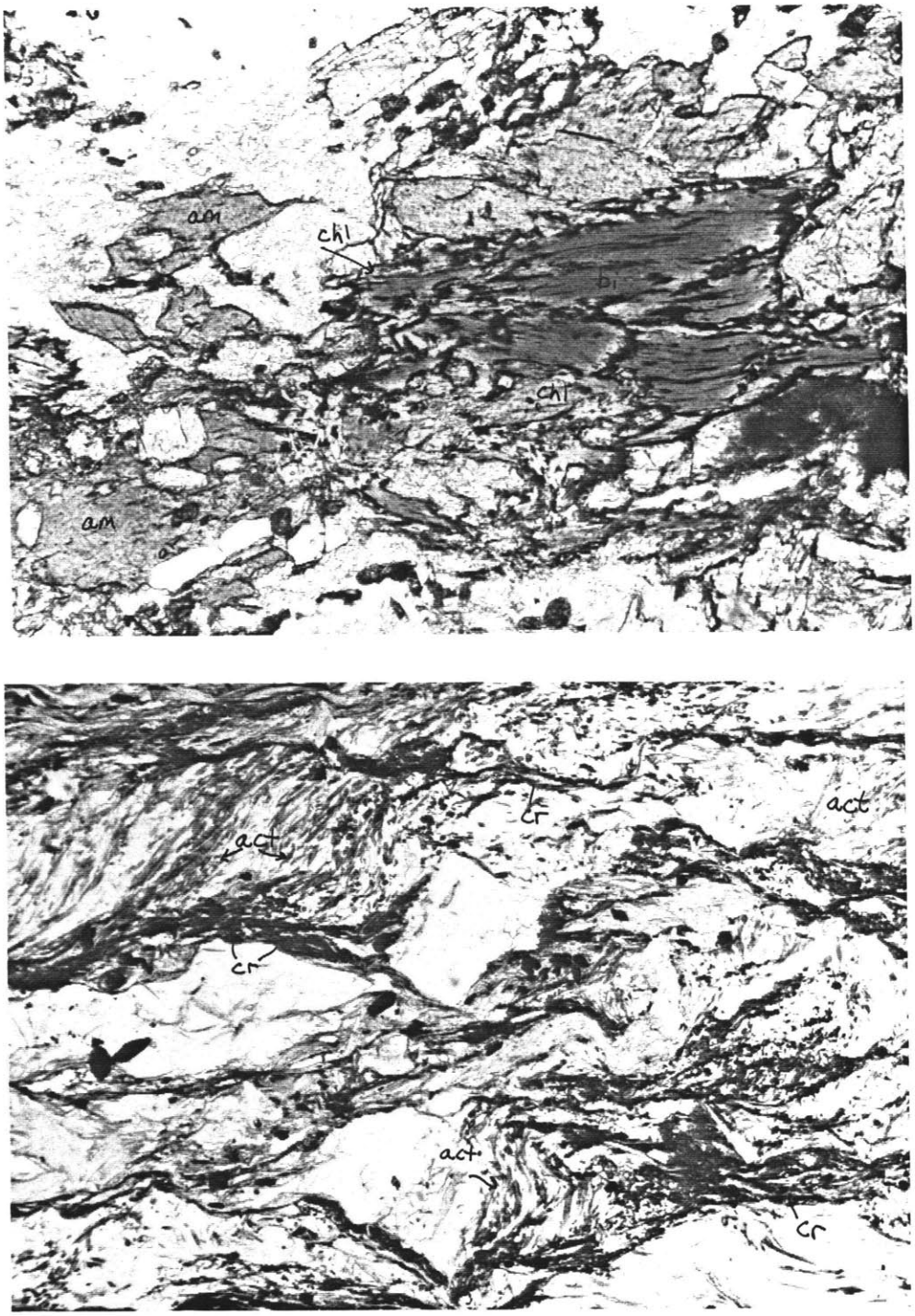

Figure 5.10: Photomicrographs of samples from the Infrapierien unit showing relations between M1 and M2 assemblages. A) Sample 84OL11 shows biotite grain reacting to chlorite; stable assemblage is blue-green amphibole + epidote; pale, high-relief grains are amphibole (am). Plane light, 2 mm across. B): Sample 84LI28 shows two generations of amphibole; the first is paler actinolite that is folded; the second is darker crossite or barroisite, oriented horizontally and parallel to the axial planar surfaces of the folded S1. Plane light, 4 mm across.

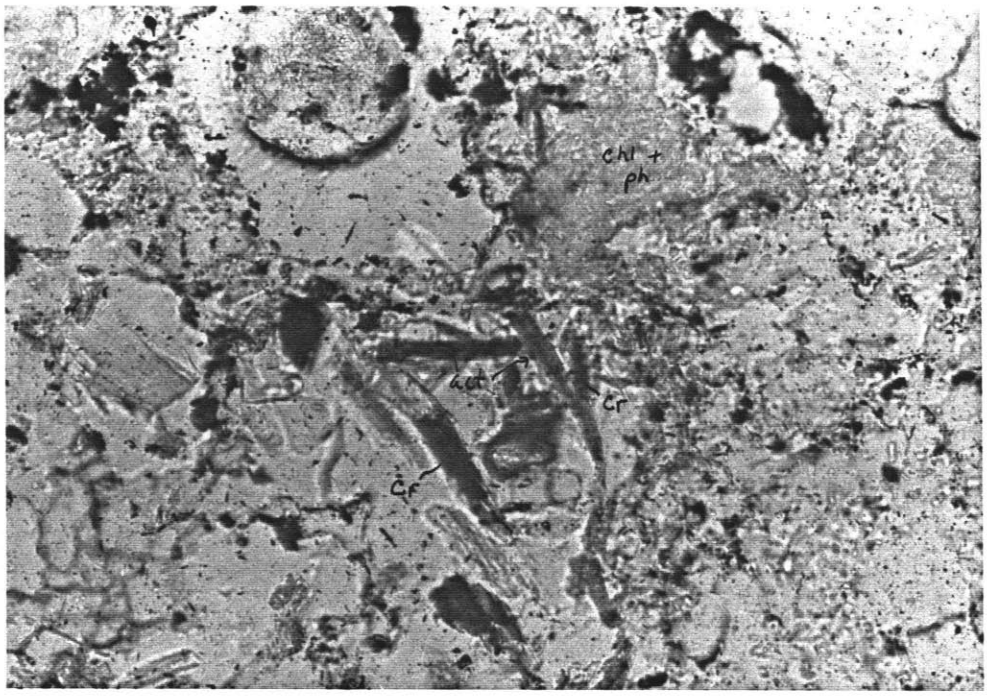

Figure 5.11: Photomicrograph of crossite + actinolite in Olympos flysch sample 84OL59. Prismatic grains in center of photo are both cr and act. Rest of photo contains qtz + ab + ph + chl. Plane light, scale 1mm across.

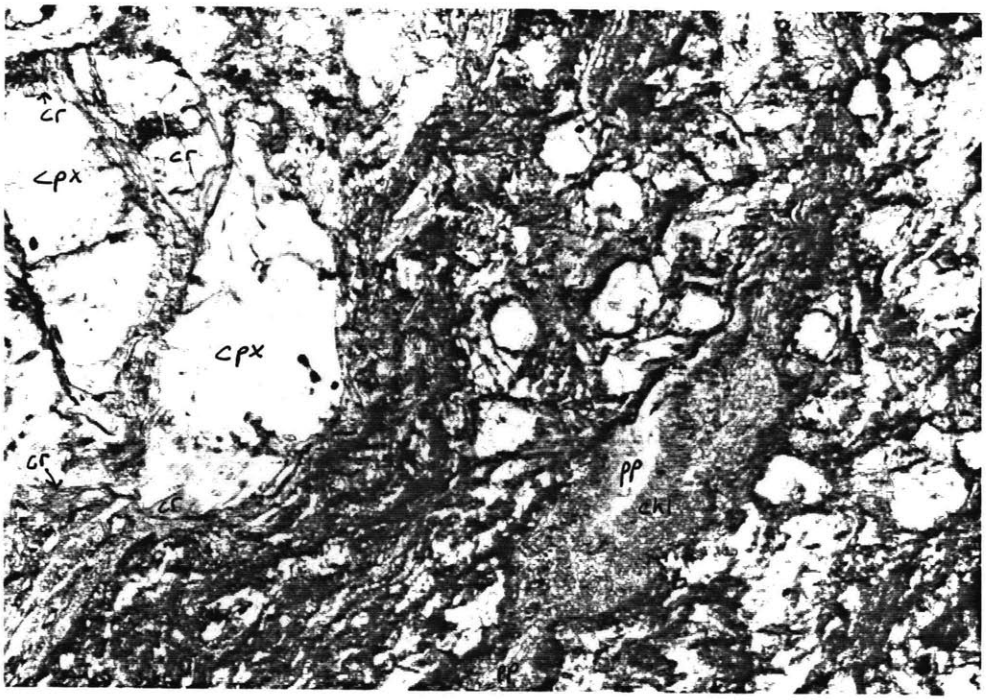

Figure 5.12: Photomicrograph of late pp + chl growing in a vein in sample 86RA6a, Ambelakia unit. Elongate grey area extending from upper right to lower center of photo contains chl (dark) + pp (light) oriented perpendicular to the vein walls (and ~perpendicular to foliation), indicating growth post-dates foliation formation. Relict augite phenocryst on left side of photo has cr grains in crack and on rims. Plane light, 2mm across.

cleavage; locally isoclinal folds are present with axial planes parallel to the foliation. In the mylonite zone of the Olympos thrust, neoblasts of albite occur surrounding porphyroblasts of K-feldspar and plagioclase.

Derycke et al (1974) report that the Ossa flysch contains lawsonite parallel to the foliation; this is interpreted to be the S3 foliation by the age of the flysch and by correlation with the Olympos flysch, thus it appears that lawsonite was stable during M3, although it is possible that in the Ambelakia unit, lawsonite was also stable during the M2 event.

M4: Prehnite-pumpellyite facies metamorphism

In the Olympos unit, pumpellyite locally occurs as unoriented sprays that are attributed to the M4 event. Late, unoriented pp + chl ± pr ± stilp fill cracks and vugs and cross-cut the earlier metamorphic and mylonitic fabric in the Ambelakia unit (Fig. 5.12). In the Pierien unit, pumpellyite has only been recognized in the metabasites between the granitic gneiss basement and the Triassic-Jurassic marble cover; here it appears as randomly oriented, post-kinematic grains (e.g. sample 85LI16; Table 5.2), and is attributed to M4. There is no clear evidence of M3 and M4 mineral assemblages in the Infrapierien unit.

METAMORPHIC MINERAL COMPOSITIONS

The focus of the microprobe analysis in this study was directed towards characterizing the range of compositions of blueschist facies minerals in the Ambelakia, Pierien, and Infrapierien units in order to constrain the pressures and temperatures of metamorphism. Due to the apparent paucity of diagnostic mineral assemblages in the other units, they have been examined in less detail. The flysch samples are strongly weathered, so only one sample (84OL59) was probed as an initial attempt to determine mineral compositions and to see if further work would be justified. It is difficult to get good analyses and most of the phases probed in the flysch yielded low totals.

Analytical Methods

Twenty samples were studied using the electron microprobe in order to characterize the mineral compositions and zoning relations in some detail. Most of the lithologies in the study area are fine- to extremely fine-grained schists and phyllites, and in many cases mineral identification could not be made without the use of the microprobe, so an additional fifteen samples were probed in a reconnaissance fashion. The analyses were performed using the JEOL 733

microprobe at M.I.T. Natural and synthetic standards were used, and Bence-Albee (1968) corrections were applied.

Representative mineral compositions in each structural unit are given in Tables 5.3-5.5. Fe^{3+} contents in amphibole were calculated using the "average Fe^{3+}" of Spear and Kimball (1984), which is the average of the maximum and minimum Fe^{3+} for normalizations which produce stoichiometric amphibole. For alkali amphiboles, a normalization using either all Fe^{2+} or all Fe^{3+} generally was non-stoichiometric; normalizations using either 1) the sum of all cations except Na, K, Ca to 13; or 2) Si =8, represented the stoichiometric maximum and minimum Fe^{3+} contents respectively.

Mineral compositions are highly variable throughout a single thin section, but I have tried to overcome this difficulty by probing phases directly in contact where possible, or within a few tens of microns.

Amphiboles

Sodic and sodic-calcic amphiboles are present in the Olympos unit (flysch), the Ambelakia unit, the Pierien unit, and the Infrapierien unit. Calcic amphiboles (actinolite and hornblende) are present in the Infrapierien and ophiolite units (Table 5.2, 5.3). Amphibole nomenclature used in this discussion follows that of Hawthorne (1981).

For the calcic and sodic-calcic amphiboles, a plot of Na(M4) vs Al^{IV} (Fig. 5.13), after Brown (1977b) illustrates the distinct gap in observed compositions between sodic and calcic amphiboles. The actinolites shown in Fig. 5.13 as "cores" are interpreted to be M1. The sodic amphiboles in Fig. 5.13 are contained in the M2 and M3 assemblages. Alkali amphiboles (M2-M3) are plotted on a Miyashiro diagram (Miyashiro, 1957) of X_{Fe2+} vs X_{Fe3+}(Fig. 5.13).

Coexisting sodic and calcic amphiboles are present in Olympos flysch sample 84OL59. Probe analyses (Table 5.3) and the plot of Figure 5.14 indicate the sodic amphibole is crossite and the calcic amphibole is actinolite.

In several samples in the Ambelakia unit, M1 actinolite cores are rimmed by M2 (or M3) crossite. (e.g. Fig. 5.5). However, other grains exhibit a patchy zoning, or more Ca-rich rims around Na-rich cores. There does not seem to be a consistent difference in composition between M1 actinolite cores and fine-grained (M2,M3) matrix actinolite; the matrix actinolites plot within the symbol for "Ambelakia core" on Fig. 5.13. Compositions of sodic amphibole from the Ambelakia unit range from glaucophane (in metabasalt) to riebeckite (in

metasandstone and impure marble) (Fig. 5.14). Where core and rim compositions of sodic amphiboles have been analyzed, these are indicated on Fig 5.14; in general rims are more Fe- and Na-rich than the cores.

In Fe^{3+} rich samples of the Pierien unit such as 85OL46, the M2-M3 amphibole is riebeckite, in most other samples the amphibole is crossite or barroisite (Fig 5.14).

Actinolite is the most abundant amphibole in mica schists of the Infrapierien unit. $Fe^{2+}/(Fe^{2+}+Mg)$ varies from 0.25 to 0.4 in actinolites of the Infrapierien unit; and cores are generally more Fe-rich than the rims. In some samples, the Na(M4) content of the M2-M3 blue-green amphiboles is highly variable, as indicated by the large error bars on Fig. 5.13.

Hornblende occurs in rare massive amphibolites within the Infrapierien unit. Representative analyses presented in Table 3 indicate that the composition ranges from Tschermakite to magnesio-hornblende. Because hornblende of this composition and actinolite do not appear to coexist in any of the samples examined, I cannot constrain the relative timing relations of these two phases; however in some samples actinolitic hornblende is rimmed by actinolite or a blue-green amphibole, suggesting that the hornblende crystallized early (M1) and the actinolite crystallized later, during M2 or M3.

In the ophiolite unit, amphibole occurs as coarse, relict hornblende rimmed by Mg-rich actinolite and as pale actinolite grains. The coarse grains have what appear to be exsolution lamellae of actinolite within the hornblende , but this is probably a replacement texture as opposed to sub-solidus cooling. $Fe^{2+}/(Fe^{2+}+Mg)$ varies from 0.2 to 0.25 in actinolites of the metabasalts from the ophiolite unit. Cores are more Fe-rich than rims. Sample 85OL30d, a pyroxenite, contains more Fe-rich actinolites, ranging from $Fe^{2+}/(Fe^{2+}+Mg)$=0.39 to 0.44.

Sodic pyroxenes

Sodic clinopyroxene has only been analyzed in two samples, one from the Ambelakia unit, and one from the Pierien unit. Several other samples from the Ambelakia samples appear to have sodic pyroxene, but due to the very-fine grain size, positive identification has not yet been made. Representative compositions are given in Table 5.3, and plotted in the Jd-Ac-Aug triangular diagram of Fig. 5.15. Calculation of endmember pyroxene components was modified from the method of Cawthorn and Collerson (1974), using Jd = Al; Ac = Fe^{3+} = Na-Al; Fe^{2+} = FeT-Fe^{3+}; Aug = (Ca + Mg + Fe^{2+})/2.

Table 5.3 Representative analyses of amphibole, pyroxene, and epidote from the study area.

	Amphiboles												Pyroxenes		Epidotes			
Sample	84OL59 gl	84OL59 act	85RA8c core	85RA8c rim	86RA6a cr	86OL14 ri	85OL46 ri	85GO42 cr	84LI26 bar	85OL13 ac	86OL47 hbl	86LO1 act	86RA5b	85OL46	85RA8c ep	85LI16 ep	84LI26 core	84LI26 rim
Unit	OLYMPOS		AMBELAKIA				PIERIEN			INFRAPIERIEN		OPH	AMB	PIERIEN	AMB	PIERIEN	INFRAPIERIEN	
MgO	9.722	16.595	15.214	8.79	8.234	7 932	5.134	7.454	12.444	13.747	8.245	19.436	3 457	0.23	0	0.045	0.021	0
Al2O3	3.741	1.655	0.796	6.188	6.804	2.075	2.083	3.58	4.552	4.191	14.95	1.46	2.153	5.67	22.066	24.646	23.052	20.861
SiO2	54.3	55.068	54.684	56.004	56.05	54.09	53.914	54.711	50.561	50.891	41.295	55.174	51.879	53.79	37.493	38.005	37.693	37.302
CaO	0.999	11.876	12.343	1.224	1.098	0.38	0.051	1.384	8.834	10 573	10.478	12.703	13.143	0.32	23.581	22.598	22.693	21.772
TiO2	0.077	0.092	0.077	0.062	0.031	0.256	0.025	0.046	0.105	0 064	0.345	0.046	0.06	0.11	0.05	0.102	0 116	0.197
MnO	0.202	0.241	0.221	0.069	0.094	0 06	0.287	0.453	0.962	0.471	0.495	0.166	0.522	0	0.028	0.079	0.34	0.285
FeO	18.978	12.185	14.249	19.053	18.017	24.008	28.177	22.695	17.105	14.189	19.033	7.631	21.553	23.42	13.05	9.901	12.346	14.949
Na2O	6.572	0.421	0.524	6.747	6.729	7.526	7.068	6.822	2.698	1.511	2.552	0.588	6 316	13.84	0	0	0	0
K2O	0.018	0.059	0	0.013	0.034	0.027	0.013	0.087	0.316	0.139	0.422	0.031	0	0	0	0	0	0
TOTAL	94.631	98.291	98.175	98.203	97.214	96.382	96.752	97.232	97.599	95.776	97.878	97.264	99.083	97.38	96.268	95.376	96.261	95.366
Si	7.952	7.827	7.878	7.938	7.981	7.965	7.989	7.976	7.409	7.509	6.178	7.781	2 055	2 130	6.237	6.236	6 229	6.307
Al(tot)	0.646	0.277	0.135	1.034	1.142	0.36	0.364	0.615	0.786	0.729	2.637	0.243	0.100	0.265	4.326	4.766	4.490	4.157
Al(iv)	0.048	0 173	0.122	0.062	0.019	0.035	0.011	0.024	0.591	0.491	1.822	0.219						
Al(vi)	0.598	0.104	0.013	0.972	1.123	0.325	0.353	0 591	0.195	0.239	0.814	0.023						
Ti	0.008	0.01	0.008	0.007	0 003	0.028	0 003	0 005	0 012	0.007	0.039	0 005	0.002	0.003	0.006	0.013	0.014	0.025
Fe3	1.097	0.094	0.074	0.646	0 628	1.265	1.568	0.968	0.494	0.278	0.479	0.116						
Fe2	1.227	1.354	1.643	1 612	1.517	1.691	1.924	1.799	1 602	1.473	1.902	0.784	0.714	0.776	1.816	1.359	1.706	2 114
Mg	2.122	3.515	3.266	1 857	1.747	1.741	1.134	1 62	2.717	3.023	1.838	4.085	0.204	0 014	0.000	0 011	0.005	0 000
Mn	0.025	0.029	0.027	0 008	0.011	0.007	0 036	0 056	0.119	0.059	0 063	0.02	0.018	0.000	0.004	0.011	0.048	0.041
Ca	0.157	1.809	1.905	0.186	0.168	0.06	0 008	0 216	1.387	1.672	1.68	1.919	0.558	0.014	4.203	3.973	4.018	3.944
Na(tot)	1.866	0.116	0.146	1.854	1.858	2.149	2 031	1 928	0.767	0.432	0 74	0.161	0.487	1.066	0.000	0.000	0.000	0 000
K	0.001	0.011	0	0.002	0.006	0.005	0.002	0.016	0.059	0.026	0.081	0.006	0.000	0.000	0.000	0.000	0.000	0.000
Na(M4)	1.765	0.085	0.064	1.713	1.802	1.882	1.974	1.745	0.473	0.25	0.185	0.048						
Na(A)	0.101	0.031	0.083	0.142	0.056	0.266	0 056	0.183	0.293	0.183	0.555	0.113						
SumA	0.257	1.839	1.988	0.327	0.224	0.326	0.065	0.4	1.68	1.854	2.235	2.032						
Fe3FeT	0.472	0.065	0 043	0.286	0.293	0.428	0.449	0.35	0.236	0.159	0.201	0.129						
FeMg	0.366	0.278	0.335	0.465	0.465	0.493	0.629	0.526	0.371	0.328	0.509	0.161						
cation sum													4 137	4.267	16.593	16 368	16.511	16.589

Table 5.4 Representative analyses of white mica, chlorite, and pumpellyite from the study area.

	PHENGITES							CHLORITES					PUMPELLYITE	
SAMPLE	84OL59	OL59 detrital	85RA8c	86GO1	85OL46	85GO1	85OL13	84OL59	86RA6a	86OL14	85OL13	86LO1	86RA6a	86RA5b
Unit	-----OLYMPOS----		---AMBELAKIA---		----PIERIEN----		INFRAPIER	OLYMPOS	---AMBELAKIA---		INFRAPIER	OPH	---AMBELAKIA---	
MgO	3.604	0.910	4.088	3.795	3.090	4.437	2.649	24.357	17.606	18.244	17.699	25.545	4.640	2.666
Al2O3	24.476	34.176	23.298	21.971	22.700	22.405	27.728	14.131	18.233	18.063	17.945	19.157	22.852	21.823
SiO2	52.482	48.713	54.120	53.394	51.810	54.581	50.078	30.591	28.045	30.704	28.316	29.496	36.670	37.070
CaO	0.022	0.026	0.099	0.053	0.040	0.038	0.000	0.059	0.066	0.132	0.074	0.070	20.266	21.868
TiO2	0.379	0.609	0.064	0.107	0.230	0.066	0.478	0.065	0.042	0.000	0.115	0.027	0.051	0.062
MnO	0.084	0.000	0.038	0.000	0.070	0.152	0.000	0.076	0.348	0.340	0.409	0.157	0.398	0.459
FeO	4.801	1.036	4.169	5.638	5.830	5.214	3.785	13.337	23.787	21.675	21.775	12.194	6.658	7.492
Na2O	0.049	1.049	0.087	0.057	0.040	0.061	0.538	0.000	0.000	0.000	0.000	0.000	0.104	0.080
K2O	10.071	8.849	9.726	9.296	7.020	10.377	10.186	0.000	0.000	0.000	0.000	0.000	0.000	0.000
Cr2O3	0.000	0.000	0.000	0.000	0.000	0.000	0.000	0.000	0.000	0.000	0.000	0.000	0.000	0.113
P2O5	0.000	0.000	0.000	0.000	0.000	0.000	0.000	0.000	0.000	0.000	0.000	0.000	0.150	0.122
TOTAL	95.968	95.368	95.689	94.311	90.830	97.331	95.442	82.616	88.127	89.158	86.333	86.646	91.789	91.755
Mg	0.359	0.089	0.405	0.384	0.320	0.436	0.265	7.596	5.448	5.475	5.532	7.542	1.139	0.661
Al	1.926	2.642	1.825	1.756	1.860	1.743	2.192	3.484	4.461	4.285	4.434	4.471	4.435	4.277
Si	3.504	3.196	3.596	3.621	3.603	3.602	3.358	6.399	5.821	6.181	5.937	5.841	6.039	6.164
Ca	0.002	0.002	0.007	0.004	0.003	0.003	0.000	0.013	0.015	0.028	0.017	0.015	3.576	3.896
Ti	0.019	0.030	0.003	0.005	0.012	0.003	0.024	0.010	0.007	0.000	0.018	0.004	0.006	0.008
Mn	0.005	0.000	0.002	0.000	0.004	0.008	0.000	0.013	0.061	0.058	0.073	0.026	0.056	0.065
Fe	0.268	0.057	0.232	0.320	0.339	0.288	0.212	2.333	4.129	3.649	3.618	2.020	0.917	1.042
Na	0.006	0.134	0.011	0.008	0.005	0.008	0.070	0.000	0.000	0.000	0.000	0.000	0.033	0.026
K	0.858	0.741	0.825	0.804	0.623	0.874	0.871	0.000	0.000	0.000	0.000	0.000	0.000	0.000
Cr	0.000	0.000	0.000	0.000	0.000	0.000	0.000	0.000	0.000	0.000	0.000	0.000	0.000	0.015
P	0.000	0.000	0.000	0.000	0.000	0.000	0.000	0.000	0.000	0.000	0.000	0.000	0.021	0.017
cation sum	6.946	6.890	6.906	6.901	6.769	6.964	6.993	19.849	19.942	19.676	19.828	19.919	16.222	16.170

Table 5.5 Representative analyses of garnet, biotite, muscovite, paragonite, and chloritoid from pelitic schists of the study area.

	GARNET	GARNET	BIOTITE	CHLORITE	MUSCOVITE	MUSCOVITE	PARAGONITE	CHLORITOID
Sample	84LI13	85LI2a	85LI2a	84LI13	84LI13	85LI2a	84LI13	84LI13
MgO	1.390	0.598	7.114	11.765	1.992	1.501	0.255	2.504
Al2O3	20.435	20.220	15.961	20.981	30.825	28.435	38.631	39.695
SiO2	36.570	38.123	37.122	25.205	51.509	48.469	47.294	24.390
CaO	4.126	12.108	0.076	0.069	0.123	0.096	0.382	0.000
TiO2	0.000	0.020	2.561	0.046	0.271	0.753	0.100	0.000
MnO	6.440	3.622	0.248	0.501	0.000	0.113	0.065	1.031
FeO	29.902	25.575	21.823	27.865	1.951	6.299	1.158	23.708
Na2O	0.000	0.000	0.038	0.000	0.790	0.186	5.594	0.000
K2O	0.000	0.000	8.622	0.000	9.062	9.883	1.111	0.000
Cr2O3	0.109	0.019	0.000	0.000	0.000	0.000	0.000	0.082
P2O5	0.000	0.000	0.000	0.000	0.000	0.000	0.000	0.028
TOTAL	98.972	100.285	93.565	86.432	96.523	95.735	94.590	91.438
Mg	0.170	0.071	0.827	3.810	0.193	0.151	0.024	0.156
Al	1.975	1.902	1.468	5.371	2.362	2.268	2.929	1.955
Si	2.999	3.042	2.896	5.475	3.349	3.280	3.042	1.019
Ca	0.362	1.035	0.006	0.016	0.009	0.007	0.026	0.000
Ti	0.000	0.001	0.150	0.008	0.013	0.038	0.005	0.000
Mn	0.447	0.245	0.016	0.092	0.000	0.006	0.004	0.037
Fe	2.050	1.707	1.424	5.062	0.106	0.357	0.062	0.829
Na	0.000	0.000	0.006	0.000	0.100	0.024	0.700	0.000
K	0.000	0.000	0.858	0.000	0.752	0.853	0.091	0.000
Cr	0.007	0.001	0.000	0.000	0.000	0.000	0.000	0.003
P	0.000	0.000	0.000	0.000	0.000	0.000	0.000	0.001
cation sum	8.011	8.005	7.652	19.832	6.883	6.986	6.884	4.000

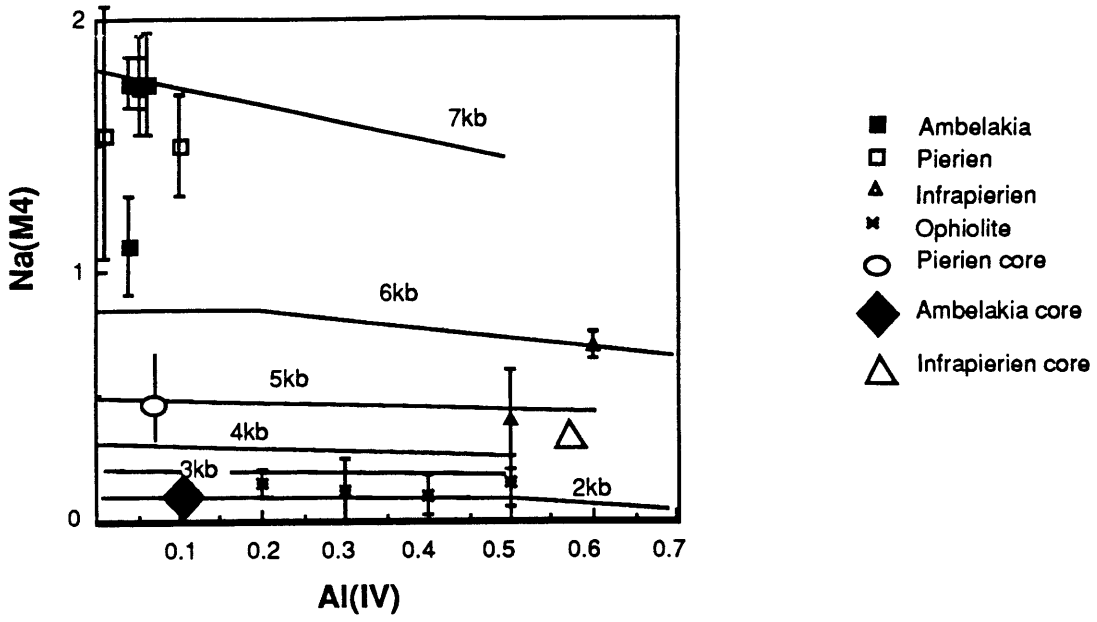

Figure 5.13: Plot of Na(M4) vs Al(IV) in sodic-calcic and calcic amphiboles after Brown (1977b). Symbols plotted represent averages of many analyses within each sample, and error bars represent standard deviation of the probe analyses. Na(M4) and Al(IV) calculated using the method of Spear and Kimball (1984). Lines indicating pressure values are from Brown (1977b); see text for discussion.

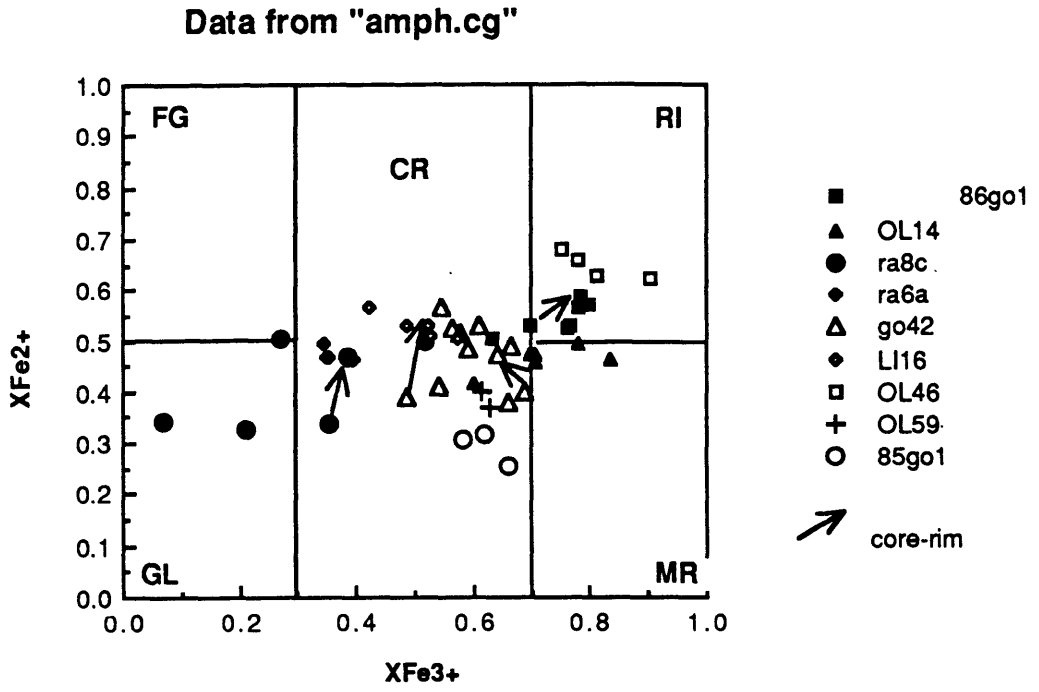

Figure 5.14: Plot of XFe^{2+} vs XFe^{3+} in alkali amphiboles from the Pierien unit (open symbols), Ambelakia unit (closed symbols) and flysch of the Olympos unit (+), after Miyashiro (1957). Fe^{3+} and Fe^{2+} calculated using the "average Fe^{3+}" calculation of Spear and Kimball (1984). FG=Ferroglaucophane, CR = crossite, RI = riebeckite, MR = magnesioriebeckite, GL = glaucophane.

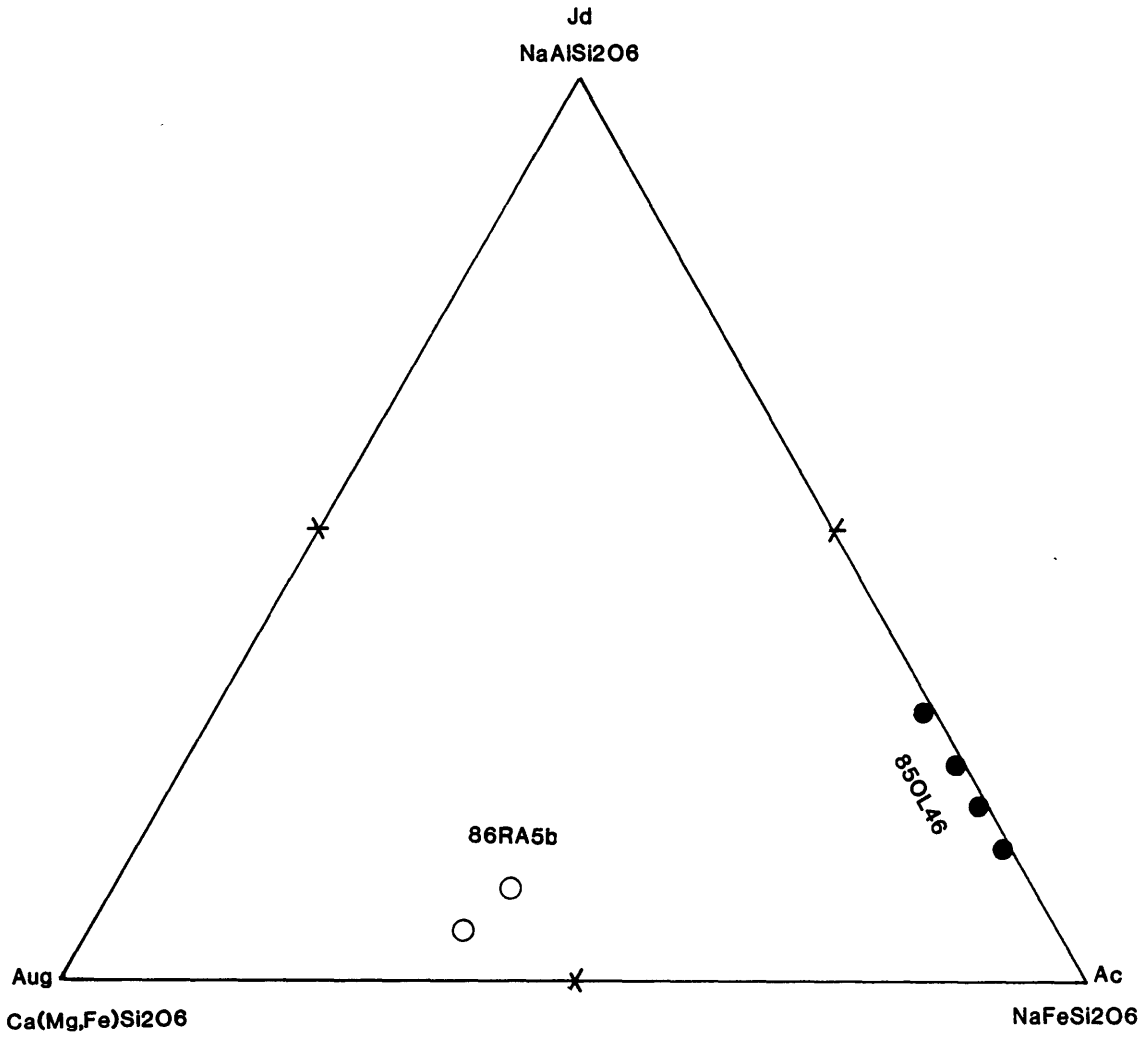

Figure 5.15: Plot of the compositions of analyzed sodic pyroxene from the Ambelakia unit and the Pierien unit in the jadeite-acmite-augite triangle.

Aegirine augite of composition ~$Jd_{10}Ac_{38}Aug_{52}$ was analyzed in one metabasaltic sample from the Ambelakia unit (86RA5b; Table 5.3; Fig 5.15). The aegirine augite occurs in a reaction rim around relict clinopyroxene that contains little or no Na_2O. The fine-grained nature and intergrowth with crossite make it difficult to identify by petrographic examination alone, so additional probe analyses would be necessary to substantiate the presence of sodic pyroxene throughout the Ambelakia unit.

Green aegirine-jadeite occurs in Pierien sample 85OL46. The jadeite content ranges from 25-30% (Table 5.3; Fig. 5.15).

Epidote

Epidote is absent in the flysch and rare in most of the Pierien unit. It is a major component of the metabasites and mica schists of the Ambelakia, Infrapierien, and ophiolite units. Representative epidote compositions are presented in Table 5.3.

Two distinct habits of epidote occur in the matrix of samples from the Ambelakia unit. One epidote is subhedral and prismatic and the other is finer-grained, anhedral, and granular; however, the probe data are insufficient to document whether these two habits are different compositions and represent different metamorphic conditions. Epidote is commonly zoned with yellow, Fe-rich cores and clear rims though zoning is often irregular, and Fe_2O_3 contents are generally greater than 8%. It also grows around relict allanite cores.

In the Pierien unit, epidote is only locally abundant ; where present, it is intergrown with sodic amphibole and phengite within the foliation planes and is thus interpreted to have grown during M2-M3. Epidote in these samples contains 10-11 wt% Fe_2O_3.

Epidote in the Infrapierien samples commonly has yellow, Fe-rich rims surrounding pale cores, and inclusions of plagioclase, sphene, and actinolite are present. In metabasite samples 84LI26 and 85RA16a, epidote contains 14-16 wt% Fe_2O_3, while in more felsic mica schists (e.g. 85OL13, 85OL32), it contains 10-11wt% Fe_2O_3.

In the ophiolite unit, epidote (zoisite) occurs as mats of extremely fine euhedral grains that replace plagioclase (saussuritization); these contain up to 5 wt% Fe_2O_3. The zoisite coexists with an Fe-rich epidote in the foliated matrix of sample 85OL30d. Preliminary analysis of metabasalt sample 86LO1 indicates that coarse, anhedral epidotes (M1?) contain less Fe_2O_3 (12.5-13%) than fine-grained euhedral epidotes (M2? or later; >14%)

White mica

White mica is an important component in rocks of all the structural units except the ophiolite unit. Mica schists occur in all the units; however I have not yet probed micas from the mica schists that occur as allochthonous blocks in the ophiolite melange. As shown in Figure 5.16, white mica compositions vary systematically between the different units, however, within a given sample, and even within an single unit, the variation is small. Geochronologic data presented in chapter 4 indicates that the micas of the Pierien and Infrapierien unit are dominantly M2 and M3 in age; however in both units M1 micas are also present in some samples. White mica in the Ambelakia unit grew during M2-M3 and in the Olympos unit during M3 (see chapter 4).

White mica contained in the foliation planes of the flysch of the Olympos unit is strongly phengitic, containing an average of 3.49±0.02 Si atoms per formula unit (p.f.u.; maximum=4). (Fig 5.16). These fine-grained metamorphic (M3) micas are intergrown with chlorite and are texturally and compositionally distinct from coarse, detrital white mica with a more variable, but lower, phengite content (Si = 3.23±0.05 p.f.u.).

White micas from the Ambelakia unit have the highest phengite component of all the white micas analyzed from this region, averaging Si =3.58-3.64 p.f.u. Although at least two generations of mica (probably M2 and M3) are visible in different foliation surfaces in thin section, the mica compositions are very consistent within a given sample (Fig 5.16; Table 5.4). Bulk composition does not seem to have a strong effect; the samples in Table 5.4 range from marble with schist laminae (86OL14) to "graywacke" metasandstone (86OL30) to metabasalt and metadacite (86RA6a, 86RA10a).

Compositions of the micas that define the D2 and D3 mylonitic foliations in the Pierien unit indicated in Table 5.4 and on Fig.5.16. These micas are strongly phengitic, ranging from ~3.43 to 3.61 Si p.f.u. In sample 86OL44b, the coarse muscovite "fish" have Si = 3.18, and the fine phengites have Si = 3.43. These two micas have been dated using the Ar/Ar technique as ~291 Ma and ~57 Ma respectively (chapter 4), and are thus correlated with M0 and M2 events. Several other samples have similar distinct muscovite and phengite relations, but these have not been probed.

Mica schists of the Infrapierien unit commonly contain two habits of white mica, as coarse-grained (up to 3 mm) porphyroblasts and as fine-grained (40-50μm) mats within the foliation planes. However, both types of mica appear to have

similar compositions (Table 5.4), and contain Si = 3.35-3.45 p.f.u. (Fig 5.16). Fine-grained amphibolite schists of the Infrapierien unit south of Mt. Olympos contain a wide range of phengite compositions. These samples are strongly weathered, and textural relations among micas and amphiboles are complex, so interpretation of the significance of this range in composition must await further, more detailed work.

In the ophiolite unit, phengite is present only in the marbles and calcareous schists that occur either as blocks in melange or as possible stratigraphic cover on top of the ophiolitic rocks. One sample from a tectonic block of marble contains phengite with Si = 3.48 p.f.u. (84OL38b); sample 86OL41c contains phengite with Si = 3.56 (Table 4). It is not clear whether this latter sample represents a sedimentary cover on the ophiolite or a block in melange, as the present contact between marble and serpentinite is sheared.

Chlorite

Chlorite occurs as a major rock-forming mineral in lithologies of the Olympos unit, the Ambelakia unit, and the ophiolite unit. Metabasites in the Pierien and Infrapierien unit have less abundant chlorite (Table 5.2). Chlorite compositions are shown on a plot of Fe/Fe+Mg versus Si (Figure 5.17).

The chlorite in the matrix of the Olympos unit has an average Fe/Fe+Mg ratio (X_{Fe}) of ~0.3, but this is based on analyses of only three grains, and may not be representative.

Chlorite in the Ambelakia unit has an average X_{Fe} ~0.4-0.5 in most samples, however, values as high as 0.7 were measured in sample 86RA10a. Chlorite composition does not seem to be different between the foliation-defining matrix grains and the late-stage alteration products, however I have not conducted a thorough, systematic study to determine whether this observation is consistent among many samples.

As noted above, M2-M3 chlorite is rare in the Pierien unit. The average X_{Fe} of chlorite in the one chl-bearing sample probed is 0.5-0.55.

In most samples collected from the Infrapierien unit, chlorite is a minor component that cross-cuts the schistosity or occurs as rims on amphibole and biotite. A notable exception is in the southern thrust sheets of the Infrapierien unit, where 85RA16 contains alternating chlorite-rich and actinolite-rich layers. Chl in this sample has X_{Fe} ~0.4, similar to that in other samples from the northern Infrapierien units (e.g. 85OL13) which has minor chlorite with X_{Fe} ~0.41-0.43.

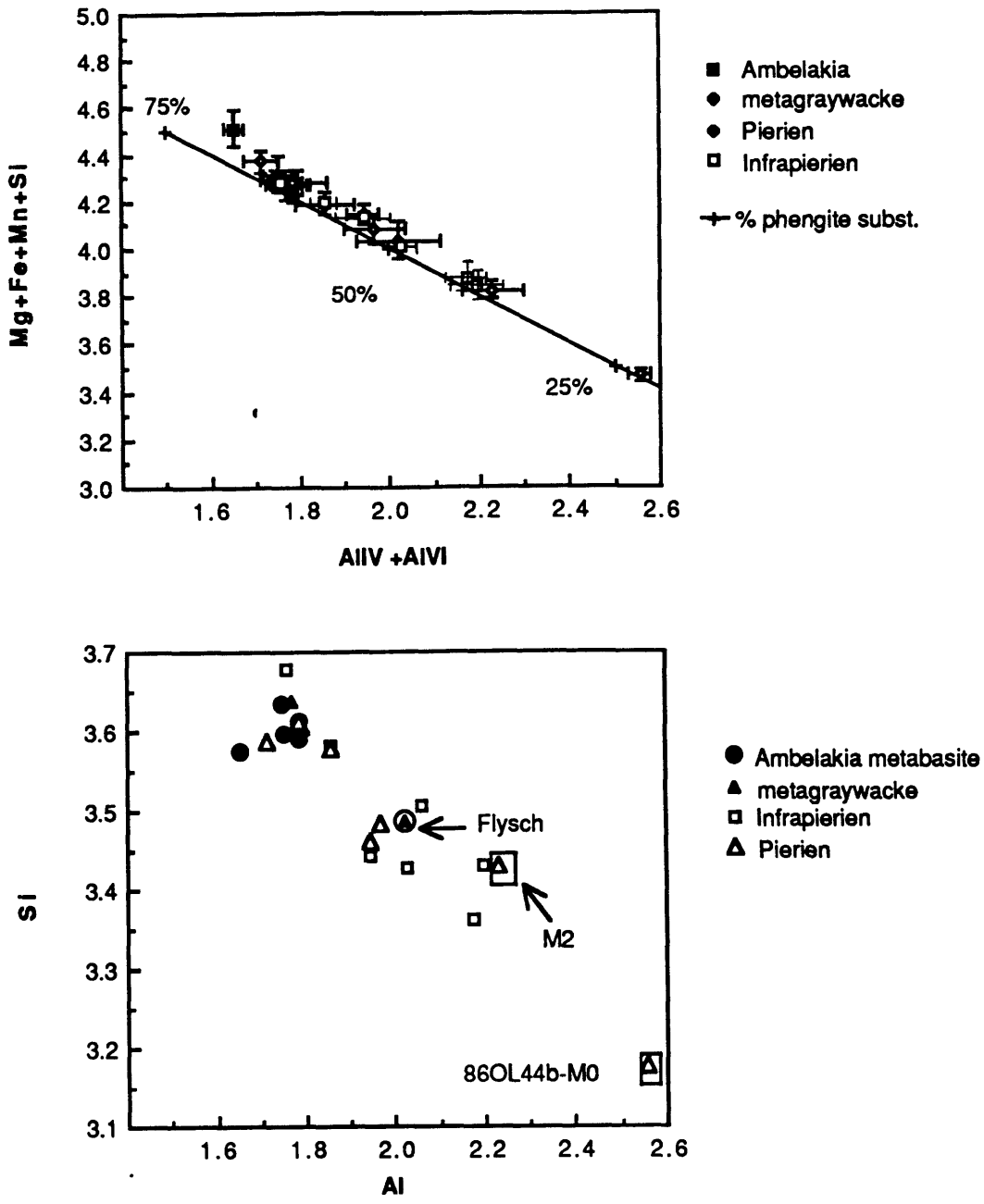

Figure 5.16 Plot of phengite contents in white micas from the Olympos region. The upper plot (a) shows the averages of white mica compositions in each sample with the sample standard deviation. The line shows the percent of phengite substitution by (Fe,Mg,Mn,Si)=Al(VI)Al(IV). Deviation from this line could reflect the presence of minor amounts of Fe^{3+}. The lower plot (b) shows Si vs Al for the same data set, indicating that all three of the cations (Fe, Mg, Mn) participate in the substitution. This plot also shows the individual samples and which unit they belong to more clearly than (a).

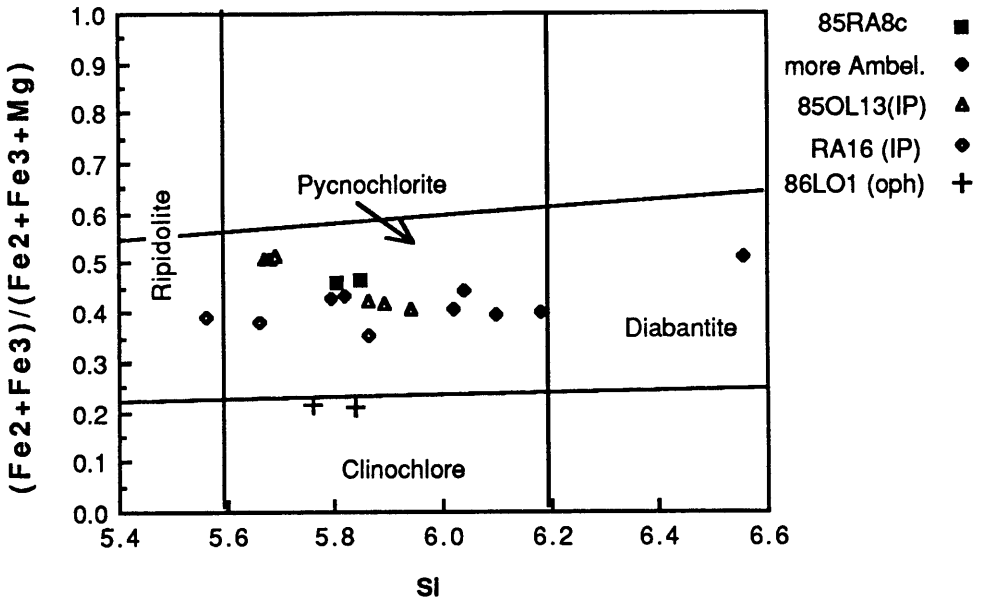

Figure 5.17: Plot of Fe(T)/Fe(T) + Mg vs Si for chlorites analyzed in this study. Nomenclature of chlorites is from Deer et al, 1966

Chlorite in the ophiolite unit is more Mg- and Mn-rich than it is in the other units and has X_{Fe} =0.2-0.22 (Table 5.4, Fig 5.17). One sample of the marble that may overlie the ophiolitic rocks on the N margin of Mt. Olympos (86OL41c) contains a strongly Mg-rich chlorite (X_{Fe} =0.1) intergrown with phengite parallel to the schistosity. Another marble, a block enclosed in serpentinite-matrix melange (84OL38b) contains abundant chlorite (X_{Fe} =0.34) as the primary phyllosilicate in the foliation planes.

Pumpellyite

Pumpellyite occurs in the Olympos, Ambelakia, and rarely in metabasites of the Pierien unit (Table 5.2, Table 5.4). In the Olympos and Ambelakia units, pumpellyite occurs parallel to the S3 foliation, but growth appears to have persisted after deformation has ceased. I have not probed enough pumpellyite to determine whether foliation-parallel (M3) and unoriented (M4) pumpellyites are different compositions. I did not probe pumpellyite in the Pierien unit.

Feldspars

Albite is the dominant composition of metamorphic feldspar in all units, with the exception of the Pierien and Infrapierien pelitic schists. Relict K-feldspar and plagioclase occur as augen in granitic gneisses of the Pierien and Infrapierien units, and detrital plagioclase and K-feldspar occur in the Olympos flysch and the Ambelakia metasediments.

In the metapelites of the Pierien unit, feldspar seems to be a minor component, and I was unable to obtain analyses on plagioclase in contact with the garnet. In sample 84LI12a, matrix plagioclase has an average composition of Ab_{94}. In the one pelitic sample analyzed from the Infrapierien unit (85LI2a), plagioclase is highly variable in composition, from Ab_{100} to Ab_{77}, and contains a significant amount of Fe_2O_3, indicating that it is oxidized.

Garnet

Garnet occurs in the M1 assemblage of the Pierien and Infrapierien units. Compositions of garnet and coexisting minerals in the metapelites of the Pierien unit are shown in Table 5.5 (Samples 84LI6a,12a,13) The garnet is dominantly almandine(up to 70%) and spessartine (12-25%).

In the massive amphibolite of the Infrapierien unit, the garnet occurs as anhedral porphyroblasts rimmed by chl + ep + Fe-oxides and appears to be a relict phase from an earlier metamorphic event (Fig. 5.6). Garnet compositions range

from X_{Al} =.58-.62, X_{Py} = .04-.06; X_{Gr} = .2-.24, and X_{Sp} = .1-.18 (Table 5.5), and no systematic core-rim zoning was detected.

Biotite

There is no evidence of biotite in samples from the Olympos, Ambelakia, or ophiolite units. Locally throughout the Pierien and Infrapierien units, biotite appears to be a relict of an earlier metamorphic event; occurring as rare, altered grains surrounded by chlorite. These relict grains have X_{Fe} = 0.44-0.52 in samples 85OL50 and 85OL32.

Biotite occurs as a major mineral in two of the Infrapierien samples studied; in amphibolite sample 86OL47, and in metapelite sample 85LI2a. In both these samples it appears to be in textural equilibrium with other phases in the rock (hbl in the former; mu + plag + ga in the latter). Biotite in sample 86OL47 contains X_{Fe} = 0.44-0.48, and in sample 85LI2a contains X_{Fe} = 0.57± 0.04 and up to 1.7 wt % TiO_2 and 0.5 wt% MnO (Table 5.5).

Chloritoid and paragonite

Chloritoid and paragonite occur in two samples from the Pierien unit, 84LI22c, and 84LI13. In sample 84LI22c the chloritoid is clearly post-kinematic. In 84LI13, chloritoid is parallel to the foliation. In both cases this is an Fe-rich chloritoid, containing 6-9% of the Mg-endmember in sample 84LI22c, and 15-16% in 84LI13 (Table 5.5)

Coexisting paragonite and muscovite in samples 84LI13 and 84LI12a contain 85-90% and 10-18% paragonite component (Na/Na+Ca+K) respectively (Table 5.5). In sample 84LI22c, coexisting paragonite and muscovite have a much broader range of compositions, from 68-88% paragonite component in the former, and 15-26% paragonite component in the latter.

RELATIVE AND ABSOLUTE AGES OF METAMORPHISM AND DEFORMATION

This section briefly summarizes the evidence for correlating the four metamorphic events with the deformation events discussed in Ch. 3 and the timing of these events as discussed in Ch. 4. The reader is referred to the previous chapters for details of the structural and geochronologic data.

In the Infrapierien and Pierien units there is abundant evidence for three metamorphic events that are associated with penetrative deformation, and possibly a fourth, retrograde, post-kinematic event. The last three events affected the Ambelakia unit, and the last two events also affected the Olympos unit. The four

events recognized include: M1: mid-Cretaceous greenschist-amphibolite facies metamorphism in the ophiolite, Pierien, and Infrapierien units; M2: early Eocene blueschist-facies metamorphism in the Pierien and Ambelakia units; M3: late Eocene blueschist-facies metamorphism in the Pierien, Ambelakia, and Olympos units; and M4: cooling and decompression under prehnite-pumpellyite facies conditions.

M1: Mid-Cretaceous greenschist-amphibolite facies metamorphism in the Ophiolite, Pierien, and Infrapierien units

In the ophiolite unit, a greenschist-facies assemblage consisting of act + ep + chl is well-developed, but foliation development is variable, so it is difficult to associate the metamorphism with a specific deformational event The local presence of two cross-cutting foliations both containing greenschist-facies minerals indicate that two periods of greenschist facies metamorphism and deformation may have affected the ophiolite unit (the second may correspond to M2). I have not directly dated the metamorphism in the ophiolite unit, but regional considerations, in addition to the structural evidence presented in Chapter 3, indicate that this event is Cretaceous in age. An important point that is worth repeating is that none of the ophiolitic rocks contain blueschist facies assemblages. This implies that the ophiolite units: 1) must have been removed from the site of (intracontinental) subduction of the Ambelakia and Pierien units and 2) were emplaced into their present positions at a later time (post -M4).

In the Infrapierien and Pierien units, the upper thrust sheets (in the northern and western portions of the study area) contain greenschist to amphibolite facies assemblages that are not strongly overprinted by younger blueschist facies assemblages. Garnet-chlorite, garnet-biotite, and hornblende-biotite-epidote are the characteristic minerals for this event in the metapelites and massive amphibolites; albite + actinolite + epidote + phengite + chlorite is the common assemblage in mica schists and amphibolite schists. Direct constraints from Ar/Ar data come only from the latter assemblage, and indicate that the phengite began to retain Ar ($T \leq 350°C$) at ~100 Ma. However, data of Yarwood and Dixon (1977) and Barton (1976) discussed in Chapter 4 suggest that lower amphibolite facies metamorphism also occurred during Early Cretaceous time. I have found no evidence of blueschist-facies metamorphism in these rocks, probably because of their high structural level in the Pelagonian nappe sequence, however, it is also possible that the bulk compositions are too felsic. This thrust sheet would have been at a high structural level relative to, and possibly in the upper plate of the A-

type subduction zone which produced the blueschists in lower thrust sheets of the Pierien unit.

The Ambelakia unit contains an older assemblage consisting of ab + act + ep ± cr ± chl that is overgrown by sodic amphibole and other phases described under M2. We do not know the age of this pre-M2 metamorphism, or where it occurred with respect to the paleotectonic positions of the Pierien and Ambelakia units. There is some suggestion in the Ar data that a Cretaceous event affected the Ambelakia unit (Chapter 4), but it is also possible that this greenschist-facies assemblage is simply an early part of the M2 metamorphic event. Because the geochronologic data are ambiguous, M1 in the Ambelakia unit may not be strictly coeval with M1 in the Pierien and Infrapierien unit, and because the M1 assemblage appears to contain sodic amphibole as well as actinolite, it is possible that pre-M2 conditions were somewhat higher pressure and/or lower temperature in the Ambelakia unit than in the other units.

M2: Early Eocene blueschist facies metamorphism, Pierien and Ambelakia units; blueschist-greenschist transition facies, Infrapierien unit.

In the Ambelakia unit, coarse sodic amphibole clearly grew after actinolite, epidote, and chlorite in some samples (Figure 5.5), possibly in response to increasing pressure and/or decreasing temperature. The stable M2 assemblage appears to consist of ab + ph + gl/cr ± act ± ep ± chl. It is unclear whether lawsonite and/or pumpellyite were in equilibrium with this assemblage; these minerals are present, but textural relations are ambiguous as to whether they were stable during M2 and/or M3. .

In the Pierien unit, the stable M2 assemblage in the granitic gneisses consisting of ab + ph ± cr/ri ± ac is not diagnostic of metamorphic grade, however the associated metabasites (e.g. 85GO1, 85LI16) contain ab + ph ± cr ± act ± chl ± ep and the presence of strongly phengitic mica (see below) suggests that this was a blueschist-facies event.

The presence of blue-green amphibole in the M2 Infrapierien assemblage ab + ph + ep ± wn/bar ± act ± stilp and the overgrowth relations described above, indicates that the Infrapierien unit passed through slightly higher pressures and/or lower temperatures than during the M1 event.

M2 is dated in the Ambelakia and Pierien units by Ar/Ar on phengite; ages range from 61-53 Ma (Schermer et al, in press; Chapter 4). In the Infrapierien unit,

one mica sample yielded a plateau age of 63 Ma, and two others suffered partial Ar loss during the early Tertiary, supporting the existence of a lower-temperature event that post-dates M1 in this unit.

M3: late Eocene blueschist-facies metamorphism in the Pierien, Ambelakia, and Olympos units

In the Ambelakia and Pierien units, M2 and M3 assemblages appear to be similar, and are distinguished as two events principally on the basis of their relationship to deformation and on constraints from Ar/Ar data. The schistosity associated with M2 is isoclinally folded and a new foliation is formed parallel to the mylonite zones between the Pierien and Ambelakia unit and the Ambelakia and the Olympos unit. The assemblage that is parallel to both foliations includes glaucophane/crossite, phengite, and chlorite; pumpellyite was stable during M3, and lawsonite may have been stable during either or both events. The presence of stable pumpellyite, a low-temperature mineral (see below) during M3 implies that lw could also have been stable at the same time. Epidote and actinolite do not appear to be in equilibrium with the M3 assemblage in some samples, where they occur as subhedral to anhedral grains that are deformed by the S3 foliation. However, in most samples the textural relations regarding the stability of act + ep are ambiguous.

M3 appears to be the first metamorphic event to affect the Olympos unit. The presence of the assemblage ab + ph + chl + pp ± lw ± cr ± act indicates that this was a blueschist-facies event. As the age of the flysch is known to be middle Eocene on the basis of fossils (Godfriaux, 1968), the metamorphism must be post-middle Eocene. Ar/Ar data constrain the age of metamorphism to 36-42 Ma (Schermer et al, in press).

M4: cooling and decompression under prehnite-pumpellyite facies conditions

Post-kinematic pp ± chl ± pr is common in the metasediments and metabasalts of the Ambelakia unit, and the flysch of the Olympos unit contains post-kinematic pumpellyite. Late pumpellyite and chlorite are also rarely present in the Pierien unit. Samples from the Infrapierien unit do not contain pumpellyite but commonly contain late chlorite. No pumpellyite has been identified in the ophiolite unit.

The structural evolution discussed in Chapter 3 suggests that the emplacement of the ophiolite unit along low-angle normal faults in parts of the study area (Fig. 5.1) occurred during D5. Because the ophiolite unit does not

contain pumpellyite where underlying rocks do, I interpret the formation of late pumpellyite and chlorite to have occurred between D3 and D5. While it may not be strictly coeval with D4 as defined on the basis of structural style, this event is termed M4. Inasmuch as the prehnite-pumpellyite facies represents lower pressure and temperature conditions than the blueschist facies, M4 is associated with the beginning of decompression and cooling of the metamorphic nappes.

DISCUSSION: CONSTRAINTS ON CONDITIONS OF METAMORPHISM

There are no well-calibrated geothermobarometers applicable to the blueschist facies assemblages from the Mt. Olympos region. Nevertheless, several mineral equilibria have been studied in detail, and the presence and absence of key phase assemblages containing minerals such as pumpellyite, lawsonite, and sodic amphiboles can be used to broadly constrain the temperatures and pressures of blueschist metamorphism. Several experimental geobarometers have been proposed in recent years; however there is much disagreement over their applicability to natural assemblages, one of the biggest difficulties being the attainment of equilibrium at high pressures and low temperatures.

Phase equilibria in the "basaltic" system Na_2O-CaO-MgO-Al_2O_3-SiO_2-H_2O (NCMASH) have been recently summarized by Liou et al (1985). Some of the experimentally-determined reactions applicable to the mineral assemblages described above are shown in Fig 5.18. In general, these reactions are discontinuous, describing the appearance and disappearance of various minerals, such as glaucophane, epidote, pumpellyite, and lawsonite. However, most of these minerals are solid solutions whose stability fields are more likely controlled by continuous reactions. Experiments and analysis of phase equilibria have generally been done in the Fe-free system, so the addition of Fe_2O_3 and FeO as system components is likely to have a significant effect on the location of reaction boundaries. Descriptions and calibrations of continuous reactions at low temperatures for metabasites are only now becoming available in the literature (e.g. Maruyama et al, 1986; Liou et al, 1985; Nakajima et al, 1977), and much experimental work needs to be done.

Phase equilibria for pelitic rocks at HP/LT conditions have recently been described e.g. (Chopin and Schreyer,1983; Koons and Thompson, 1985) and may prove to be valuable quantitative thermobarometers, however, the general absence of Al-rich bulk compositions in the study area precludes use of such equilibria. The abundance of granitic rocks in the Pierien and Infrapierien unit

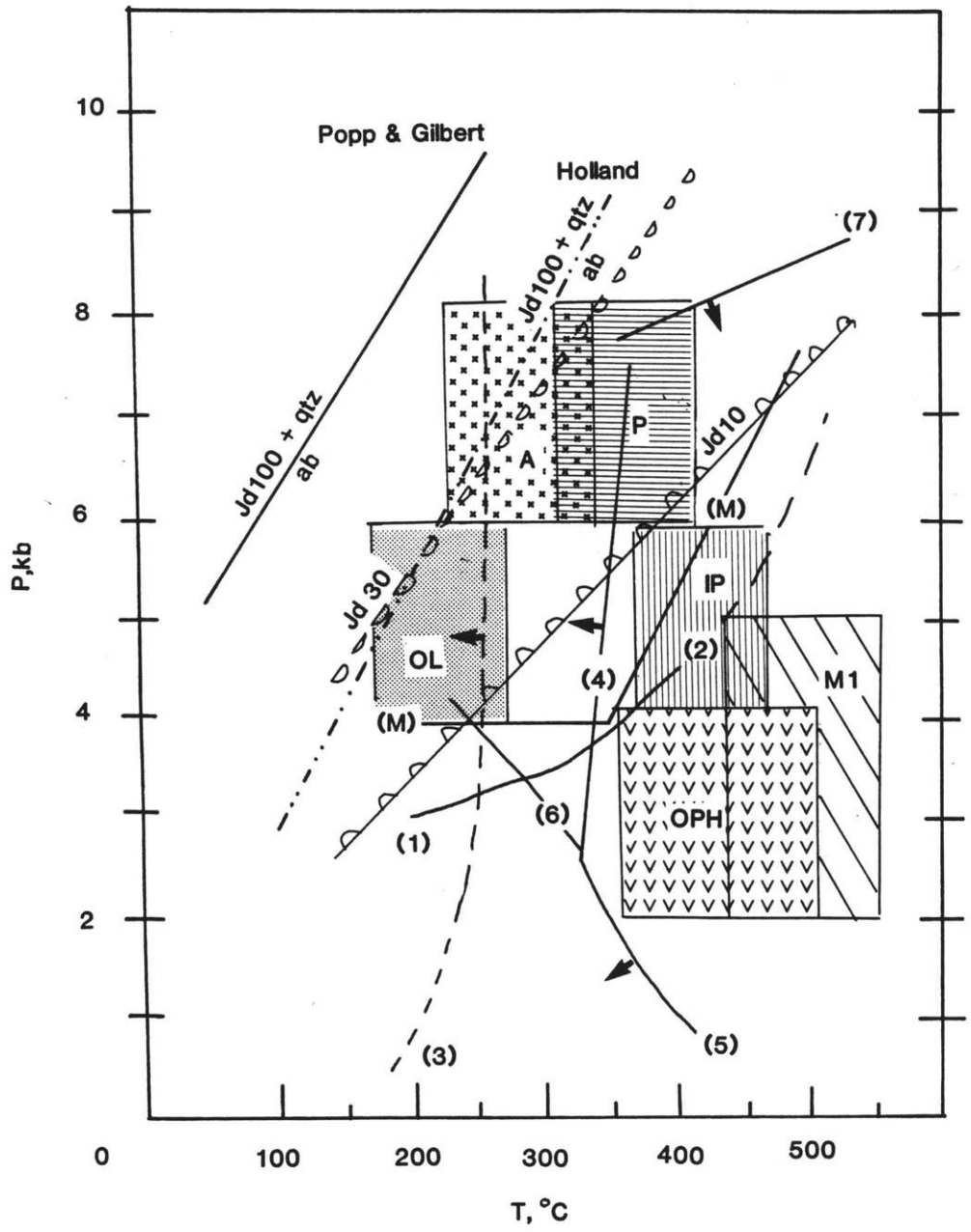

Figure 5.18: P-T diagram showing location of various phase equilibria in the system NCMASH. See text for details. Adopted from Liou et al, 1985. Location of jadeite$_{100}$ + qtz = ab from Popp and Gilbert (1972) and Holland (1980); location of curves for Jd$_{10}$ and Jd$_{30}$ computed from data in Popp and Gilbert; see text for details. Numbered curves correspond to equilibria discussed in text; (M) indicates glaucophane stability limits of Maresch (1977). Arrows indicate effect of addition of Fe_2O_3 as a system component. Boxes indicate preferred estimates of P-T conditions in each unit: dot pattern, OL= Olympos unit; crosses, A= Ambelakia unit; horizontal lines, P= M2,M3 in Pierien unit; vertical lines, IP= M2,M3 in Infrapierien unit; diagonal lines = M1 in Pierien and Infrapierien unit, v's, OPH= M1 in ophiolite unit.

Table 5.6 Comparison of estimates of pressures and temperatures of metamorphism obtained from using various different techniques discussed in the text.

METHOD / UNIT	Min. Eq.	Na(M4) in amph.	Al_2O_3 Na-amph	Na-px XJd	Phengite (Velde)	Phengite (Massone)
Olympos (M3)	P>3 kb T<225-250°C	P~7 kb	P> 4.5 kb (min)		P~3 kb	P~10 kb
Ambelakia (M2,M3)	P>4kb T<350°C	P~7kb	P~5-7kb	P~5kb	P~6kb	P~12-14kb
Pierien (M2,M3)	P>4kb T<400°C	P~6-7kb	P>4-5kb (min)	P~7.5kb	P~5-7kb	P~11-13 kb
Infrapierien (M2,M3)	P ?? T~350-450°C	P~4-6kb			P~5-7kb	P~9-12 kb
Pierien, Infrapierien (M1)	P ?? T~425-550°C	P~2-5 kb			P~2-3kb	P~3-5kb
Ophiolite (M1)	P<4kb T350-450°C	P~2-3kb				

makes it difficult for any diagnostic assemblages to form at all but the highest grades of metamorphism. .I will first summarize constraints on metamorphic conditions obtained from consideration of phase equilibria and the stability of various index minerals. This will be followed by a discussion of the semi-quantitative (for blueschists) and quantitative (for pelites) equilibria that can be applied to the assemblages and the mineral compositions present in the study area. Pressure-temperature estimates using various techniques applied to the blueschists of the study area are compared in Table 5.6.

Constraints from mineral equilibria and the stability of index minerals

Mineral stability fields

Lawsonite

The first appearance of lawsonite (+ qtz + H_2O) occurs at 170-180°C and P=4-5 kb (Nitsch, 1968; cited in Winkler, 1979). At higher temperatures, experiments by Liou (1971) on the reactions

$$lm = lw + qtz + H_2O \quad (1)$$

and

$$lw + qtz = wr \quad (2)$$

indicate that lawsonite is stable at P>3kb at 200°c and P>5 kb at ~400°C. The upper temperature stability of lawsonite is less well-constrained as it depends on by which reaction lawsonite breaks down to epidote (zoisite); none of these have been determined experimentally. Liou et al (1985) locate the reaction

$$lw + pp = zo + chl + qtz + H_2O \quad (3)$$

at T~225°C over.a broad range of pressures. Most workers agree that lawsonite is not stable above ~300°C.

Pumpellyite and Prehnite

Several reactions illustrating the stability limits of pumpellyite are shown on Figure 5.18. Arrows indicate the effects of the addition of Fe_2O_3 to the system (from Liou et al, 1985). The presence of pumpellyite constrains the temperature of metamorphism to less than ~300°C. The reaction:

$$pp + chl + qtz = zo + tr + H_2O \quad (4)$$

has been determined experimentally by Maruyama et al (1985) to be located at 300°C, 3 kb and 350°C, 6 kb. Thus, constraints from reactions 1-4 indicate that the assemblage lw + pp is stable at T< 225°; P>3kb.

The formation of prehnite and pumpellyite during very low-grade metamorphism has been known since the work of Coombs (1960). The assemblages pp + pr + chl; pp + chl + ep, and pp + pr + hm are restricted to low

temperature and low pressure in part by reaction (4), separating the prehnite-pumpellyite facies from the prehnite-actinolite facies (Liou et al, 1985). Additional limiting reactions studied by Liou et al, 1985, and shown on figure 5.18, include:

$$pr + chl + qtz = cz + tr + H_2O \quad (5),$$

and

$$pr + chl + qtz = pp + tr + H_2O \quad (6).$$

These reactions limit pr + pp-bearing assemblages to P<1.5 kb at T~400°C and to T<300°C at higher pressures. Both of these reactions are displaced toward lower temperatures with addition of Fe_2O_3 to the system.

Sodic amphibole

Experimental studies on the synthesis of pure Mg- end-member glaucophane by Carman and Gilbert (1983) have located the stability field at >10 kb at 300°C. However, the addition of Fe2O3, a common component of natural glaucophanes, significantly enlarges the stability field. The data summarized by Maresch (1977) for Fe-bearing glaucophanes indicates that glaucophane is stable above 4 kb between 200-300°C, and with an upper temperature limit at ~450°C at 7 kb (Figure 5.18).

Reactions occurring at the transition from blueschist to greenschist-facies has been studied by Maruyama et al (1986). They located the reaction:

$$cz + gl + qtz + H_2O = tr + chl + ab \quad (7),$$

which is univariant in the system NCMASH, at 350±10°C, 7.8±0.2 kb and 450±10°c, 8.2±0.4 kb. The addition of Fe_2O_3 displaces the reaction toward lower pressures and higher temperatures and is broadly consistent with the upper temperature limit determined by Maresch (1977) (Fig 5.18). The progression of assemblages 1) gl + lw (+ chl + pp); 2) gl + pp (+ chl + ep) and 3) gl + ep (+ chl + act) occurs with increasing temperature through the blueschist facies (Liou et al, 1985).

Epidote and actinolite

Epidote and actinolite are stable over a wide range of pressure-temperature conditions, from low P and T in the pumpellyite-actinolite facies to low P and higher T in the epidote-actinolite facies, to moderate P and T in the greenschist facies. The stability of zoisite or clinozoisite is more limited than that of Fe-rich epidotes; and occurs under low-grade (as opposed to very-low-grade) conditions, above T~350°C where lawsonite is unstable (Winkler, 1979, p. 74). The transition from greenschist facies to amphibolite facies, indicated by the appearance of hornblende (instead of actinolite) and garnet, the disappearance of chlorite (as chl

+ mu), and the transformation of albite to more An-rich plagioclase, occurs at ~500-550°C (Winkler, 1979).

Phase equilibria constraints on P,T conditions

M1: Greenschist-amphibolite facies metamorphism

The assemblage sp + chl in the ultramafic rocks of the ophiolite unit is not diagnostic of metamorphic grade; however, if T >400-450°C, metamorphic olivine would have formed from serpentine, thus the metamorphism is constrained to greenschist grade or lower. Nance (1981) describes metamorphic olivine from the Livadi ophiolite complex (Fig. 5.1), and attributes it to an early upper greenschist-lower amphibolite facies metamorphism that is subsequently retrogressed under greenschist facies conditions. The persistence of serpentine minerals implies low X_{CO2} conditions (Winkler, 1979).

Mineral assemblages in metabasalts and gabbros of the ophiolite unit are also consistent with greenschist facies metamorphism. The assemblage act + ab + chl + ep forms in basaltic rocks at temperatures between ~350 and 450°C (Winkler, 1979), however there are no well-defined constraints on the pressure during metamorphism. Whole-rock major element analyses of two metagabbros from the ophiolite unit and one metabasalt from the Ambelakia unit presented in Chapter 2 (Appendix A2, samples 86GO18, 86RA22, 86RA6a) indicate that although the bulk compositions are broadly similar, blueschist-facies minerals such as Na-amphibole and lawsonite did not form in the ophiolitic rocks. The absence of blueschist facies minerals in rocks of appropriate bulk composition indicates pressures less than ~4 kb and/or temperatures greater than ~350° C.

M2, M3, and M4: Blueschist and Prehnite-Pumpellyite facies metamorphism

In the Olympos unit, the presence of lw + pp + chl implies T<225-250°C and P>3 kb for M3 based on the mineral equilibria discussed above. If the crossite and actinolite were also in equilibrium with the above assemblage, the minimum pressure is ~4 kb from the glaucophane stability curve of Maresch (1977).

In the Ambelakia unit, the probable coexistence of lw + cr + pp during M2 and M3 implies P >4 kb at 300°C and P>6 kb at 400°C. Because lw is rare, it is difficult to determine if lw + pp was a stable assemblage; if so, the temperatures for M2 and M3 were similar to those for the Olympos unit, and T<~225-250°C. If cr + ep was stable at the expense of lw, the approximate upper temperature limits of blueschist facies metamorphism are given by the data of Maruyama et al (1986) and Maresch (1977) to be ~400°C at 6 kb and ~500°C at 8 kb. The coexistence of chl + pp ± pr

and the absence of sodic amphibole and epidote during M4 indicate lower pressures and temperatures, with approximate P<4 kb and T<300°C.

In the Pierien unit, no critical low-temperature minerals such as lw or pp are present, but the presence of crossite and phengite compositions similar to those in the Ambelakia unit (see below) appear to indicate similar pressures. The geochronologic data discussed in chapter 4 provides an indirect temperature constraint, that Ar was retained in earlier-formed white micas during the M2 and M3 events, thus temperatures were probably less than ~350°C, the approximate closure temperature of Ar in phengite.

In the Infrapierien unit, M2 and M3 assemblages appear to represent higher temperatures. The presence of winchite, barroisite, and actinolite instead of glaucophane-crossite is evidence for higher T conditions. However, there are no constraints on the pressure of metamorphism from mineral equilibria; constraints from phengite compositions indicate a relative pressure with respect to the pressure in the Ambelakia unit (see below).

Thermobarometric constraints

Several well-calibrated thermobarometers exist for pelitic rocks. However, due to the paucity of rocks of pelitic bulk composition in the study area, I can only apply these equilibria to samples from the upper parts of the Pierien and Infrapierien units, which appear to have had a long and complicated metamorphic history (see chapter 3). Because no alumino-silicate minerals could be identified, we are limited to Al_2SiO_5-absent equilibria. Calibrated equilibria that can be applied to the pelitic assemblages present in the study area include 1) garnet-biotite geothermometry (Ferry and Spear, 1978), and 2) garnet-chlorite geothermometry (Dickenson and Hewitt, 1986; Lang and Rice, 1987). Semi-quantitative calibrations of geobarometers for blueschist facies rocks include 1) the phengite content of white mica (Velde, 1965; Massonne and Schreyer, 1987); 2) the Al_2O_3 content of sodic amphibole(Maruyama et al, 1986); 3) the Na(M4) content of calcic amphiboles (Brown, 1977b); and 4) the jadeite content of sodic pyroxene (Holland, 1980, 1983; Popp and Gilbert, 1972).

The garnet-biotite geothermometer is only applicable to sample 85LI2a, from the Infrapierien unit as other samples containing this assemblage have abundant evidence for textural disequilibrium and/or replacement of biotite by chlorite (e.g. 86OL47, 84LI6,12a,13). The garnet-chlorite thermometer can be applied to the samples from the upper part of the Pierien unit in the Sarandoporou area (84LI6a,

12a, 13). Both of these assemblages are part of the M1 metamorphic event. The phengite and sodic and calcic amphibole barometers can be applied to many of the samples in the Infrapierien, Pierien, Ambelakia, and Olympos units to determine conditions during M2 and M3. Jadeitic pyroxene has only been probed in two samples, 86RA5b from the Ambelakia unit and 85OL46 from the Pierien unit.

Garnet-biotite geothermometry

The garnet-biotite geothermometer, calibrated by Ferry and Spear (1978), utilizes the temperature dependence of Fe-Mg exchange in garnet and biotite as expressed by the following reaction:

$$Mg_3Al_2Si_3O_{12} + KFe_3AlSi_3O_{10}(OH)_2 = Fe_3Al_2Si_3O_{12} + KMg_3AlSi_3O_{10}(OH)_2 \quad (8)$$

Activity-composition relationships and data for ΔH, ΔS, and ΔV (Hodges and Crowley, 1985) are presented in Table 5.7. Garnet and biotite rim compositions and calculated temperatures from the only sample with the appropriate assemblage, Infrapierien sample 85LI2a, are listed in Table 5.8.

A wide variation of plagioclase compositions and analytical difficulties prevents use of the garnet-muscovite-plagioclase-quartz and garnet-muscovite-plagioclase-biotite barometers calibrated by Hodges and Crowley (1985) at this time, however we hope that further work will resolve these difficulties. I could not obtain good analyses of this plagioclase, so pressure estimates using this analytical data would be subject to extremely large errors. Perhaps further work on this or other thin sections from this sample will allow us to obtain better data.

Mean temperatures calculated from garnet-biotite geothermometry range from ~500°C to 535°C for assumed pressures from 4-13 kb. Although I do not have enough data to rigorously calculate errors, a nominal precision of ±50°C is appropriate to use in a relative comparison with other samples from the study area, although the potential inaccuracy in determination of absolute temperature is likely to be considerably larger (Hodges and McKenna, 1987). The calculated temperatures are consistent with the mineral assemblage, providing support for the argument, based on textural relations, that this is an equilibrium assemblage.

Garnet-chlorite geothermometry

The garnet-chlorite assemblages described from the Pierien unit were analyzed to determine metamorphic temperatures using two calibrations of the

Table 5.7: Thermodynamic data and activity-composition relations for garnet biotite geothermometry (Ferry and Spear, 1978) and garnet-chlorite geothermometry (Dickenson and Hewitt, 1986; Lang and Rice, 1987).

Equilibrium	ΔH(cal)	ΔS(cal/mol-K)	ΔV(cal/bar)
Ref:			
(1) pyrope + annite = almandine + phlogopite	12454	4.622	0.057
(2) 1/5 Mg-Chl + 1/3 almandine = 1/5 Fe-chl + 1/3 pyrope	4109.8	1.365	0.0122

Activity-composition relations:

Biotite (ideal):

$$a_{ann} = (X_{ann})^3$$
$$a_{phlog} = (X_{phlog})^3$$

Garnet:
Ref. (1)

$$a_{alm} = [X_{alm} \cdot \exp(((1.5T(K)-3300) \cdot (X_{py}X_{gr})) / RT(K))]^3$$

$$a_{py} = [X_{py} \cdot \exp(((3300-1.5T(K)) \cdot (X_{gr}^2 + X_{al}X_{gr} + X_{gr}X_{sp})) / RT(K))]^3$$

$$a_{gr} = [X_{gr} \cdot \exp(((3300-1.5T(K)) \cdot (X_{py}^2 + X_{al}X_{py} + X_{py}X_{sp})) / RT(K))]^3$$

Chlorite (ideal):

$$a_{Fe}^{Chl} = (X_{Fe}^{Chl})^5$$
$$a_{Mg}^{Chl} = (X_{Mg}^{Chl})^5$$

References:
(1) Hodges and Crowley, 1985
(2) Derived from Lang and Rice, 1987

Table 5.8: Summary of garnet and biotite compositions and temperatures obtained from garnet-biotite geothermometry.

	AVG gar rim	st. dev.	AVG bi	st. dev.
MgO	0.501	0.181	6.756	0.330
Al2O3	19.926	0.281	14.950	1.465
SiO2	37.762	0.248	36.679	0.668
CaO	11.260	1.813	0.464	0.521
TiO2	0.099	0.056	1.625	0.595
MnO	10.469	4.800	0.547	0.105
FeO	19.447	3.851	24.869	2.365
Na2O	0.000	0.000	0.054	0.018
K2O	0.000	0.000	7.977	1.295
TOTAL	99.562	0.699	93.921	0.867
Mg	0.060	0.022	0.796	0.049
Al	1.892	0.021	1.391	0.114
Si	3.042	0.015	2.898	0.015
Ca	0.971	0.152	0.040	0.045
Ti	0.006	0.003	0.096	0.034
Mn	0.716	0.332	0.037	0.008
Fe	1.309	0.252	1.646	0.181
Na	0.000	0.000	0.008	0.003
K	0.000	0.000	0.804	0.127
cation sum	8.003	0.016	7.716	0.091
Xalm	0.4283	0.069		
Xpy	0.0196	0.007		
Xgr	0.3177	0.055		
Xsp	0.2343	0.086		
Xann			0.5746	0.037
Xphlog			0.2781	0.024
XMn			0.0128	0.0028
T, °C at 13 kb	538			
T, °C at 7 kb	522			

Table 5.9: Summary of garnet and chlorite compositions and temperatures obtained from the two calibrations of the garnet-chlorite geothermometer discussed in the text.

	84L16a							
Mineral	GARNET1	GARNET2	GARNET3	CHLOR1	CHLOR2	CHLOR3	GARNET4	CHLOR4
MgO	1.707	1.691	1.754	8.712	11.16	10.613	1.732	11.068
Al2O3	20.474	20.709	20.832	18.936	21.851	21.783	20.514	21.682
SiO2	36.924	36.691	37.017	20.002	24.932	24.094	36.542	23.827
CaO	1.66	1.743	1.717	0.171	0.087	0.121	1.8	0.048
TiO2	0.029	0.045	0.045	0.072	0.018	0.034	0.062	0.072
MnO	7.296	7.147	7.172	0.551	0.559	0.654	8.432	0.588
FeO	31.828	31.751	31.997	39.549	29.061	31.41	30.933	29.519
Cr2O3	0.114	0.122	0.042	0	0	0	0.179	0
TOTAL	100.032	99.899	100.576	87.993	87.668	88.709	100.194	86.804
Mg	0.207	0.206	0.212	3.023	3.583	3.42	0.211	3.614
Al	1.965	1.99	1.987	5.194	5.546	5.55	1.971	5.597
Si	3.007	2.991	2.996	4.655	5.369	5.209	2.979	5.219
Ca	0.145	0.152	0.149	0.043	0.02	0.028	0.157	0.011
Ti	0.002	0.003	0.003	0.013	0.003	0.006	0.004	0.012
Mn	0.503	0.493	0.492	0.109	0.102	0.12	0.582	0.109
Fe	2.168	2.165	2.166	7.698	5.233	5.679	2.109	5.407
Cr	0.007	0.008	0.003	0	0	0	0.012	0
cation sum	8.005	8.007	8.006	20.735	19.855	20.011	8.025	19.97
mg/fe	0.096	0.095	0.098	0.393	0.685	0.602	0.1	0.668
Xmg chl				0.282	0.406	0.376		
	avg garnet							
Xal	0.717						0.689	
Xpy	0.069						0.069	
Xgr	0.048						0.051	
Xsp	0.166						0.19	
aPy	0						0	
aAl	0.365						0.324	
probe points used	ga-chl1 avg		ga-chl	ga-chl 4				
Dickensen,Hewitt 1986								
T(K) at 6 kb:	1098		908	849				
T(K) at 3 kb:	1075		932	888				
Lang,Rice, 1987								
T(K) 6kb	1023		878	834				
T, °C	750		605	561				

Table 5.9 (continued)

	84LI12a					84LI13					
	GARNET 1	GARNET 2	GARNET 3	CHLOR 1	CHLOR 2	GARNET1	GARNET2	GARNET3	CHLOR1	CHLOR2	CHLOR3
MgO	1.705	1.083	0.781	12.159	13.072	1.348	1.39	1.312	11.765	11.548	12.044
Al2O3	20.533	20.662	20.811	21.029	21.899	20.023	20.435	20.571	20.981	21.94	22.403
SIO2	36.851	37.400	37.224	25.936	26.149	36.48	36.57	36.773	25.205	27.324	24.429
CaO	3.384	8.262	7.961	0.140	0.036	4.006	4.126	3.947	0.069	0.083	0.041
TIO2	0.000	0.063	0.042	0.030	0.018	0.029	0	0.074	0.046	0.05	0.083
MnO	6.854	5.745	8.227	0.377	0.421	6.201	6.44	7.689	0.501	0.422	0.449
FeO	29.983	26.913	24.888	26.050	26.302	30.114	29.902	30.24	27.865	26.173	27.705
Cr2O3	0.087	0.109	0.122			0.067	0.109	0.13	0	0	0
TOTAL	99.397	100.237	100.056	85.721	87.897	98.268	98.972	100.736	86.432	87.54	87.154
Mg	0.207	0.130	0.094	3.920	4.105	0.166	0.17	0.158	3.81	3.623	3.863
Al	1.973	1.956	1.976	5.360	5.437	1.95	1.975	1.964	5.371	5.441	5.681
Si	3.005	3.004	2.999	5.609	5.508	3.014	2.999	2.978	5.475	5.75	5.256
Ca	0.296	0.711	0.687	0.032	0.008	0.355	0.362	0.343	0.016	0.019	0.009
Ti	0.000	0.004	0.003	0.005	0.003	0.002	0	0.005	0.008	0.008	0.013
Mn	0.473	0.391	0.561	0.069	0.075	0.434	0.447	0.527	0.092	0.075	0.082
Fe	2.045	1.808	1.677	4.711	4.634	2.081	2.05	2.048	5.062	4.606	4.985
Cr	0.000	0.000	0.000	0.000	0.000	0.004	0.007	0.008	0	0	0
cation sum	8.005	8.011	8.006	19.706	19.770	8.007	8.011	8.031	19.832	19.522	19.89
mg/fe	0.101	0.072	0.056	0.832	0.886	0.08	0.083	0.077	0.753	0.787	0.775
Xal	0.677	0.595	0.555			0.722					
Xpy	0.069	0.043	0.031			0.067					
Xgr	0.098	0.234	0.228			0.091					
Xsp	0.157	0.129	0.186			0.121					
aPy	0.000	0.000	0.000			0					
aAl	0.301	0.201	0.165			0.366					
pts used	avg ga1-3 avg chl 1,2		gar1 avg chl 1,2		gar3 avg chl 1,2	pts used:	avg gar, chl				
Dickenson, Hewitt, 1986						Dickenson,Hewitt, 86					
T(K) @ 6 kb	684					T(K) @6 kb	726				
Lang, Rice						Lang, Rice, 1987					
T(K) 6kb	748		782		692	T(K) @6 kb	756				
T deg C	475		509		419	T, deg C	483				
T(K), 3kb	742		776		686	T(K) @3 kb	750				
T deg C	469		503		413	T, deg C	477				

garnet-chlorite thermometer, one by Dickenson and Hewitt (1986), and the other derived by subtracting the chlorite-biotite equilibrium empirically derived by Lang and Rice (1987) from the garnet-biotite geothermometer of Ferry and Spear (1978). Activity-composition relationships and data for ΔH, ΔS, and ΔV are shown in Table 5.7. The Dickenson and Hewitt (1986) calibration uses ideal solution models for both garnet and chlorite; the equilibrium derived from the Lang and Rice (1987) calibration uses the non-ideal solution model for garnet of Hodges and Crowley (1985). In general, the two calibrations differ by ~<50°C.

The garnet-chlorite results are more variable than the garnet-biotite results, and the T calculated for an assumed pressure of 6 kb ranges from 561-750°C (834-1033 K) in sample 84LI6a, 419-509°C (692-782K) for 84LI12a, and 483°C (756K) for 84LI13.

The temperatures calculated for sample 84LI6a are too high given the presence of chlorite instead of biotite, and the presence of chloritoid in sample LI13, indicating that this sample probably is not in equilibrium. This is supported by textural evidence (Fig. 5.3) that the garnet grew prior to the formation of the chl + par + mu foliation. However, the other two samples yield temperatures of ~400-500°C which are within the stability field of chloritoid (<550°C; Winkler, 1979) and are consistent with the observation that the garnets in these samples are in textural equilibrium with chlorite.

The three samples discussed here come from approximately (±50 m) the same structural level and are <1 km apart in small area near the base of the Triassic marbles that cover the basement of the Pierien unit in the Sarandoporou area, so it is unlikely that they would have experienced widely different P-T conditions. Although it is possible that small domains of M1 equilibrium mineral compositions survived retrogression under M2 and M3 metamorphism and associated deformation, it is apparent that further analysis would be needed to confirm the preliminary conclusion from samples 84LI12a and 84LI13 that M1 temperatures were ~450°C.

Phengite geobarometry

White micas become more phengitic in composition with increasing pressure (e.g. Velde, 1965; Cipriani et al, 1971; Sassi and Scolari, 1974 Guidotti and Sassi, 1976). The substitution of "phengite", or "celadonite" component, $(Fe,Mg)Si \leftrightarrow Al^{VI}Al^{IV}$) into the mica structure has been investigated experimentally

by Velde (1965) and Massonne and Schreyer (1987), and empirically (and qualitatively) by Guidotti (1973); Cipriani et al, 1971; and Guidotti and Sassi (1977, 1986). As summarized by Guidotti and Sassi, the Na-K substitution in white mica is a function of temperature, whereas the celadonite (phengite) substitution is a strong function of pressure and a weak function of temperature. The experimental studies of Velde (1965) and Massonne and Schreyer (1987) give widely different results for the quantitative relation between phengite content and pressure. The experiments were performed on the Fe-free system K_2O-MgO-Al_2O_3-SiO_2. Neither experiment was reversed, and both workers discussed problems related to the attainment of equilibrium during experimental runs, including the metastable presence of micas of the "wrong" polytype. The Velde (1965) experiments were performed at P<4.5 kb and extrapolated to higher pressures; this calibration shows a strong temperature dependence at pressures greater than 4 kb and temperatures greater than~400°C. The experiments of Massonne and Schreyer (1987) were conducted at pressures up to 24 kb and have shallower dP/dT slopes than the Velde calibration. The two calibrations are shown in Fig 5.19, along with the average phengite compositions for each structural unit; for clarity the detailed phengite data from the Olympos region (Table 5.4; Fig 5.16) have been omitted from this diagram, but comparison of Figs 5.16 and 5.19 indicates the range of compositions and possible pressures.

The extremely high phengite contents of virtually all metamorphic micas from the Olympos region (excluding coarse muscovite in granitic rocks interpreted to be relict (M0 or prior) phases indicates high metamorphic pressures. There is a systematic increase in phengite content with structural depth, from the Infrapierien unit (Si=3.35-3.45) to the Pierien unit (3.48-3.61) to the Ambelakia unit (3.58-3.64). The one Olympos flysch sample has phengite compositions intermediate between Infrapierien and Pierien rocks.

The small variation in phengite compositions within samples, even where more than one generation of phengite is observed, does not allow us to determine whether there may have been M1 phengites of a different composition than M2 and M3 phengites. However, the intergrowth of phengite, chlorite, and sodic amphibole in the Ambelakia and Pierien units suggests that the compositions in these units reflect M2 and M3 conditions. In the Infrapierien unit, two phengites (85OL50, 85OL32) have been dated by Ar/Ar and Rb/Sr as M1 in age (chapter 4), but experienced partial Ar loss during M2. These phengites are similar in composition to the phengite in sample 84LI26, which has been dated by Ar/Ar as M2, so it is

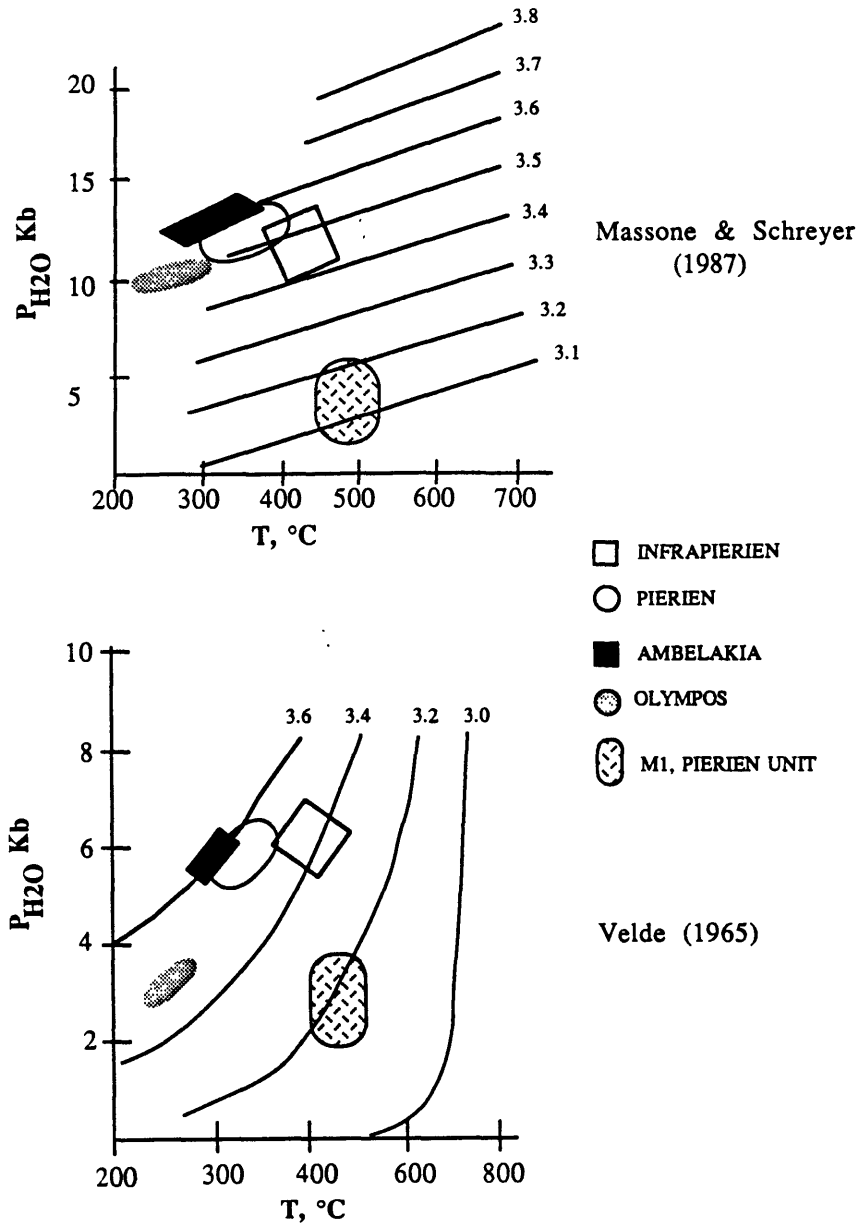

Figure 5.19 Comparison of calibrations of the phengite geobarometer by Massonne and Schreyer (1987) (top) and Velde (1965) (bottom). Averages for phengite data in each unit analyzed in this study are shown by the symbols; the shape of the symbols indicates the approximate range in phengite composition in each unit. The temperatures are not quantitatively constrained; however they are consistent with the available data (see text).

possible that either the pressure did not change while the temperature decreased from M1 to M2, or that any change was not recorded in the phengite component of the mica.

The mineral assemblages discussed above and the constraints from Ar/Ar data (Chapter 4) suggest that M2-M3 temperatures did not exceed ~350-400°C; at T=300-400°C, the Velde (1965) data imply the phengites in the study area formed at pressures varying from 3-4 kb in the Olympos unit to 5-7 kb in the Infrapierien unit to >6-7 kb in the Ambelakia unit. In contrast, the Massonne and Schreyer data imply pressures of ≥10 kb for the Olympos and Infrapierien units and 12-15 kb for the Ambelakia unit. Because the mineral assemblages of rocks in the Olympos region do not contain the limiting assemblage ksp + qtz + phlogopite in addition to phengite, these pressures should be minimum estimates. The crude barometric constraints from amphibole and pyroxene compositions discussed below and the phase equilibria discussed above are more consistent with the lower pressure estimates obtained from the Velde (1965) calibration and by comparison with HP/LT terranes in the Alps and the Franciscan complex of California, however, in detail, the actual pressures seem to be underestimated by the Velde calibration and overestimated by the Massonne and Schreyer calibration (compare Figures 5.18 and 5.19).

Because the calibrations discussed above only considered $MgSi \leftrightarrow Al^{VI}Al^{IV}$ exchange, it is probable that consideration of the effect of the addition of Fe to the system will resolve the differences between the Massonne and Schreyer (1987) data and the phase equilibria constraints. The phengites analyzed in this study contain significant amounts of FeO (Table 5.4), so any shift in the position of the curves would be reflected in the pressure estimated using this barometer.

Constraints from sodic and calcic amphibole compositions

Brown (1974,1977b) determined an empirical relation between the crossite content of calcic amphibole and the pressure of metamorphism. In the buffered assemblage Ca-amph -Na amph (solid solution) + mt + ab + chl + H_2O (± stilp, qtz), the Na(M4) content of the amphibole increases with increasing pressure. Brown (1974) identified the reaction

cr + ep + H2O = Ca-amph + ab + chl + Fe oxide (9)

as the buffering reaction in metabasites from New Zealand and Japan.

The Na content of actinolite will only be pressure dependent in assemblages containing ab + chl + mt. In crossite-bearing rocks which lack magnetite, there will

be less Na(M4) in actinolite (Brown, 1977b), and (pure) actinolite and crossite may coexist.

Maruyama et al (1986) conducted experiments on reactions thought to represent the transition from blueschist to greenschist facies. They discovered that in the buffered assemblage Na amphibole + ep + act + chl + ab + qtz, the Al_2O_3 content of sodic amphibole decreases with decreasing pressure, until the reaction (in the Fe-free system)

$$cz + gl + qtz + H20 = tr + chl + ab \qquad (7)$$

occurs at the low-pressure end of the blueschist facies field. In the system containing Fe_2O_3, it is the Fe^{3+}/Al content that increases with decreasing pressure, causing an effective Al_2O_3 decrease. They obtained consistent results between pressures estimated from Al_2O_3 content of sodic amphibole and those obtained from the jadeite content of pyroxene (see below).

In the Mt. Olympos region, most of the sodic amphiboles are crossite, and in Fe-rich rocks, riebeckite is more common. A plot of Al_2O_3 in sodic amphibole vs X_{Fe} (Fig 5.20) in chlorite shows the range of compositions in M2 and M3 assemblages that contain both minerals; where no chlorite is present, the amphibole composition is plotted at $X_{Fe} = 0$ (Fig 5.20). The lines indicating pressure are taken from Maruyama et al (1986) correlation of observed Al_2O_3 contents with pressures determined by other methods. For the calcic amphiboles, a plot of Na(M4) vs Al^{IV} (Fig. 5.13), after Brown (1977b) illustrates the variability in observed compositions. As most of these determinations are from the cores of grains rimmed by sodic amphibole, they probably reflect M1 metamorphic conditions and do not correspond to the same P-T conditions as those recorded by the sodic amphibole, and indeed this is the case, where the sodic amphiboles record higher pressures corresponding to M2 and M3 metamorphism.

These geobarometers have not been well-calibrated in terms of absolute pressure, as they are mainly based on comparison of several blueschist terranes, many of which do not have well-constrained P-T conditions themselves. This is particularly a problem for the lower pressure part of the blueschist facies, where jadeite is unstable. However, there seems to be a general consistency among the pressure determinations using amphibole compositions in the Ambelakia and Pierien units. Pressures obtained from Al_2O_3 content for M2-M3 (sodic) amphiboles are 4-5 kb for unbuffered assemblages and 5-6 kb for buffered ones. Using the Na(M4) content, the cores (M1?) record ~4-4.5 kb, and rims (M2?) record 6-7 kb (Figure 5.20).

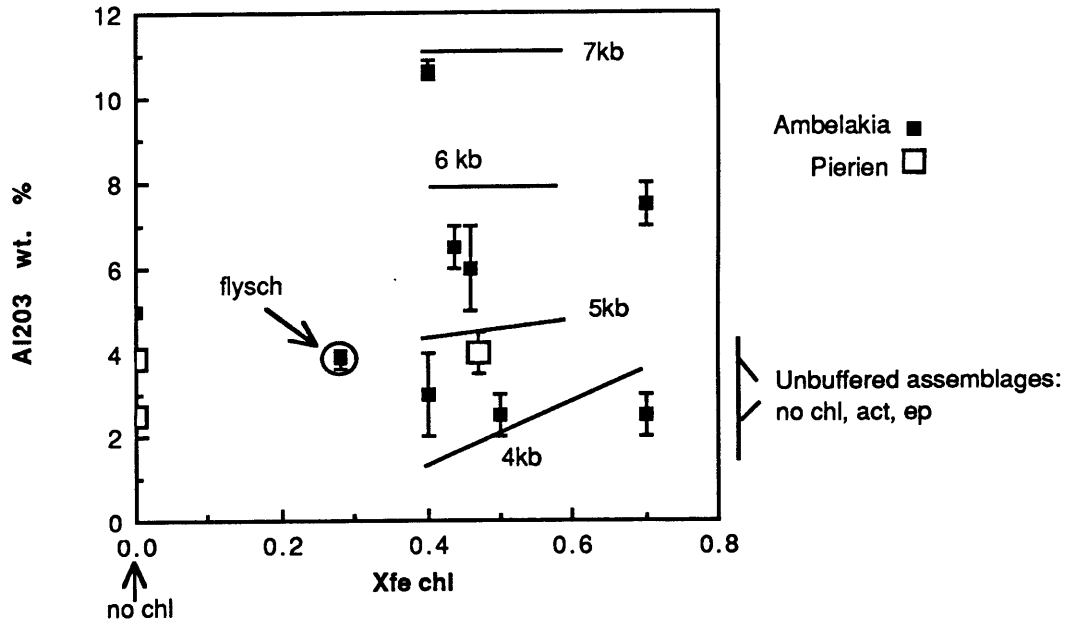

Figure 5.20: Plot of Al2O3 content in sodic amphibole vs X_{Fe} in chlorite. Where chlorite is not present in the sample, the amphibole composition is plotted at X_{Fe} = 0. Lines indicating pressure estimates are from Maruyama et al, (1986). Unbuffered assemblages only reflect minimum pressures.

Constraints from sodic pyroxene compositions

Pure jadeite has not been found in the Olympos region, although it is common in blueschists of the Cycladic belt further south in Greece. However, a sodic pyroxene, a solid solution between jadeite ($NaAlSi_2O_6$)-acmite ($NaFeSi_2O_6$) and augite ($Ca(Mg,Fe)Si_2O_6$) is locally present in the Pierien and Ambelakia unit. The reaction ab =jd + qtz has been investigated by a number of workers (Birch and LeComte, 1960; Newton and Smith, 1967; Newton and Kennedy, 1968; Boettcher and Wyllie, 1968; Popp and Gilbert, 1972; Holland, 1980). Most of the experiments were performed at high temperatures (~500-700°C) and extrapolations to lower (and higher) temperatures are inconsistent among the models. Although many workers use the Holland (1980) model, Maruyama and Liou (1987) discuss several inconsistencies in these data when applied at low temperatures, in particular where temperature is constrained by oxygen isotope data and well-calibrated phase equilibria, such as the presence of aragonite or pumpellyite. Maruyama and Liou (1987) use the Popp and Gilbert data, which puts the end-member reaction at higher pressure and has a shallower P-T slope. For comparison, the Popp and Gilbert (1972) and Holland (1980) curves are shown in Fig 5.18, along with isopleths of X_{Jd} calculated as discussed below.

The high acmite component in the sodic pyroxenes from the Pierien unit (85OL46, Table 5.3) allows use of an ideal one-site mixing model for Ac-Jd; however for the more augite-rich compositions in the Ambelakia unit (86RA5b, Table 5.3), a more complicated activity-composition model is required (e.g. Holland, 1983). Nevertheless most workers use $a_{Jd} = X_{Jd}$ (e.g. Brown and Ghent, 1983; Maruyama and Liou, 1987), which gives minimum pressure estimates. The compilation of Popp and Gilbert (1972) yields the following P-T points on the curve Jd_{100} + qtz = ab: 8.2 kb at 200°C and 14.5 kb at 500°C. Using the equation (Essene and Fyfe, 1967)

$$\frac{RT\ln X_{Jd}^{cpx}}{X_{ab}^{plag}} = \Delta V \Delta P \qquad (10)$$

with R = gas constant in cal/deg/mole; T in Kelvin, P in bars, and the ΔV for the reaction determined by Popp and Gilbert of 19.68 cm^3=0.407 cal/bar, we determined P=4.7 kb at 300°C for the Ambelakia sample (X_{Jd}=0.1) and P=7.4 kb at 300°C for the Pierien sample (X_{Jd} =0.3)

Although the Holland (1980) curve for pure jadeite is at lower pressures than that of Popp and Gilbert (1972), the non-ideal activity-composition models of Holland (1983) cause the X_{Jd} isopleths to converge at low temperatures, so that even low X_{Jd} compositions fall at high pressures (9-10 kb for Pierien; 7-9 kb for Ambelakia rocks). The absence of pure jadeite and the presence of albite in the samples from the study area constrains the maximum pressures to P<11 kb at 400°C, based on the data of Holland (1980).

The metamorphic conditions for events M1-M4 as constrained from the various methods discussed above are summarized in Table 5.6. My preferred P-T estimates, based on consideration of all the data together, despite the somewhat inconsistent results, is shown in Figure 5.18. The fields shown on this diagram are consistent with the phase equilibria constraints and with constraints from sodic amphibole and pyroxene compositions. However, the phase equilibria mainly provide minimum pressure estimates. The *relative* pressures between the different structural units are consistent with the phengite geobarometry, however, the *absolute* pressures can only be broadly constrained by the amphibole and pyroxene compositions, because the two phengite barometers yield such different estimates. It is impossible at this point to quantify the errors associated with these estimates because none of the reactions 1-7 in Figure 5.18 may be directly responsible for the observed parageneses in the samples studied. In addition, as the reactions are determined for the Fe-free system, any calibration uncertainties would not be directly applicable. The boxes indicated in Fig. 5.18 of ~±50°C, ±1 kb minimum are probably useful relative uncertainties and are in part constrained by the proximity of the reaction curves 1-7.

The preferred P-T estimates shown in Figure 5.18 are: M1: 2-4 kb, 425-550°C for the Infrapierien and Pierien units, with similar pressure and perhaps somewhat lower temperatures (350-450°C) for the ophiolite unit; M2 and M3: 4-6 kb, 350-450°C for the Infrapierien unit; 6-8 kb, 275-375°C for the Pierien unit, 6-8kb, 200-350°C for the Ambelakia unit, and 4-6 kb, 150-250°C for the Olympos unit. The textural relations for M2 and M3 are ambiguous(as discussed above), so it is difficult to determine separate P-T fields for these events in each unit,. Nevertheless, the conclusion in chapter 3 that the Olympos and Ambelakia/Pierien units were juxtaposed during D3/M3 suggests that M3 in the Ambelakia and Pierien units may occupy the lower temperature, lower pressure corners of the fields outlined in Figure 5.18, closer to the field outlined for the Olympos unit.

PRESSURE-TEMPERATURE-TIME EVOLUTION OF THE MT. OLYMPOS REGION: A SPECULATIVE TECTONIC MODEL

The broad pressure and temperature constraints on metamorphic events M1-M4, combined with the Ar/Ar data discussed in Chapter 4 and the structural data discussed in Chapter 3 allow us to interpret the metamorphic evolution of the Mt. Olympos region in terms of the regional tectonic setting of the convergence of the Apulian and European plates. I will first present a brief summary of the regional relations and the events discussed above.

Convergence between the Apulian and European plates and consumption of Mesozoic Tethyan ocean floor resulted in the obduction of ophiolites onto the Apulian margin during latest Jurassic to Early Cretaceous time. In many places in the Hellenides and Dinarides, this event is known to be pre-Albian, however, the ocean basin apparently did not completely close until latest Cretaceous to Paleocene time (Mercier et al, 1975; Vergely, 1976; Burchfiel, 1980; Sengor and Yilmaz, 1981). Continued convergence throughout the Cretaceous and Tertiary produced a west-vergent and westward-younging fold and thrust belt in the Hellenides that lay to the west of the suture zone (the Vardar zone; see chapter 1). Early Alpine events involved imbrication of the basement of both the Apulian and European (Rhodopean) plates, while younger (post-Eocene) deformation involved only the carbonate cover (at least in the thrust sheets that are visible in the mountain belt today). Deformation of this carbonate cover began in the Eocene in the Mt. Olympos region and progressed westward through Oligocene, Miocene, and Pliocene time, and continues today at the present Hellenic trench. The opening of the Aegean back-arc basin apparently began at ~12 Ma (Angelier, 1978).

In the Mt. Olympos region, I have demonstrated the existence of four distinct metamorphic events; at least the first three of these were associated with thrusting and folding of the basement and continental margin of the Apulian plate. The preferred interpretations of the pressure and temperatures of these events are shown in Figure 5.18 for each individual unit and in Figure 5.21 for each event M1-M4. M1 involved greenschist- to lower amphibolite-facies metamorphism of the ophiolite unit, the Infrapierien unit, and the Pierien unit during the early to middle Cretaceous (~100 Ma). P-T conditions at the metamorphic maximum may have been ~4 kb; 450-550°C. M2 resulted in blueschist-greenschist transition facies metamorphism in the Infrapierien unit and blueschist facies metamorphism in the Pierien and Ambelakia units during Paleocene-early Eocene time (~61-53 Ma).

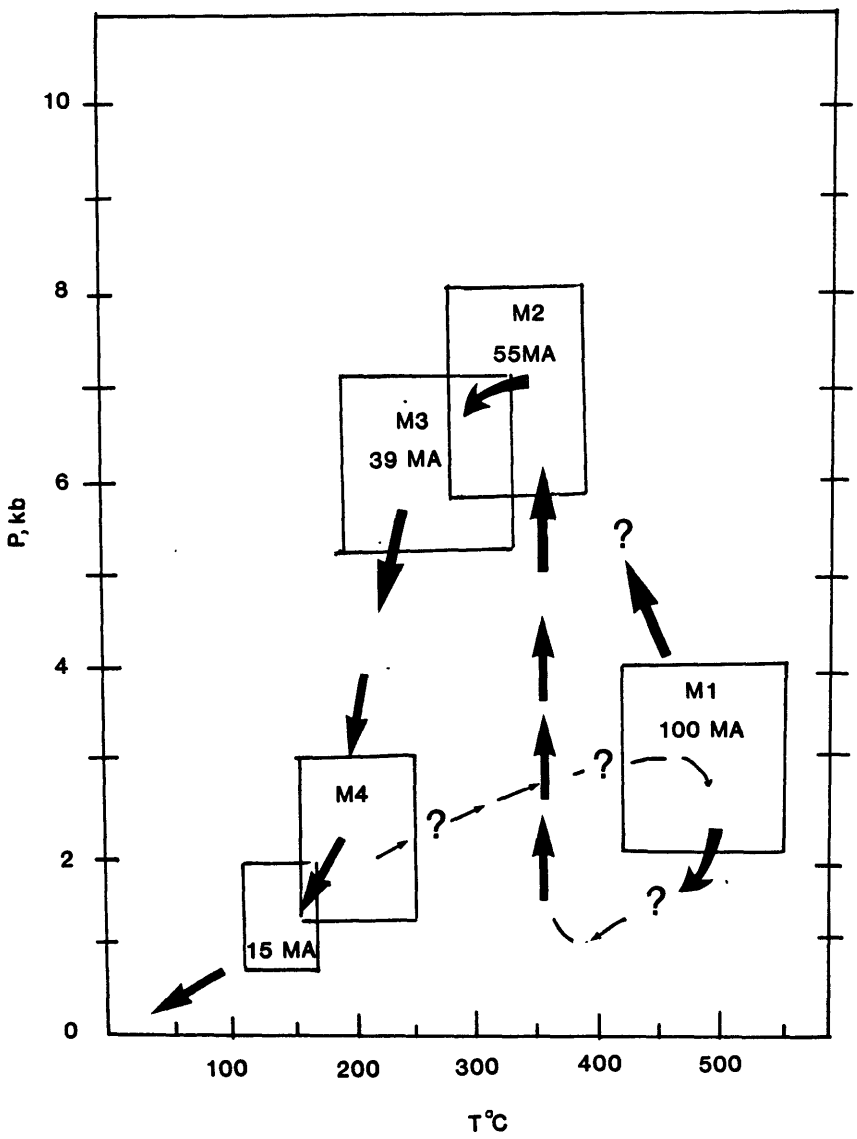

Figure 5.21 Schematic P-T diagram depicting the metamorphic evolution of rocks in the study area. Points labelled M1 to M4 are discussed in the text. Ages are constrained by Ar/Ar data discussed in more detail in chapter 4. Small arrows indicate possible prograde path leading to peak T conditions during M1; however we have no constraints on this path. Heavy arrows indicate the P-T-time evolution as interpreted from the data in this study; the path leading from M1 to M2 is speculative, but the path from M2-M4 is constrained by superposition of mineral assemblages.

Pressure and temperature estimates are ~4-6 kb, 350-400°C for the Infrapierien unit; ~6-8kb, ~275-375°C for the Pierien unit, and ~6-8 kb, 250-325°C for the Ambelakia unit. M3 produced blueschist-facies assemblages in the Pierien, Ambelakia, and Olympos units during late Eocene (36-42 Ma) time. P-T conditions may have been the same as M2 for the Pierien unit, but temperature seems to have decreased to <300°C, at P≤5-7 kb, for the Ambelakia unit; in the Olympos unit P ≥ 5 kb and T<225-250°C during M3. M4 resulted in prehnite-pumpellyite facies conditions in the Ambelakia, Olympos, and possibly the Pierien and Infrapierien units at P <4 kb, T<300°C. Constraints from Ar data indicate the structurally lowest parts of the Pierien unit (and thus probably the Ambelakia and Olympos units as well) passed through T~100-150°C during early to middle Miocene time (16-23 Ma).

The P-T-t evolution presented above and shown on Figure 5.21 indicates a counter-clockwise P-T path for the Infrapierien, Pierien, and Ambelakia units. There are no constraints on the shape of the path between M1 and M2, however, the metamorphic assemblages and the Ar data discussed in chapter 4 suggest that M1 conditions were the maximum temperatures reached by these units, so a continual (though potentially episodic) temperature decrease is required by the data. It is probable, given the 40Ma time span between M1 and M2, that M1 and M2 were related to completely different tectonic events and that the ophiolite, Infrapierien and Pierien units experienced some uplift and cooling during this time prior to subduction during M2. M2 and M3 resulted in the subduction of continental crust; the ophiolite unit was not affected, and appears to represent the "upper plate", along with higher thrust sheets of the Pierien and Infrapierien units, of this "A-type" (Bally, 1975) subduction zone. In this regard it is important to note that there is an overall decrease in temperature and probable increase in pressure from top to bottom within the nappe stack during the M2 and M3 events, although in detail, the error bars on P and T for each event overlap substantially. In addition there is an overall increase in pressure and decrease in temperature from M1 to M3, with M4 at still lower temperatures.

We interpret the metamorphic evolution of the Mt. Olympos region to reflect the episodic subduction of thin sheets of continental crust from Paleocene to late Eocene time, approximately contemporaneous with the closure of the ocean basin between Apulia and Europe. Basement imbrication apparently began <u>before</u> collision had occurred, during M1. The thrust sheets of the Infrapierien and Pierien units are thicker than the thrust sheets produced during D2 and D3, and peak

metamorphic temperatures were higher than in later events. The early (D1) event may have been similar to the "classic" overthrust models of Oxburgh and Turcotte (1974), that would produce a clockwise P-T path as modelled by England and Thompson (1984). The P-T loops modelled by these workers reflect the thrusting of hot rocks above cold rocks and thickening of the crust; relaxation of the perturbed geotherm requires that the rocks in the lower plate heat up after thrusting has stopped and during subsequent erosion. Such a path is in sharp contrast to the counter-clockwise path apparently travelled by the rocks in the Mt. Olympos region

Whether or not the M1 P-T path followed the "classic" pattern, shown by the lower curve in Fig. 5.18, this path was interrupted by the initiation of subduction within the continental crust. Events D2 and D3 resulted in a counter-clockwise P-T "loop" as thrust sheets were subducted to depths ≥20 km, at T≤350°C. It is probable that the Olympos unit was not subducted as deeply as the Ambelakia and Pierien units, so that these latter units experienced some decompression during D3. Later folding events were closely followed by normal faulting (discussed in more detail in Chapter 3), resulting in the decompression and cooling of the Olympos and Ambelakia units and at least the lower thrust sheets of the Pierien and Infrapierien units (M4). This decompression and cooling is consistent with these units being in the lower plate of a normal fault below the ophiolite nappe. While there is no evidence for contemporaneous heating followed by cooling of the ophiolite nappe during this time, it is probable that the rate of movement toward the surface (see below) was sufficiently fast and the depth reached by the upper plate was sufficiently shallow to prevent prograde (or subsequent retrograde) assemblages from forming in upper plate rocks.

Apparently, continued underthrusting of cool, surface sedimentary rocks, and the rapid evolution of thrusting to normal faulting and uplift (relative to the surface) allowed the underthrust rocks to remain at high-pressure, low-temperature conditions from ~60 Ma until ~40 Ma without heating up and obliterating the blueschist-facies assemblages. This is consistent with the thermal models of Draper and Bone, (1980); and Rubie, (1984), which suggest that under conditions where either the thrust zone is "refrigerated" by continual underthrusting of cool rocks as decompression is occurring, or if movement toward the surface occurs within ~26 Ma after subduction ceases, the blueschist-facies assemblages are preserved.

CONCLUSIONS

Four distinct metamorphic events occurred during continental basement imbrication, subduction, and uplift during the Alpine orogeny in Greece. The first event, M1, consists of upper greenschist to lower amphibolite facies metamorphism of the highest structural levels, the ophiolite, Infrapierien, and Pierien units. Based on dating of greenschist facies minerals, and regional considerations for the amphibolite facies event, M1 occurred during early to middle Cretaceous time. This was followed by continental subduction and metamorphism of the Infrapierien, Pierien, Ambelakia, and Olympos units under blueschist-greenschist transition facies (Infrapierien unit) to blueschist facies conditions during M2 and M3 in early Eocene and late Eocene time. M2 and M3 temperatures appear to decrease downward, from ~400°C in the Infrapierien unit to ~200°C in the Olympos unit. Maximum pressures of ~6-8 kb were recorded in the Ambelakia and Pierien units. Although the dominant lithology in the Infrapierien and Pierien basement units is granitic gneiss that contains only phengitic mica ± riebeckite and acmite as evidence for high-P metamorphism, metabasites within these units contain more typical blueschist-facies assemblages. The final metamorphic event, M4, reflects relative uplift and cooling through prehnite-pumpellyite facies conditions. Although decompression of the blueschists began during M3 as the Ambelakia and Pierien units were thrust over the Olympos unit, it was continued by normal faulting that may have begun during M4 and certainly occurred shortly thereafter. The period of extension and cooling was apparently broadly contemporaneous with opening of the Aegean back-arc basin, and was superimposed on the previously formed thrust belt.

Subduction of continental crust proceeded by stripping off thin thrust sheets of the basement and cover (<6 km overall thickness presently exposed above the Olympos unit) and by continual underthrusting of cool surface material to depths ≥20 km. Underthrusting maintained low temperatures at these depths for ~20 Ma until decompression and cooling occurred by erosion and normal faulting.

Chapter 6: CONCLUSIONS: TECTONIC HISTORY OF THE MT. OLYMPOS REGION

Introduction

The overall purpose of this thesis is to provide a detailed analysis of the deformation and metamorphism that occurred during the Alpine orogeny in the Mt. Olympos region, in order to better understand the thermal and structural evolution of the crust during collisional orogeny. After establishing that continental (A-type) subduction occurred in the Mt. Olympos region, I have attempted to constrain the timing and P-T conditions of the deformation and metamorphism that accompanied the collision of the Apulian plate with the European plate. Some of the general questions that I have attempted to address in this study of an A-type subduction zone include the following: 1) How deep can continental crust be subducted; how much of it disappears and how much of it is incorporated into the orogen? 2) How does the crust deform during A-type subduction and what are the pressure-temperature conditions during deformation? 3) If subducted crust is incorporated into the mountain belt, how does it become exposed at the surface? In this chapter, I will summarize the important results and conclusions that have been described in the previous chapters and will attempt to place the results in the context of these overall dynamic and tectonic questions.

Summary of constraints on the tectonic history of the Mt. Olympos region

Five major tectonostratigraphic units have been identified in the study area (Ch. 2): The lowest unit (Olympos unit), is composed of parautochthonous, very low-grade Mesozoic platform carbonates and Lutetian (Eocene) flysch. Previous workers have correlated this unit with the margin of the Apulian plate. This is overlain in thrust contact by the Ambelakia unit, a tectonically complex sequence of blueschist-facies metavolcanic and metasedimentary rocks. The third unit, the Pierien unit, consists of blueschist-facies Paleozoic granitic gneiss overlain by Mesozoic marble, internally imbricated and thrust over the Olympos and Ambelakia units. Blueschist -greenschist transition facies quartzofeldspathic and amphibolitic gneiss and schist of the fourth unit, the Infrapierien unit, are found in both thrust and normal fault contact over lower units. The highest unit, the ophiolite unit, includes late Jurassic ophiolitic rocks generally in normal fault contact over all lower units.

The tectonostratigraphic data indicate that the Mt. Olympos region is composed of several thrust nappes of upper continental crust; there are no oceanic rocks between the more external carbonate platform of the Olympos unit and the continental basement and cover nappes of the Pierien and Infrapierien units.

Inasmuch as the continental rocks have been deformed and metamorphosed under blueschist facies conditions, we can conclude that A-type subduction did occur in this part of the Hellenides. The observation that the ophiolites are present only at the highest structural levels, combined with the southwesterly direction of nappe transport interpreted from the structural analysis in chapter 3, implies that the oceanic basin from which the ophiolites were derived must have lain to the northeast of the Pelagonian zone, and that continental crust was continuous westward to the external Hellenides (i.e. the Pelagonian zone was part of the Apulian plate rather than a separate microcontinent). Another implication of the tectonostratigraphic data is that the Ambelakia unit was deposited on continental crust, and the presence of blueschist facies parageneses in both the Ambelakia and Pierien units indicates that upper continental crustal sequences were subducted to depths greater than 20 km during the Alpine orogeny.

Rb-Sr and $^{40}Ar/^{39}Ar$ ages from metamorphic rocks provide constraints on the absolute ages of several of the metamorphic and deformational episodes, and on the time-temperature history of the crust during orogenesis. The low temperatures of metamorphism in this part of the Hellenides have resulted in the preservation of age gradients in the Ar release spectra. This study shows that a wealth of information can be derived from $^{40}Ar/^{39}Ar$ dating of micas recrystallized at low temperatures, because the age gradients, interpreted to be diffusive loss profiles, can constrain both initial crystallization and younger metamorphic or deformational events which may be obscured by Rb/Sr mineral-whole rock dates.

Diffusive-loss profiles in 40Ar/39Ar spectra from hornblende, white mica, and biotite samples indicate that the upper two units preserve evidence of four distinct thermal events while the lower units were affected only by Eocene and younger events: 1) 295-300 Ma crystallization of granitic intrusions, with cooling from >550°C to <325°C by 285 Ma; 2) 100 Ma greenschist to blueschist-greenschist transition facies metamorphism (T~400-500°C) and imbrication of continental thrust sheets; 3) 53-61 Ma blueschist facies metamorphism and deformation of the basement and continental margin units (Ambelakia and Pierien units) at T<350-400°C; 4) 36-40 Ma thrusting of blueschists over the Olympos carbonate platform, and metamorphism at T~200-300°C. A fifth event is indicated by diffusive loss profiles in microcline spectra from the basement units. These are interpreted to reflect the beginning of decompression and cooling to T<100-150°C at 16-23 Ma, associated with normal faulting which continued until Quaternary time. During early to middle Tertiary time, a cooling rate of >10°C/Ma below peak metamorphic

temperatures of ~350-400°C allowed preservation of the blueschist facies mineral assemblages as they were uplifted from depths of >20 km.

Incomplete resetting of mica ages in all units constrains the temperature of metamorphism during continental (A-type) subduction to T≤350°C, the approximate closure temperature for Ar in muscovite. Micas grown during earlier metamorphic events lost ~10-40% 39Ar during subsequent HP/LT metamorphism. Ar release spectra from phengites grown during Eocene metamorphism and deformation record the ages of the Ar loss events.

A-type subduction resulted in the superposition of high pressure-low temperature assemblages on earlier higher T, lower P assemblages. Four metamorphic events can be distinguished; and earlier greenschist facies (M1), two blueschist facies events (M2,M3) and a late- to post-kinematic prehnite-pumpellyite facies event (M4). Pressures and temperatures of metamorphism have been estimated from phase assemblages and compositions of sodic amphiboles and pyroxenes and the phengite content of white mica. These constraints indicate M2-M3 conditions in the Olympos unit were T<250°C, P≥4-6 kb; in the Ambelakia unit P ~6-8 kb; T ~250-350°C and in the Pierien unit P ~6-8kb, T ~300-425°C. Blueschist-greenschist transition facies metamorphic conditions in the Infrapierien unit are estimated at P ~3-6kb and T ~350-400°C.

Structural and Metamorphic Evolution

Based on a combination of field, geochronologic, and petrologic data, I recognize the following sequence of events related to the collision of Apulia and Europe during the Alpine orogeny: D0): Greenschist-amphibolite facies metamorphism and deformation of the Pierien and Infrapierien units may include both early Alpine and Paleozoic events that can not be differentiated in the study area. D1) Thrust imbrication, mylonitization, NE-SW trending isoclinal folds, and blueschist-greenschist facies metamorphism of continental nappes (Pierien,Infrapierien) may have signaled the beginning of collision. Rb/Sr and 40Ar/39Ar ages indicate this event occurred at ~100 Ma. D2) Blueschist-facies metamorphism (6-8 kb, 350-400°C) of the Ambelakia unit and parts of the Pierien unit was accompanied by the formation of foliation, isoclinal folds, and NE-SW mineral lineation. Thrust faults that juxtaposed the Pierien,Infrapierien, and Ambelakia units were were active during this event, dated by Ar/Ar at ~53-61 Ma. D3) Thrusting of Ambelakia and Pierien units over the Olympos unit produced NE-SW trending isoclinal folds and stretching lineations and 50-300 m-thick mylonite

zones at thrust faults. Sense-of-shear indicators indicate the hanging wall moved towards the SW over the footwall. Thrusting produced ductile fabrics but did not overprint the blueschist-facies mineral assemblages formed during D2 with higher T phases. M3 blueschist facies metamorphism occurred at P>4-6 kb, T<250°C. D4) Thrust faults were folded by close to open NW-SE trending folds. These folds were previously interpreted (Barton, 1975) to represent NE-vergent thrusting of basement rocks over parautochthon; however, we can show that this event overprints the older, thrust-related fabrics. F4 folds rotated thrust faults to produce apparent normal sense of shear on thrusts on the western margin of the Olympos window. Late-kinematic prehnite-pumpellyite facies metamorphism may have occured during the D4 event. D5) Low-angle normal faults locally cut out 3-6 km of structural section and displace ophiolitic rocks down to NNE and NE so they are in fault contact with all lower structural units. D6) Broad folding about NE-SW axes caused further steepening of thrust surfaces and preserved low-angle normal fault segments on the NW and SE flanks of Mt. Olympos. D7) High-angle normal faults juxtapose ophiolitic rocks against the lower parts of the Olympos unit on the eastern flank of Mt. Olympos and cut Neogene and Quaternary conglomerates. Brittle extensional structures in D7 affect both hanging wall and footwall, indicating extension occurred at a relatively shallow level. Ar/Ar cooling ages indicate extension and uplift may have begun in early-middle Miocene time.

The SW-vergence of the major thrusting events (D2, D3) indicates that the ocean from which the ophiolitic terranes were derived originally lay NE of the carbonate platform of Apulia (Olympos unit). This in turn suggests that only one ocean basin lay between Apulia and Europe in this region prior to Paleocene collision. Intracontinental blueschist-facies metamorphism began prior to emplacement of blueschist facies rocks on lower grade Olympos unit carbonate rocks; however, high pressure-low temperature conditions continued as imbrication of the Apulian margin proceeded from NE to SW. Thrusting and normal faulting were both responsible for rapid decompression of blueschist-facies rocks without subsequent heating.

Characteristics of continental collision and subduction in the Hellenic Alps

In the Olympos region, convergence between Apulia and Europe resulted in episodic imbrication of thin (<5km) slices of the upper continental crust over a ~90-Ma period, from Early Cretaceous to post Eocene time (D1 to D4). Basement-

involved thrusting was SW- (foreland-) directed. The main regional implications of the D1-D3 geometric and kinematic data are twofold: 1) obduction and imbrication may have occurred prior to final collision between the Pelagonian basement (probably attached to the Apulian plate) and the European plate and 2) because the ophiolites rode "piggy-back" on top of the continental nappes and there was no oceanic terrane between theFlambouron and Olympos unit rocks, the oceanic rocks must have been derived from an ocean basin to the NE, and could not have come from a basin to the SW, as postulated by Barton (1976, 1979).

The relation between events D1-D4 and the presence of Oligocene and Miocene debris from the Pelagonian nappes in the Mesohellenic trough to the west (Brunn, 1956) records the overall cooling, uplift, and erosion of the thrust belt as deformation progressed toward the foreland. Metamorphic conditions progressed from blueschist-greenschist transition facies to blueschist to prehnite-pumpellyite facies with time and as lower structural levels were deformed. Continued compression and progression of deformation from the Olympos region toward the foreland is well documented by the progressive younging of flysch and the age of the youngest rocks deformed in the various thrust sheets of the external Hellenides (e.g. Jacobshagen et al, 1978).

Deformation under high pressure-low temperature conditions began at ~60 Ma, and continued until <40 Ma. Even though temperatures were low (<400°C; see chapters 4,5), both the crystalline basement rocks and carbonates behaved ductiley. D4 and later events occurred at lower pressures and temperatures. Apparently the continued underthrusting of cool surface rocks maintained a relatively low geothermal gradient because the blueschists are not overprinted by greenschist facies assemblages (e.g. Rubie, 1984).

Alpine deformation in the study area involved subduction of the continental basement of the Pelagonian zone. Thrust sheets of the Paleozoic basement rock are relatively thin (<500m locally), and must have been detached from the lower crust. The upper parts of the basement may have been subducted to depths >20 km, but were subsequently decompressed during thrusting above carbonate rocks of the Olympos unit, and uplifted and exhumed by the removal of tectonic overburden by normal faulting and erosion. Because the lower crustal portions of the Flambouron nappes are not exposed, and the crust here is only moderately thick (45-50 km; Makris, 1977; Geise et al, 1982), the lower parts of the continental crust may have been subducted into the mantle.

Significance of normal faulting and the preservation of blueschists

In addition to missing crustal material from below the basement thrust sheets, the present exposure of the blueschist facies rocks suggests that material is missing from above as well. Blueschist facies rocks metamorphosed at depths >20 km were underthrust by lower-grade rocks, but both low-angle and high-angle normal faults have also played an important role in the uplift and exhumation of the high pressure-low temperature rocks. The maximum apparent displacement that we can attribute to D5 and D7 normal faults is ~6 km, the approximate thickness of the exposed thrust sheets between the ophiolite unit and the Olympos unit. An unknown thickness of rocks could have been removed by erosion as clasts of Pelagonian metamorphic rocks are abundant in the Oligocene-Miocene Mesohellenic molasse basin west of the Olympos region. Nevertheless, the thickness of sediments in this basin cannot account for the apparent ~15 km discrepancy because the formation that contains abundant debris derived from the Pelagonian zone is only ~3 kilometers thick (Brunn, 1956; Papanikolaou et al, 1988).

We have been able to indirectly constrain the timing of the beginning of uplift of blueschist facies rocks to early to mid-Miocene time on the basis of cooling ages of potassium feldspars (Schermer et al, in press; chapter 4). Direct constraints from the age of faulted strata only bracket the timing of D5 low-angle normal faults to post Eocene, pre-Neogene time. It is clear, however, that normal faulting closely followed thrust faulting in the Olympos region, and may have been broadly contemporaneous with continued local folding (D6). In a regional context, D5 and D7 extensional deformation occurred while thrust faulting was still continuing to progress westward through the external Hellenides out to the present-day Hellenic trench.

The identification of low-angle normal faults that occur at the base of the ophiolite unit in the Mt. Olympos region has important regional implications. Low-angle faults are commonly mapped as thrust faults in the absence of good kinematic indicators; there is still some controversy over whether low-angle normal faults actually initiate or are active at low angles (e.g. Wernicke, 1981; Miller et al, 1983; Jackson, 1987). We are just beginning to realize the significance and characteristics of extensional deformation within convergent regimes (e.g. Royden and Burchfiel, 1987). The recognition of low-angle normal faults with significant displacement may require reexamination of contacts mapped as thrust faults throughout the Pelagonian zone and perhaps throughout the Hellenides.

The contemporaneous nature and parallelism of extensional and compressional structures in the Hellenides is a well-known and engimatic problem in Mediteranean tectonics. This "back-arc" extension may be occuring as a result of the collapse of over-thickened crust (e.g. Dalmayrac and Molnar, 1981; Royden and Burchfiel, 1987) or in response to slab retreat processes such as those described by Royden (1987) for the Appenines and Royden and Burchfiel (in press) for the Alps and Carpathians. While our data do not provide dynamic constraints on the processes responsible for extension in northern mainland Greece, we can demonstrate that normal faulting rapidly followed thrusting, caused significant (>3 km) uplift of metamorphic rocks in the Olympos region, and was essentially antiparallel to the thrusting direction.

A-type subduction: problems and possible solutions

In many collisional orogens, several hundreds of kilometers of shortening of upper crustal rocks are inferred from geologic relations. The absence of sufficient exposed basement to account for the shortened cover sequences requires subduction of significant amounts of lower crust (e.g. Milnes, 1978; Burchfiel, 1980; Bally, 1981; Hodges et al, 1983). However, several problems arise when we consider that the crust in the Mt. Olympos region was not only subducted, but also was metamorphosed at high P-low T conditions without overprinting by high temperature assemblages. The assumption that continental crust is too bouyant to be subducted has been examined by Molnar and Gray (1979), who concluded that tens to hundreds of kilometers of continental crust could be subducted if either the upper crust was detached from the lower crust or if an oceanic plate was attached to the leading edge of the subducted continental plate. As both of these conditions appear to have obtained in the Olympos region, subduction of the upper parts of the crust to ~20 km depth is not unreasonable.

The second problem associated with A-type subduction zones is a thermal one: how can underthrusting and thickening of radiogenic crust result in the low-temperature metamorphic conditions that we observe in the rocks from the Olympos region? A related question is that onced the blueschists are formed, how are they exhumed and exposed at the surface without evidence of overprinting at higher temperatures? Thermal modelling of continental thrust sheets predicts increasing temperatures as the perturbed geotherm relaxes during uplift and erosion (e.g. Oxburgh and Turcotte, 1974; England and Thompson, 1984). Thus, in order to produce high pressure-low temperature conditions, it is necessary to

"refrigerate" the A-type subduction zone so that the geothermal gradients of <20°C/km necessary for blueschist formation are maintained (e.g. Draper and Bone, 1980; Rubie, 1984). The thermal models of Draper and Bone (1980) and Rubie (1984) suggest that under conditions where either the thrust zone is refrigerated by continual underthrusting of cool surface rocks as decompression is occurring, or if movement toward the surface occurs within ~26 Ma after subduction ceases, the blueschist-facies assemblages are preserved.

In the Mt. Olympos region, both continued underthrusting of cool, surface sedimentary rocks, and the rapid evolution of thrusting to normal faulting and uplift (relative to the surface) allowed the underthrust rocks to remain at high-pressure, low-temperature conditions from ~60 Ma until ~40 Ma without heating up and obliterating the blueschist-facies assemblages. Because the thrust sheets in the Olympos region are thin (<5km), if they were underthrust and remained at depth under conditions of a normal continental geothermal gradient (20-30°C/km) for ~10^5 years, a temperature increase of ~100-200°C would occur that would be sufficient to overprint blueschist-facies rocks with greenschist-facies assemblages.

Average cooling rates calculated from the geochronologic data using the different closure temperatures and different ages of minerals (Ch. 4) are ~10°C/Ma. Assuming a 10-20°C/km subduction zone geothermal gradient, this cooling rate can be converted to a 0.5-1 mm/yr "uplift rate" (reflecting movement toward the surface). The P-T conditions and ages of the M3 and M4 events (~20 km in 38 Ma to a maximum average rate between M3 and M4 of 18 km in <13 Ma) result in "uplift rates" of 0.6-1.4 mm/yr. These relatively slow average rates would not be fast enough to preserve the blueschist-facies assemblages unless the uplift was synchronous with continued refrigeration of the subduction zone by underplating surface sediments (e.g. Rubie, 1984; Cloos, 1985). Nonetheless, it is also possible that tectonic uplift (e.g. by normal faulting) resulted in short-lived rapid uplift rates during one or more events. The data presented here are insufficient to resolve a shorter cooling interval than the 13 Ma (minimum) that may have elapsed between the closure of Ar diffusion in white mica (36 Ma) and microcline (23 Ma; see chapter 4). While we cannot quantitatively constrain the mechanism and rate of uplift of the blueschists, we have nonetheless documented both an extended period (~20 Ma) of high pressure-low temperature metamorphism and significant younger normal fault events. Thus it seems likely that both syn-subduction underplating and uplift along normal faults were important in the preservation of blueschists in the Mt. Olympos region.

CONCLUSIONS

The detailed study of the structural geology, geochronology, and metamorphic petrology in the Mt. Olympos region provides the following constraints on the Alpine tectonic evolution of this part of the Hellenides: 1) Deformation occurred over a long period of time (>90 Ma) and was episodic, but produced consistent foreland-directed emplacement of thin upper crustal thrust sheets throughout most of Cretaceous-Eocene time. 2) Deformation of the continental crust of the Pelagonian zone included basement-involved thrusting and continental subduction that may have begun before collision of the Apulian and European plates. 3) Metamorphic conditions evolved from upper greenschist-amphibolite facies to blueschist facies to prehnite-pumpellyite facies with time. 4) Compressional deformation was rapidly followed by extension. The present-day geometry of the metamorphic nappes is controlled by the extensional deformation, which was partly responsible for rapid uplift of the blueschist-facies rocks, and was synchronous with overall convergence in Hellenic arc. 5) Syn-subduction cooling and decompression combined with tectonic denudation to form and preserve blueschist-facies assemblages in thrust sheets of detached upper to middle continental crust.

REFERENCES

Albaréde, F., 1978, The recovery of spatial isotope distributions from stepwise degassing data: Earth and Planetary Science Letters, v. 39, p. 387-397.

Altherr, R., Harre, W., Kreuzer, H., Okrusch, M., and Seidel, E., 1977, On the age of the high-pressure metamorphism in Sifnos (Greece): Preliminary report, in Biju-Duval, B., and Montadert,L., eds., International Symposium on the structural history of Med. Basins, Split: Paris, Editions Technip, p. 315-316.

Altherr, R., Schliestedt, M., Okrusch, M., Siedel, E., Kreuzer, H., Harre, W., Lenz, H., Wendt, I., and Wagner, G.A., 1979, Geochronology of high-pressure rocks on Sifnos (Cyclades, Greece): Contrib. Mineral. Petrol, v. 70, p. 245-255.

Ampferer, O., 1906, Über das Bewegungsbild von Faltengebirgen: Jahrb. Geol. Reichsanst, v. 56, p. 539-622.

Angelier, J., 1978, Tectonic evolution of the Hellenic Arc since the late Miocene: Tectonophysics, v. 4, p. 23-36.

Aubouin, J., 1959, Contribution a l'étude géologique de la Grèce septentrionale: les confins de l'Epire et de la Thessalie: Annales Géologiques des Pays Helléniques, v. 10, p. 483.

Bally, A.W., 1975, A geodynamic scenario for hydrocarbon occurrences: Proc. Ninth World Petroleum Congress, v. 2, p. 33-44.

Bally, A.W., 1981, Thoughts on the tectonics of folded belts, in K.R. McClay and N.J. Price,, Thrust and Nappe Tectonics: Oxford, Blackwell, p. 13-32.

Baroz, F., Bebien, J., and Ikenne, M., 1987, An example of high-pressure low-temperature metamorphic rocks from an island-arc: the Paikon Series (Innermost Hellenides, Greece): Jour. Metamorphic Geol., v. 5, p. 509-527.

Barton, C.M., 1975a, Mount Olympos, Greece: A study of thrust belt tectonics: Cambridge University, England, Unpubl. Ph.D. Thesis, 260 p.

Barton, C.M., 1975b, Mount Olympos, Greece: New light on an old window: Journal of the Geological Society of London, v. 131, p. 389-396.

Barton, C.M., 1976, The tectonic vector and emplacement age of an allochthonous basement slice in the Olympos area, N.E. Greece: Soc. Géol. de France Bull., v. 18, p. 253-258.

Barton, C.M., 1979, Structural evolution of the Vardar root zone, northern Greece: Discussion and reply: Geological Society of America Bulletin, v. 90 Pt. 1, p. 125-128.

Barton, C.M., and England, P.C. , 1979, Shear heating at the Olympos (Greece) thrust and the deformation properties of carbonates at geological strain rates: Geological Society of America Bulletin, v. 90, p. 483-492.

Bebien, J., Ohnenstetter, M., and Vergely, P., 1980, Diversity of the Greek ophiolites: birth of oceanic basins in transcurrent systems: Ofioliti, Special Issue, v. 2, p. 129-197.

Bell, T.H., Etheridge, 1973, Microstructures of mylonites and their descriptive terminology: Lithos, v. 6, p. 337-348.

Bence, A.E., and Albee, A.L., 1968, Empirical correction factors for the electron microanalysis of silicates and oxides: Journal of Geology, v. 76, p. 382-403.

Birch, F., and Le Comte, P., 1960, Temperature-pressure plane for albite composition: American Journal of Science, v. 258, p. 209-217.

Blake, M.C., Jr., Bonneau, M., Geyssant, J., Kienast, J.R., Lepvrier, C., Maluski, H., and Papanikolaou, D. , 1981, A geologic reconnaissance of the Cycladic blueschist belt, Greece : Geological Society of America Bulletin, Pt. 1, v. 92, p. 247-254..

Boettcher, A.L., and Wyllie, P.J., 1968, Jadeite stability measured in the presence of silicate liquids in the system $NaAlSiO_4$-SiO_2-H_2O: Geochimica Cosmochimia Acta, v. 32, p. 999-1012.

Brodie, K.H., and Rutter, E.H., 1985, On the relationship between deformation and metamorphism with special reference to the behaviour of basic rocks, in Thompson, A.B., and Rubie, D.C., eds., Metamorphic Reactions: Kinetics, Textures, and Deformation: New York, Springer-Verlag, p. 118-137.

Brown, E.H., 1974, Comparison of the mineralogy and phase relations of blueschists from the North Cascades, Washington, and greenschists from Otago, New Zealand: Geological Society of America Bulletin, v. 85, p. 333-344.

Brown, E.H., 1977a, Phase equilibria among pumpellyite, lawsonite, epidote, and associated minerals in low grade metamorphic rocks: Contrib. Mineral. Petrol., v. 64, p. 123-136.

Brown, E.H., 1977b, The crossite content of Ca-amphibole as a guide to pressure of metamorphism: Jour. Petrol., v. 18, p. 53-72.

Brown, E.H., and Bradshaw, J.Y., 1979, Phase relations of pyroxene and amphibole in greenstone, blueschist and eclogite of the Franciscan Complex, California: Contrib. Mineral. Petrol. , v. 71, p. 67-83.

Brown, E.H., and Ghent, E.D., 1983, Mineralogy and phase relations in the blueschist facies of the Black Butte and Ball Rock areas, northern California Coast Ranges: American Mineralogist, v. 68, p. 365-372.

Brunn, J.H., 1956, Contribution a l'etude geologique du Pinde sepentrional et d'une partie de la Macedoine: Ann. Geol. Pays. Hellen., v. 8, 258 pp.

Burchfiel, B.C., 1980, Eastern European Alpine System and the Carpathian orocline as an example of collision tectonics: Tectonophysics, v. 63, p. 31-61.

Carlson, W.D., and Rosenfeld, J.L., 1981, Optical determination of topotactic aragonite-calcite growth kinetics: Metamorphic implications: Journal of Geology, v. 89, p. 615-638.

Carman, J.H., and Gilbert, M.C., 1983, Experimental studies on glaucophane stability: American Journal of Science, v. 283-A, p. 414-437.

Carmignani, L., Franceschelli, M., Pertusati, P.C., Memmi, I., and Ricci, C.A., 1982, An example of compositional control of the celadonitic content of muscovite and the incoming of biotite in metapelites (Nurra, NW Sardinia): Neues Jahrbuch Miner. Abh., v. H.7, p. 289-311.

Cawthorn, R.G., and Collerson, K.D., 1974, The recalculation of pyroxene end-member parameters and the estimation of ferrous and ferric iron content from electron microprobe analyses: American Mineralogist, v. 59, p. 1203-1208.

Celet, P., and Ferrière, J., 1978, Les Hellénides internes: Le Pélagonien: Eclogae Geol. Helv., v. 73, p. 467-495.

Chopin, C., and Maluski, H., 1980, 40Ar-39Ar dating of high pressure metamorphic micas from the Gran Paradiso area (Western Alps): evidence against the blocking temperature concept: Contrib. Mineral. Petrol., v. 74, p. 109-122.

Chopin, C., and Schreyer, W., 1983, Magnesiocarpholite and magnesiochloritoid: two index minerals of petlitic blueschists and their preliminary phase relations in the model system MgO-Al_2O_3-SiO_2-H_2O: American Journal of Science, v. 283-A, p. 72-96.

Cipriani, C., Sassi, F.P., and Scolari, A., 1971, Metamorphic white micas: definition of paragenetic field: Schweiz. Miner. Petr. Mitt., v. 51, p. 259-302.

Cloos, M., 1985, Thermal evolution of convergent plate margins: thermal modelling and re-evaluation of isotopic Ar-ages for blueschist in the Franciscan Complex of California: : Tectonics, v. 4, p. 421-433.

Coombs, D.S., 1960, Lower grade mineral facies in New Zealand: 21st International Geological Congress, Copenhagen, 1960, v. 13, p. 339-351.

Crawford, W.A., and Hoersch, A.L., 1972, Calcite-aragonite equilibrium from 50°C to 150°C: American Mineralogist, v. 57, p. 995-998.

Dalmayrac, B., and Molnar, P., 1981, Parallel thrust and normal faulting in Peru and constraints on the state of stress: Earth and Planetary Science Letters, v. 55, p. 473-481.

Dalrymple, G.B., Alexander, E.C., Jr., Lanphere, M.A., and Kraker, G.P. , 1981, Irradiation of samples for 40Ar/39Ar dating using the Geological Survey TRIGA Reactor: U.S. Geol. Survey Professional Paper 1176 1176, 55 pp.

Dalrymple, G.B., and Lanphere, M.A., 1969, Potassium-argon dating: San Francisco, W.H. Freeman, 258 p.

Davis, E., and Migiros, G., 1979, Granitic intrusions into the metamorphic system in eastern Thessaly: Pract. Acad. Ath., v. 54, p. 349-367.

Deer, W.A., Howie, R.A., and Zussman, J., 1966, An introduction to the rock-forming minerals: London, Longman, 528 p.

Dercourt, J., Aubouin, J., Savoyat, E., Desprairies, A., Terry, J., Vergely, P., Mercier, J., Godfriaux, I., Ferrière, J., Fleury, J.-J., Celet, P., and Clément, B., 1977, Réunion extraordinaire de la Société Géologique de France en Grèce: Bull. Soc. Géol. France, v. XIX, p. 5-70.

Dercourt, J., Zonenshain, L.P., Ricou, L.-E., Kazmin, V.G., Le Pichon, X., Knipper, A.L., Grandjacquet, C., Sbortshikov, I.M., Geyssant, J., Lepvrier, C., Pechersky, D.H., Sibuet, J.-C, Savostin, L.A., Sorokhtin, O., Westphal, M., Bazhenov, M.L., and Biju-duval, B., 1986, Geological evolution of the Tethys belt from the Atlantic to the Pamirs since the Lias: Tectonophysics, v. 123, p. 241-315.

Dérycke, F., and Godfriaux, I., 1976, Métamorphismes "schistes bleus et schistes verts" dans l'Ossa et le Bas-Olympe (Thessalie-Grèce): Bull. Societé. Géol. France, (7), v. XVIII, p. 252.

Dérycke, F., and Godfriaux, I., 1978, Découverte de microfaunes paléogènes dans le flysch métamorphique de Spilia (Ossa, Grèce): Comptes Rendus de l'Académie des Sciences (Paris), v. 286, p. 555-558.

Dickenson, M.P., Hewitt, D.A., 1986, A garnet-chlorite geothermometer [abs.]: Geological Society of America Abstracts with Programs, v. 18, p. 584.

Dodson, M.H., 1973, Closure temperature in cooling geochronological and petrological systems: Contrib. Mineral. Petrol., v. 40, p. 259-274.

Draper, G., and Bone, R., 1980, Denudation rates, thermal evolution, and preservation of blueschist terrains: Journal of Geology, v. 89, p. 601-613.

Dungan, M.A., Vance, J.A., and Blanchard, D.P., 1983, Geochemistry of the Shuksan greenschists and blueschists, North Cascades, Washington: variably fractionated and altered metabasalts of oceanic affinity: Contrib. Mineral. Petrol., v. 82, p. 131-146.

Durr St., Altherr, R., Keller, M., and Siedel, E., 1978, The median Aegean crystalline belt: stratigraphy, structure, metamorphism, and magmatism, in Cloos, H., and others, eds., Alps, Appenines, Hellenides: Stuttgart, E. Schweizerbart'sche Verlagbuchhandlung, p. 455-477.

England, P.C., and Richardson, S.W., 1977, The influence of erosion upon the mineral facies of rocks from different metamorphic environments: Jour. Geol. Soc. Lond., v. 134, p. 201-213.

England, P.C., and Thompson, A.B., 1984, Pressure-temperature-time paths of regional metamorphism, Part I: Heat transfer during the evolution of regions of thickened continental crust: Journal of Petrology, v. 25, p. 894-928.

Essene, E.J., and Fyfe, W.S., 1967, Omphacite in Californian metamorphic rocks: Contrib. Mineral. Petrol., v. 15, p. 1-23.

Ferriere, J., 1982, Paléogéographies et tectoniques superposées dans les Hellénides internes: les massifs de l'Othrys et du Pélion (Grèce continentale): Société Géologique du Nord Publ. 8, p. 982.

Ferry, J.M., and Spear, F.S., 1978, Experimental calibration of the partitioning of Fe and Mg between garnet and biotite: Contrib. Mineral. Petrol., v. 69, p. 315-318.

Fleck, R.D., Sutter, J.F., and Elliot, D., 1977, Interpretation of discordant 40Ar/39Ar age-spectra of Mesozoic tholeiites from Antarctica: Geochimica Cosmochimica Acta, v. 41, p. 15-32.

Fleury, J.J., and Godfriaux, I., 1974, Arguments pour l'attribution de la série de la fenêtre de l'Olympe (Grèce) à la zone de Gavrovro-Tripolitza: présence de fossiles du Maestrichtien et de l'Eocène inférieur (et moyen?): Ann. Géol. Soc. Nord., v. 94, p. 149-156.

Geise, P., Reutter, K-J., Jacobshagen, V., and Nicolich, R., 1982, Explosion seismic crustal studies in the Alpine-Mediterranean region and their implications to tectonic processes: Alpine-Mediterranean Geodynamics, v. , p. 39-74.

Gill, J., 1981, Orogenic andesites and plate tectonics: Berlin, Springer Verlag,

Godfriaux, I., 1977, L'Olympe: Bull. Soc. Géol. France, v. XIX, p. 45-49.

Godfriaux, I. , 1968, Etude géologique de la région de l'Olympe (Grèce): Annales Géologiques des Pays Helléniques, v. 19, p. 1-271.

Godfriaux, I. and Pichon, J.F., 1979, Sur L'importance des evenements tectoniques et metamorphique d'age tertiaire en Thessalie septentrionale (Olympe, Ossa, Flambouron): Ann. Soc. Geol. Nord., v. 99, p. 367-376.

Godfriaux, I., Ferrière, J., and Schmitt, A., 1988, Le developpement en contexte continental d'un metamorphism HP/BT: Les "schistes bleus" Tertiares Thessaliens: Bulletin of the Geological Society of Greece, v. XX, p. 175-192.

Godfriaux, I., Laduron, D., Pichon, J.F., and Schmitt, A., 1979, Analyse á la microsonde électronique de quelques assemblages minéralogiques des métabasites en Ossa (Thessalie septentrionale, Grèce): VIIé R.A.S.T., Lyon, p. 225.

Guidotti, C.V., 1973, Compositional variation of muscovite as a function of metamorphic grade and assemblage in metapelites from N.W. Maine: Contrib. Mineral. Petrol., v. 42, p. 33-42.

Guidotti, C.V., and Sassi, F.P., 1976, Muscovite as a petrogenetic indicator mineral in pelitic schists: Neues Jahrbuch Miner. Abh., v. 127, p. 97-142.

Guidotti, C.V., and Sassi, F.P., 1986, Classification and correlation of metamorphic facies series by means of muscovite b0 data from low-grade metapelites: Neues Jahrbuch Miner. Abh., v. 153, p. 363-380.

Hansen, E., 1966, Methods of deducing slip-line orientations from the geometry of folds: Annual Report, Director of the Geophysical Lab., Wash., D.C., v. 65, p. 387-405.

Hansen, E., 1971, Strain Facies: Berlin, Springer-Verlag, 207 p.

Harrison, T.M., 1981, Diffusion of 40Ar in hornblende: Contrib. Mineral. Petrol., v. 78, p. 324-331.

Harrison, T.M., Duncan, I., and McDougall, I., 1985, Diffusion of 40Ar in biotite: Temperature, pressure, and compositional effects: Geochimica Cosmochimica Acta, v. 49, p. 2461-2468.

Harrison, T.M., and Heizler, Matthew T., 1987, Multiple trapped Argon isotopic components revealed by 40Ar/39Ar isochron analysis [abs.]: EOS (American Geophysical Union Transactions), v. 68, p. 431.

Harrison, T.M., McDougall, 1980a, Investigations of an intrusive contact, northwest Nelson, New Zealand-I. Thermal, chronological and isotopic constraints: Geochimica Cosmochimica Acta, v. 44, p. 1985-2003.

Harrison, T.M., and McDougall, I., 1980b, Investigations of an intrusive contact, northwest Nelson, New Zealand-II. Diffusion of radiogenic and excess 40Ar in hornblende revealed by 40Ar/39Ar age spectrum analysis: Geochimica Cosmochimica Acta, v. 44, p. 2005-2020.

Harrison, T.M., and McDougall, I., 1981, Excess 40Ar in metamorphic rocks from Broken Hill, New South Wales: implications for 40Ar/39Ar age spectra and the thermal history of the region: Earth and Planetary Science Letters, v. 55, p. 123-149.

Harrison, T.M., and McDougall, I., 1982, The thermal significance of potassium feldspar K-Ar ages inferred from 40Ar/39Ar age spectrum results: Geochimica Cosmochimica Acta, v. 46, p. 1811-1820.

Hart, S.R., and Brooks, C., 1977, The Geochemistry and evolution of the early Precambrian mantle: Contrib. Mineral. Petrol., v. 61, p. 109-128.

Hawthorne, F.C., 1981, Crystal chemistry of the amphiboles, in D.R. Veblen,, Ed., Amphiboles and other Hydrous Pyriboles-Mineralogy: Reviews in Mineralogy 9A, p. 1-102.

Heizler, Matthew T., and Harrison, T. Mark, 1988, Multiple trapped Argon isotopic components revealed by 40Ar/39Ar isochron analysis: Geochimica Cosmochimica Acta, v. 52, p. 1295-1303.

Hellman, P.L., Smith, R.E., and Henderson, P., 1979, The mobility of the rare earth elements: evidence and implications from selected terrains affected by burial metamorphism: Contrib. Mineral. Petrol., v. 71, p. 23-44.

Henjes-Kunst, F., and Kreuzer, H., 1982, Isotopic dating of pre-Alpidic rocks from the island of Ios (Cyclades, Greece): Contrib. Mineral. Petrol., v. 80, p. 245-253.

Hodges, K.V., Bartley, J.M., and Burchfiel, B.C., 1982, Structural evolution of an A-type subduction zone, Lofoten-Rombak area, northern Scandinavian Caledonides: Tectonics, v. 1, p. 441-462.

Hodges, K.V., and Crowley, P.D., 1985, Error estimation and empirical geothemobarometry for pelitic systems: American Mineralogist, v. 70, p. 702-709.

Hodges, K.V., and McKenna, L.W., 1987, Realistic propagation of uncertainties in geologic thermobarometry: American Mineralogist, v. 72, p. 671-680.

Hodges, K.V., and Spear, F.S., 1982, Geothermometry, geobarometry, and the Al2SiO5 triple point at Mt. Moosilauke, New Hampshire: American Mineralogist, v. 67, p. 1118-1134.

Holland, T.J.B., 1980, The reaction albite=jadeite+quartz determined experimentally in the range 600-1200 C: Am. Min., v. 65, p. 129-134.

Holland, T.J.B., 1983, The experimental determination of activities in disordered and short-range ordered jadeitic pyroxenes: Contrib. Mineral. Petrol., v. 82, p. 214-220.

Huneke, J.C., and Smith, S.P., 1976, The realities of recoil: 39Ar recoil out of small grains and anomalous age patterns in 39Ar-40Ar dating: Proc. 7th Lunar Sci Conf , p. 1987-2008.

Hynes, A., 1980, Carbonatization and mobility of Ti, Y, and Zr in Ascot formation metabasalts, SE Quebec: Contrib. Mineral. Petrol, v. 75, p. 79-87.

Hynes, A.J., Nisbet, E.G., Smith, A.G., Welland, M.J., and Rex, D.C., 1972, Spreading and emplacement ages of some ophiolites in the Othris region (eastern central Greece): Zeitschrift der Deutschen Geologischen Gesellschaft, v. 123, p. 455-468.

Institute for Geology and Mining Research, Greece, Geologic map of Greece, Elassona 1:50,000 sheet: Athens, I.G.M.E.

Institute for Geology and Mining Research, Greece, Geologic map of Greece, Deskati 1:50,000 sheet: Athens, I.G.M.E.

Jacobshagen, V., Dürr, S., Kockel, F., Kopp, K.O., and Kowalezyyk, G., 1978, Structure and geodynamic evolution of the Aegean region, in Cloos, H., and others, eds., Alps, Appenines, Hellenides: Stuttgart, E. Schweizerbart'sche Verlagbuchhandlung, p. 538-564.

Johannes, W., and Puhan, D., 1971, The calcite-aragonite transition, reinvestigated: Contrib. Mineral. Petrol., v. 31, p. 28-38.

Katsikatsos, G. and Migiros, G., 1987, Geologic map of Greece, Rapsani sheet, scale 1:50,000: Athens, I.G.M.E.

Katsikatsos, G., Migiros, G., and Vidakis, M., 1982, Structure géologique de la region de Thessalie Orientale (Grèce): Ann. Géol. Soc. Nord, v. C1, p. 177-188.

Koons, P.O., and Thompson, A.B., 1985, Non-mafic rocks in the greenschist, blueschist and eclogite facies: Chem. Geol., v. 50, p. 3-30.

Kvale, A., 1953, Linear structures and their relation to movement in the Caledonides of Scandinavia and Scotland: Quart. Jour. Geol. Soc. Lond., v. 109, p. 51-73.

Lang, H.M, and Rice, J.M., 1985, Geothermometry, geobarometry and T-X(Fe-Mg) relations in metapelites, Snow Peak, Northern Idaho: Journal of Petrology, v. 26, p. 889-924.

Latsoudas, Ch., 1985, Geologic map of Greece, Kondariotissa 1:50,000 sheet: Athens, I.G.M.E.

Liou, J.G., 1971, P-T stabilities of laumontite, wairakite, lawsonite, and related minerals in the system $CaAl_2Si_2O_8$-SiO_2-H_2O: Journal of Petrology, v. 12, p. 379-411.

Liou, J.G., Maruyama, S., and Cho, M., 1985, Phase equilibria and mineral pargeneses of metabasites in low grade metamorphism: Mineralogical Magazine, v. 49, p. 321-333.

Lister, G.S., and Snoke, A.W., 1984, S-C Mylonites: Journal of Structural Geology, v. 6, p. 617-638.

Lister, G.S., and Williams, P.F., 1979, Fabric development in shear zones: theoretical controls and observed phenomena: Journal of Structural Geology, v. 1, p. 283-297.

Makris, J., 1977, Geophysical investigations of the Hellenides: Hamburger Geophys. Einzelschriften 27, 98 pp.

Maresch, W.V., 1977, Experimental studies on glaucophane: an analysis of present knowledge: Tectonophysics, v. 43, p. 109-125.

Maruyama, S. Cho, M., and Liou, J.G., 1986, Experimental investigations of blueschist-greenschist transition equilibria: Pressure dependence of Al_2O_3 contents in sodic amphiboles- A new geobarometer: Geol. Soc. Am. Mem., v. 164, p. 1-16.

Maruyama, S., and Liou, J.G., 1987, Clinopyroxene- a mineral telescoped through the processes of blueschist facies metamorphism: J. Metamorphic. Petrol., v. 5, p. 529-552.

Maruyama, S., Liou, J.G., and Sasakura, Y., 1985, Low-temperature recrystallization of Franciscan greywackes from Pacheco Pass, California: Mineral. Mag., v. 49, p. 345-355.

Massone, H.-J., and Schreyer, W., 1986, High-pressure syntheses and X-ray properties of white micas in the system K_2O-MgO-Al_2O_3-SiO_2-H_2O: Neues Jahrbuch Miner. Abh., v. 153, p. 177-215.

Massone, H.-J., and Schreyer, W., 1987, Phengite geobarometry based on the limiting assemblage with K-feldspar, phlogopite, and quartz: Contrib. Mineral. Petrol., v. 96, p. 212-224.

Mattinson, J.M., 1978, Age, origin and thermal histories of some plutonic rocks from the Salinian Block of California: Contrib. Mineral. Petrol., v. 67, p. 233-245.

Mercier, J., 1968, Étude géologique des zones internes des Hellenides en Macèdoine centrale (Grèce): Annales Géologiques des Pays Helléniques, v. 20, p. 1-792.

Mercier, J., Vergely, P., and Bebien, J. , 1975, Les ophiolites helléniques "obductés" au Jurassique supérieur sont-elles les vestiges d'un océan tethysien ou d'une mer marginale péri-européene?: Comptes Rendus Sommaires des Seances de la Soc. Géol. de France, v. 17, p. 108-112.

Migiros, G., 1985, Geologic map of Greece, Gonnoi 1:50,000 sheet: Athens, I.G.M.E.

Milnes, A.G., 1978, Structural zones and continental collision, central Alps: Tectonophysics, v. 47, p. 369-392.

Miyashiro, A., 1957, The chemistry, optics and genesis of the alkali amphiboles: Journal of Faculty of Science, University of Tokyo, Section II, v. 11, p. 219-272.

Molnar, P., and Gray, D., 1979, Subduction of continental lithosphere: some constraints and uncertainties: Geology, v. 7, p. 58-62.

Mountrakis, D., 1984, Structural evolution of the Pelagonian zone in northwestern Macedonia, Greece, in Dixon, J.E., and Robertson, A.H.F, eds., The Geological Evolution of the Eastern Mediterranean: Geol. Soc. Lond. Spec. Publ. 17, p. 581-590.

Mountrakis, D., 1986, The Pelagonian zone in Greece: A polyphase-deformed fragment of the Cimmerian continent and its role in the geotectonic evolution of the eastern Mediterranean: Jour. Geology, v. 94, p. 335-347.

Mountrakis, D., Sapountzis, E., Kilias, A., Eleftheriadis, G., and Christofides, G., 1983, Paleogeographic conditions in the western Pelagonian margin in Greece during the initial rifting of the continental area: Canadian Journal of Earth Science, v. 20, p. 1673-1681.

Nakajima, T., Banno, S., and Suzuki, T., 1977, Reactions leading to the disappearance of pumpellyite in low-grade metamorphic rocks of the Sanbagawa metamorphic belt in Central Shikoku, Japan: Jour. Petrol., v. 18, p. 163-284.

Nance, Damian, 1981, Tectonic history of a segment of the Pelagonian zone, northeastern Greece: Canadian Journal of Earth Science, v. 18, p. 1111-1126.

Nance, R. D., 1977, The Livadi mafic-ultramafic complex and its metamorphic basement, N.E. Greece: Cambridge University, England, Unpubl. Ph.D Thesis, 183 p.

Newton, R.C., and Kennedy, G.C., 1968, Jadeite, analcite, nepheline, and albite at high temperatures and pressures: American Journal of Science, v. 266, p. 728-735.

Newton, R.C., and Smith, J.V., 1967, Investigations concerning breakdown of albite at depth in the earth: Journal of Geology, v. 45, p. 268-286.

Nitsch, K. H., 1971, Contrib. Mineral. Petrol., v. 30, p. 240-260.

Okay, A.I., and Özgul, N., 1984, HP/LT metamorphism and the structure of the Alanya Massif, southern Turkey: an allochthonous composite tectonic sheet, in Dixon, J.E., and Robertson, A.H.F, eds., The Geological Evolution of the Eastern Mediterranean, Geol. Soc. Lond. Spec. Publ. 17,p. 429-439.

Oxburgh, E.R., and Turcotte, D.L., 1974, Thermal gradients and regional metamorphism in overthrust terrains with special reference to the Eastern Alps: Schweiz. Miner. Petrogr. Mitt. , v. 54, p. 641-662.

Papanikolaou, D., and Stojanov, R., 1983, Geological correlations between the Greek and Yugoslav parts of the Pelagonian metamorphic belt: I.G.C.P. No. 5 Newsletter, v. 5, p. 146-152.

Papanikolaou, D., and Zambetakis-Lekkas, A., 1980, Nouvelles observations et datation de la base de la série pélagonienne (s.s.) dans la région de Kastoria, Grece: Comptes Rendues Acad. Sci. Paris, serie D, v. 291, p. 155-158.

Papanikolaou, D.J., 1984a, An introduction to the geology of Greece: the pre-Alpine units. I.G.C.P. Project #5, Field Guide: Athens, Univ. Athens, Dept. Geology, 64 pp.

Papanikolaou, D.J., 1984b, The three metamorphic belts of the Hellenides: a review and a kinematic interpretation, in Dixon, J.E., and Robertson, A.H.F, eds., The Geological Evolution of the Eastern Mediterranean: Geol. Soc. Lond. Spec. Publ. 17, p. 649-659.

Papanikolaou, D.J., 1978, Contribution to the geology of the Aegean sea: the island of Andros: Annales Géologiques des Pays Helléniques, v. 29, p. 477-553.

Papanikolaou, D.J., 1981, Some problems concerning correlations within the metamorphic belts of the Pelagonian and the Rhodope, in Karamata, S. and Sassi, F.P., eds., : I.G.C.P. Project #5 Newletter 3, p. 119-123.

Papanikolaou, D.J., Lekkas, E., Mariolakis, I., and Mirkou, R., 1988, Geodynamic evolution of the Mesohellenic basin: Bulletin of the Geological Society of Greece, v. XX, p. 17-36.

Pearce, J.A., and Cann, J.R., 1973, Tectonic setting of basic volcanic rocks determined using trace element analyses: Earth and Planetary Science Letters, v. 19, p. 290-300.

Pearce, Julian A., and Norry, Michael J., 1979, Petrogenetic implications of Ti, Zr, Y, and Nb variations in volcanic rocks: Contrib. Mineral. Petrol., v. 69, p. 33-47.

Popp, P.K., and Gilbert, M.C., 1972, Stability of acmite-jadeite pyroxenes at low pressure: American Mineralogist, v. 57, p. 1210-1231.

Purdy, J.W., and Jaeger, E., 1976, K-Ar ages on rock forming minerals from the Central Alps: Mem. 1st. Geol. Univ. Padova , p. 1-32.

Ramsay, J.G., 1967, Folding and fracturing of rocks: New York, McGraw-Hill, 568 p.

Ricou, L.E., Marcoux, J., and Whitechurch, H., 1984, The Mesozoic organization of the Taurides: one or several ocean basins?, in Dixon, J.E., and Robertson, A.H.F, eds., The Geological Evolution of the Eastern Mediterranean: Geol. Soc. Lond. Spec. Publ. 17, p. 349-360.

Robbins, G.A., 1972, Radiogenic argon diffusion in muscovite under hydrothermal conditions [M.S. thesis]: Providence, Rhode Island, Brown University, 42 pp.

Robertson, A.H.F., and Dixon, J.E., 1984, Introduction: aspects of the geological evolution of the Eastern Mediterranean, in Dixon, J.E., and Robertson, A.H.F, eds., Geological Evolution of the Eastern Mediterranean: Geol. Soc. Lond. Spec. Publ. 17, p. 1-74.

Roddick, J.C., 1978, The application of isochron diagrams in 40Ar/39Ar dating: a discussion: Earth and Planetary Science Letters, v. 41, p. 233-244.

Roddick, J.C., Cameron, W.E., and Smith, A.G., 1979, Permo-Triassic 40Ar/39Ar ages from Greek ophiolites and associated rocks: Nature, v. 279, p. 788-790.

Royden, L.H., 1987, Segmentation and configuration of subducted lithosphere in Italy: an important control on thrust belt and fore-deep evolution: Geology, v. 15, p. 714-717.

Royden, L.H., and Burchfiel, B.C., 1987, Thin-skinned N-S extension within the convergent Himalayan region: gravitational collapse of a Miocene topographic front, in Coward, M.P., J.F.Dewey, and P.L. Hancock, eds., Continental Extensional Tectonics: Geol. Soc. Lond. Special Pub. 28, p. 611-619.

Royse, F., Warner, M.A., and Reese, D.C., 1975, Thrust belt structural geometry and related stratigraphic problems, Wyoming-Idaho-northern Utah: R.M.A.G. Symposium on Deep Drilling Frontiers in Central Rocky Mountains, v. , p. 41-54.

Rubie, D.C., 1984, A thermal-tectonic model for high-pressure metamorphism and deformation in the Sesia Zone, Western Alps: Journal of Geology, v. 92, p. 21-36.

Sassi, F.P., and Scolari, A., 1974, The b0 value of the potassic white micas as a barometric indicator in low grade metamorphism: Contrib. Mineral. Petrol., v. 45, p. 143-152.

Schermer, E. R., 1987, Age and tectonic significance of blueschist from the Mt. Olympos region, Greece: EOS (American Geophysical Union Transactions), v. 68, p. 431.

Schermer, E.R., and Burchfiel., B.C., 1987, Alpine deformation and metamorphism during continental subduction and uplift, Mt. Olympos region, Greece [abs.]: Geological Society of America Abstracts with Programs, v. 19, p. 832.

Schermer, E.R., Lux, D.R., and Burchfiel, B.C., in press, Age and tectonic significance of metamorphic events in the Mt. Olympos region, Greece: Bull. Geol. Soc. Greece.

Schmitt, A., 1981a, L'ensemble volcanique et sédimentaire de l'unité tectonique de l'Ossa (Thessalie orientale, Grèce): Ann. Geol. Soc. Nord, v. C1, p. 23-38.

Schmitt, A., 1981b, Sur la présence de Cunéolines dans les marbres charriés sur la plateforme de l'Olympe (Thessalie - Grèce): Ann. Soc. Geol. Belgium, v. 104, p. 61-65.

Schmitt, A., 1982, Tectonique tangentielle dans la fenetre de L'Olympe (Thessalie, Grece): IX'ieme R.A.S.T., v. 9, p. 572.

Schmitt, A., 1983, Nouvelles contributions a l'étude géologique des Pieria, de l'Olympe, et de l'Ossa (Grèce du Nord):`These, Faculte Polytechnique de Mons (Begium), 215 p.

Sengor, A.M.C., and Yilmaz, Y., 1981, Tethyan evolution of Turkey: a plate tectonic approach: Tectonophysics, v. 75, p. 181-241.

Simpson, C., and Schmid, S.M., 1983, Microstructural indicators of sense of shear in shear zones: Geological Society of America Bulletin, v. 94, p. 1281-1288.

Smith, A.G., 1971, Alpine deformation and the oceanic areas of the Tethys, Mediterranean and Atlantic: Geological Society of America Bulletin, v. 82, p. 2039-2070.

Smith, A.G., Hynes, A.J., Menzies, M., Nisbet, E.G., Price, I., Welland, M.J.P., and Ferriére, J., 1975, The stratigraphy of the Othris mountains, eastern central Greece: a deformed Mesozoic continental margin sequence: Eclog. Geol. Helv., v. 68, p. 463-481.

Smith, A.G., and Woodcock, N.H., 1976, The earliest Mesozoic structures in the Othris region, Eastern Central Greece: Bulletin, Geological Society of France, v. 18, p. 245-351.

Smith, A.G., Woodcock, N.H., and Naylor, M.A., 1979, The structural evolution of a Mesozoic continental margin, Othris mountains, Greece: Journal of the Geological Society of London, v. 136, p. 589-603.

Spear, F.S., and Kimball, K.L., 1984, Recamp- a FORTRAN IV program for estimating Fe3+ contents in amphiboles: Computers & Geosciences, v. 10, p. 317-325.

Spray, J.G., Bébien, J., Rex, D.C., and Roddick, J.C., 1984, Age constraints on the igneous and metamorphic evolution of the Hellenic-Dinaric ophiolites, in Dixon, J.E., and Robertson, A.H.F, eds., Geological Evolution of the Eastern Mediterranean: Geol. Soc. Lond. Spec. Publ. 17, p. 619-627.

Spray, J.G., and Roddick,J.C., 1980, Petrology and 40Ar/39 Ar geochronology of some Hellenic subophiolitic rocks: Contrib. Mineral. Petrol., v. 72, p. 43-55.

Steiger, R.H., and Jaeger, E., 1977, Subcommission on geochronology: convention on the use of decay constants in geo- and cosmochronology: Earth and Planetary Science Letters, v. 36, p. 359-362.

Taylor, S.R., and McLennan, S.M., 1985, The Continental Crust: its Composition and Evolution: Oxford, Blackwell Scientific Publications, 312 p.

Thiébault, F., and Triboulet, C., 1984, Alpine metamorphism and deformation in phyllites nappes (external Hellenides, southern Peloponnesus, Greece): Geodynamic implications: Journal of Geology, v. 92, p. 185-199.

Thompson, R.N., Morrison, M.A., Hendry, G.L., and Parry, S.J., 1984, An assessment of the relative roles of crust and mantle in magma genesis: an elemental approach: Philos. Trans. Roy. Soc. London, v. A310, p. 549-590.

Trumpy, R., 1963, Sur les racines des nappes helvetiques, in M.D. Delga,, ed., Livre a la Memoire du Professeur Paul Fallot: Paris, Société Géologique de France, p. 419-430.

Turner, F.J., 1981, Metamorphic Petrology: Mineralogical, Field, and Tectonic Aspects: New York, McGraw-Hill, 524 p.

Turner, G., 1968, The distribution of potassium and argon in chondrites, in Ahrens, L.H., ed., Origin and distribution of the elements: London, Pergamon Press, p. 387-398.

Velde, B., 1965, Phengite micas: Synthesis, stability, and natural occurrence: American Journal of Science, v. 263, p. 886-913.

Velde, B., 1967, Si+4 content of natural phengites: Contrib. Mineral. Petrol., v. 14, p. 250-258.

Vergely, P., 1976, Chevauchment vers l'ouest et retrocharriage vers l'est des ophiolites; deux phases tectoniques au cours du Jurassique supérior-Eocrétace dans les Hellenides internes: Soc. Géol. de France Bull., v. 18, p. 233-246.

Vergely, P., 1984, Tectonique des ophiolites dans les Hellenides internes (déformations, métamorphismes et phénomènes sédimentaires): Consequences sur l'evolution des regions Tethysiennes occidentalesThese, Universite de Paris-Sud, Centre D'Orsay, no. 2924: 661 p.

Wagner, G.A., Reimer, G.M., and Jaeger, E., 1977, Cooling ages derived by apatite fission track, mica Rb-Sr and K-Ar dating: the uplift and cooling history of the Central Alps: Mem. 1st Geol. Mineral. Univ. Padova 30.

Winkler, H.G.F., 1979, Petrogenesis of metamorphic rocks, Fifth edition: New York, Springer-Verlag, 348 p.

Wood, David A., Joron, Jean-Louis, and Treuil, Michel, 1979, A re-appraisal of the use of trace elements to classify and discriminate between magma series erupted in different tectonic settings: Earth and Planetary Science Letters, v. 45, p. 326-336.

Yarwood, G.A., 1978, The structure, metamorphism, and geochronolgoy of the High Pieria mountains, N. Greece: Unpubl. Ph.D. thesis, Scotland, Univ. of Edinburgh.

Yarwood, G.A., and Aftalion, M., 1976, Field relations and U-Pb geochronology of a granite from the Pelagonian zone of the Hellenides (High Pieria, Greece): Soc. Géol. de France Bull., v. 18, p. 259-264.

Yarwood, G.A., and Dixon, J.E., 1977, Lower Cretaceous and younger thrusting in the Pelagonian rocks of the High Pieria, Greece: Sixth Colloq. Aegean Region, Athens , p. 269-280.

York, D., 1966, Least-squares fitting of a straight line: Canadian Journal of Physics, v. 44, p. 1079-1086.

York, D., 1969, Least squares fitting of a straight line with correlated errors: Earth and Planetary Science Letters, v. 5, p. 320-324.

Zeitler, P.K., and Fitzgerald, J.D., 1986, Saddle-shaped 40Ar/39Ar age spectra from young, microstructurally complex potassium feldspars: Geochimica Cosmochimica Acta, v. 50, p. 1185-1199.

Zimmerman, J., Jr., and Ross, J.V., 1976, Structural evolution of the Vardar root zone, northern Greece: Geological Society of America Bulletin, v. 87, p. 1547-1550.

Zimmerman, J., Jr., and Ross, J.V., 1979, Structural evolution of the Vardar root zone, northern Greece, Discussion and reply: Geological Society of America Bulletin, v. 90, Pt. 1, p. 125-128.

PLATE 1

GEOLOGIC MAP OF THE MT. OLYMPOS REGION , N. THESSALY, GREECE

ELIZABETH R. SCHERMER

1988

EXPLANATION

QUATERNARY AND NEOGENE

- Qal — Unconsolidated alluvium
- Qc — Alluvium, consolidated alluvium, scree, cemented talus, landslide, covered areas, undivided
- Qol — Older, consolidated alluvium; boulder conglomerate
- Ngc — Conglomerate, sandstone, marl

OPHIOLITE UNIT

- Mzm — Marble, cipolin: Mzm1: blocks in melange; Mzm2: ?Upper Cretaceous overlap sequence
- cs — calcareous schist, chloritic phyllite, psammite
- ms — chlorite-phengite schist
- sp/spg — sp: serpentinite, serpentinized pyroxenite, dunite, mafic phyllite; spg: undifferentiated serpentinite, amphibolite
- ga — amphibolite gneiss, schist, gabbro, greenstone

FLAMBOURON INFRAPIERIEN UNIT

RELATIVE AGES BELOW TJm UNKNOWN

PALEAMBELA NAPPE
- TJm — Triassic-Jurassic thick-bedded marble
- fgs — felsic muscovite -epidote schist, augen schist, fine-grained gneiss

LIVADI NAPPE
- TJm — Triassic-Jurassic thick-bedded marble
- fbs — blue and purple mica schist
- fa2 — fa2: amphibolite gneiss, schist, intercalated with felsic gneiss, mica schist
- lm — lm: thin grey marble layers in fa2
- fam — fam: massive amphibolite layers in fa2
- fg2 — granitic gneiss, minor amphibolite

ZILIANA NAPPE
- TJm — Triassic-Jurassic thick-bedded marble
- fa3 — amphibolite schist and gneiss, mica schist, and chlorite schist

FLAMBOURON PIERIEN UNIT

- TJm — Triassic-Jurassic thick-bedded marble
- fa1 — amphibolite schist, augen schist, mica schist
- fg1 — granitic gneiss, lesser amphibolite gneiss
- fgg — granitic gneiss
- fgr — weakly-foliated biotite granite, biotite-hornblende granodiorite: 295 Ma (Ar/Ar)

RELATIVE AGES UNKNOWN

AMBELAKIA UNIT

RELATIVE AGES UNKNOWN
- as — blue and green mica schist, metabasalt, felsic mica gneiss
- am — thin-bedded marble, cherty marble, interbedded with blueschist and psammite
- acs — calcareous schist; metasandstone, phyllite

OLYMPOS UNIT

- Tf — Eocene flysch; sandstone, siltstone, calcareous siltstone, pebble conglomerate
- Tl — Eocene thin-bedded limestone intercalations in Tf
- KTl — Upper Cretaceous-Eocene thin- to thick-bedded crystalline limestone

- Depositional contact (inferred, concealed)
- Thrust fault (dipping 20, overturned, inferred, concealed)
- High-angle reverse fault
- High-angle normal fault (ball on downthrown side; dipping 60, inferred, concealed)
- Low-angle normal fault or listric normal fault (dipping 20, inferred,concealed)
- Bedding (overturned, horizontal, vertical)
- Primary metamorphic foliation (mylonitic foliation in mylonite zones)
- Mylonite zone
- Secondary foliation where two are visible in outcrop
- Axial plane of minor fold
- Mineral lineation, stretching lineation
- Antiform
- Synform
- Overturned antiform
- Overturned synform
- Minor fold axis, phase unknown
- F1 minor fold axis (plunging 20, symmetric, fold pair with NW vergence)
- F2 minor fold axis (plunging 20, symmetric, fold pair with NW vergence)
- F3 minor fold axis (plunging 20, symmetric, fold pair with NW vergence)
- F4 minor fold axis (plunging 20, symmetric, fold pair with NW vergence)

LOCATION OF MAP SHEETS

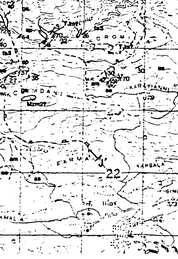

N

0 1 2 3 4

Kilometers

TOPOGRAPHIC BASE FROM HELLENIC ARMY
GEOGRAPHICAL SERVICE 1970

PLATE 2

GEOLOGIC CROSS SECTIONS OF THE MT. OLYMPOS REGION, GREECE

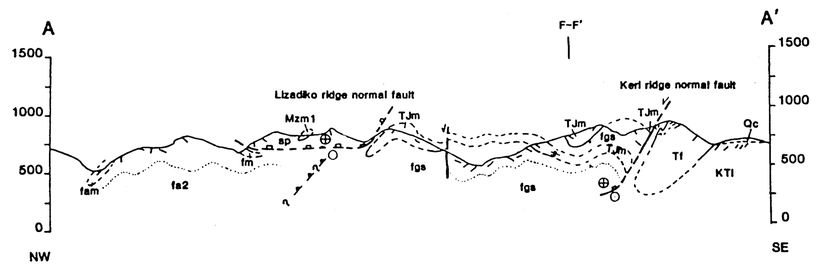

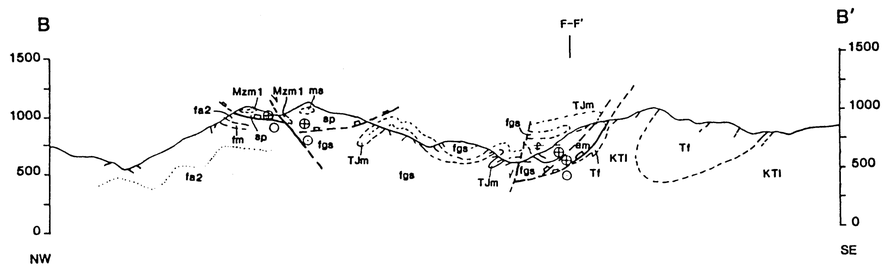

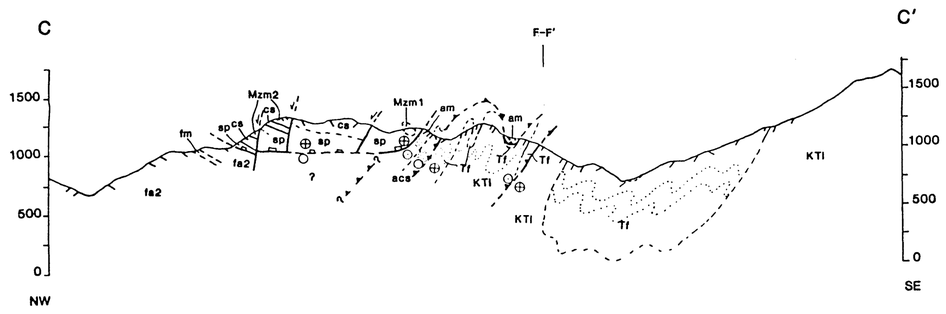

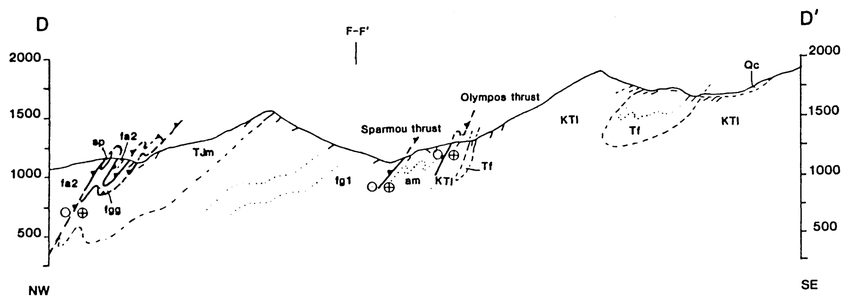

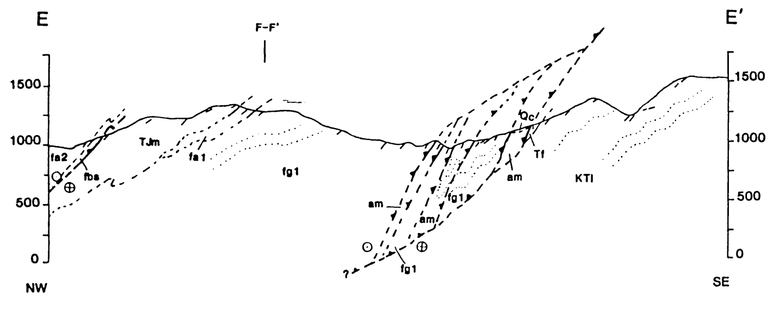

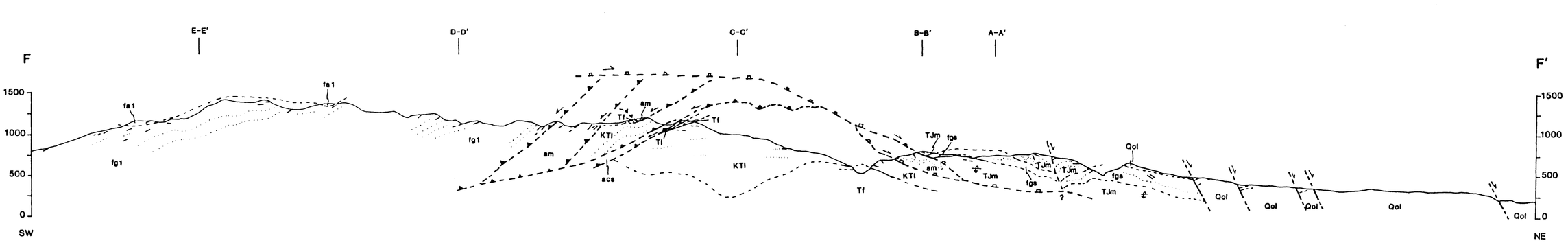

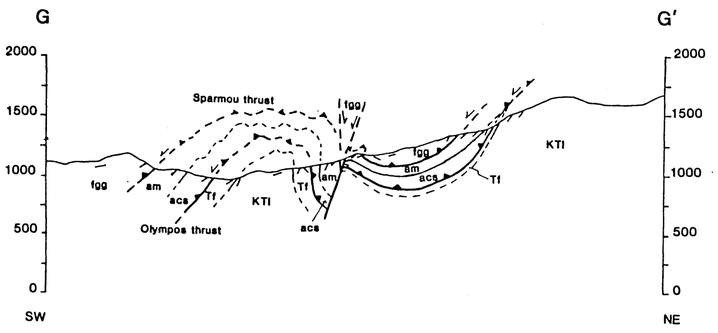

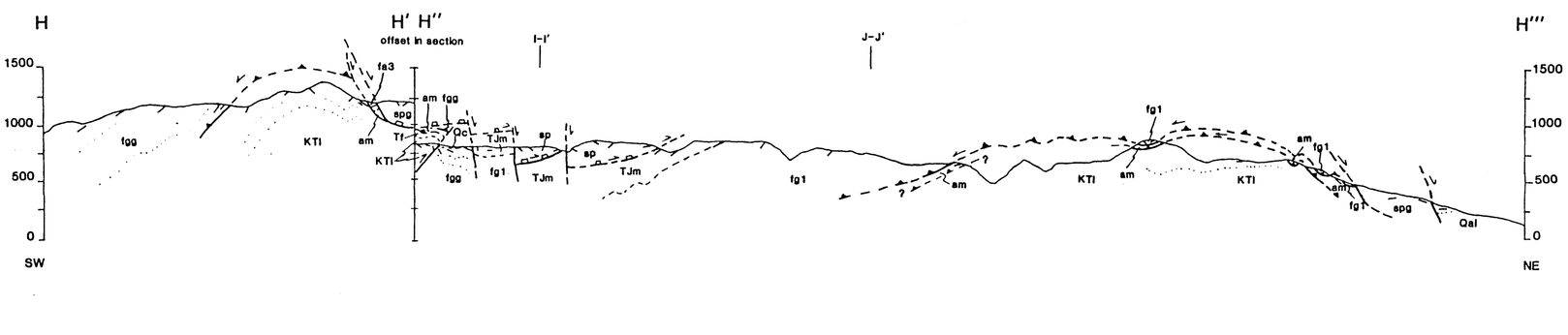

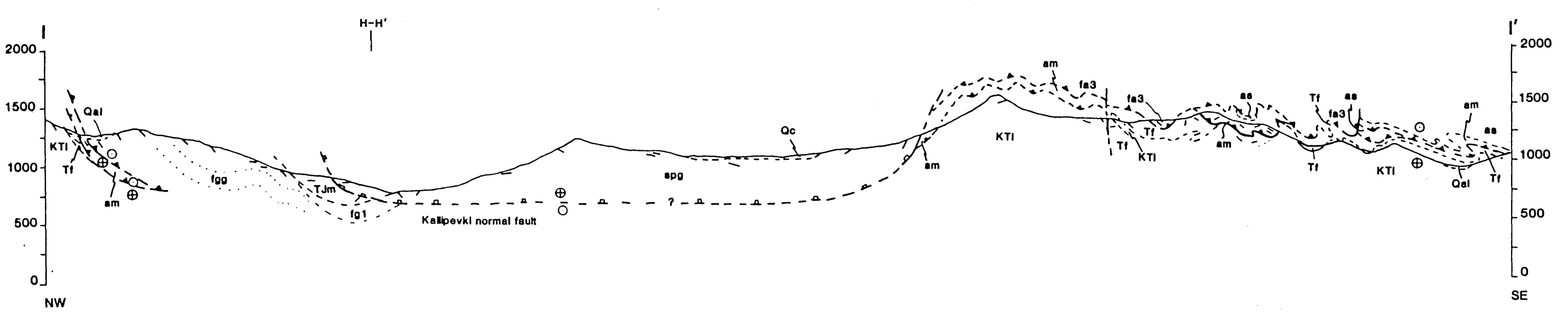

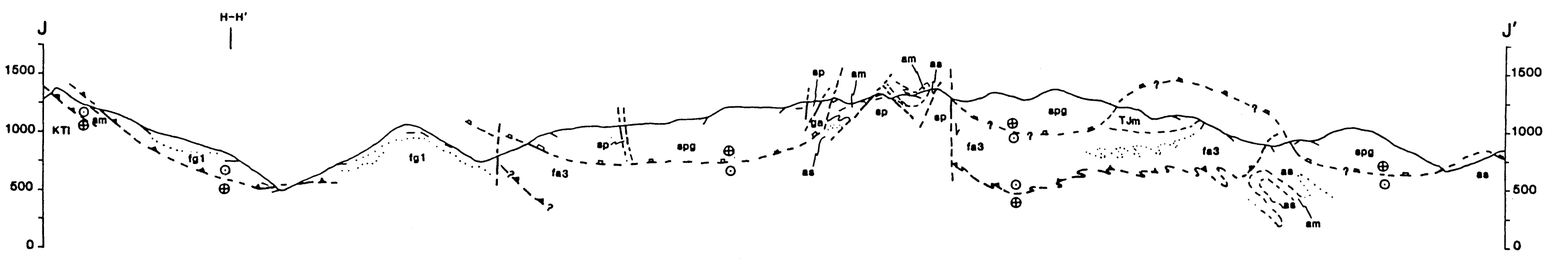

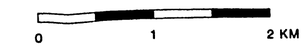

NO VERTICAL EXAGGERATION

VERTICAL SCALE: METERS ABOVE SEA LEVEL

EXPLANATION

- dip of bedding or foliation along line of section
- overturned
- form of folded bedding or foliation
- stratigraphic contact
- high angle fault
- thrust fault
- low-angle normal fault or listric normal fault